NOAA Technical Report NWS 44

Distributed Modeling:
Phase 1 Results

Michael Smith
Victor Koren
Bryce Finnerty
Dennis Johnson

February 1999

U.S. DEPARTMENT OF COMMERCE
National Oceanic and Atmospheric Administration
National Weather Service

Preface

This report is basically a compilation of the work performed in HRL from 1995 to the present investigating the use of NEXRAD data for hydrologic modeling. Over this time span, some of the results in this report were published in journals or presented at conferences. It was decided to place the majority of the results into a final document that could be distributed to interested groups as well as referenced in future reports.

As the work has progressed over a multi-year time span, more data has become available for analysis. For example, the analyses in Chapter 2 were based on the 9 months of available NEXRAD data, while the hydrologic simulations in Chapter 5 used 3 years of data.

The authors would like to thank Dr. Lee Larson and Dr. Charles Hoffeditz for their support during their terms as Chief of the Hydrologic Research Lab. The comments of John Schaake, Jay Breidenbach, Rich Fulton, Dennis Miller, and D.J. Seo are appreciated. The helpful review and comments by Billy Olsen, Bill Lawrence, John Schmidt, and others at ABRFC are acknowledged and appreciated.

Table of Contents

Table of Contents

1. Introduction

1.1 Scope

For hydrologic modeling, the basic premise surrounding the use of NEXRAD and other radar precipitation estimates is that higher resolution data will lead to better simulations. Until recently, standard procedures within the NWS River Forecast System have called for models to be calibrated and operational real time forecasts to be made using raingage measurements. Phase I of the Distributed Modeling Project, originally developed by Lindsey (1993), Lindsey (1994), and continued by Smith, (1996), attempts to address the questions: 'How can Stage III precipitation estimates be used with existing NWS hydrologic models and procedures to improve simulations?'; 'Can the Sacramento model be used in lumped and semi-distributed modes with Stage III?'; 'If a sufficient period of Stage III data is not available for calibration, can guidelines be developed for a priori hydrologic model parameter adjustment so that historically derived parameters can be modified for use with finer resolution Stage III data'? and 'What level of basin sub-division will give the optimum simulation results?' In other words, Phase I addresses the situation of distributed model *inputs*, not distributed model *parameters*. While many fully distributed parameter models already exist, research has first been directed towards answering several basic questions concerning the use of the gridded Stage III data. In Phase II of this project, it is envisioned that hydrologic models having distributed parameters as well as being forced by distributed inputs will be investigated.

The study area chosen for this work is the Illinois River above Tenkiller Ferry Lake in Oklahoma. Hourly streamflow data is available for 8 basins in this watershed, and the ABRFC has the longest duration archive of hourly Stage III data. The basins were chosen as they are unregulated headwater basins. Figure 1-1 displays the location map of the study basins.

The primary purpose of the research under Phase 1 is to address issues related to the RFC scale of basins. However, the results may shed light on issues dealing with forecasting the response of smaller basins.

1.2 Goals of Phase 1.

Two main goals are identified for Phase I:

1. Evaluate the improvement gained through the use of distributed inputs to existing NWSRFS hydrologic models. Before moving to a fully distributed parameter hydrologic model in future research, we want to first determine if any improvement can be gained by using distributed inputs rather than lumped inputs. A semi-distributed modeling approach will be examined in which existing basins will be disaggregated into a number of sub-basins, each receiving a spatially averaged
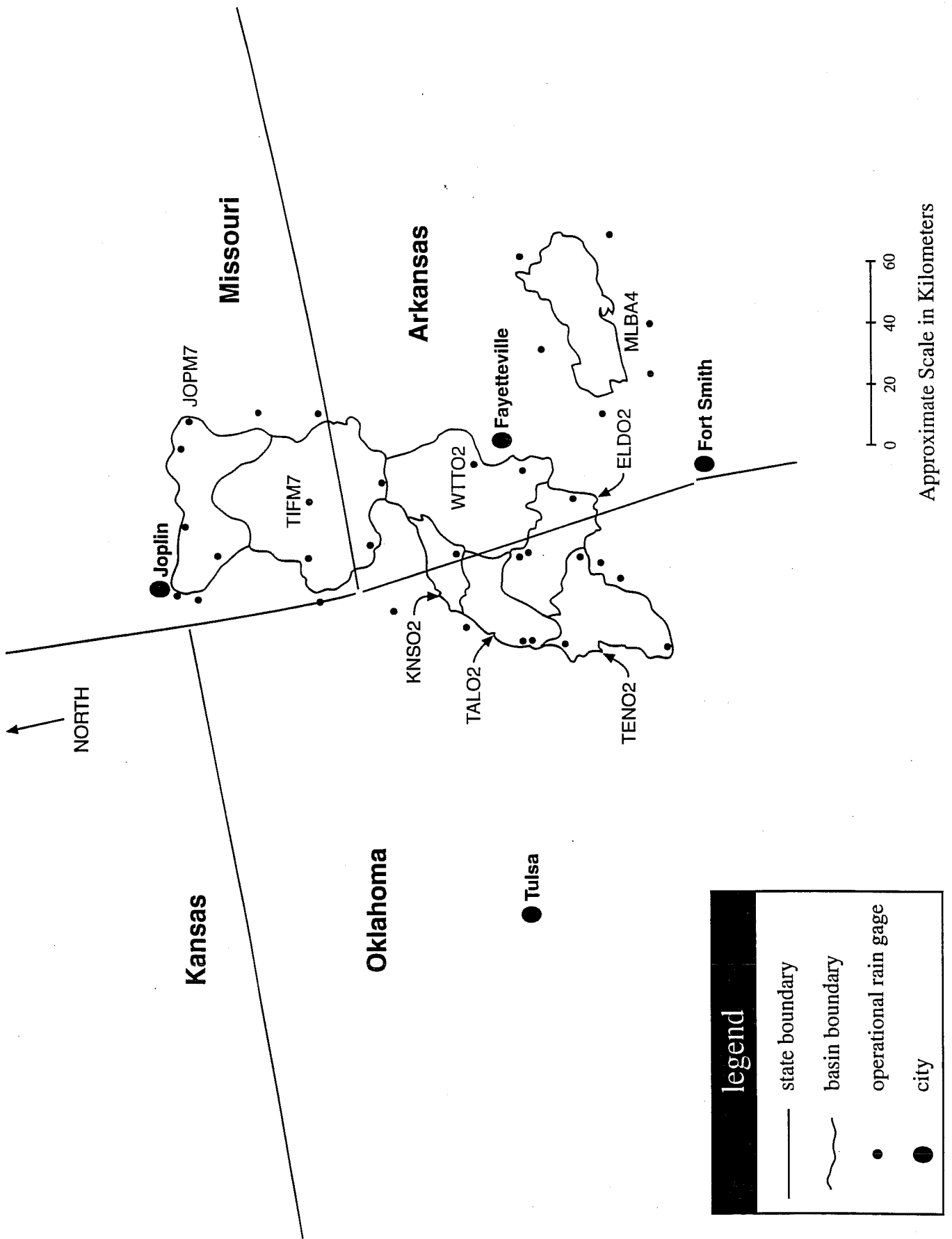
Figure 1-1 Location Map of Basins in Study Area

precipitation input.

Figure 1-2 presents the modeling approach investigated in this research. On the left side of the figure is the current method for lumped parameter modeling to generate hydrographs at a forecast point. Lumped parameters are developed for the Sacramento model through calibration using upwards of 45 years of precipitation and streamflow data. Precipitation input to the models is in the form of a 6-hour mean areal precipitation (MAP) value most commonly determined by Thiessen weighting of rain gage reports. Due to reporting limitations in the rain gage network, the minimum time step was set at 6 hours.
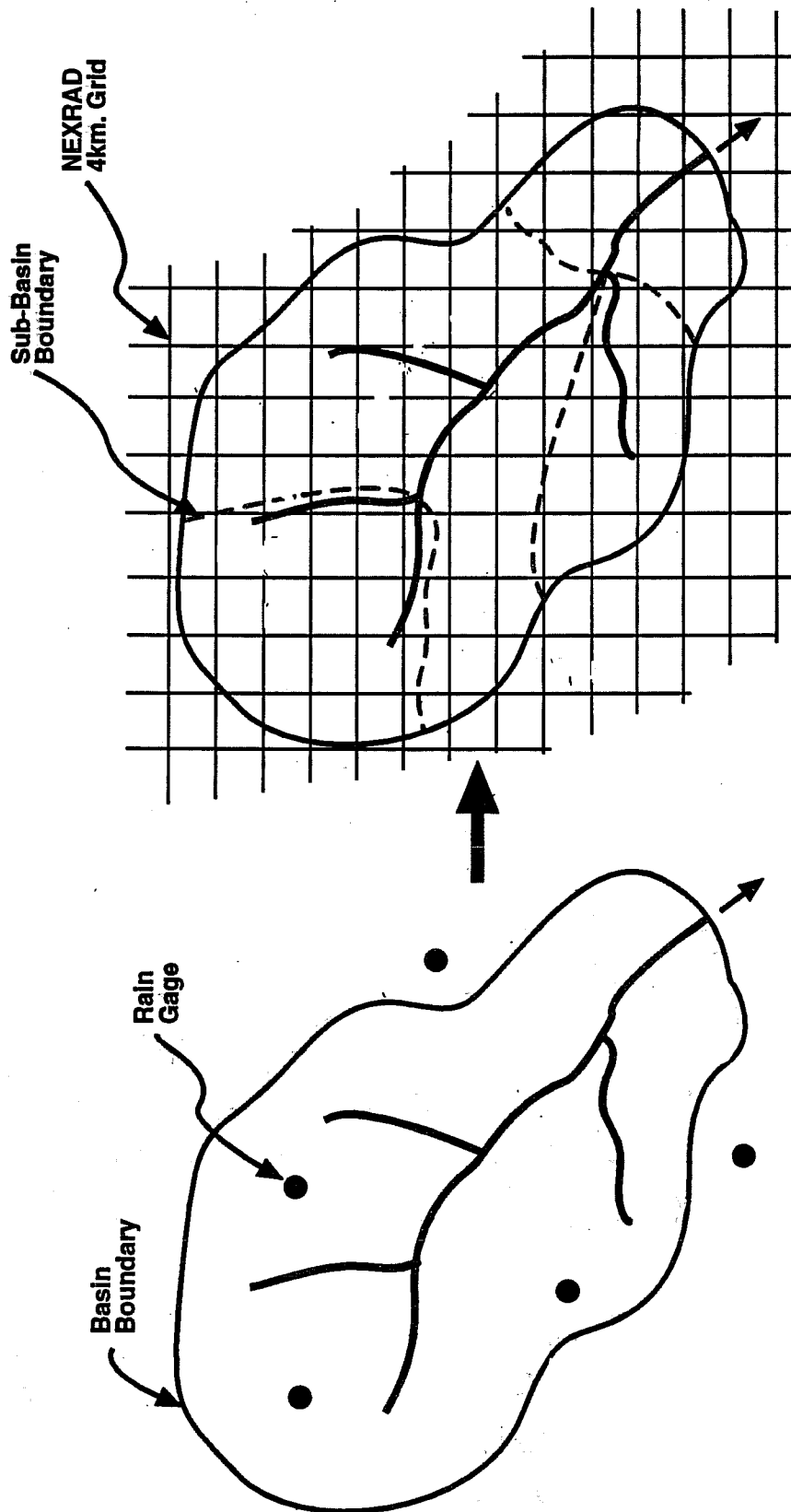
The right hand side of Figure 1-2 presents the semi-distributed modeling approach. In essence, this approach models a basin by disaggregating the area into a number of constituent sub-basins. For each of these sub-basins, Stage III data is used to define a mean areal precipitation value (MAPX). Hopefully, disaggregation will capture the essential spatial variability in the rainfall to provide an improvement over lumped modeling. In addition, each sub-basin will have its own unique unit hydrograph. Routing of sub-basin hydrographs to the main basin outlet will be accomplished by having each sub-basin unit hydrograph reflect both the transformation of runoff depth to discharge as well as the translation of the sub-basin hydrograph to the main basin outlet. Parameters for the Sacramento model will be developed through calibration or a priori adjustment of the lumped calibrated parameters. A key question posed by this formulation is how to parameterize and calibrate a semi-distributed hydrologic model given only observed streamflow information at the outlet.

2. Develop tools and procedures to enable RFC personnel to more effectively use the NEXRAD data for hydrologic modeling. Examples of such tools include methods of deriving synthetic unit hydrographs for sub-basins in semi-distributed modeling. In addition, additional capabilities need to be added to the Interactive Calibration Program (ICP) to enable RFC personnel to do hydrologic modeling at finer time scales. These enhancements include being able to plot hourly discharge data and to provide statistics based on shorter time step information. In addition, a new operation for performing Muskingum-Cunge routing between sub-basins is desirable. Such a channel routing procedure would help limit modeling uncertainty to the rainfall-runoff processes.

1.3 Overview of the report

If a semi-distributed modeling format is to be used, then some method of parameterization and calibration needs to be developed. A significant effort was directed towards the investigation of the sensitivity of Sacramento model runoff components to the scale of precipitation forcing. These analyses are presented in Chapter 2.

In Chapter 3, comparisons of mean areal precipitation values derived from two types of raingage networks (MAP) are compared to operational areal means computed from the gridded Stage III data (MAPX). These analyses were conducted to evaluate the assumption that in flat terrain, the long term mean annual areal mean precipitation derived from radar data should be similar to that derived by a raingage network. In the first set of analyses, MAP values computed from the

NEXRAD 4km. Grid

Sub-Basin Boundary

Semi - Distributed Modeling

- 1 - hour mean areal rainfall from NEXRAD

- rainfall - runoff model parameters adjusted for sub - basins

Rain Gage

Basin Boundary

Lumped Parameter Modeling

- 6 - hour mean areal rainfall from point measurements

- spatially averaged parameters for rainfall - runoff models

Figure 1-2 Approach to River Basin Modeling at Finer Scales

National Climatic Data Center (NCDC) cooperative observer network are compared to operational MAPX values for a 7 month period for 8 basins from the Tulsa RFC. In the second set of analyses, MAP values derived from the operational raingage network are compared to operations MAPX values for the same nine basins over a three year period. The hydrologic modeling implications of any differences between MAP and MAPX values are discussed.

Chapter 4 presents the results of numerical analyses investigating the optimum level of basin disaggregation. Few guidelines exist in the literature to aid the hydrologist in answering the question: "Given the availability of gridded precipitation measurements, to what level must a lumped basin be disaggregated in order to improve hydrograph simulation"? In this chapter, the effects of random noise in the gridded rainfall data on peak flow and volume are presented.

In Chapter 5, the main findings of Phase I are presented: results of lumped and semi-distributed simulations using Stage III inputs. Improvements over rain gage based hydrologic modeling are discussed. Approaches for deriving sub-basin unit hydrographs are described, as well as the limitations of using the standard S-Curve method to derive a one-hour unit graph from a six-hour unit graph. In addition, discussion is provided concerning the calibration of lumped and semi-distributed sub-basins using Stage III. Chapter 6 is a natural continuation of Chapter 5 in that issues related to sub-basin parameters are discussed.

While each chapter contains a section on results and conclusions, Chapter 7 serves to present a list of overall conclusions. A series of recommendations is provided in Chapter 8. Graphs and other information too numerous to present in the main body of the report are included in the Appendices.

References

Lindsey, S.D., 1994, 'Distributed Modeling Project Plan', Internal Publication, Hydrologic Research Lab, National Weather Service, February.

Lindsey, S.D., 1993, 'Strategy for Utilizing Radar-Based Precipitation Estimates for River Forecasting .' Proceedings of the Symposium on Engineering Hydrology, ASCE, C.Y. Kuo, editor,, 940-945.

Smith, M. B., 1996, 'Distributed Modeling Project Plan -Phase 1: Distributed Inputs', Internal Publication, Hydrologic Research Lab, National Weather Service, September.

2.0 The Sensitivity of the Sacramento Model to Precipitation Forcing of Various Spatial and Temporal Scales.

2.1 Introduction

The Sacramento Soil Moisture Accounting Model (SAC-SMA) model is a conceptual rainfall runoff model with spatially lumped parameters (Burnash, 1995; Burnash et al., 1973). Within the National Weather Service, it is generally applied to river basins ranging from 300 km^2 up to 5000 km^2. Basin sizes vary according to hydrologic region, geomorphology, forecast point requirements, and available data. The SAC-SMA model is generally run at a 6-hour time step but can run at any time step. Inputs to the SAC-SMA model are 6-hour mean areal precipitation (MAP) and 6-hour mean areal potential evaporation (MAPE). MAPE is estimated from pan evaporation data or monthly mean potential evaporation, and may also be calculated from synoptic data. The SAC-SMA model parameters are manually and automatically calibrated with the objective of making the model simulation match historical observed discharge data. Calibration usually requires at least 8 years of historical input precipitation data for continuous simulation and comparison to observed discharge (U. of Arizona, 1995). An additional 8 years of historical data are recommended for model verification. Therefore, the calibrated parameters are inherently tied to the spatial and temporal scale, terrain, geographic location, and gage networks from which they are calibrated.

As a result of the calibration parameters being linked to the historical rain gage network, a direct utilization of the gridded Stage III data cannot be made without understanding how the SAC-SMA model responds to precipitation forcing at various spatial and temporal scales. Optimally, a lumped basin that is disaggregated into sub-basins should be recalibrated to reflect the model's response to a different scale and type of precipitation forcing (i.e., 6 hour gage MAP values vs. 1 hour gridded radar precipitation estimates) (Bradley and Kruger, 1998). Obled et al. (1994) followed this procedure when they modeled a basin in a lumped fashion and then as a collection of 9 constituent sub-basins. However, For the NWS, less than 3 years of Stage III data are available for recalibration of the SAC-SMA model, which is an insufficient length of time for calibration and validation of model parameters. Comprehensive procedures exist within the NWS for the calibration of the SAC-SMA on lumped basins provided there is stream gage data available. However, it is unclear how to recalibrate the model parameters on the disaggregated sub-basins due to the absence of stream gages at internal points. Thus, the NWS faces the unique problem of using a semi-distributed modeling approach for operational forecasting, without a sufficient period of high resolution Stage III data or observed discharge data with which to calibrate the sub-basins. Until an adequate Stage III calibration data set is available, improved understanding is required concerning SAC-SMA model parameter adjustments to account for model response to different scales of precipitation inputs.

This section presents the results of the sensitivity of the SAC-SMA model runoff component volumes to Stage III gridded precipitation estimates at numerous space-time scales. There are no actual hydrographs being presented in this section, simply the runoff component volumes. Although model parameters are tied to the space-time scale, terrain, and gage network characteristics from which they are calibrated, this section shows similar model results from a wide range of model parameters. Therefore, the results presented are considered to be generally applicable to the SAC-SMA model response and are not tied to the parameters used. A primary assumption in the analysis is that the 6-hour Stage III MAPs are equal to the historical 6-hour gage MAPs because gage data is used by the Stage III multi-sensor field. In addition, the calibrated SAC-SMA model parameters are assumed to be applicable to input MAPs estimated from Stage III data as well as gage network data.

2.2 Review of related research

Hydrologic model response to precipitation inputs of various spatial and temporal resolutions has been the subject of numerous investigations. Many studies have approached this problem from the standpoint of rain gage sampling and density. Recently, the implementation of radar has enabled hydrologists to begin the evaluation of model response to gridded precipitation estimates. Intuitively, one would hypothesize that the use of higher resolution data leads to better model results. Surprisingly, there does not seem to be a clear trend in the literature that supports this hypothesis.

In an oft-referenced work, Wilson et al. (1979) concluded that ignoring the spatial variability of precipitation input, even when the total depth of rainfall is preserved, can have significant influences on the runoff hydrograph. Their findings were based on the analysis of a 67 km² basin and two levels of synthetic precipitation definition: in the first case, one gage was used to define the input to a lumped parameter model, while in the second, 20 gages were used. Based on limited testing, Shanhltz et al. (1981) arrived at a similar conclusion, as did Beven and Hornberger (1982) who suggested that:

'....(the) incorporation of distributed inputs would lead to improvements in simulating catchment hydrographs.'

On the other hand, Obled et al. (1994) used 21 rain gages to define the input to 9 sub-basins representing a 71 km² basin. They presumed that providing distributed inputs to the model would improve simulations, especially if parameter re-optimization was allowed. However, their semi-distributed representation of the basin produced slightly worse results than a lumped representation combined with coarser precipitation input, even after recalibration of the model parameters. The authors were unable to prove the value of using distributed rainfall inputs to improve hydrologic predictions, noting that:

'better dynamics expected in the discharge from better information on rainfall pattern is not demonstrated in (the) goodness-of-fit criteria'.

Krajewski et al. (1991) saw more influence from temporal resolution of rainfall inputs than from spatial variability. Given the very small size of the basin (7.5 km^2), the authors concluded that their results were reasonable. However, Pessoa et al. (1993) found that simulated hydrographs from an 840 km^2 basin using distributed radar-rainfall inputs were not significantly different than simulated hydrographs produced from lumped radar-rainfall inputs. Significant differences were realized, however, when lumped rainfall inputs were defined as the arithmetic means of up to 5 randomly selected radar pixels.

Kouwen and Garland (1989) examined the effects of radar data resolution on runoff hydrographs produced from a distributed parameter model, and attempted to define guidelines for the appropriate level of rainfall input resolution. They found that coarser resolution radar input sometimes produced better simulation results due to smoothing of errors present in finer resolution data. However, they also recognized that local circumstances dictate whether radar data smoothed into a coarser grid would be appropriate. Their study also presented significant differences between runoff hydrographs produced by rain gage only data and radar data.

Kenner et al. (1996) recognized the need to identify the scale dependencies of critical hydrologic parameters. Preliminary results were obtained when a 963.5 km^2 basin was modeled as a single lumped area and as a collection of 5 sub-basins. In limited tests on a single extreme event, the semi-distributed approach produced better agreement with the observed hydrograph than the lumped approach. However, the results may be affected by the fact that neither approach was calibrated.

In a recent study, Shah et. al. (1996) examined the spatial variability of rainfall on a small (10.55 km^2) basin for various levels of antecedent moisture conditions. Spatial averaging of rainfall inputs led to adequate simulations under wet conditions. However, greater errors resulted when spatially averaged rainfall fields were used with dry antecedent moisture conditions, indicating a linkage between spatial variability of rainfall and the distribution of soil moisture which subsequently controls the generation of runoff.

Ogden and Julien (1994) found severe reductions in peak discharge due to a reduction in rainfall excess which was directly attributed to the aggregation of radar inputs. Their analysis used high resolution radar inputs and a gridded rainfall runoff model on watersheds less than 150 km^2.

Wood et al. (1988) introduced the concept of a representative elementary area (REA) to account for the small-scale heterogeneities in the macro scale models. The REA represents the threshold scale where statistical representations of smaller areas can replace actual patterns of variability. For the 525 km^2 Little Washita catchment Wood (1995) estimated the threshold scale to be on the order of 5 to 10 km^2. However, Fan and Bras (1995) argued that the REA concept has limited utility in hydrology because the REA is scale dependent, and it can vary on individual storm events.

Nalbantis (1995) developed guidelines for adjusting certain hydrologic model parameters to account for changes in temporal modeling scales. He addressed the problem of lumped parameter models calibrated with daily information that were then used at shorter time intervals to simulate flood events. Often, this situation arises when continuous daily rainfall and streamflow data are available for long periods, but an insufficient period of shorter time interval data is available for proper calibration at shorter time intervals. His proposed strategy involved calibrating the model at a daily time step, then adjusting certain time-dependent withdrawal coefficients to derive a model to be used at a 1 hour time step. The daily model would be operated continuously. At the onset of a flood event, the derived hourly model would be initialized using the states of the continuous daily model. His results showed that the prediction of initial values of the 1 hour state variables related to slow response of a basin can be done quite accurately. However, he could not produce an automated method to reliably transfer the rapid response state variables from the daily to the hourly scale without requiring significant tuning.

2.3 Method

In order to examine the response of the SAC-SMA model to Stage III precipitation inputs at various spatial and temporal resolutions, a collection of synthetic sub-basins is created. The synthetic sub-basins correspond to regular aggregations of HRAP bins within a 64x64 HRAP bin matrix. These sub-basins range in size from 1x1 HRAP bin up to 64x64 HRAP bins, as shown in Table 2-1. MAP inputs for the sub-basins are calculated from a 64x64 HRAP bin, 1-hour, Stage III precipitation data set that encompasses a calibrated test basin at Eldon, Oklahoma. Figure 2-1 shows the 64x64 HRAP bin experimental data set and the Eldon test basin. Figures 2-2a, b, c, d, e, f, and g show the scaling of MAP inputs for a 1 hour accumulation of a Stage III precipitation field and the resulting areal averaging of the high intensity event over the range of synthetic sub-basin scales analyzed. Figure 2-2 clearly illustrates the loss of intensity that occurs when averaging precipitation forcing over increasingly larger areas.

Sacramento model parameters were taken from a preliminary calibration of the Baron Fork at Eldon, Oklahoma, U.S.A., whose drainage area is 795 km^2. A 6 hour MAP time series for the basin was derived using historical rain gage data. Observed mean daily flow records for the stream gage at Eldon were obtained from the U.S. Geological Survey. The calibration time step was 6 hours. It is worth emphasizing that these SAC-SMA parameters, calibrated at 6 hours, and for a 795 km^2 basin, were applied without change to each of the synthetic sub-basins in the subsequent analyses. It should also be noted that the drainage area of the Baron Fork corresponds roughly to the 8x8 HRAP bin area. The calibrated parameters are assumed to be reasonable for the entire 64x64 HRAP bin area, and the area is assumed to have similar rainfall runoff processes throughout.

Figure 2-1 on following page: Location of the Illinois River basin (lightly highlighted) and the calibrated test basin of the Baron Fork of the Illinois River at Eldon, Oklahoma (darker highlighting). The basin is in the straddles the border of Oklahoma and Arkansas, which is located on the southern plains of the United States. The 64x64 HRAP bin Stage III test data set is shown by the square area surrounding the test basin. Precipitation is seen to the west and north of the experimental area.

.Hot_Springs

.llardanelle

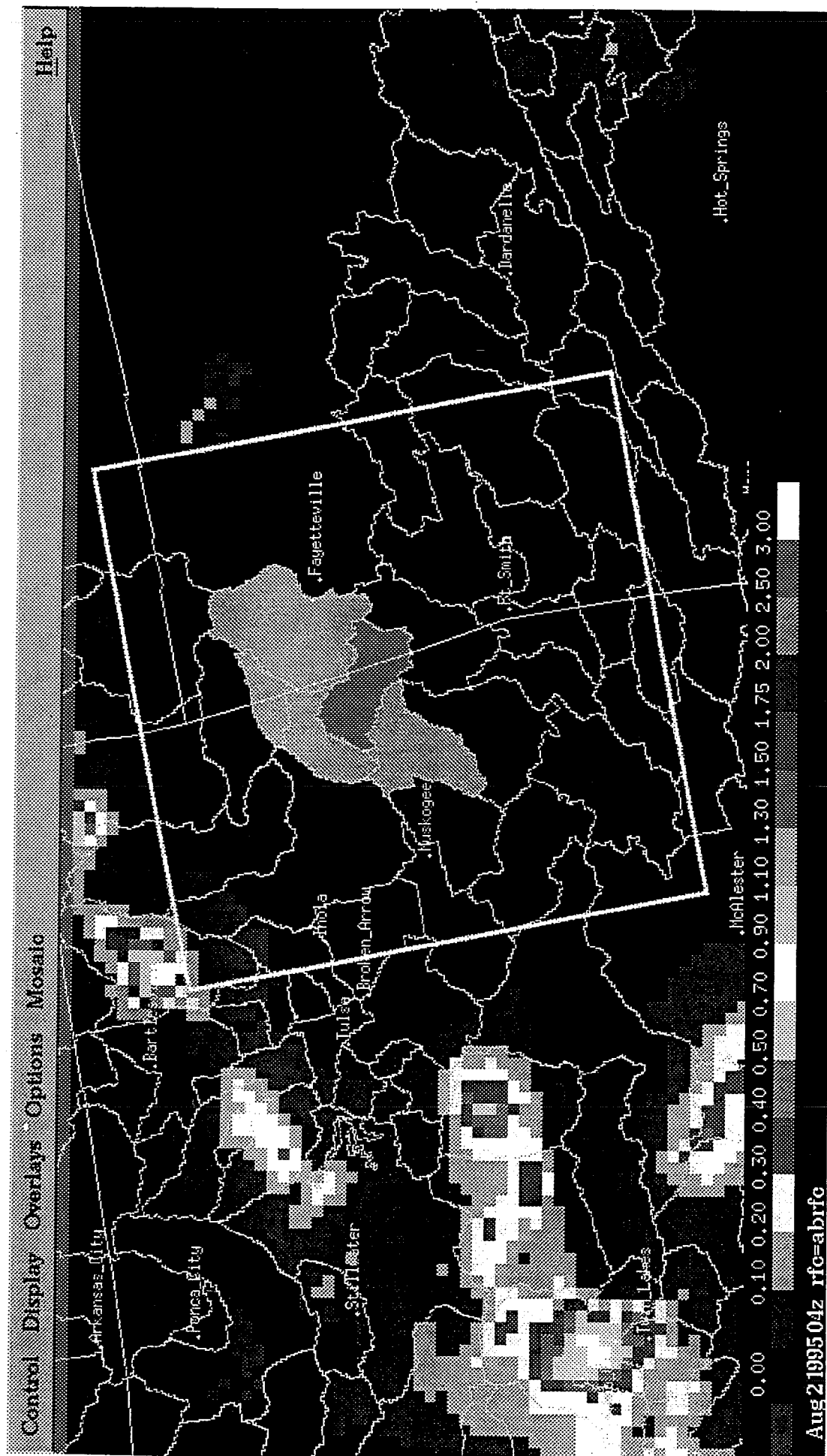.Fayetteville

.Ft_Smith

.Muskogee

.Bart

.Tulsa

.Broken_Arrow

.McAlester

.Arkansas_City

.Ponca_City

.Stillwater

0.00   0.10 0.20 0.30 0.40 0.50 0.70 0.90 1.10 1.30 1.50 1.75 2.00 2.50 3.00

Aug 2 1995 04z rfc=abrfc

Figure 2-1

Following pages:

Figure 2-2: Spatially Aggregated Stage III Precipitation Field Over Northeastern Oklahoma, January 16, 1994, 20:00z.

a) Stage III 1-hour precipitation field in units of millimeters (z-axis) and over a spatial extent of 64x64 HRAP bins. Each bin has an individual value relative to its neighbors, and is used as input to the lumped SAC-SMA hydrologic model. Thus, 64^2 or 4096 individual SAC-SMA model runs are used over this area for every hour of model simulation. (Maximum value: 19.01 mm)

b) Same data as shown in a) except it has been averaged in 2x2 HRAP bins. This field has $64^2/2^2=1024$ individual values and will require the same number of SAC-SMA model runs to analyze. Notice that the averaging procedure reduces the peaks of actual values shown in a). (Maximum value: 15.73 mm)

c) Same data as shown in a) except it has been averaged in 4x4 HRAP bins. This field has $64^2/4^2=256$ individual values. Notice that each individual group appears as a "tic-tac-toe" board or grid boxes. This may create the false impression that values have been grouped 3x3 rather than 4x4. The values being plotted are at the **corner** of each square, not centered upon the square, thus a tic-tac-toe board has 16 corners rather than 9 squares. (Maximum value: 11.56)

d) Same data as shown in a) except it has been averaged in 8x8 HRAP bins. This field has $64^2/8^2=64$ individual values. Notice that this field only very coarsely resembles the original field shown in a) and this is the scale at which the Eldon, OK test basin most closely represents. (Maximum value: 9.11 mm)

e) Same data as shown in a) except it has been averaged in 16x16 HRAP bins. This field has $64^2/16^2=16$ individual values. (Maximum value: 6.32 mm)

f) Same data as shown in a) except it has been averaged in 32x32 HRAP bins. This field has $64^2/32^2=4$ individual values. This field is arguably a poor representation of the original spatial distribution of data (Maximum value: 2.11 mm)

g) The entire field has now been averaged into a single, 64x64 value requiring only a single run of the SAC-SMA model. This corresponds to the lumped model run for the entire 64x64 HRAP bin experimental area. (Maximum value: 1.45 mm)

(a)

(b)

(c)

(d)

space (HRAP bins)

precip. depth (mm)

2.8
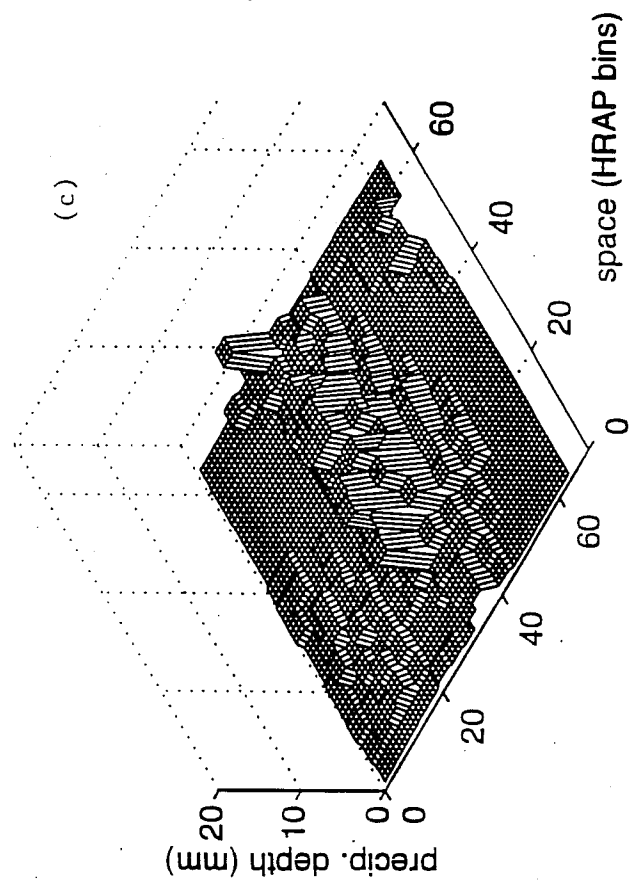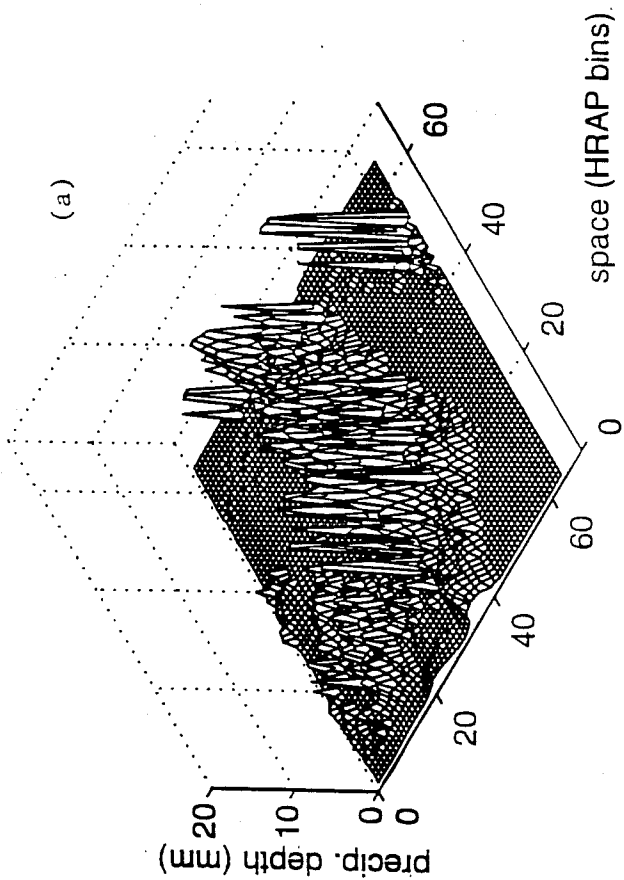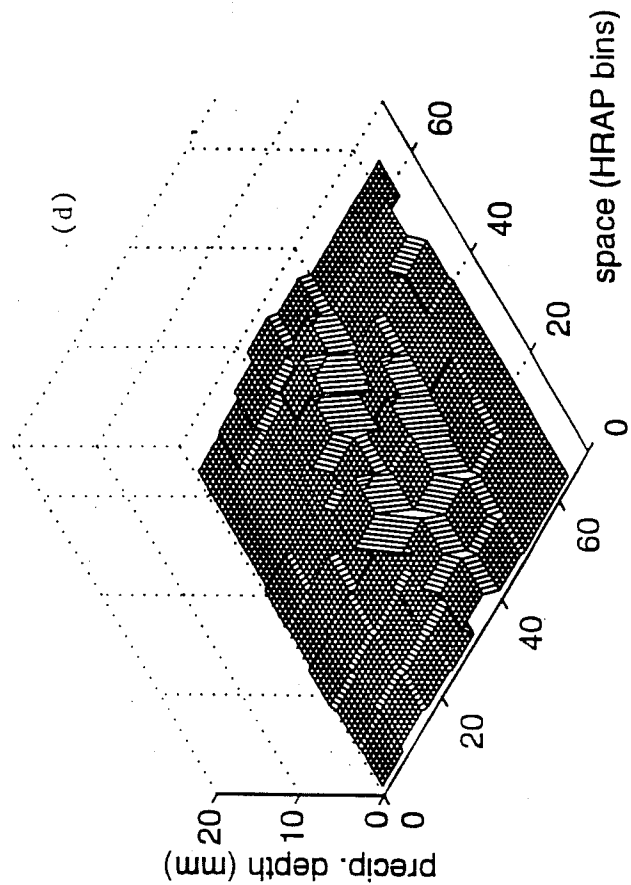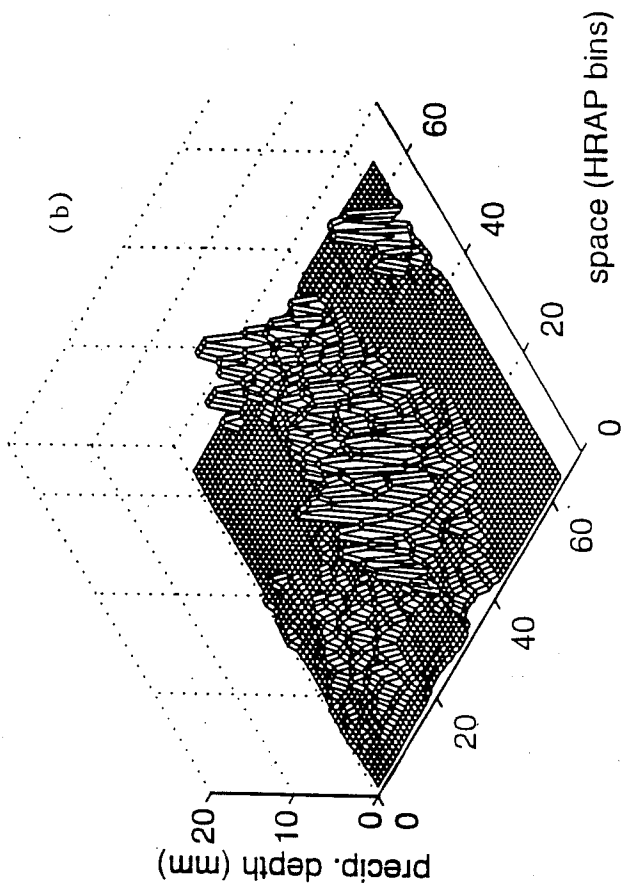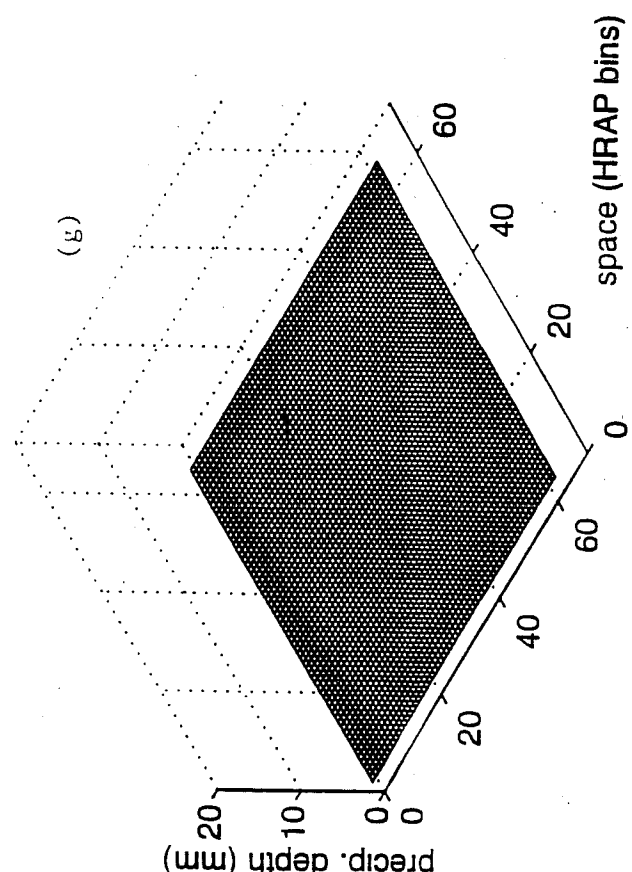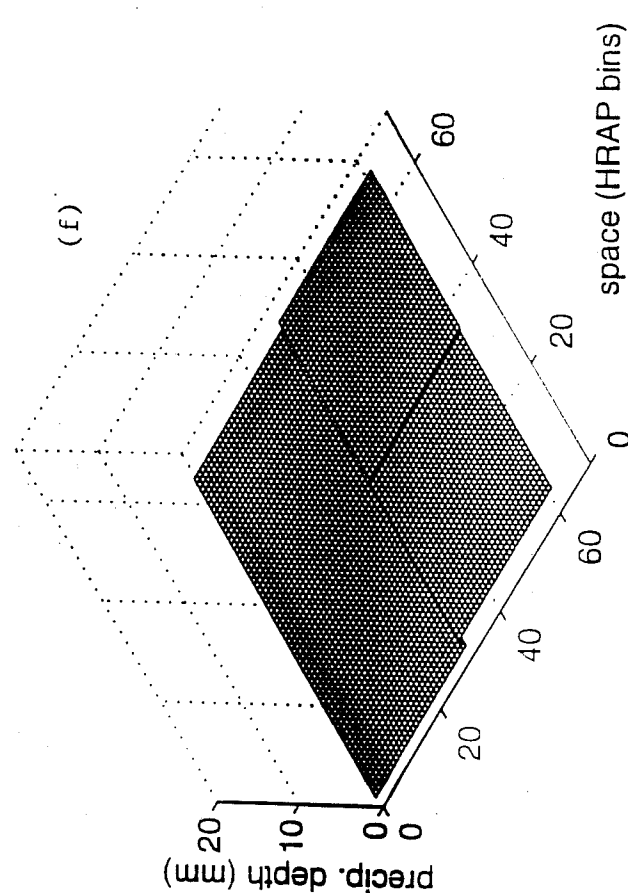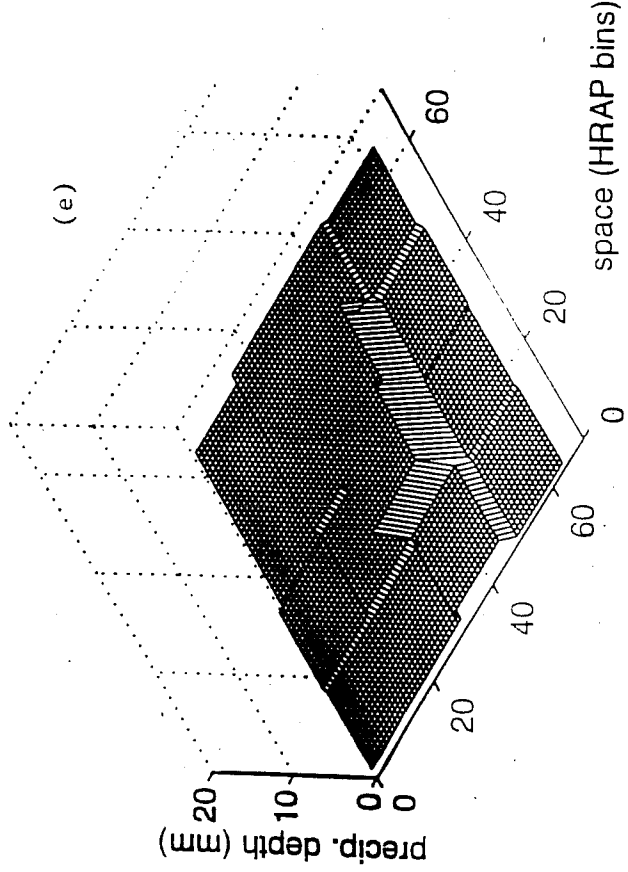
Within this framework, the sensitivity of the SAC-SMA runoff components to precipitation forcing at various scales is analyzed. The SAC-SMA model is run in a continuous mode for the entire 9-month period using model time steps of 1, 3, and 6 hours, and for each of the spatial scales listed in Table 2-1. The Stage III data set covers the eastern portion of the Tulsa, Oklahoma, river forecasting region and spans from May 7, 1993 through January 31, 1994. This time period records the very wet summer which resulted in the "Great Flood of '93" in the Midwestern United States. Soil moisture accounting is performed over the entire 64x64 HRAP bin area and is maintained independently for every sub-basin and at each space-time scale analyzed.

Table 2-1: Sub-basin Scale Dimensions and Units

Sub-basin Size (HRAP Bins)	Sub-basin Size (km)	Sub-basin Size (km^2)	Number of Sub-basins Representing Entire Area
1 x 1	4 x 4	16	4096
2 x 2	8 x 8	64	1024
4 x 4	16 x 16	256	256
8 x 8	32 x 32	1,024	64
16 x 16	64 x 64	4,096	16
32 x 32	128 x 128	16,384	4
64 x 64	256 x 256	65,636	1

Storm characteristics are difficult to describe for the large 64x64 HRAP bin area, however, some general storm information is useful to understanding the regional climate in the study area. Rain was detected in the 64x64 study area for 2163 hours of the 6480 total hours of data between May 7, 1993 and January 31, 1994. The average hourly precipitation coverage was 22% of the total area with a mean hourly precipitation depth of 0.37 mm/64x64 HRAP bins, given the presence of rain. There were approximately 45 events in the 9 month period that had a storm peak with greater than 40% coverage in the 64x64 area and had a mean peak depth in the covered area of greater than 4 mm.

For comparison, runoff volumes generated by sub-basins within a given level of disaggregation are spatially averaged over the entire 64x64 HRAP bin area. Routing of the runoff components through a unit hydrograph or channel network is not performed in this analysis. The

precipitation inputs for the 3-hour and 6-hour time scale analysis are derived from summing the 1-hour data.

The model components analyzed include: precipitation depth, impervious runoff, direct runoff, surface runoff, interflow, percolation, total evapotranspiration, supplemental baseflow, primary baseflow, total channel inflow, water balance errors, and evapotranspiration demand. Figure 2-3 shows the general contribution of the various runoff components of the SAC-SMA model to the runoff hydrograph. Figure 2-4 shows the fundamental conceptualization of the SAC-SMA model, including all soil moisture storages, runoff components, and exchanges between the atmosphere and land surface components. The names of the model components are specific to the conceptual formulation of the SAC-SMA model and are not general terms of hydrologic science. Output summary statistics are calculated over the 9-month period for all 13 model components and all sub-basin scales analyzed. Statistics include mean, variance, maximum, minimum, and cumulative depth values at all sub-basin scales. The analysis in this section only presents certain statistics, runoff components, and time scale cases in order to highlight the most significant results.

2.4 Results

2.4.1 Spatial Analysis

Perhaps the most extreme change in modeling strategy for a River Forecast Center would be to convert from 6-hour lumped parameter modeling using gage-derived precipitation estimates to 1-hour semi distributed modeling using precipitation estimates derived from NEXRAD. This first series of analyses addresses such a dramatic change.

Figure 2-5 clearly shows the sub-basin scale sensitivities of the relative change in SAC-SMA model runoff component volumes for the 1-hour model time step. Recall that the SAC-SMA parameters are uniformly applied to each sub-basin. Each increase in basin resolution results in a 4 fold increase in the number of sub-basins being used to model the 64x64 HRAP bin test area. The runoff components are scaled relative to their value generated at the 8x8 spatial scale because that is the approximate spatial scale of the calibrated test basin. The SAC-SMA model generates surface runoff when the two storage reservoirs, tension and free water storages, representing the upper soil layer become saturated. Figure 2-3 shows surface runoff is the fast response rising limb of the hydrograph. As seen in Figure 2-5, surface runoff is the most spatially sensitive component of the SAC-SMA model, and decreases to zero as the spatial scale increases to 64x64 HRAP bins. Surface runoff is also very sensitive at the finer spatial scales analyzed.

Interflow is the second fastest responding runoff component in the model followed by supplemental baseflow. These runoff components represent the falling limb of the hydrograph as shown in Figure 2-3. Interflow is conceptualized as the lateral flow from the upper soil layer and is generated from the upper zone free water storage reservoir. Supplemental baseflow is the fast responding baseflow component and is generated from the lower zone free supplemental water reservoir. Figure 2-5 shows interflow and supplemental baseflow are also quite sensitive to spatial

Hydrograph Positions Where Runoff Types are Generally Most Significant
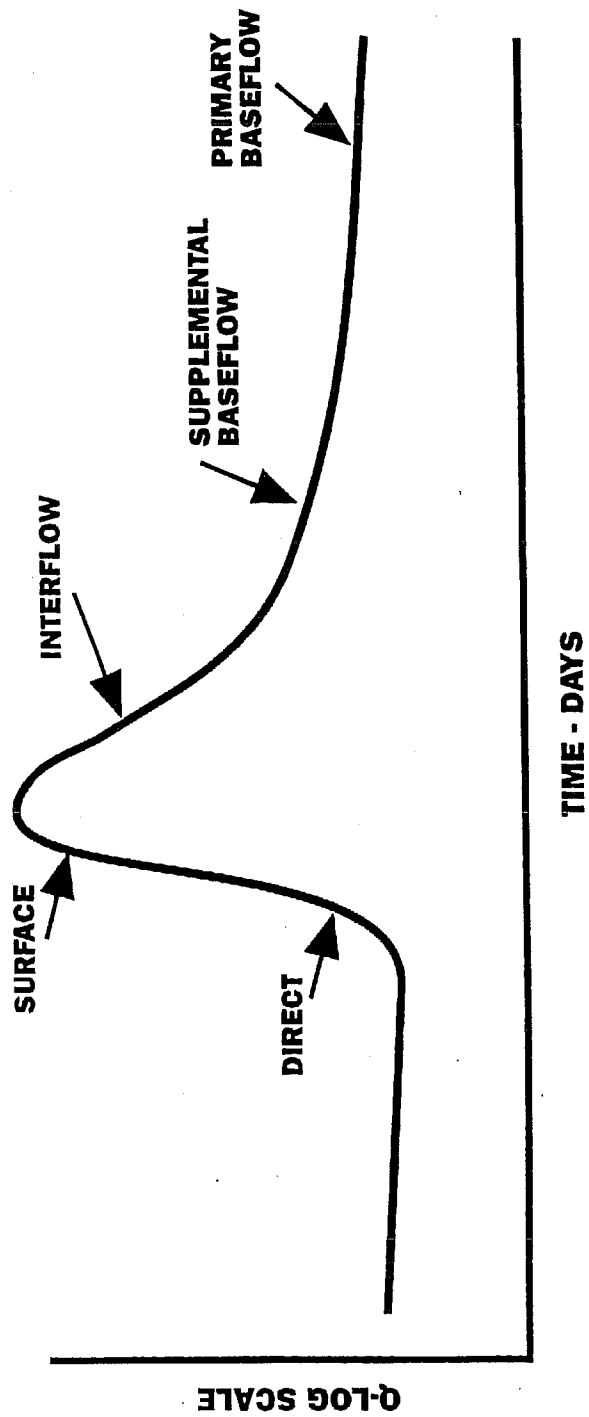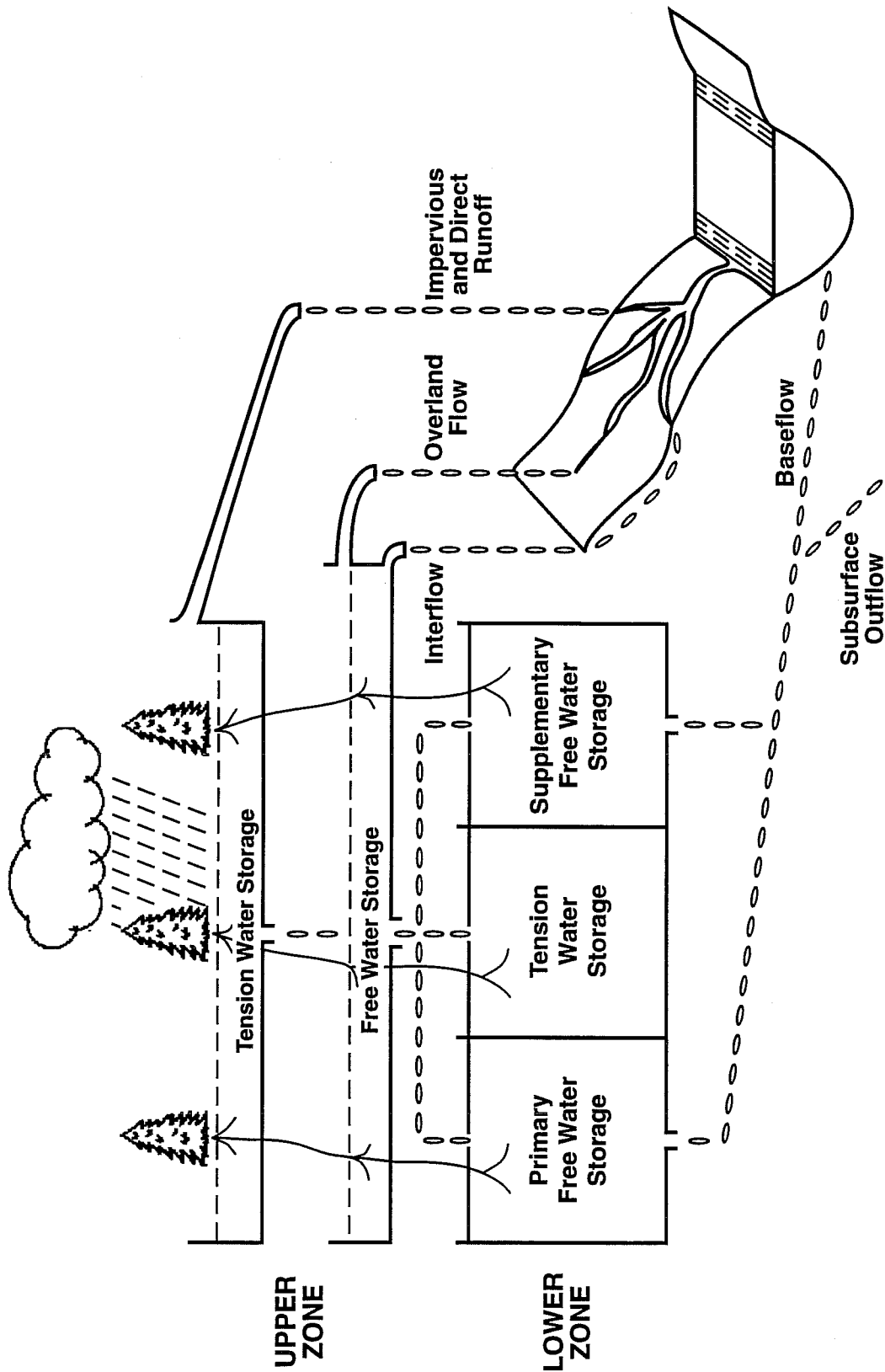
Figure 2-3

Figure 2-4 Conceptual Representation of the Sacramento Soil Moisture Accounting Model
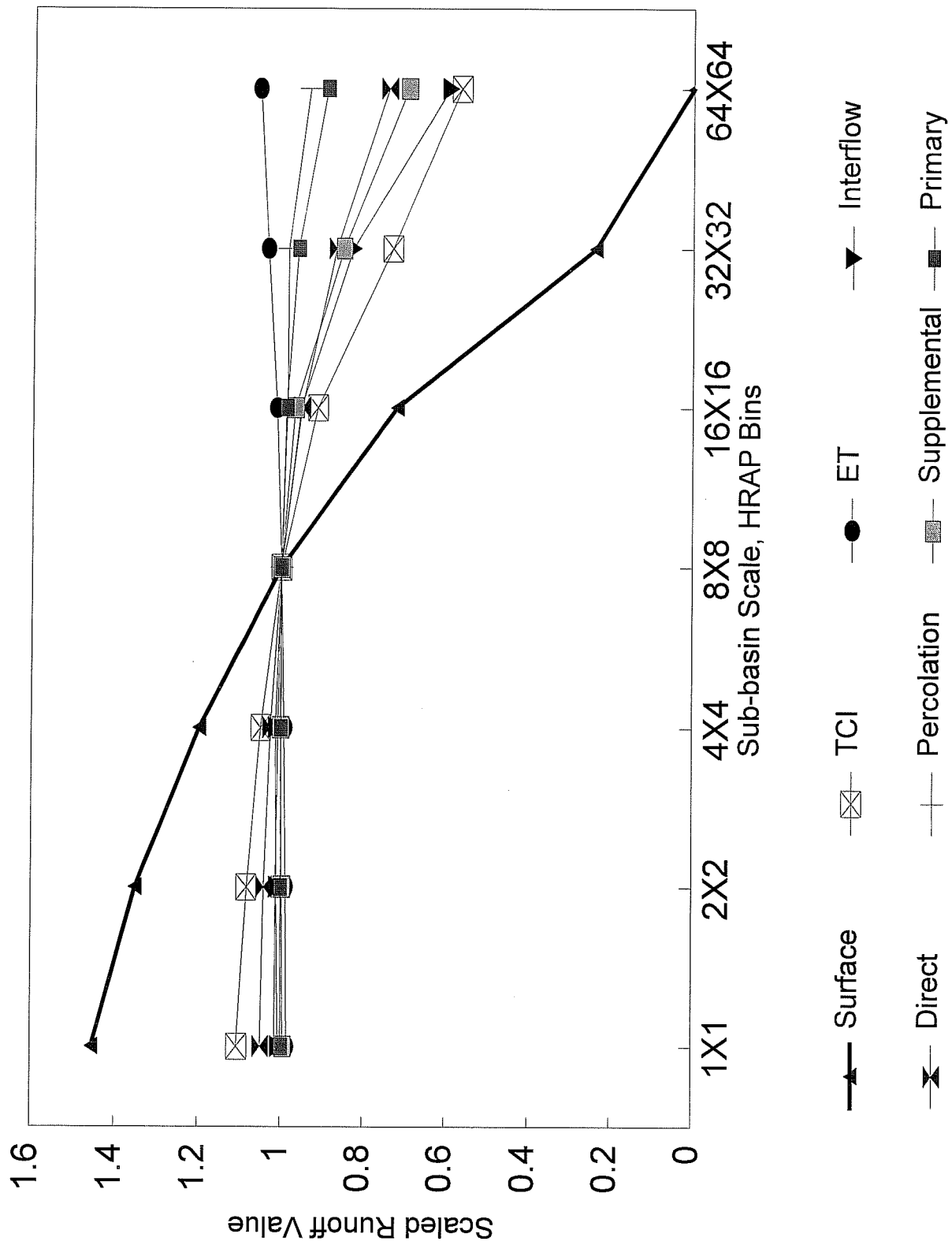Showing the Various Storages and Corresponding Runoff Components

Figure 2-5. Relative Sensitivity of Runoff Component to Sub-Basin Scale. Runoff values have been normalized bye the value at the 8x8 scale.

scale and they both decrease as the sub-basin scale increases. However, they do not prove to be very sensitive at spatial scales less than the 16x16 sub-basin size. The figure shows how the reduction of surface runoff, interflow, and supplemental baseflow contribute to the overall reduction of total channel inflow as the sub-basin scale increases. Percolation, direct runoff, and primary baseflow also exhibit a decrease in runoff volume as the spatial scale increases. Capturing the spatial precipitation intensity characteristics exhibited in the Stage III data by using smaller sub-basins without parameter recalibration accentuates the fast response runoff components, while having less impact on the slower response components of the SAC-SMA model.

Evapotranspiration decreases as the sub-basin scale decreases, as shown in Figure 2-5. The long-term water balance is maintained in the SAC-SMA model because the increase in total channel inflow, produced at the finer spatial scales, results in less soil water available for evapotranspiration during the drying periods. The SAC-SMA model scale dependency displayed in Figure 2-5 is primarily attributed to the spatial averaging of high intensity precipitation events that produce significant runoff (see Fig 2-2a-g). Increasing sub-basin scale decreases the mean areal precipitation (MAP) to the extent that it does not satisfy the SAC-SMA upper zone tension and free water storages, which decreases the frequency and runoff volume from those events which produce runoff at the smaller spatial scales. Therefore, increasing the spatial scale increases the volume of precipitation held in tension water storage where it evapotranspires into the atmosphere and reduces total channel inflow. Georgakakos et al. (1996) also noticed that a lumped application of the SAC-SMA model holds more water in storage as compared to a semi distributed application of the model. The results shown in Figure 2-5 for surface runoff agree with those generated by Famighetti and Wood (1994) on an ll.7 km^2 basin. However, Pessoa et al. (1993) detected very little difference in hydrologic model response generated from a lumped versus fully distributed implementation of radar rainfall data on an 840 km^2 basin.

The spatial analysis indicates that parameters derived from the 6-hour MAP inputs at a given spatial scale cannot be distributed to sub-basins of different spatial scales and a 1-hour model time step, without introducing significant biases in the volume and timing of SAC-SMA model runoff components. Therefore, disaggregating a basin to capture the spatial variability of precipitation must be accompanied by recalibration to remove biases in model simulation. All results presented must be viewed according to the fundamental assumptions and limitations of the analysis and may vary geographically.

2.4.2 Temporal Analysis

The time scale analysis is performed to investigate the effects of changing from the 6-hour model time step, most commonly used for current operational forecasting, to the 1-hour time step of the Stage III precipitation data. In the NWS a 6-hour MAP typically represents the lower bound in temporal resolution because the rain gage networks currently used for forecasting procedures are too sparse and don't report frequently enough to produce meaningful hourly precipitation estimates. The temporal analysis assumes the 6-hour MAP from the Stage III products are similar to the 6-hour

MAPs derived from gage data. This assumption is reasonable because Stage III precipitation estimates are merged with "ground truth" gage data.

.Modeling at finer time steps is expected to increase forecast lead times and increase forecasting accuracy in fast response basins. For example, if a 6-hour time step is used, the NWS River Forecasting System (NWSRFS) must collect and process data for the entire time interval before the data is run through the models to generate a river forecast. NWSRFS uses a fixed time interval and data is generally reported at fixed times, there is no means for a sliding type of time interval. If a rain event occurs in the first 2 hours of the 6 hour time step, then all 6-hours must elapse before the data is posted to the system for processing. In this example, a 1 hour time step increases the forecast lead time by approximately 4 hours while more accurately representing the intensity of the precipitation.

Figure 2-6 displays the percent change in SAC-SMA model runoff component volumes when changing from a 6-hour time scale to a 1-hour time scale while holding the model parameters constant. Values in Figure 2-6 represent the differences in 9-month totals in each of the runoff component volumes. The figure shows that surface runoff is the most temporally sensitive model component at the finer sub-basin scales. Surface runoff at the 8x8 spatial scale increases by over 21 percent when changing to the shorter 1-hour time scale. Interflow at the 8x8 spatial scale is shown to increase by 20 percent when changing from the 6-hour to the 1-hour time scale, but is not as sensitive as surface runoff at the finer spatial scales. Supplemental baseflow decreases with decreasing time scale and is more sensitive at the finer spatial scales analyzed. Total channel inflow also increases when changing from a 6-hour to a 1-hour time step and is more sensitive at the finer spatial scales.

The results shown in Figure 2-6 are primarily attributed to the temporal averaging of high-intensity, short-duration precipitation events which tend to produce surface runoff. This temporal sensitivity of the SAC-SMA runoff volumes could suggest that the hydrologic processes in the region are operating at a finer time scale than 6 hours. The temporal information contained in the 1-hour Stage III products may possibly be used to improve hydrologic forecasting. Moreover, the temporal analysis indicates that the parameters calibrated at the 6-hour time step cannot be applied at the 1-hour time step without introducing the volume biases shown in Figure 2-6. Changing the model time scale and keeping the model parameters fixed redistributes runoff between the rising limb (surface) and the falling limb (interflow) of the runoff hydrograph, as well as between near surface and groundwater runoff components. These runoff volume biases are particularly important because they are most significant in the fast response surface runoff and interflow components of the hydrograph, which are the most critical model elements in flood forecasting. In general, the results displayed in Figures 2-5 and 2-6 indicate that the utilization of finer space-time scale precipitation estimates, without parameter adjustments, introduces SAC-SMA runoff volume and timing errors. These runoff volume and timing errors could potentially result in degradation of the predictive ability of the model if used at finer time scales.

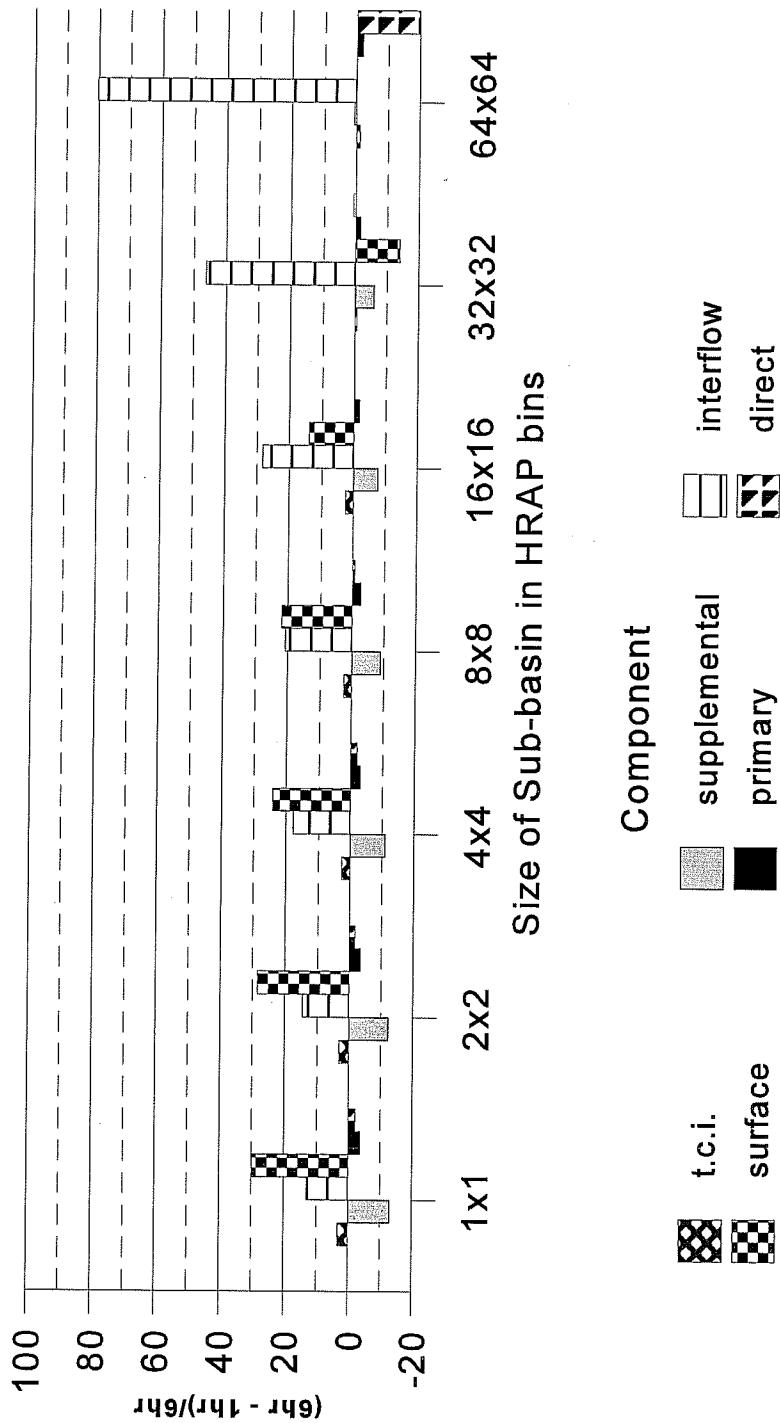Figure 2-6   Percent change in runoff component due to change in time step 6 hour to 1 hour at same basin scale with no change in SAC-SMA parameters. Example: At 8x8 sub basin scale, going from 6 hour calibration time step to a 1 hour OFS time step (using Nexrad) would result in 21%increase in surface flow, 20% increase in interflow, and a 9 % decrease in supplemental base flow. Total channel inflow (TCI) would increase about 3%.

2.4.3 Adjustment of Parameters for Space-Time Scales

One possible method for applying SAC-SMA model parameters at different space-time scales is to make adjustments to parameters in order to minimize the biases created by changing the precipitation intensity (precipitation depth/event duration) across space-time scales. The previous section established that surface runoff is the most sensitive runoff component to space-time scales. The following sections analyze the sensitivity of the runoff components to changes in the upper zone free water maximum (UZFWM) and upper zone tension water maximum (UZTWM) threshold parameters which are known to dominate the generation of surface runoff in the SAC-SMA model. Almost every parameter in the SAC-SMA model could potentially effect surface runoff but they were not analyzed in this work. Caution should be exercised because UZFWM and UZTWM also control interflow, percolation, supplemental baseflow and evapotranspiration components of the SAC-SMA model. Percolation changes have an impact on lower zone free and tension water storages, which directly affect supplemental and primary baseflow recharge and evapotranspiration.

Obled et al. (1994) disaggregated a lumped basin into 9 constituent sub-basins and recalibrated the parameters of their semi-distributed hydrologic model using 9 distinct runoff events over a 16 year period to account for the higher resolution rainfall input fields. However, the 9 months of Stage III data available for the present study are not sufficient for a recalibration of the SAC-SMA parameters, as continuous simulation over an 8 year period is recommended to obtain parameters that are insensitive to the data period selected (U. of Arizona, 1995). Until a sufficient length of record of data is available to calibrate the SAC-SMA model for various space-time scales using Stage III precipitation inputs, alternative approaches to adjusting model parameters need to be developed.

2.4.3.1 Upper Zone Free Water Parameter

The separation of fast responding surface runoff and interflow from the slow response baseflow runoff is primarily controlled by the upper zone free water maximum parameter (UZFWM). Bae and Georgakakos (1994) identify this parameter as the most sensitive when examining high flows, where lowering the parameter value has more influence than increasing the value. Their results indicate that the influence of UZFWM is reduced when both high and low flows are considered.

An analysis of upper zone processes is performed by changing the relative size of the upper zone free water maximum parameter. The UZFWM value of 18 mm was taken from a preliminary calibration and trial runs are made at 50% increases and decreases, 27 mm and 9 mm respectively. Figure 2-7 illustrates that the UZFWM parameter derived at one scale is not applicable across different scales because surface runoff volumes are not preserved. Figure 2-7 shows that UZFWM must be increased when modeling at finer space or time scales in order to accommodate the higher intensity precipitation events and preserve surface runoff volumes. This affect is more pronounced when the UZFWM parameter is small, which is in agreement with Bae and Georgakakos (1994). The figure also shows that surface runoff is sensitive to UZFWM at both the 1-hour and 6-hour
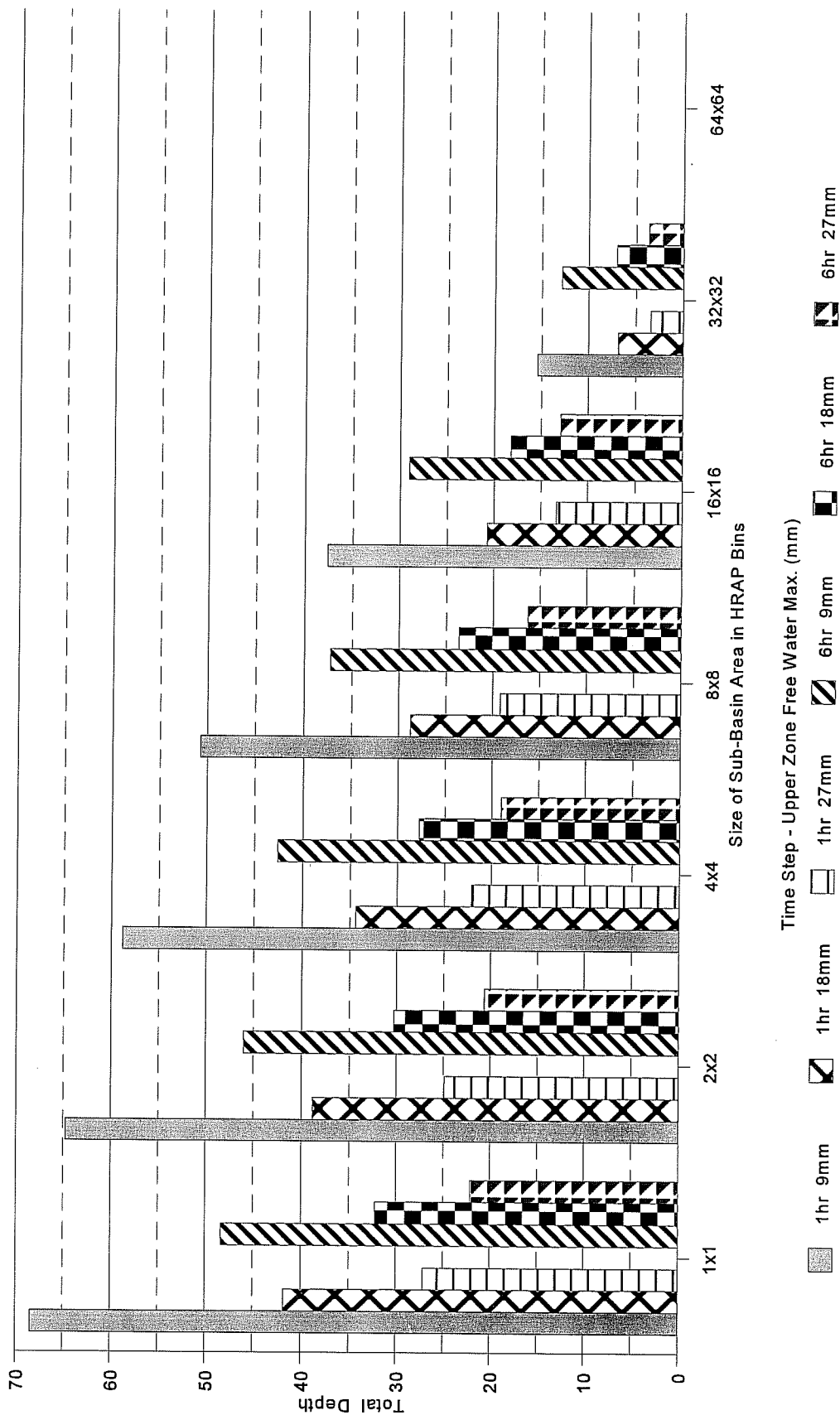
Figure 2-7. Variation of surface runoff depth versus sub-basin size for Calibration time step of 6 hours and OFS time step of 1 hour. Total depths are for 9 month simulation. 3 values of Upper Zone Free Water Max were used to investigate how to adjust parameters (re-calibrate) when moving from a lumped 6 hour calibration to semi distributed segment definition at 1 hour time step. Calibrated UZFWM is 18mm. Example: A basin at the 8X8 scale (32km by 32km) is calibrated on a lumped basis at 6 hour time step. For OFS, basin is divided into 4 subasins (4x4 scale) and 1 hour time step is used. To preserve the same volume of surface runoff (24 mm), the calibrated value of UZFWM must be adjusted to around 23 mm.

model time steps. Consider an example illustrated in Figure 2-7 in which a basin at the 8x8 HRAP bin scale is calibrated at a 6-hour time step. If one chooses to disaggregate the basin into 4 sub-basins (i.e., a move to the 4x4 scale) the UZFWM must be increased from 18 mm to approximately 27 mm in order to preserve the same volume of surface runoff.

Secondary effects of UZFWM adjustments are presented in Figures 2-8, 2-9, and 2-10. Figure 2-8 shows that interflow is very sensitive to changes in UZFWM for all spatial scales analyzed, and at both the 1-hour and 6-hour time steps. Increasing UZFWM increases interflow at all spatial scales, which is the opposite effect that the parameter change has on surface runoff. Figures 2-7 and 2-8 clearly illustrate how the UZFWM parameter controls the contribution of runoff from surface (rising limb of hydrograph) or interflow (falling limb) because an increase in surface runoff results in a decrease in interflow. Changing UZFWM has a wide range of impacts on percolation across the numerous space-time scales presented in Figure 2-9. UZFWM affects both the volume of water available for percolation and the rate of percolation in the SAC-SMA model. The results in Figure 2-9 show no clear relationship between scale, UZFWM, and percolation, which indicates a more in-depth percolation analysis is required. Figure 2-10 shows that supplemental baseflow is sensitive to the UZFWM parameter across all space-time scales analyzed and in much the same way the parameter affects percolation. This model behavior is expected because soil water percolates from the upper zone free water reservoir down to the lower zone soil moisture reservoirs, one of which is the lower zone free supplemental baseflow reservoir.

Adjustment of the SAC-SMA model UZFWM parameter is shown to be capable of compensating for biases created from applying the model at space-time scales different from which it is calibrated. However, adjusting the UZFWM parameter also has a significant and opposite effect on interflow, and a wide range of effects on percolation and supplemental baseflow. These complex interactions effect the timing, volume, and shape of the resulting runoff hydrograph. Thus, adjusting UZFWM effects the exchange of water between fast and slow response runoff as well as between the upper and lower zone soil moisture. Figures 2-7, 2-8, 2-9, and 2-10 demonstrate the complex problems inherent to recalibrating model parameters when distributing them spatially and temporally.

2.4.3.2 Upper Zone Tension Water Parameter

Upper zone tension water maximum storage capacity (UZTWM) must be satisfied in the SAC-SMA model before precipitation enters the upper zone free water storage where interflow and percolation take place. The tension water storage also controls evapotranspiration, which accounts for 77% of the losses in the water balance for the 9 month simulation period. Therefore, UZTWM also controls runoff generation in the SAC-SMA model in much the same way the UZFWM parameter does, and may also be recalibrated to account for runoff volume biases caused from
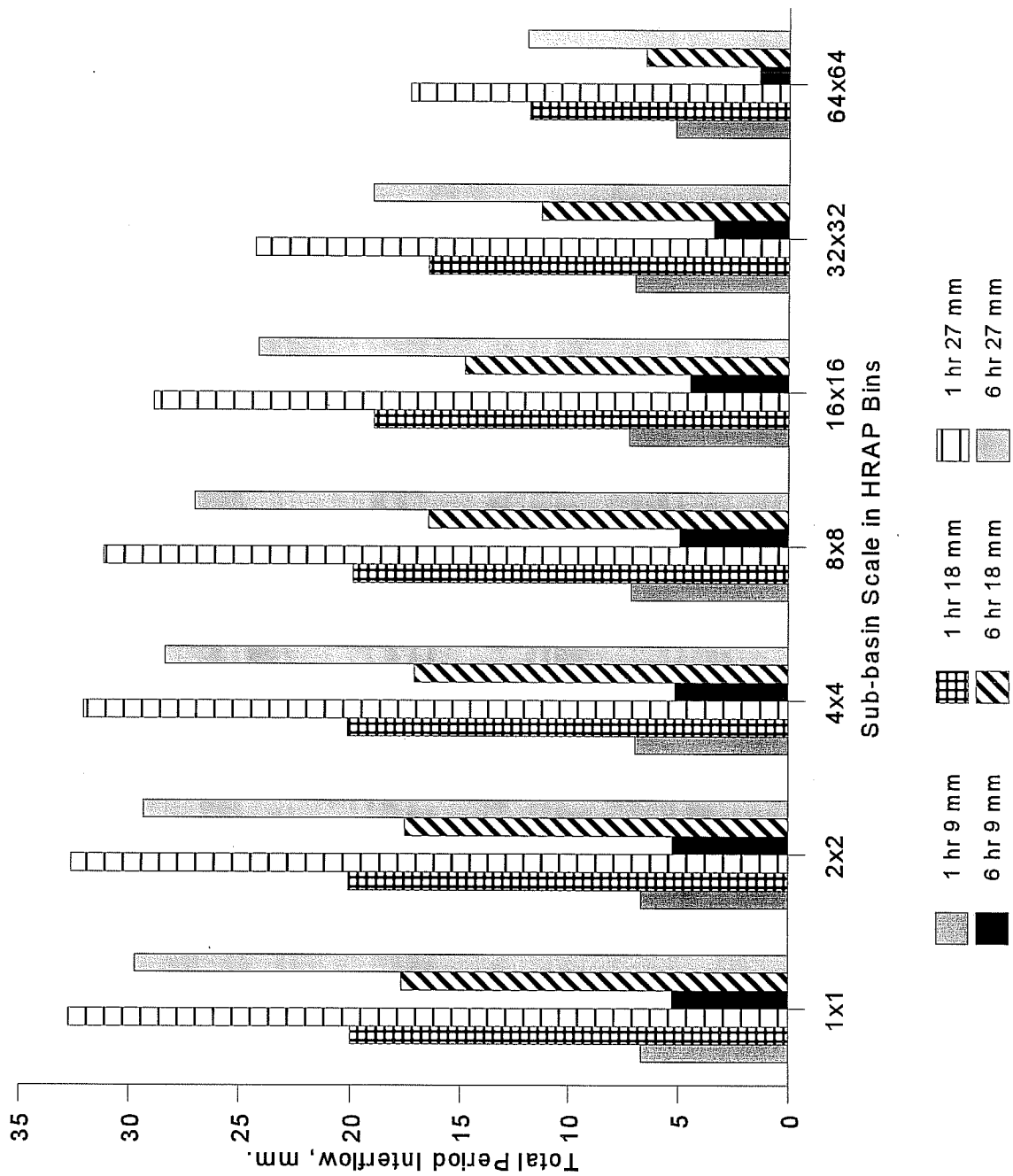
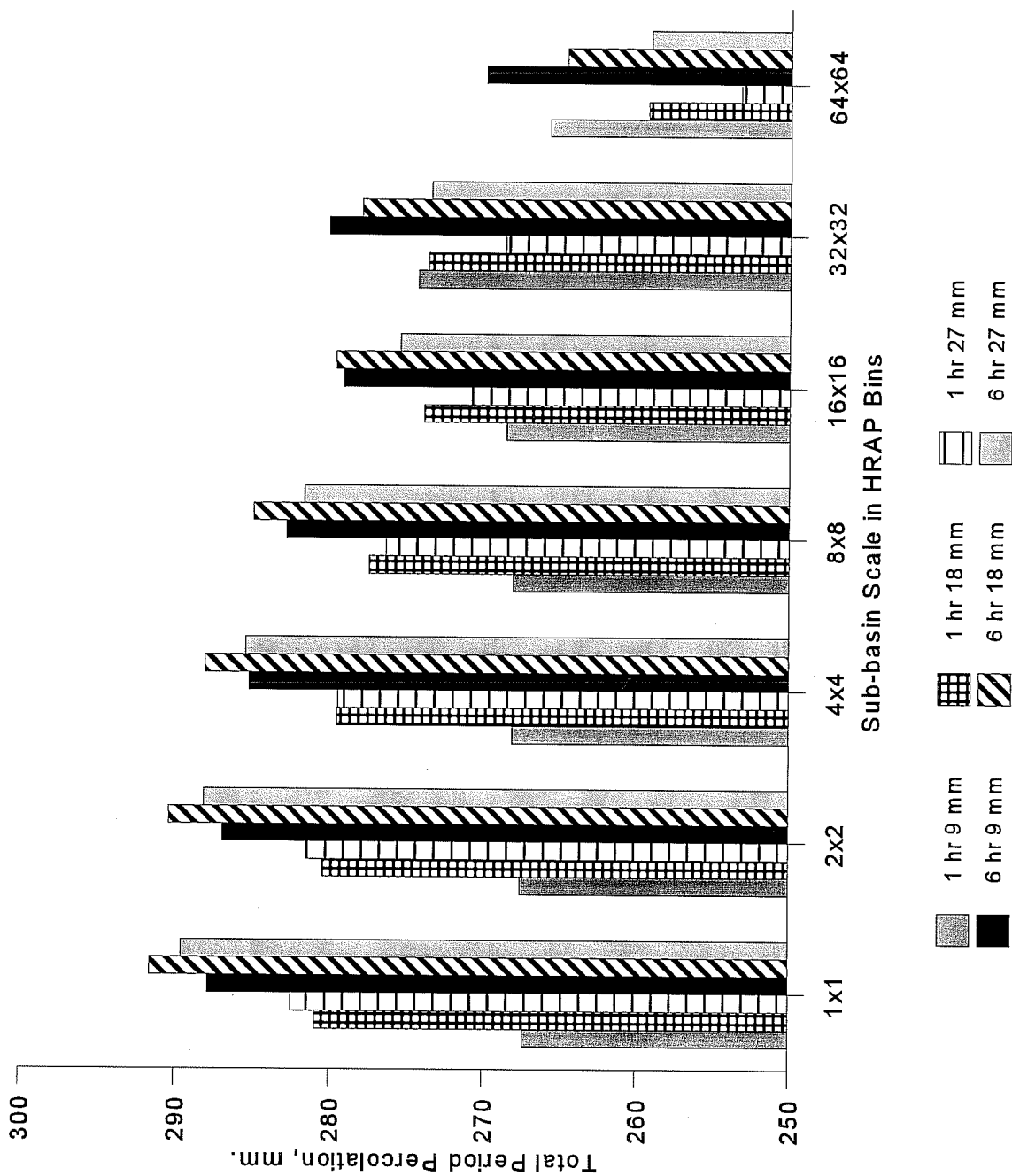Figure 2-8 Sensitivity of Interflow Generation to Sub-basin Scale and UZFWM for Two Time Steps

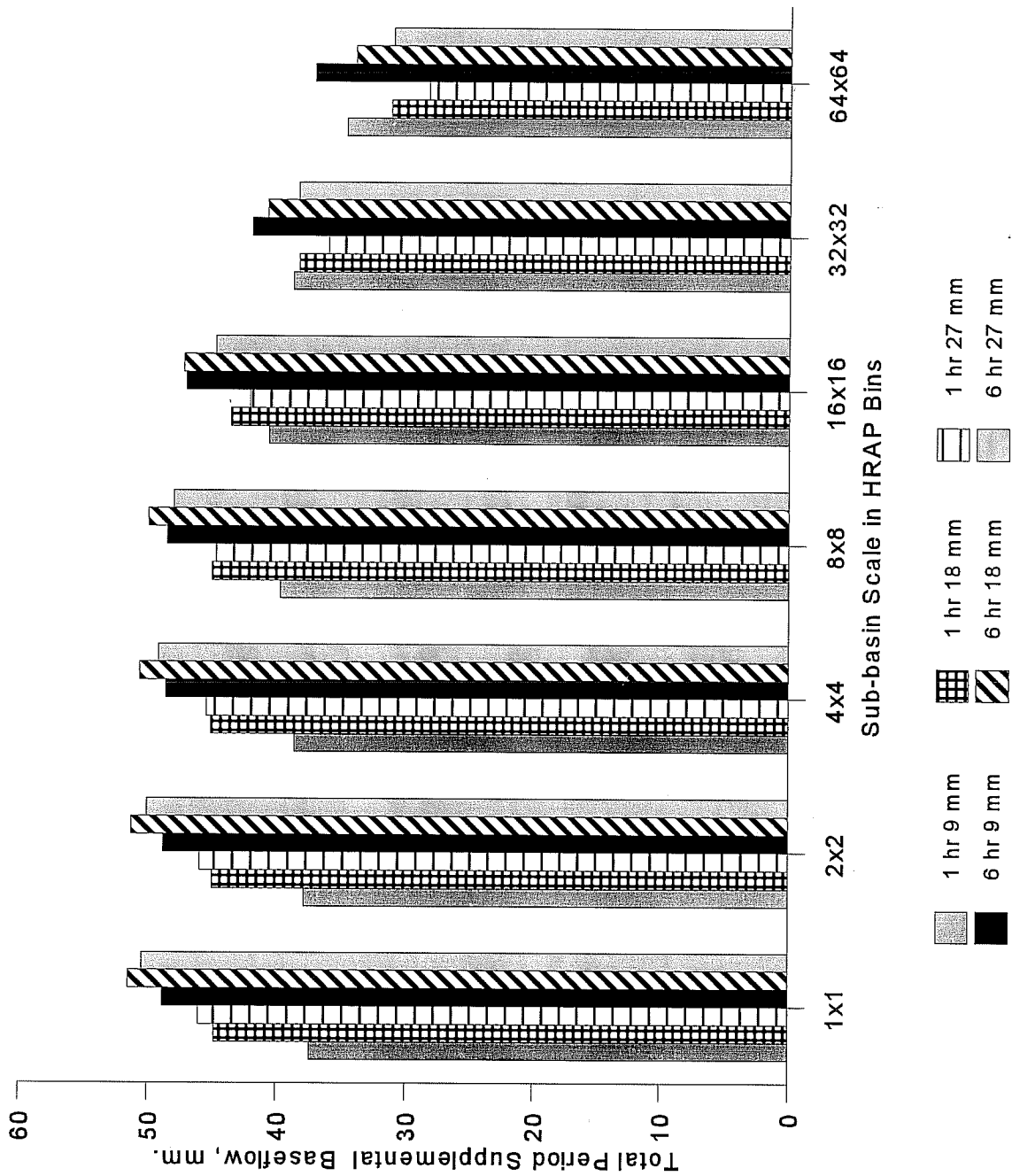Figure 2-9 Sensitivity of Percolation to Sub-basin Scale and UZFWM for Two Time Steps

Figure 2-10 Sensitivity of Supplemental Baseflow Generation to Sub-basin Scale and UZFWM for Two Time Steps

applying model parameters across different space-time scales. The UZTWM parameter is calibrated at 40 mm for the test basin and trials are run for values of 20 mm, 40 mm, 60 mm, and 80 mm.

Figure 2-11 shows that increasing UZTWM decreases surface runoff for all space-time scales analyzed. However, the effects of UZTWM on surface runoff also exhibit the complex interaction with interflow, percolation, and supplemental baseflow, just as the UZFWM parameter does in Figures 2-7, 2-8, 2-9, and 2-10. Surface runoff is more sensitive to the UZFWM parameter than the UZTWM parameter, but either may be used to adjust surface runoff volumes at all space-time scales analyzed.

Figure 2-12 shows that evapotranspiration, ET, is sensitive to recalibration of the UZTWM parameter for all space time scales analyzed. In general, ET is maximized at the calibrated UZTWM value of 40mm and ET decreases as the parameter is either increased or decreased. ET is shown to increase as the sub-basin spatial scale increases and when changing from the 1-hour to 6-hour time step. Both observations are related to more precipitation residing in tension water storage as opposed to becoming runoff. Although a clear trend of ET as a function of UZTWM is not present in Figure 2-12, the effect of space-time scales on ET is of the same order of magnitude as the changes in the other most sensitive SAC-SMA model components. In fact, any increases in ET are balanced by decreases in total channel inflow across all space-time scales. This result strongly suggests a more in-depth study of scale impacts on ET and the long-term soil water balance is required. Figures 2-11 and 2-12 further illustrate that SAC-SMA model parameter adjustments can correct for certain biases created from applying the model at space-time scales for which the parameters are not calibrated. However, changing model parameters causes a complex and poorly understood redistribution of water between the various runoff components in the model which results in new volume and timing biases in both the short-term storm runoff and the long-term water balance.

2.5 Comparison of the SAC-SMA sensitivity to other conceptual models

The previous sections showed that the SAC-SMA model runoff components were sensitive to spatial scales of the Stage III precipitation inputs., To understand how the scale dependency relates to the model structure, and if the SAC-SMA model is an unique case of scale dependency, a similar analysis was performed with a few other conceptual models.

2.5.1. Model scale examples

Historically, less emphasis has been placed on the scale dependency inherent to the rainfall-runoff model as opposed to the scale of rainfall. Analysis of the spatial variability of rainfall can give a qualitative sense of this scale dependency such as the Representative Elemental Area (REA) concept, however, quantitative measures of physical scale is highly model dependent. For example,
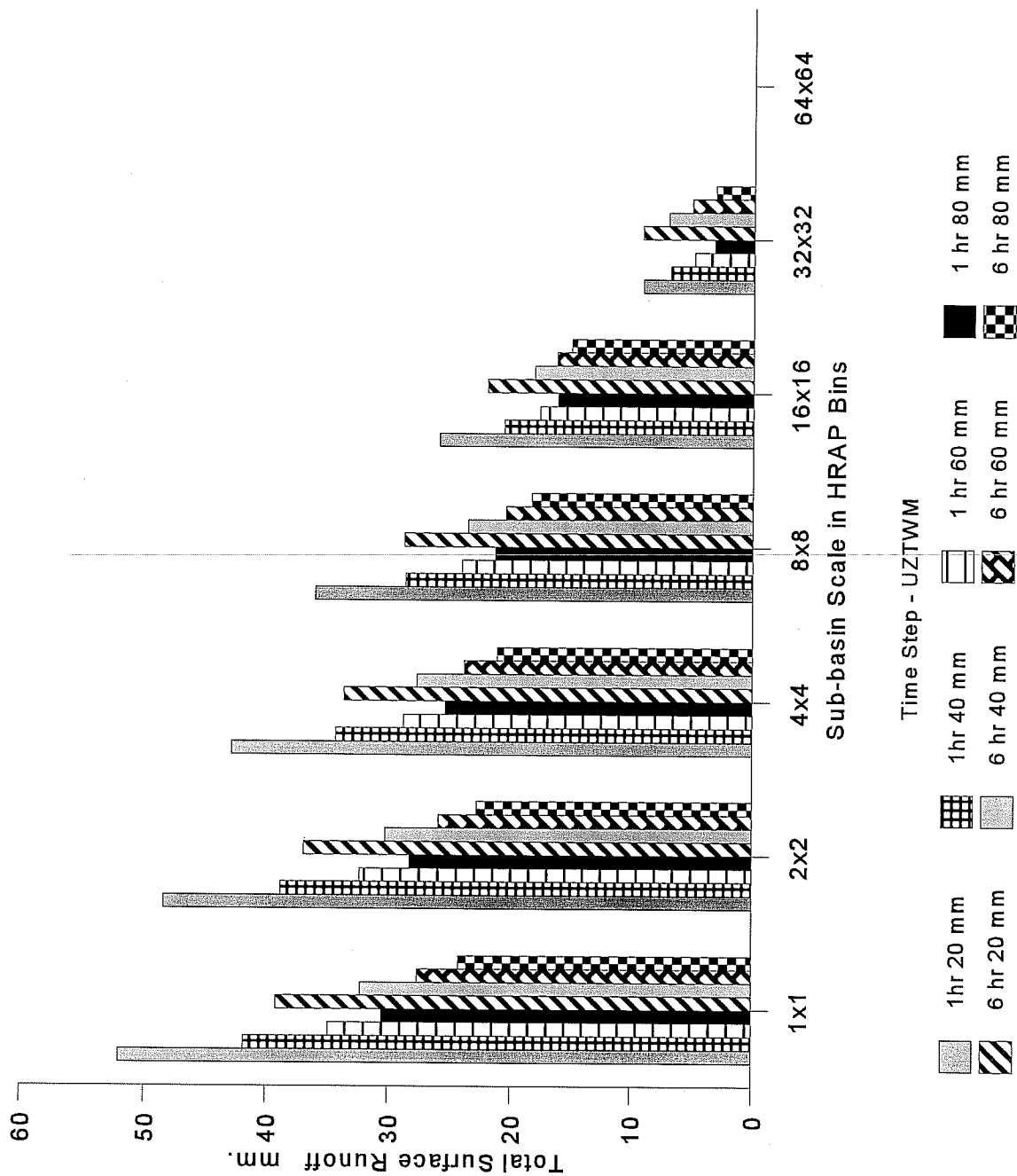
Figure 2-11 Sensitivity of Surface Runoff to Sub-basin Scale and UZTWM for Two Time Steps
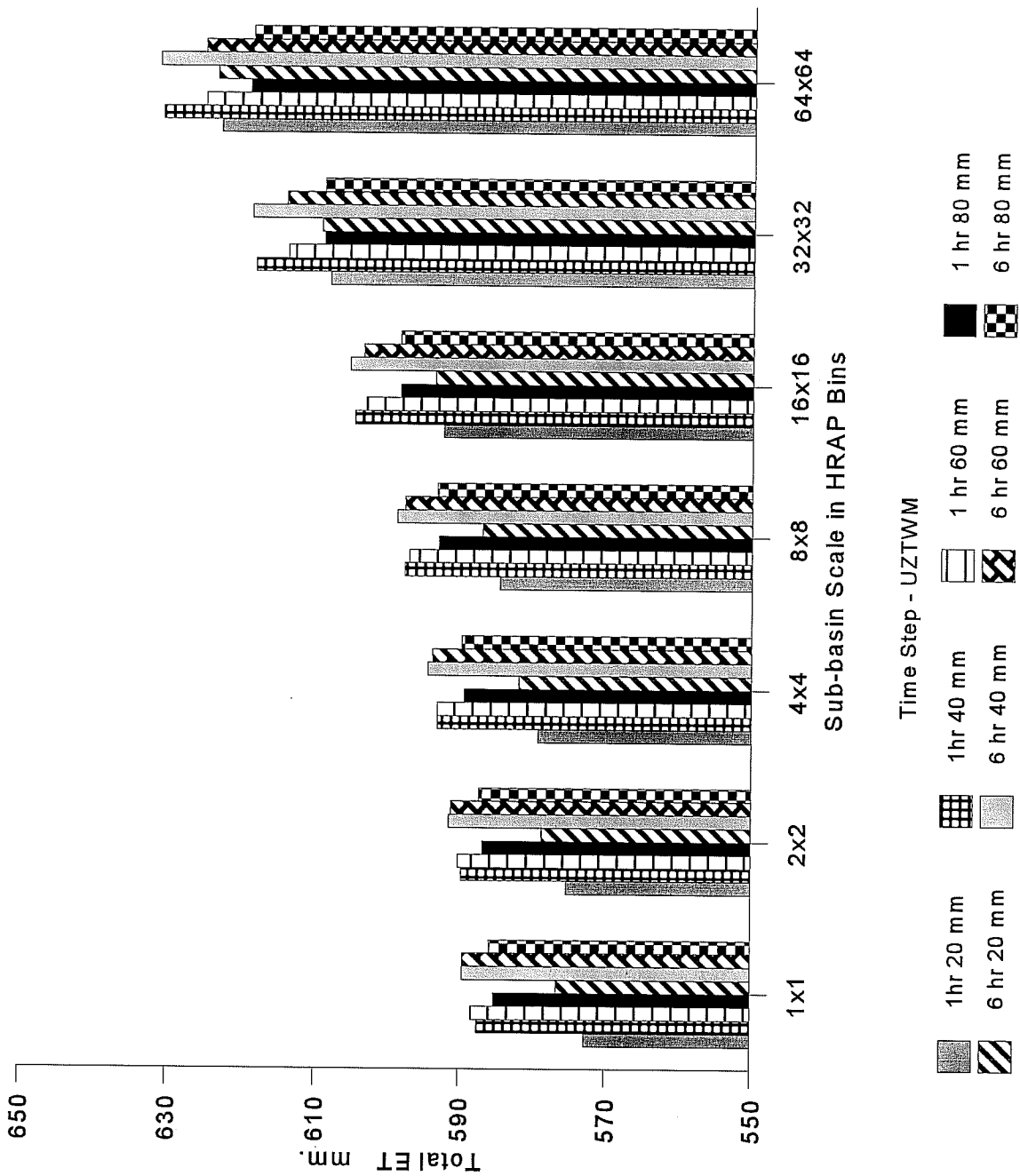
Figure 2-12 Sensitivity of ET to Sub-basin Scale and UZTWM for Two Time Steps

2.26

the linear rainfall-runoff relationship in Equation 2-1 is not sensitive to the spatial variability of rainfall given that the spatial averages of rainfall preserve the total volume of precipitation.

$$\overline{R}_A^{(k)} = \alpha(t)\overline{P}_A \qquad (2\text{-}1)$$

where $\overline{R}_A^{(k)}$ is runoff averaged over an area A using scale k estimates of runoff, $\overline{P}_A$ is a mean areal rainfall, and $\alpha(t)$ is the scale independent parameter for the rainfall-runoff relationship.

The rainfall-runoff model, however, becomes scale dependent if, for example, its parameter is a linear function of the rainfall rate:

$$R_i = \beta(t)P_i, \; P_i = \beta(t)P_i^2 \qquad (2\text{-}2)$$

Runoff from an area A (say, a river basin) can be aggregated from runoffs simulated at a finer scale, R_i,

$$\overline{R}_A^{(k)} = \frac{1}{N_k}\sum_{i=1}^{N_k} R_i^{(k)} \qquad (2\text{-}3)$$

where N_k is a number of k-scale elements in the area A. Combination of Equations 2-2 and 2-3 leads to

$$\overline{R}_A^{(k)} = \beta^{(k)}(t)\frac{1}{N_k}\sum_{i=1}^{N_k}(P_i^{(k)})^2 = \beta^{(k)}(t)[(\sigma^{(k)})^2 + (\overline{P}^{(k)})^2] \qquad (2\text{-}4)$$

where $\sigma^{(k)}$ is the spatial standard deviation of rainfall averaged over scale k, and $\overline{P}^{(k)}$ is the mean value of k-scale rainfall that is equal to the rainfall averaged over an entire area, $\overline{P}_A$. For a scale independent unbiased model the right sides of Equation 2-4 should be equal at any scale less than the area A. It leads to a relationship between the model parameter $\beta^{(k)}(t)$ at different scales. Simple equation can be drawn after substituting a coefficient of rainfall variation, $C_v^{(k)}$, instead of a standard deviation

$$\beta^{(k+n)}(t) = \beta^{(k)}(t)\frac{1 + (C_v^{(k)})^2}{1 + (C_v^{(k+n)})^2} \qquad (2\text{-}5)$$

Equation 2-5 shows how to preserve a constant average runoff over an area A by adjusting the model parameter $\beta^{(k)}(t)$. The adjustment depends on differences of rainfall variability at different

2.27

scales. The results of an analysis of 3 years of high resolution (4x4 km) radar precipitation estimates over a 256x256 km region in the southern plains of the United States shows that the coefficient of spatial variation of precipitation differs significantly at different averaging scales. As a result, the model parameter $\beta^{(k)}(t)$ will vary greatly from scale to scale. Figure 2-13 plots the ratio of $\beta^{(k)}(t)/\beta^{(0)}(t)$ versus $L^{(k)}/L^{(0)}$ where $L^{(0)}$ is the finest resolution of the radar estimates (4x4 km), $L^{(k)}$ is the k-scale, $\beta^{(0)}$ is the coefficient at the finest resolution, and $\beta^{(k)}$ is the coefficient at the k-scale. Figure 2-13 clearly illustrates that the coefficient in Equation 2-2 changes significantly from scale to scale.
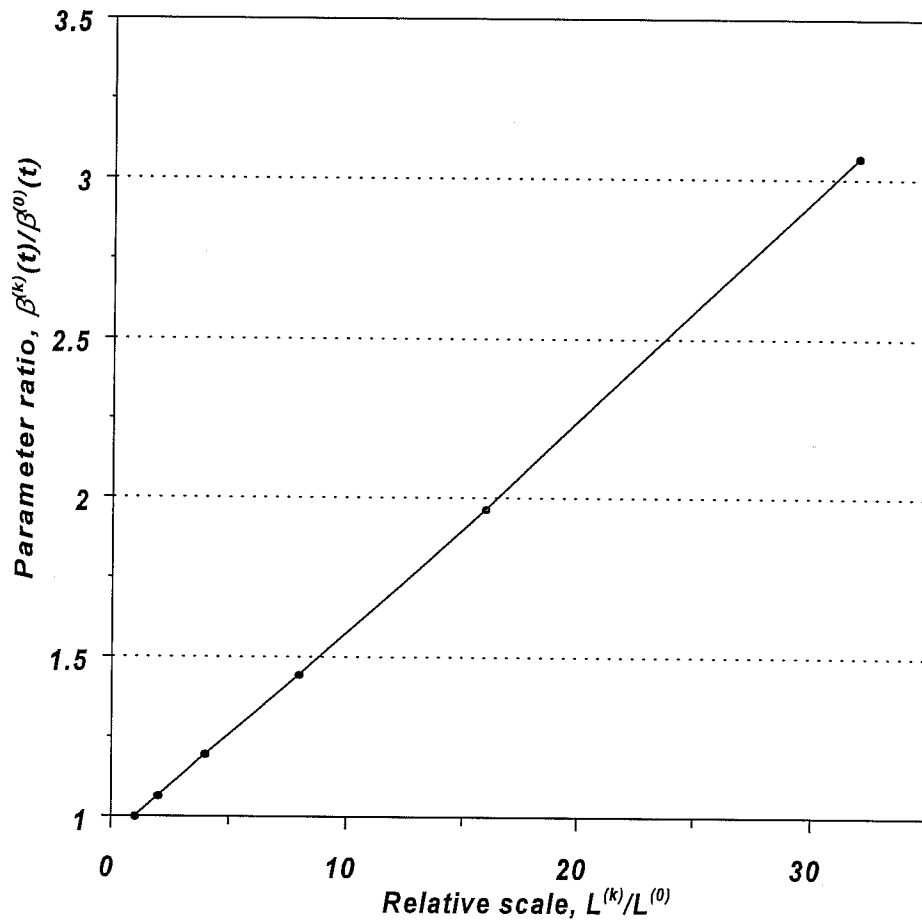
Figure 2-13. Scale dependency of a point type rainfall runoff model parameter, $\beta^{(k)}(t)$, which is constant for a given scale, k, and varies accross scales as a function of rainfall variability

2.5.2 Hydrologic models analyzed

This study is focused on comparative analyses of scale dependency of lumped hydrological models with different formulations of the infiltration processes. Three lumped hydrological models of differing complexity were used in the study: the SAC-SMA model, the Oregon State University (OSU) multi layer model (Mahrt and Pan, 1984), and the Simple Water Balance (SWB) model (Schaake et al., 1996). The first two models are typical point models that do not account for the spatial variability within the basin. The SWB model implicitly accounts for the spatial variability in precipitation data and model states. A fourth model, a reformulated version of the SAC-SMA model which accounts for the spatial variability of rainfall, was also analyzed.

2.5.2.1 The OSU Model.

The OSU model was used as the land surface hydrologic parameterization in the Oregon State University one-dimensional planetary boundary layer model (Ek and Mahrt, 1991). The model is based on the finite difference solution of the one-dimensional Richards' equation (Dingman, 1993) in the multi-layer vertical soil column. The Richards' equation is a physically based infiltration model derived from Darcy's law under the assumption of an isotropic, homogeneous soil column. Surface runoff is calculated under the assumption of the Hortonian, infiltration-excess, type of rainfall-runoff partitioning,

$$R_s = \max\{(P - I_{\max}), 0\} \tag{2-6}$$

A maximum infiltration rate, I_{max}, is estimated based on the water flux at the soil surface:

$$I_{\max} = D(\Theta_s) \frac{\Theta_s - \Theta_1}{\Delta z} + K(\Theta_s) \tag{2-7}$$

where $D(\Theta_s)$ and $K(\Theta_s)$ are the soil water diffusivity and conductivity under conditions of saturation, Θ_s, Δz is the upper layer thickness, and Θ_1 is the water content of the upper soil layer, usually 5-10 cm. Two to ten layer versions of the model were used in the analyses.

The OSU model explicitly accounts for the effect of vegetation on evapotranspiration by the inclusion of the canopy resistance scheme. However, it does not account for the effect of spatial variability in hydrologic variables. Most of the parameters in the OSU model are usually derived using the soil and vegetation classification information (Chen et al., 1996). However, a few parameters have to be adjusted if the model is applied to a specific river basin.

2.5.2.2 The SWB Model.

The Simple Water Balance model (SWB) has a two-layer structure with both a physical and statistical basis for the model parameters (Schaake et al., 1996). A thin upper layer consists of the vegetation canopy and the soil surface. A lower layer includes both the root zone of the vegetation and the ground water system. Capacities of each layer are model parameters. The supply of water to the lower zone is the excess of precipitation from the upper layer, P_{excess}. This water is available for partitioning into surface runoff and infiltration into the lower layer. The surface runoff equation was derived based on probabilistic averaging of the point infiltration-excess equation, assuming

$$R_s = \frac{P_{excess}^2}{P_{excess} + D_{LZ}(1 - e^{-K_{dt}\,dt})} \qquad (2\text{-}8)$$

exponential distribution functions of precipitation and soil moisture capacity,

where D_{LZ} is a water deficit of the lower zone, dt is the simulation time step, and K_{dt} is a model parameter that accounts for the temporal scale. The model has five parameters which are calibrated using historical data.

2.5.2.3 Reformulated Sacramento Model.

The SAC-SMA model was reformulated in order to account for the spatial variability of rainfall. The reformulated Sacramento model (REF-SAC) replaces actual patterns of rainfall at the river basin scale with a distribution function of rainfall. Mean areal excess rainfall can be estimated assuming that Equation 2-6 applies at any point in a basin, the upper zone tension water deficit is uniformly distributed over the basin, and only rainfall is spatially variable,

$$\overline{P}_{excess} = \int_{\overline{D}_{UZTW}}^{\infty} A(P - \overline{D}_{UZTW}) f(P) dP \qquad (2\text{-}9)$$

where $f(P)$ is a distribution function of rainfall. Figure 2-14 graphically shows the meaning of the reformulation where the SAC-SMA produces zero excess rainfall and therefore zero surface runoff, if the mean areal rainfall of 29 mm is less than the upper zone tension water deficit of 41 mm. However, the reformulated version produces some amount of excess rainfall (shaded area in Figure 2-14) depending on the distribution function of rainfall. The same assumptions were used to estimate mean areal surface runoff from Equation 2-7 with an additional assumption that point excess rainfall has the same distribution function as rainfall.
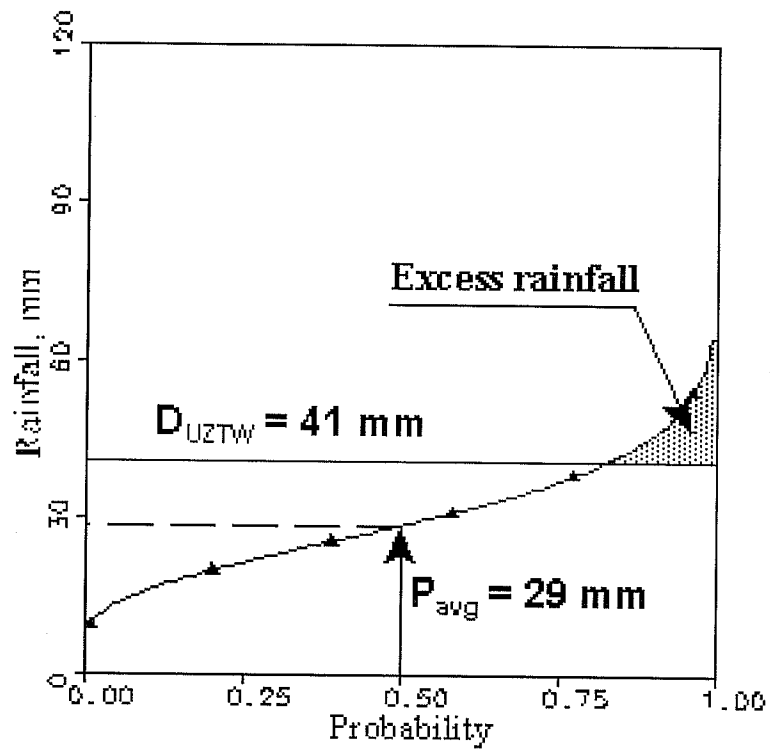
Figure 2-14. Probabilistic averaging of excess rainfall
using a distribution function of rainfall, where P_{avg} and the
distribution function are evaluated at every time step

To apply the REF-SAC model, a spatial distribution function of rainfall must be estimated at each time step where SWB model assumes the distribution function to be constant in time. High resolution radar data provides the best available information about the spatial distribution of rainfall which allows the precipitation distribution function to be estimated at every time step. This approach is impossible to apply using only conventional land based rain gage networks because the spatial structure of the precipitation over headwater basins is not adequately sampled by gage networks. An analysis of the spatial variability of hourly Stage 3 precipitation grids indicates that a gamma distribution can be used as an approximation to the empirical distribution (Koren, 1993; Schaake et al., 1996),

$$f(P) = \frac{\lambda^v}{\Gamma(v)} P^{v-1} e^{-\lambda P}$$

(2-10)

where λ and v are the distribution function parameters which can be estimated using mean areal precipitation and coefficient of variation, $C_{v,P}$. The distribution function parameters were estimated for each time step using only the radar bins with measured rain within the simulation area. Simulated excess rainfall and surface runoff were multiplied by the percentage of the rainy area to get average values over an entire basin area.

2.5.3 Results and discussion

2.5.3.1 Comparison of different model results.

Runoff components generated by each model (a ten layer version if the OSU model was used in this test) were cumulated for the entire period and averaged over the test area, 256x256 km. Figure 2-15 is a plot of the relative change in the surface runoff volume simulated by the different models over the 3 year period as a function of the grid scale. Surface runoff changes at each grid scale are defined as the difference between the total cumulated surface runoff at that scale and the total cumulated surface runoff at the finest scale (4x4 km). These changes have been scaled relative to the total cumulated surface runoff generated at the finest scale.

Table 2-2. Averaged hourly values of rainy area fraction and coefficient of rainfall variation at different grid scales

Scale, km^2	4x4	8x8	16x16	32x32	64x64	128x128	256x256
Coefficient of variation	2.07	1.99	1.85	1.63	1.30	0.85	0.00
Covered area, %	100	98	95	89	79	64	45

2.33

Figure 2-15 shows that each model produced less surface runoff with increasing scale size. Surface runoff is gradually reduced within the range of 20% till the scale of 32x32 km. At scales greater than 32x32 km there is a faster reduction in surface runoff with a wide range of variability from one model to the other. The main factor governing runoff reduction at the smaller scales is rainfall variability over a rainfall averaging area. At the larger scales, the rainfall coverage becomes the major factor controlling runoff reduction. As seen in Table 2-2, area covered by rain was less than 50% at the largest scale. The rainy area fraction in the table was weighted by the rain rate, while averaging for the total test period. The coefficient of rainfall variation at the larger scales were about two times less than the coefficient at the finer scales.

The scale dependency of simulated surface runoff is inherent in the model structure due to the model's method of partitioning rainfall into runoff and losses. The OSU model is the most scale dependent with surface runoff reduction close to 100% at the largest scale. The reason for this is that surface runoff in the OSU model is generated by excess rainfall above the soil moisture flux on the soil surface, which is estimated as a ratio of the soil moisture gradient, as shown in Equation 2-9. Excess rainfall can vary significantly over an area depending on the rainfall rates which differ significantly across scales. The SAC-SMA model showed much less scale dependency than the OSU model. The surface runoff calculation in the SAC-SMA model is a saturation-excess type. There will not be any surface runoff (excluding a small amount of runoff from impermeable areas) generated prior to the fill-up of the tension and free water storages of the upper zone. The rainfall rate will not affect surface runoff during the first phase of runoff when initial rainfall losses are generated. This will reduce scale dependency of the total flood runoff simulated by the SAC-SMA model on the rainfall rate compared to the OSU model.

As expected, the SWB model was less scale dependent then the SAC-SMA and OSU models because its infiltration equation implicitly accounts for the spatial variability of rainfall. However, reduction of surface runoff at the larger scales exceeded 30%. One of the reason for this reduction at the larger scales was that the areas covered by rain were significantly reduced at the 128x128 km and 256x256 km scales, 0.64 and 0.45 respectively. Where as Table 2-1 shows, the finer 4x4 km and 8x8 km scales have 1.0 and 0.98 covered areas respectively. The SWB model assumes that rain covers the entire area and this assumption is clearly violated at the larger spatial scales.

The reformulated SAC-SMA model was found to be the least sensitive to grid scale. At the largest scale of 256x256 km the model underestimated surface runoff by about 20% compared to 60% by the original SAC-SMA model. Because the spatial distribution of rainfall and rain coverage were estimated at each time step, the reformulated SAC-SMA model produced more reasonable results over a wide range of spatial scales.

As seen in Figure 2-16, all models showed much less scale dependency in total runoff. Total runoff was calculated as a sum of surface and groundwater flows for the OSU and SWB models, and as a sum of six runoff components: surface, interflow, primary and supplemental baseflow, permanent and variable impermeable area flow, for the SAC-SMA model. The total runoff reduction was about three times less than the surface runoff reduction. The models ranking
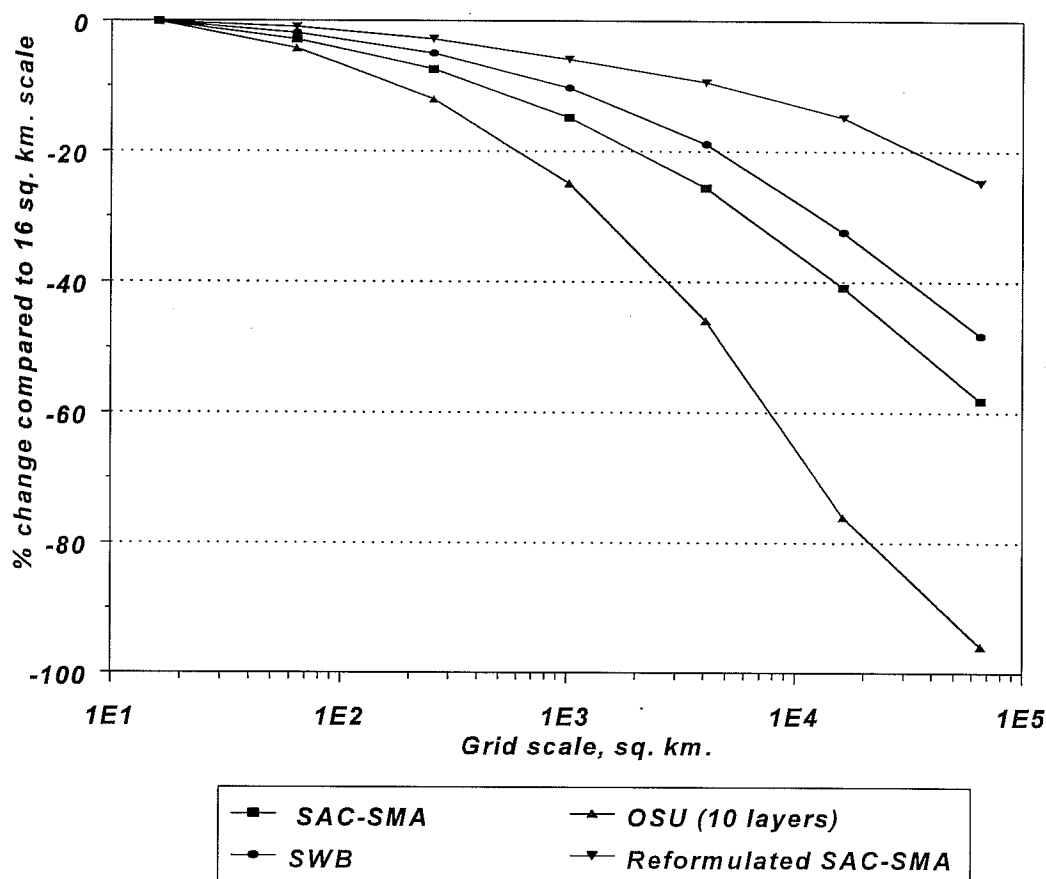
Figure 2-15. Scale dependency of surface runoff, simulated by different models, and expressed in percent change in surface runoff as compared to the finest scale value. Statistics are aggregated for all synthetic sub-basins in the test area continuously over 3.5 year period

based on the scale dependency of total runoff were close to that based on the surface runoff dependency order: the OSU model was the most scale dependent, and the reformulated SAC-SMA model was the least scale dependent. The only difference was that the SAC-SMA model became a little less scale dependent than the SWB model. There is less scale dependency in the total runoff because surface and subsurface components usually change in opposite directions as the scale increases. That is, the surface runoff decreases at the larger scales while the subsurface

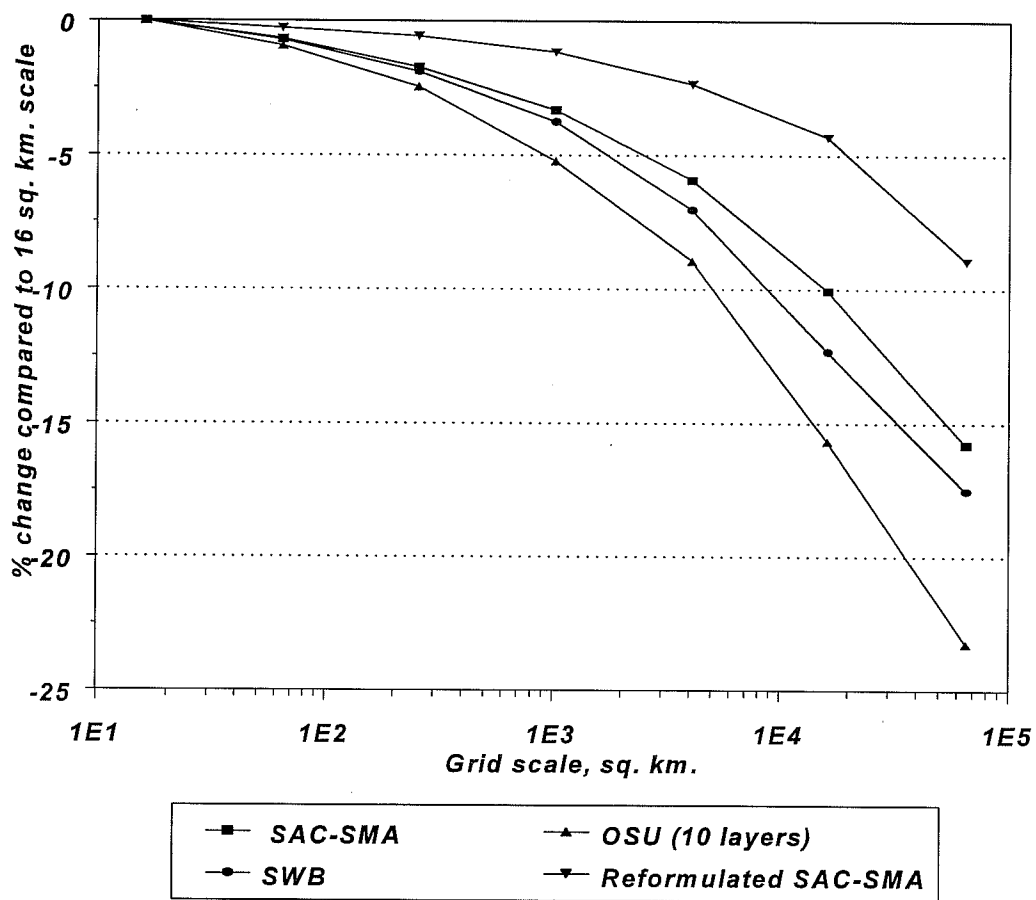Figure 2-16. Scale dependency of total runoff simulated by different models. Total runoff is less sensitive to scale than surface runoff shown in Figure 2-15.

component increases. The SAC-SMA model multi-interaction between runoff components reduces the effect of the surface runoff scale dependency in the total runoff significantly.

2.5.3.2 Rainfall-runoff partitioning in the SAC-SMA model.

The importance of the rainfall-runoff partitioning mechanism was seen during flood events. Figure 2-17a is a plot of the runoff coefficient during a specific flood event, April 12, 1994, simulated using total channel inflow from the SAC-SMA model outputs at different grid scales. The runoff coefficient is defined as the ratio of accumulated runoff to accumulated precipitation, for a given time interval. At the beginning of the flood, when initial losses are satisfied, the runoff coefficient is rather stable and does not vary much from scale to scale. Once initial losses have been satisfied, the runoff coefficient varies significantly over different scales with the highest values at the finest scale. Most of the rainfall during the storm was stored in the soil at the 128x128 km scale, and the runoff coefficient was close to zero during the entire flood event. As a result, soil moisture content increased during the flood and was the greatest for the lowest resolution as shown in Figure 2-17b.

The reformulated SAC-SMA model showed less scale dependency in rainfall-runoff partitioning. The range of the runoff coefficient variability across scales was narrower during the same flood event, as shown in Figure 2-18a. The 128x128 km scale has a higher runoff coefficient at the beginning of the flood event because of different soil moisture states from the continuous run. Soil moisture content at the end of the flood was close for all grid scales, as shown in Figure 2-18b.

2.37

a)
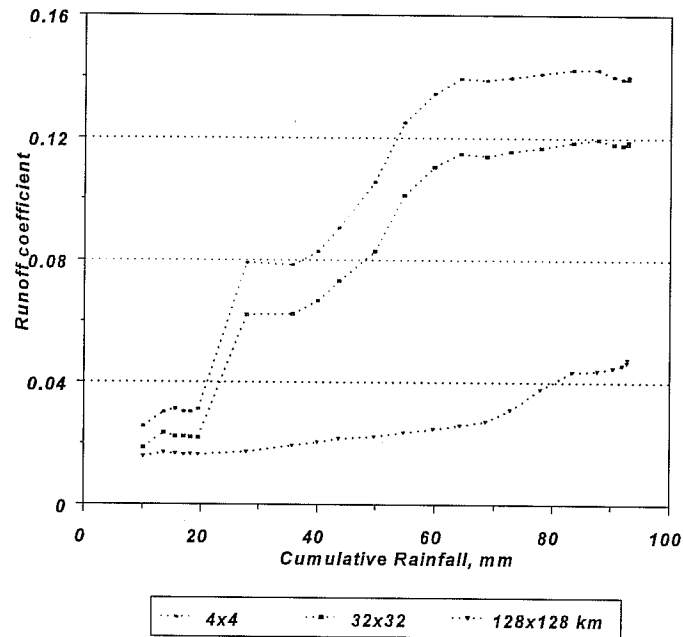
b)

Figure 2-17. Dynamics of the SAC-SMA model outputs during a
single flood event (04/12/94) generated at different scales:
a) Runoff coefficient versus cumulative rainfall
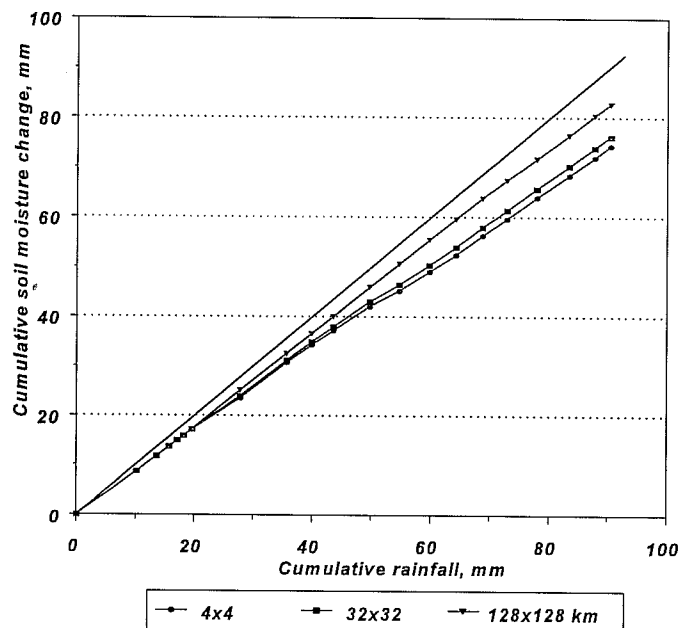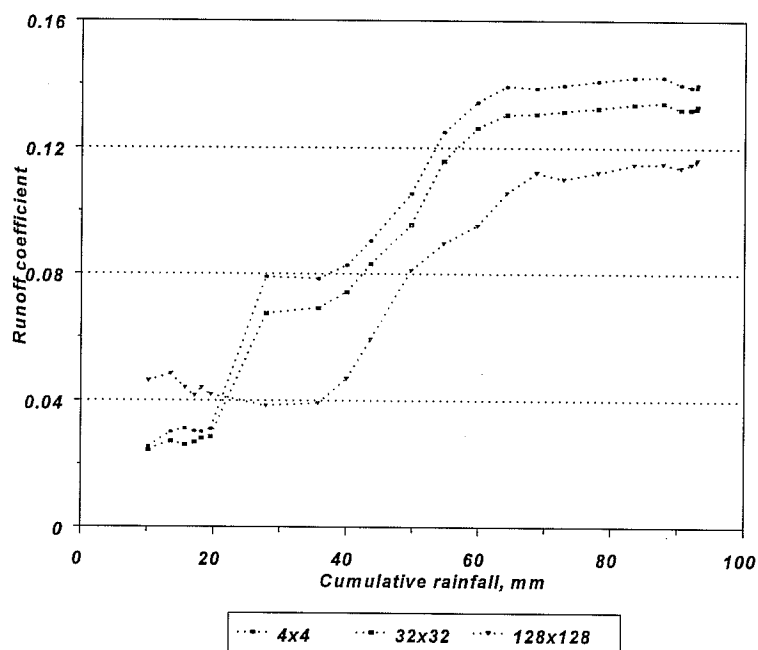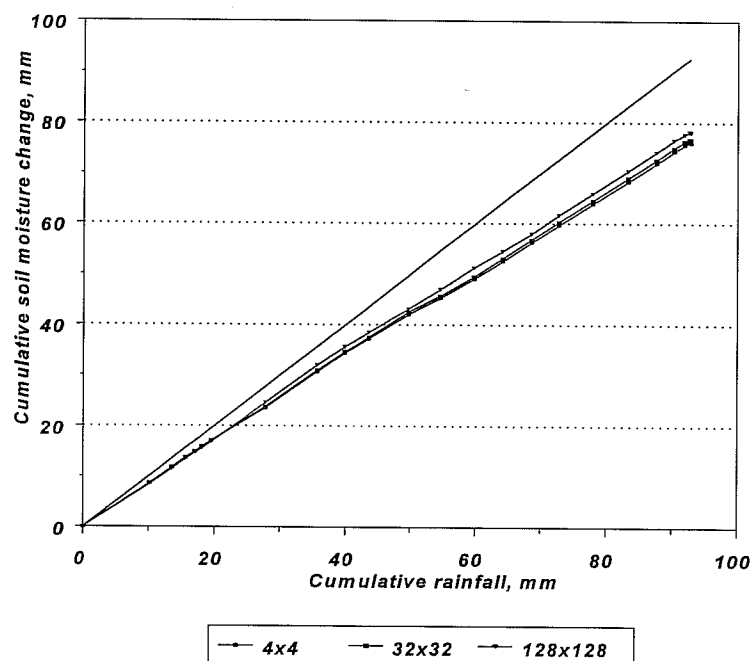b) Soil moisture change versus cumulative rainfall

a)

Figure 2-18. Dynamics of the reformulated SAC-SMA model outputs during a single flood event (04/12/94) generated at different scales: a) Runoff coefficient versus cumulative rainfall b) Soil moisture change versus cumulative rainfall

2.39

2.6 Conclusions

The sensitivity of the SAC-SMA model to precipitation inputs at various space-time scales while holding the parameters constant was explored by developing a rainfall runoff scale driver. The results presented were realized when running a continuous version of the SAC-SMA model in a lumped fashion at many different space-time scales while using mean areal precipitation inputs derived from gridded Stage III data. At the time of this analysis, a relatively short period (9 months) of NEXRAD data was available

The SAC-SMA model runoff components were found to be sensitive to both spatial and temporal scales of the Stage III precipitation inputs. The analysis revealed a general increase in surface runoff, interflow, supplemental baseflow, and total channel inflow when moving to finer spatial scales and maintaining constant hydrologic model parameters. Evapotranspiration decreased as spatial scale decreased which offset the increase in total runoff in the 9 month water balance. Decreasing the time scale of the model from 6 hours to 1 hour, while holding the spatial scale constant, resulted in a significant increase in surface runoff, interflow, and total channel inflow. Decreasing the time scale caused a decrease in the supplemental and primary baseflows.

These space-time scale effects on the SAC-SMA hydrologic model response may be attributed to the space-time averaging of high intensity, short duration, runoff generating precipitation events. And this space-time scale sensitivity suggests that potential improvements to the SAC-SMA model simulations may be possible by using the Stage III gridded precipitation estimates and modeling at finer space-time scales. Additional research will explore these possibilities by evaluating the finer resolution simulated hydrographs as compared to observed hydrographs.

At least for nested synthetic basins of regular size, adjusting model parameters was shown to be a method for preserving volume biases in a single runoff component when biases were created from applying the SAC-SMA model parameters to space-time scales for which the model was not calibrated. However, simple parameter changes resulted in a complex exchange and redistribution of water in other model runoff components and cannot account for space-time scale effects on the overall volume, timing, and shape of the SAC-SMA runoff hydrograph.

The results presented highlight the need for a greater understanding of the space-time distribution of SAC-SMA model parameters. The analysis indicated that parameters derived at a given space-time scale cannot be applied at different scales without introducing significant runoff volume biases. These biases were displayed in the redistribution of runoff volume between fast and slow response components, as well as between near surface and groundwater response. All results presented must be viewed according to the fundamental assumptions and limitations of the analysis and may vary geographically.

Comparative analysis showed that all selected models produced less surface and total runoff, and more evapotranspiration with increasing scale size. Rainfall variability was a primary factor of runoff reduction at the smaller scales, and rainfall coverage became a major factor at the larger scales. Although all selected models were scale dependent, the level of dependency varied significantly with different formulations of the rainfall-runoff partitioning mechanism. The point type OSU model with a pure infiltration-excess mechanism was the most sensitive to the rainfall spatial variability. The better representation of the soil moisture profile by using more soil layers did not reduce scale dependency. Mixed saturation/infiltration-excess type models, such as the original and reformulated SAC-SMA models, were less sensitive to the scale. The rainfall rate induced scale dependency of the fast runoff components on the rainfall rate was reduced significantly during the first phase of flood when a saturation-excess mechanism was dominated.

Probabilistic averaging of the point processes reduces scale dependency, as demonstrated by the SWB and reformulated SAC-SMA models. Effectiveness of the probabilistic averaging varies depending on the scale, and was reduced with increased scale size because rainfall coverage and rain area locations became an important factor. Continuous assimilation of a distribution function of rainfall and rainy area fraction significantly reduced scale dependency of the SAC-SMA model at the larger scales.

All models showed less scale dependency in total runoff compared to surface runoff because surface and subsurface runoff components usually changed in opposite directions as the scale increased. That is, the surface runoff decreased at the larger scales while the subsurface component increased. It suggests that neglecting the subsurface-groundwater component by compensating it in a surface runoff component can lead to an increase in the model scale dependency.

The analysis was focused on the scale dependency of different models rather than on their performances compared to measured data. If well calibrated, a more scale dependent model may give better results at the applied scale basin than a less scale dependent model. Importance of the scale sensitivity of the model depends on the specific application. In the local rainfall-runoff forecasting over dense gauge regions it is important to use a model that showed a high accuracy in rainfall-runoff simulations, and could be calibrated properly using historical data. Less scale dependent models are desirable when rainfall-runoff simulations are performed over large ungaged regions and there is a need in transferring of model parameters from different size basins.

2.7 References

Bae, D.H., and Georgakakos, K.P., 1994. Climate variability of soil water in the American Midwest: Part 1. Hydrologic Modeling. Journal of Hydrology, 162: 355-377.

Beven, K.J., and Hornberger, G.M., 1982. Assessing the effect of spatial pattern of precipitation in modeling stream flow hydrographs. Water Resources Bulletin, 18(5): 823-829.

Bradley, A.A., and Kruger, A., 1998, 'Recalibration of Hydrologic Models for use with WSR-88D Precipitation Estimates', Preprints of the American Meteorological Society Special Symposium on Hydrology, Phoenix, Arizona, 11-16 January, 302-305.

Burnash, R.J.C., 1995. The NWS River Forecast System - Catchment Modeling. Computer Models of Watershed Hydrology, Singh, V.P., ed., pp. 311-366.

Burnash, R.J.C., Ferral, R.L., and McGuire, R.A., 1973. A generalized streamflow simulation system - conceptual modeling for digital computers. U.S. Department of Commerce, National Weather Service and State of California, Department of Water Resources.

Chen, F., K. Mitchell, J. Schaake, Y. Xue, H-L. Pan, V. Koren, Q. Y. Duan, M. Ek, and A. Betts, 1996. Modeling of land surface evaporation by four schemes and comparison with FIFE observations. J. Geophys. Res., 101, D3: 7251-7268

Dingman, S. L., 1993. Physical Hydrology, Prentice Hall, Englewood Cliffs, New Jersey 07632.

Ek, M., and L. Mahrt, 1991. OSU 1-D PBL model user's guide. Dep. of Atmos. Sci., Oreg. State Univ., Corvallis, Oreg.

Famiglietti, J.S., and Wood E.F., 1994. Application of multiscale water and energy balance models on a tall grass prairie. Water Resources Research, 30(11): 3079-3093.

Fan, Y., and Bras, R.L., 1995. On the concept of a representative elementary area in catchment runoff. Hydrological Processes, 10th Anniversary issue: 69-80.

Fulton, R.A., Breidenbach, J.P., Seo, D.J., Miller, D.A., and O'Bannon, T., 1997. The WSR-88D rainfall algorithm. Submitted to Weather and Forecasting.

Georgakakos, K.P., Guetter, A.K., and Sperfslage, J.A., 1996. Systems for forecasting flows and their uncertainty. ASCE North American Water and Environment Congress, 22-28 June, Anaheim, California. CD-ROM.

Greene, D.R., Hudlow, M.D., and Farnsworth, R.K., 1979. A multiple sensor rainfall analysis system. Preprint volume: Third Conference on Hydrometeorology (Bogota), American Meteorological Society, Boston, pp. 44-53.

Greene, D.R., and Hudlow, M.D., 1982. HRAP project. National Weather Service, Hydrologic Research Laboratory, Silver Spring, MD, U.S.A., internal publication.

Hudlow, M.D., 1988. Technological developments in real-time operational hydrologic forecasting in the United States. Journal of Hydrology, 102: 69-92.

Kenner, S.J., Brich, S., Yang, Y., Hjelmfelt, M.R., and Pielke, R.A., 1996. Atmospheric and surface hydrologic simulation of an extreme flood event, Second Int'l Scientific Conference on the Global Energy and Water Cycle, 17-21 June, Washington D.C., pp. 17-18.

Klazura, G.E., and Imy, D.A., 1993. A description of the initial set of analysis products available from the NEXRAD WSR-88D System. Bulletin of the American Meteorological Society, 74(7): 1293-1311.

Kouwen, N., and Garland, G., 1989. Resolution considerations in using radar rainfall data for flood forecasting. Canadian Journal of Civil Engineering, 16: 279-289.

Krajewski, W.F., Lakshmi, V., Georgakakos, K.P., and Jain, S.C., 1991. A monte carlo study of rainfall sampling effect on a distributed catchment model. Water Resources Research, 27(1): 119-128.

Mahrt, L., and H. Pan, 1984. A two-layer model of soil hydrology. Boundary-Layer Meteorology, 29: 1-20

Nalbantis, I., 1995. Use of multiple-time-step-information in rainfall runoff modelling, Journal of Hydrology, 165: 135-159.

Obled, C. H., Wendling, J., and Beven, K., 1994. The sensitivity of hydrological models to spatial rainfall patterns: an evaluation using observed data. Journal of Hydrology, 159: 305-333.

Ogden, F.A., and Julien, P.Y., 1994. Runoff model sensitivity to radar rainfall resolution, Journal of Hydrology, 158: 1-18.

Pessoa, M.l., Bras, R.L., and Williams, E.R., 1993. Use of weather radar for flood forecasting in the sieve river basin: a sensitivity analysis. Journal of Applied Meteorology, 32(3): 462-475.

Schaake, J.C., 1989. Importance of the HRAP grid for operational hydrology. U.S./Peoples Republic of China Flood Forecasting Symposium, Portland, OR, NOAA/NWS, 331 - 355.

Schaake, J. C., V. I. Koren, Q.-Y. Duan, K. Mitchell, and F. Chen, 1996. Simple water balance model for estimating runoff at different spatial and temporal scales. J. Geophys. Res., vol. 101, No D3: 7461-7475.

Seo, D.J., and Smith, J.A., 1996. Characterization of climatological variability of mean areal rainfall through fractional coverage. Water Resources Research, 33(7): 2087-2095.

Seo, D.J., R.A. Fulton, J.P. Breidenbach, D.E. Miller, and E.F. Friend, 1995. Final report for interagency memorandum of understanding among the NEXRAD program, WSR-88D Oper. Support Facil. and the Natl. Weather Serv. Off. of Hydrol., Hydrol. Res. Lab., Jan, 1995.

Shah, S.M.S., O'Connell, P.E., and Hosking, J.R.M., 1996. Modeling the effects of spatial variability in rainfall on catchment response 2: Experiments with distributed and lumped models. Journal of Hydrology, 175: 89-111.

Shanhltz, V.O., Ross, B.B., and Carr, J.C., 1981. Effect of spatial variability on the simulation of overland and channel flow. Transactions of the ASAE, 24(1): 124-138.

Shedd, R.C., and Fulton, R.A., 1993. WSR-88D precipitation processing and its use in National Weather Service hydrologic forecasting. Proceeding of ASCE International Symposium on Engineering Hydrology, San Francisco, California, July 25-30, 1993.

Shedd, R.C., and Smith, J.A., 1991. Interactive precipitation processing for the modernized National Weather Service. Preprints, Seventh International Conference on Interactive Information and Processing Systems for Meteorology, Oceanography, and Hydrology, New Orleans, Louisiana, American Meteorological Society, pp. 320-323.

Smith, J.A., D.J. Seo, M.L. Baeck, and M.D. Hudlow, 1996. An intercomparison study of NEXRAD precipitation estimates. Water Resources Research, 32(7): 2035-2045.

Smith, J.A., and W.F. Krajewski, 1994. Estimation of parameters for the NEXRAD rainfall algorithms. Final report to the hydrologic research laboratory, Off. of Hydrol., Natl. Weather Serv., Natl. Ocean. Atmos. Admin., Silver Spring, MD, 1994.

University of Arizona, Progress Report. 1995-1996 Cooperative Agreement NA37WH0385 by Department of Hydrology and Water Resources, The University of Arizona, to the Hydrologic Research Laboratory of the U.S. National Weather Service, June 1995.

Wilson, CB., Valdes, J.B., and Rodriguez-Iturbe, I., 1979. On the influence of the spatial distribution of rainfall on storm runoff. Water Resources Research, 15(2): 321-328.

Wood, E.F., Sivapalan, M., Beven, K., and Band, L., 1988. Effects of spatial variability and scale with implications to hydrologic modeling. Journal of Hydrology, 102: 29-47.

Wood, E.F., 1995. Scaling behavior of hydrological fluxes and variables: empirical studies using a hydrological model and remote sensing data. Hydrological Processes, 10th Anniversary issue, 21-36.

3. Comparison of Mean Areal Precipitation Estimates from NEXRAD Stage III and Operational Raingage Networks

3.1 Operational MAPX vs. Operational MAP

3.1.1 Problem Description

Until recently, precipitation input for operational forecasting has been based solely on point rain gage measurements that are converted into mean areal precipitation estimates. With the nationwide advent of the Weather Surveillance Radar - 1988 Doppler (WSR-88D) systems known as Next Generation Weather Radar (NEXRAD), the NWS and others have the opportunity to use hourly 4 km precipitation estimates for hydrologic modeling (Hudlow, 1988; Klazura and Imy, 1993). As outlined in Chapter 1, one of the approaches to using Stage III data to improve simulation accuracy is to perform lumped modeling with MAPX data as input.. One aspect of this investigation is to understand the differences between rain gage-derived and radar-derived estimates of mean areal precipitation, since often both are used for operational forecasting in the same basin. In addition, one of the assumptions regarding Stage III data is that long term areal means defined using gridded radar estimates and rain gage point estimates are the same.

A review of the literature indicates that differences between MAP and MAPX do exist. In an early study, Smith et. al (1975) noticed a general underestimation of daily mean areal rainfall derived by radar compared to that derived from a raingage network. Barge et. al (1979) compared raingage and radar- derived mean areal rainfall estimates for a 6 day storm sequence. They were clearly able to identify causes for large differences in the two estimates. Collier et. al (1975) were able to show that the addition of rain gages used in calibrating radar led to improved estimates of areal rainfall. For a 7 month period, Finnerty and Johnson (1997) compared MAP values derived from the NCDC gage network with MAPX values for several basins near Tulsa, Oklahoma. Their findings indicated that the mean areal precipitation estimates derived from NEXRAD are biased low compared to gage-derived estimates. Borga et. al, (1995) compared several radar derived mean areal estimates with several gage products. In streamflow simulations limited to one storm event, they investigated the hydrologic impacts of the differences in the mean areal products. Goodhew and Mylne (1992) compared daily mean areal estimates from various density gage networks to those based on data from a single radar. Their analysis spanned a two year period. Agreement between the two estimates was found to vary with distance from the radar, amount of gage recorded precipitation, radar calibration, and location under the radar umbrella. In their experiments using a single event model, Kull and Feldman (1988) found that at least on one occasion, radar-based runoff simulations were well below those of the observed data. Finnerty et. al (1997) found that parameters for the SAC-SMA are strongly linked to the temporal and spatial scale of precipitation forcing, implying that hydrologic model parameters calibrated from raingage networks may not be suitable for use with the gridded NEXRAD data.

In light of these findings, it is important that the two estimates of precipitation forcing be understood. Two objectives of this investigation are identified: 1) to examine the statistical differences between radar derived and gage derived estimates of mean areal precipitation, and 2) to investigate the potential impacts of these differences on streamflow simulations generated with a hydrologic model commonly used within the National Weather Service.

This initial study is not aimed at investigating the accuracy of the two mean areal precipitation products themselves, but rather to provide a comparison. Differences in these products will undoubtedly have implications on calibrated parameters, mean areal precipitation estimates, and climate and hydrologic modeling.

3.1.2 Methodology

The Tulsa River Forecast Center was chosen as the site for these comparisons for several reasons. This area has the longest archive of radar data available and it has a relatively dense raingage network in comparison to some areas of the country. In addition, there are a number of unregulated headwater basins already being modeled by the ABRFC. The density of the raingage network is in reference to the operational gages and the network of gages used in producing the Stage II radar precipitation estimates. The basic framework of the methodology includes : 1) Obtain operational 6-hour MAP estimates from the Tulsa River Forecast Center data archives for the period from 1993 to 1996; 2) From the same 1993 to 1996 period, obtain operationally-derived 1-hour MAPX's for the same basins and aggregate to a 6-hour time step; 3) Perform various analyses to illustrate differences and similarities between the two mean areal precipitation products; 4) Compare the effects of these inputs on hydrologic simulations produced by one of the hydrologic models used by the National Weather Service.

3.1.3 Data

A total of 8 basins were used in the study of precipitation comparisons, with 3 of these basins being subsequently used in the study of the effects of the precipitation products on the hydrologic simulations. The basins are located mainly on the Oklahoma-Arkansas-Missouri border. Most of the study area stretches north from Fort Smith up to the Mark Twain National Forest. Figure 3-1 provides a location map of the region with the Arkansas River noted as well as the original 8 basins and several other prominent features of the area. Also shown are the operational rain gages used to compute MAP values. Table 3-1 provides information regarding the basins.
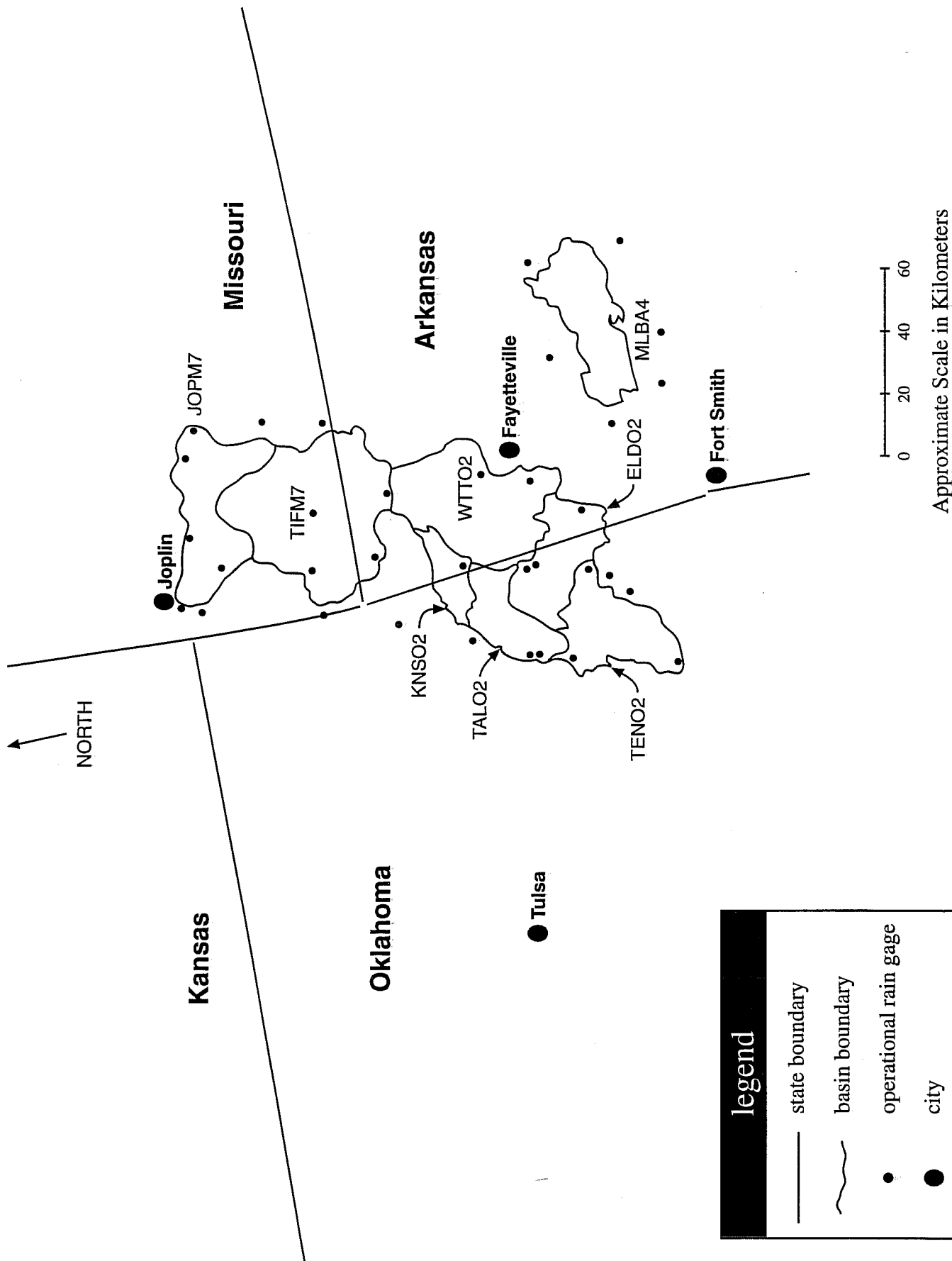
Figure 3-1 Location Map of Study Basins and Operational Rain Gages

Table 3-1. Study basin descriptions and relevant information.

No.	Basin Name	Lat./Long. Centroid	Area (km^2)
1	ELDO2: Eldon, OK	35.91/94.59	795
2	JOPM7: Joplin, MO	36.9/94.17	1106
3	KNSO2: Kansas, OK	36.23/94.58	285
4	MLBA4: Mulberry, AR	35.69/93.72	1103
5	TALO2: Talequah, OK	36.08/94.78	552
6	TENO2: Tenkiller Ferry Dam, OK	35.79/94.88	894
7	TIFM7: Tiff City, MO	36.6/94.25	2259
8	WTTO2: Watts, OK	36.12/94.32	1645

3.1.3.1 Operational Gage Network

Each RFC within the NWS utilizes data from an operational network of precipitation gages to derive MAP values. Details of this procedure can be found in National Weather Service (1993). Gages in the operational network report at a variety of time steps, most commonly 1, 3, 6, and 24 hours. In general, rainfall reports from different gages are accumulated to derive 24 hour totals. Missing gage data is estimated from surrounding gages using a $1/d^2$ weighting procedure, where d is the distance between the estimator station and the station being estimated. A daily MAP value is computed using one of several weighting options, the most common being a Thiessen polygon method. Daily MAP estimates are then distributed into 6 hour periods based on the precipitation values of the recording gage closest to the centroid of the basin in each of 4 quadrants. Figure 3-1 shows the location of the operational gages in the ABRFC operational network.

This product may or may not be exactly reproducible, due to changes in the operational gage network; however, it is noted that it is considered to be an accurate representation of the precipitation based on the gage network operating at the time.

3.1.3.2 Stage III Precipitation

MAPX products are derived from the gridded hourly Stage III precipitation estimates. A brief description of the NEXRAD products is provided here. Additional information can be found in Finnerty et al. (1997), Shedd and Fulton, (1993), Seo and Johnson, (1995), and Fulton et. al (1997). The NEXRAD product used in this work begins with the raw reflectivity data produced from the radar sites. This raw reflectivity is transformed into precipitation estimates by using a "reflectivity-rainfall" relationship, also known as a "Z-R" relationship. This is now known as the Stage I product and there are known errors in these precipitation estimates (Smith and Krajewski, 1994; Seo et al., 1995; Smith et al., 1996). An attempt to account for these errors results in the processing of the data by utilizing "ground truth" gage measurements to remove a mean-field bias in the radar precipitation estimates, the resulting product is known as a Stage II product. Finally, the estimates are merged with overlapping radar fields in a gridded system known as the NWS Hydrologic Rainfall Analysis Project (HRAP) to form a Stage III product (Greene and Hudlow, 1982). The HRAP projection system is a polar stereo graphic projection grid. The grid size varies with location because of the non-equal area projection, but is approximately 4x4 km^2. The merged data is often referred to as multi-sensor HRAP precipitation estimates or HRAP precipitation estimates. Essentially one can think of Stage III products as radar derived distributions "warped" to match gage recorded precipitation values.

Stage III is the final radar product of an RFC and reflects enhancements and corrections made by a "hydrometeorological analysis and support" (HAS) forecaster at the RFC. The HAS forecaster checks the Stage III products and analyzes the meteorological system which is responsible for the precipitation. The HAS forecaster may then correct or alter the Stage III product if it is believed that the radar or gages used in the Stage II product are erroneous. Hourly MAPX values are computed from the Stage III data as a spatial average of all the gridded precipitation measurements over a particular basin.

Both the operational MAPs and the MAPXs are considered by the NWS to be very reliable real-time mean areal precipitation estimate over the basin, having been derived from two unique sources of data. Time series of over 4,000 MAP/MAPX pairs for each of the basins were derived for analysis.

3.1.4 Results

In these results, we present a variety of data comparing gage based MAP's and MAPX products. Cumulative amounts for both the MAP and MAPX estimates are compared, as well as monthly and seasonal totals. Additionally, a number of storms were investigated. The arrival times, storm totals, storm distributions, and return periods were investigated. Because of the large amount of data, the findings are summarized and specific examples are provided to illustrate the general results.

Summary of Results

1) Long Term Cumulative Sums - The gage based MAP's tend to be higher than the radar based MAPX's. This is true to varying degrees for most of the basins investigated. The basin KNSO2 had cumulative MAPX values that tended to be only slightly higher than the MAP values for most of the study period, while MLBA4 and TIFM7 had fairly good agreement between MAPX and MAP values over the course of the study period. The remainder of the basins have the MAP values being higher most of the time. This result was found by summing the MAP and MAPX values for each month over the study period and calculating the monthly MAPX/MAP ratios. Table 3-2 presents the average of the 40 monthly rations for each basin. In some of the basins the ratios are closer than others, but on average, the MAPX's are 5 to 10% less than the MAP's. Exceptions to this are the basins KNSO2, MLBA4, and TIFM7, for which the MAPX/MAP ratio fluctuated over the period. The underestimation would seem to be a logical extension of the results found by Smith et. al (1996) whose gage-radar bin intercomparisons suggested a systematic underestimation relative to gage observations.

Table 3-2 - Average ratio of MAPX values to MAP values.

BASIN NAME	MAPX/MAP
ELDO2	0.901
JOPM7	0.955
KNSO2	1.153
MLBA4	1.014
TALO2	0.941
TENO2	0.93
TIFM7	1.012
WTTO2	0.961

Also, overall biases or differences in precipitation amounts were calculated by summing total precipitation over the study period for each year and for the season from May 1 to October 31. This season was selected because of known precipitation estimation errors by the radar in the winter months (Smith et al., 1996). These results are illustrated in Table 3- 3. Note that most of the total bias is achieved in the season from May 1 thru October 31, which is not terribly unexpected as most of the precipitation occurs in these

Table 3-3 - Total study period biases and total seasonal precipitation (inches).

	ELDO2	JOPM7	KNSO2	MLBA4	TALO2	TENO2	TIFM7	WTTO2
MAY 1 thru October 31 - MAP	115.4	117.9	86.1	97.8	106.1	116.6	112.1	94.9
MAY 1 thru October 31 - MAPX	100.6	105.6	90.2	101.6	96.2	104.7	105.4	91.3
Seasonal Difference (MAPX-MAP)	-14.8	-12.3	+4.1	+3.8	-9.9	-11.9	-6.7	-3.6
Ratio of MAPX/MAP	0.87	0.89	1.05	1.04	0.91	0.90	0.94	0.96
TOTAL PRECIP. - MAP	165.5	155.5	129.1	153.8	152.3	163.8	151.2	140.0
TOTAL PRECIP. - MAPX	146.4	139.9	134.6	153.7	139.1	148.9	146.9	134.4
Total Difference (MAPX-MAP)	-19.0	-15.6	+5.4	-0.1	-13.2	-14.9	-4.3	-5.6
Ratio of MAPX/MAP	0.88	0.90	1.04	1.0	0.91	0.91	0.97	0.96

3.7

months. The overall average bias is 5.4% (MAPX being less than MAP). This is very promising at first glance, but is not entirely true, as will be discussed.

2) Monthly Precipitation - - The conditional average monthly precipitation for the MAPX values is higher than the MAP values. While the gage based MAP's tended to produce higher monthly (and storm totals), the MAPX's tended to report fewer increments of precipitation. There were exceptions to this, but in general this tended to be the case. Figures 3-2, 3-3, and 3-4 illustrate the average 6 hour mean precipitation (conditioned on the occurrence of precipitation) for the gage and NEXRAD based estimates over the study period for basins WTTO2, ELDO2, and KNSO2 respectively.. Basically, the radar estimates show the storm events occurring in much fewer intervals. Thus, ignoring the underestimation problems of the radar and given cases where the radar and the gages predicted the same depth of rainfall, the radar estimates tended to be more intense and less spread out. Also, it was found that the radar data often showed rainfall as occurring earlier than did the gage data even at these 6 hour increments. Ongoing investigations using 1-hour data show this occurs much more frequently at this smaller time step, which is expected (Finnerty and Johnson, 1997).

The results presented in Figures 3-2, 3-3, and 3-4 could be the result of two factors. First, the operational gage network for deriving MAP values is different than the gage network used in the processing of the NEXRAD estimates to derive MAPX values. Hourly, 3-hourly, 6-hourly, and daily rain gage reports are used in the MAP algorithm, while predominately hourly gages which report at the top of the hour are used in the processing of NEXRAD data. Second, the strategies used to define a 6-hour MAP and MAPX estimates are quite different. As described earlier, in the MAP algorithm a 24 hour MAP is derived from the various reports, and then distributed into four six-hour periods based on the temporal distribution of precipitation at nearby stations. This strategy may tend to spread out the precipitation. If suitable data at nearby stations cannot be found, then the 24-hour MAP value is uniformly distributed over four 6-hour periods. For example, for basins WTTO2 and ELDO2 between April, 1993 and November, 1996, 71 and 60 cases respectively were found in which a uniform distribution was used. In contrast to the MAP algorithm, hourly MAPX values are derived from the Stage III data and then aggregated into six-hour MAPX values for use in the hydrologic model.

These differences will have varying effects on hydrologic models. In the case of continuous simulation "bucket" models such as the Sacramento Soil Moisture Accounting Model (SAC-SMA), the effects of precipitation biases are cumulative. Current investigations and experiences within the NWS show that the SAC-SMA has difficulty in handling some short duration, high intensity events.

3) No clear trend for this short period could identified in the MAPX/MAP ratios. In general, MAPX values, as supported by other conclusions in the paper, tend to be lower than MAP values. Also, most of the basins tended to have several periods where monthly MAPX/MAP ratios were greater than 1.0. These tended to be in the winter months between November and March. Examples of this are illustrated in Figures 3-5, 3-6, and 3-7, which depict the ratios of MAPX to MAP for the WTTO2, ELDO2, and KNSO2 basins, respectively, for the study period. Also shown in these figures
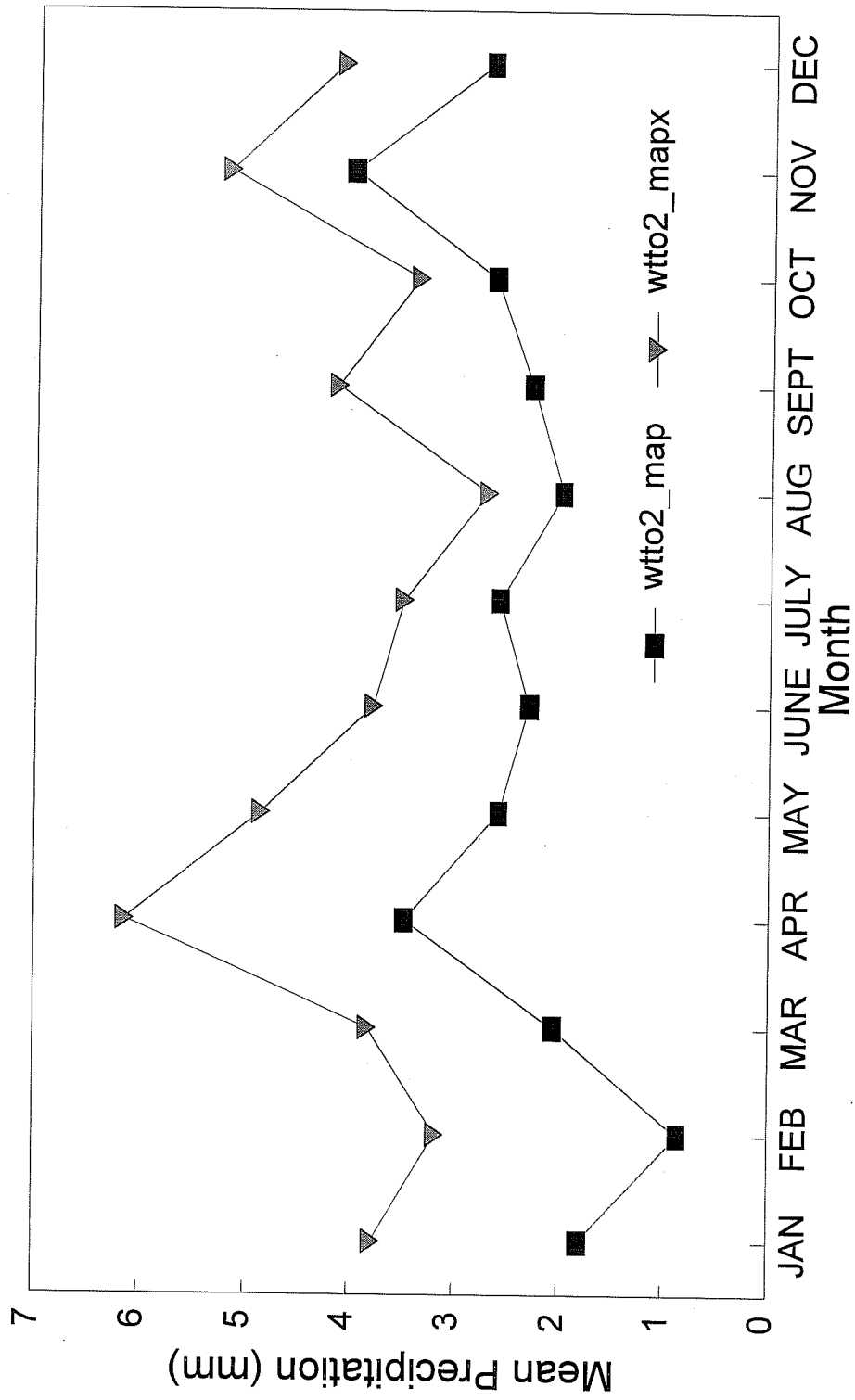
Figure 3-2 WTTO2: MAPX and MAP Conditional Mean Precipitation
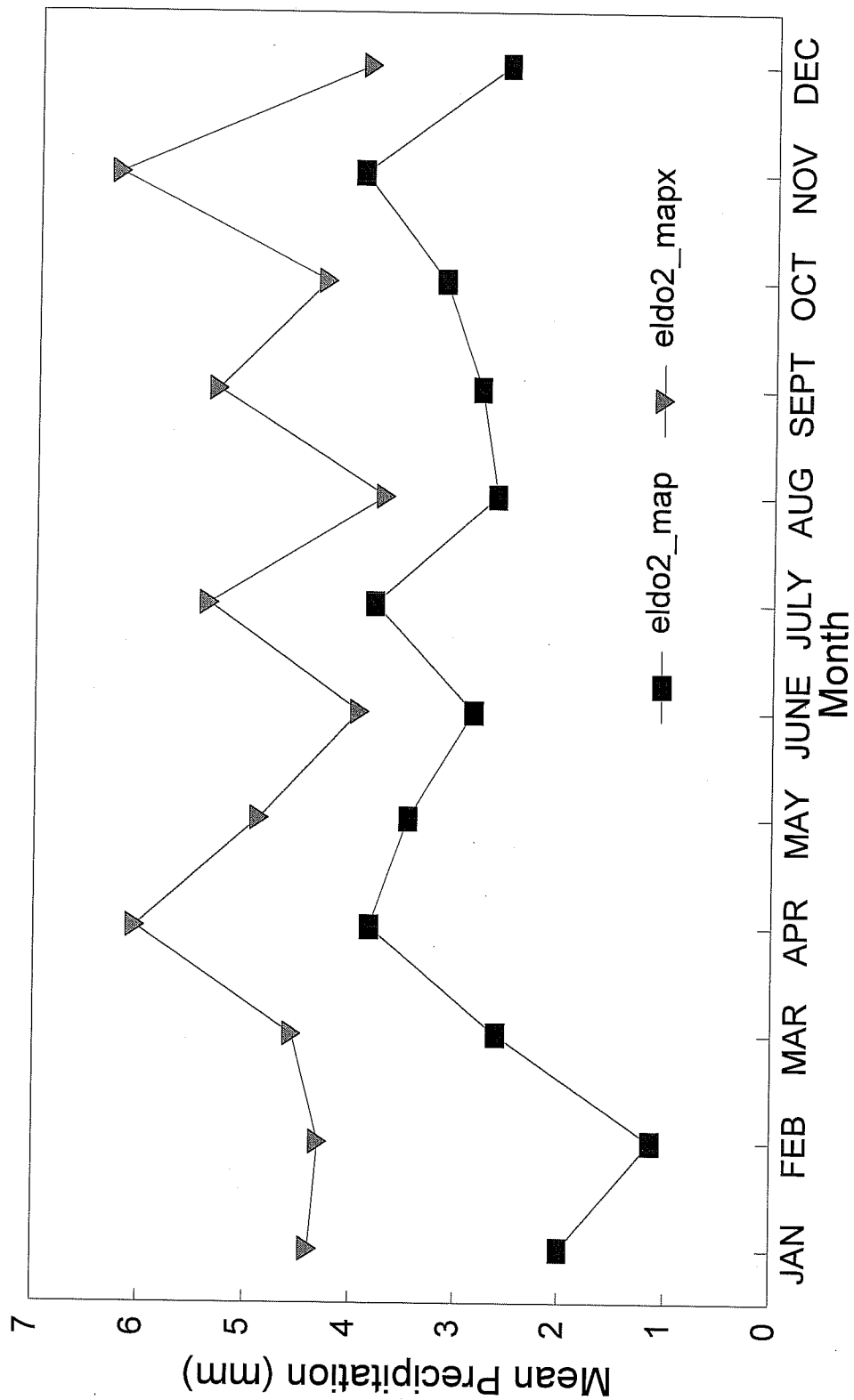
Figure 3-3 ELDO2: MAPX and MAP Conditional Mean Precipitation
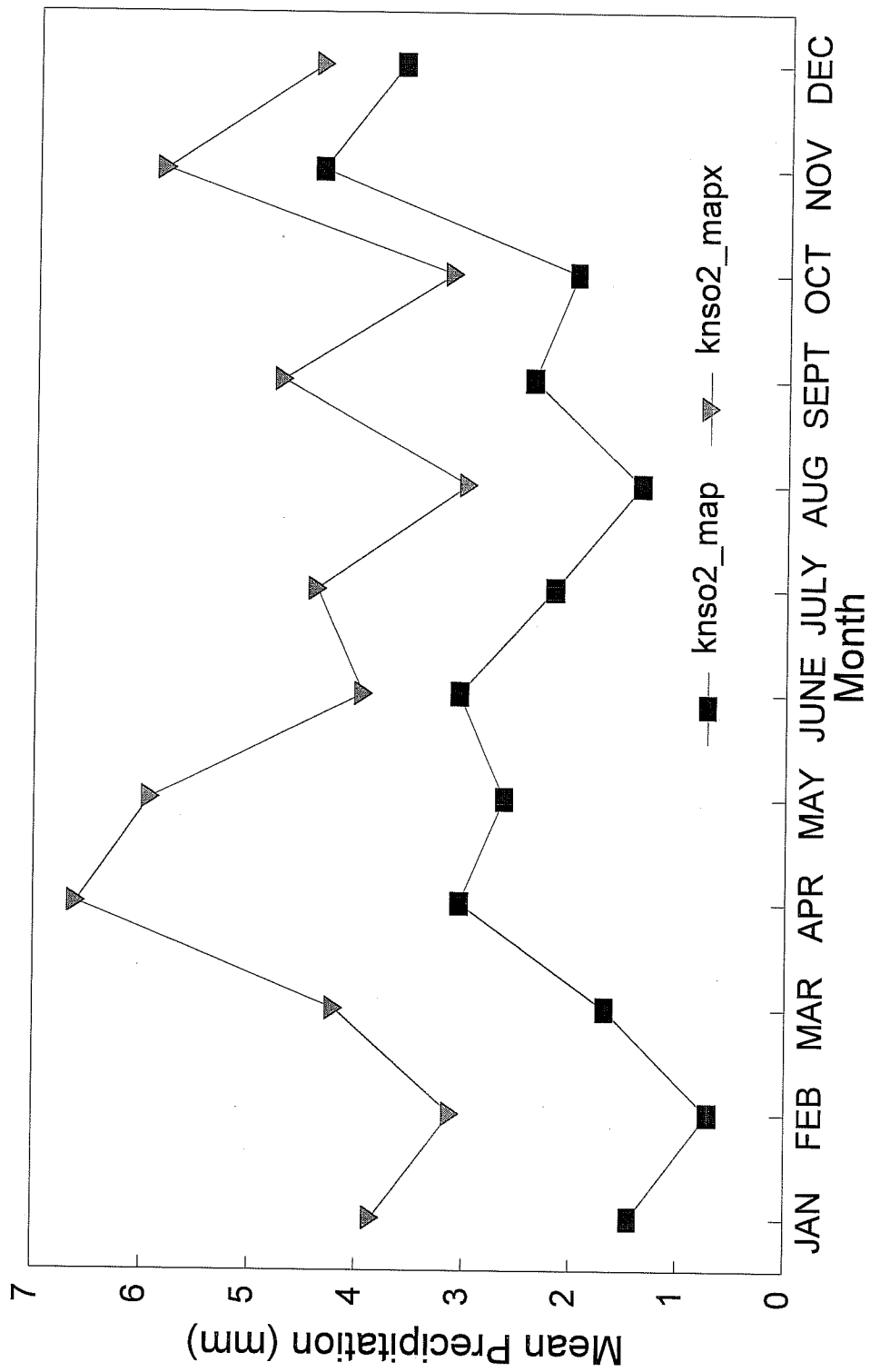
Figure 3-4   KNSO2: MAPX and MAP
Conditional Mean Precipitation

Figure 3-5   WTTO2
MAPX/MAP Ratio and %Runoff Bias

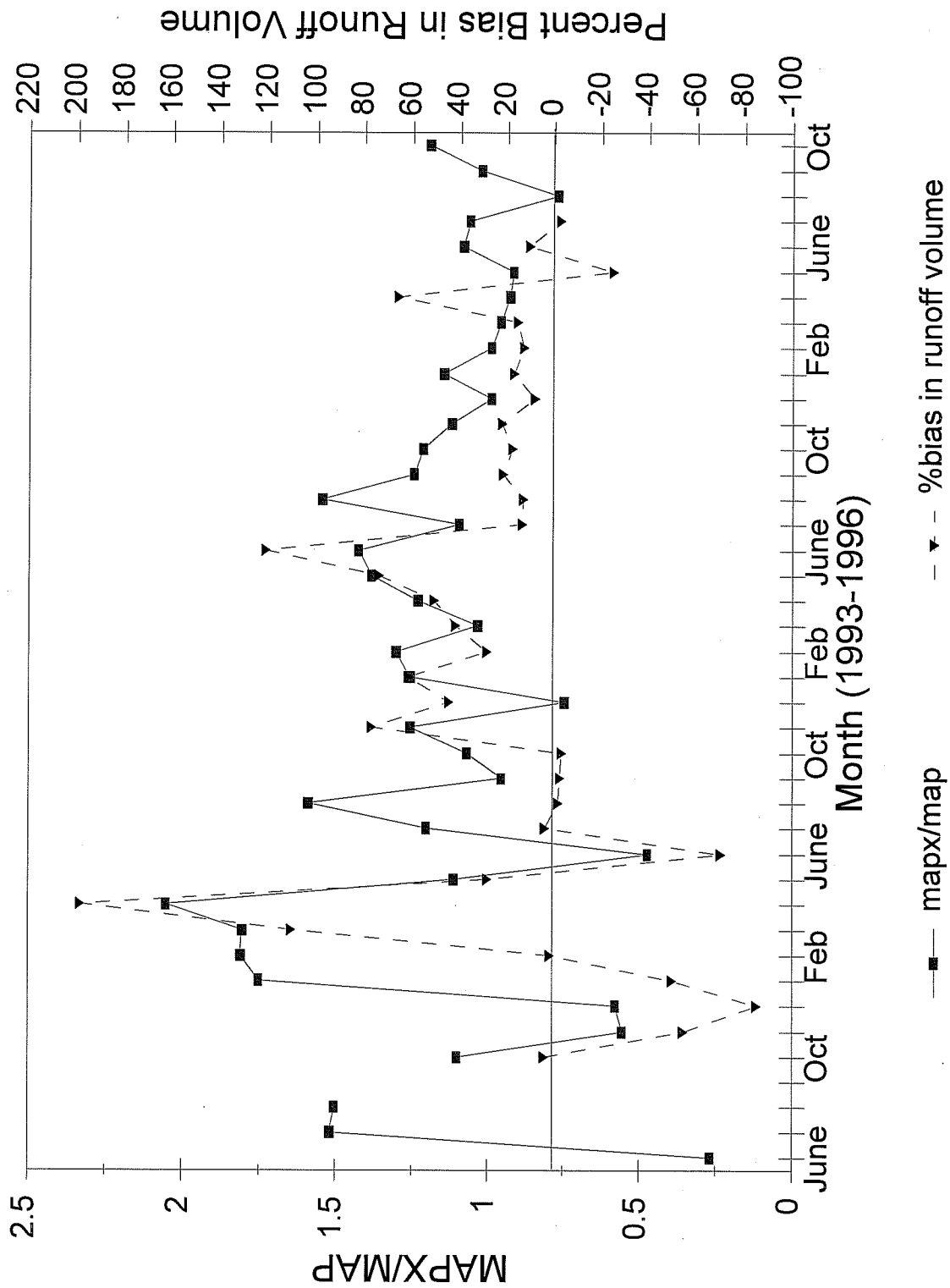Figure 3-6 ELDO2
MAPX/MAP Ratio and %Runoff Bias

Figure 3-7   KNSO2
MAPX/MAP Ratio and %Runoff Bias

are percent runoff biases. These bias plots will be discussed in later sections. The MAPX/MAP value of zero in September of 1993 is due to missing data for that month. The reader may notice a periodic signal, or time when the MAPX/MAP ratios approach 1.0, occurring during the winter months for each year. This signal, which is stronger in some basins than others, is the result of the MAPX values being closer to the MAP values. Note that the MAP and MAPX values tend towards one another for the winter months and then the average bias accumulates in the period from Spring to Fall.

This result is contradictory to current theory, which generally indicates that the radar should more drastically under predict precipitation in typical winter storm systems due to beam overshoot (Smith et al., 1997). This departure from expected behavior is one of the most significant and puzzling findings of the study. The overall average biases were on the order of 5% for the 3+ year study period; however, if the radar is erroneously over predicting in the winter, then the overall biases would be considerably greater.

While this continues to be investigated, it could be a result of a phenomenon known as "bright band" reflectivity (Battan, (1973), Collier et al.,(1979), Hopper et al.,(1991)). In short, bright band reflectivity is caused when a radar beam passes through a zero degree isothermal layer in the atmosphere. Precipitation above this line is more in the form of frozen particles. As this frozen precipitation passes through the zero degree isotherm it begins to melt, producing particles or water coated ice droplets. These droplets are capable of reflecting high levels of energy, thus producing false echos, which appear as areas of high rainfall.

While bright band reflectivity can occur at all ranges, ranges beyond 50 km from the radar site have historically used a "bi-scan maximization" technique. This technique essentially utilizes two beam heights from the radar, selecting the maximum of the two returns for estimating precipitation (Smith et. al, 1997). This technique was used in nearly all of the data of this study. The bi-scan maximization technique was effectively turned off in February, 1996. It should be noted, first, that bright band will still be present and algorithms to help detect and reduce this phenomenon are being studied, and secondly, the bright band reflectivity is present in all NEXRAD products as it is an artifact of the raw reflectivity. Stage III may have this effect reduced as the HAS forecasters may recognize this occurring in the storm system and correct for it.

Another possible explanation for the winter MAPX/MAP ration to approach a value of one is that in winter, for frozen precipitation events, personnel at ABRFC often switch to a gage only field in the processing of the NEXRAD data. In other words, gridded hourly precipitation fields are constructed from rain gage reports without the radar measurements.

3.1.5 Implications for Hydrologic Modeling

In order to evaluate the hydrologic effects of the MAP versus MAPX differences, streamflow simulations were performed for 3 of the 7 basins using the two precipitation products as input to the SAC-SMA. The basins chosen were WTTO2, ELDO2, and KNSO2, having drainage areas of 1646,

895, and 285 km2, respectively.

As mentioned earlier, the SAC-SMA is widely used within the NWS and interested readers are referred to Burnash et al.,(1973) and Burnash (1995) for detailed descriptions of the model. In short, the SAC-SMA is a conceptual model consisting of several tension water and free water reservoirs representing the active portions of the soil. Deficits accumulated in the tension water zones must be satisfied before water may move to the free water reservoirs. Fast response surface runoff is generated after upper zone tension and free water storages are full. Moisture is released from the free water reservoirs at different rates and summed with surface runoff to derive a total runoff volume hydrograph. Unit hydrographs are used to transform runoff volumes to discharges.

Parameters for the SAC-SMA for each of the 3 basins were derived through manual calibration using historical gage-derived MAP time series and observed mean-daily flow from the U.S. Geological Survey. Statistics from the calibration of the 3 basins in this study appear in Table 3-4 where the percent bias is computed as follows:

$$Bias = \frac{\sum_{i=1}^{N} (S_i - O_i)}{\sum_{i=1}^{N} O_i} \cdot (100) \qquad (3\text{-}1)$$

where:

Bias = Percent Bias

S = Simulated mean daily flow forced with radar data, cubic meters per second day (cmsd).

O = Simulated mean daily flow forced with gage data, cmsd.

N = Number of discharge pairs

Table 3-4. Calibration Statistics for Three Study Basins

Basin	Period	%Bias
WTTO2	1971-1992	4.85
ELDO2	1971-1985	4.78
KNSO2	1971-1992	4.85

A slight positive bias was realized in the historical calibration of all three basins. Nonetheless, it was felt that the parameter sets were acceptable for the generation of simulated flows using the operational MAP and MAPX time series.

Streamflow simulations for the three basins were performed for the period October, 1993 to July, 1996. Two simulations were produced for each basin: one using the MAPX time series and the other using the MAP values. Model simulations were run using a 6 hour time step. It should be emphasized that in each of the three basins, the same SAC-SMA parameters were used for both simulations. Simulated discharge values were averaged to derive a mean daily flow time series in units of cmsd, facilitating the use of existing NWS software for statistical analysis. Table 3-5 presents the results of these statistical analyses.

The bias statistic in Table 3-5 is computed using the basic form of Eq. 3-1, but modified as shown in Eq. 3-2:

$$Bias = \frac{\sum_{i=1}^{N} (R_i - G_i)}{\sum_{i=1}^{N} G_i} \cdot (100) \tag{3-2}$$

Bias =   Percent Bias
R =   Simulated mean daily flow forced with radar data,   Cubic meters per second day (cmsd).
G =   Simulated mean daily flow forced with rain gage data, cmsd
N =   Number of discharge pairs

The total bias is computed as the difference of the average monthly simulated and observed flows divided by the average monthly observed flow. It can be seen from Table 3-5 that the simulations produced from the two input forcings are significantly different on a seasonal basis.

Table 3-5. Percent and Absolute Biases in Monthly Runoff Volumes Generated Using MAP and MAPX Time Series. Period is October 1993 to July 1996

Basin	WTTO2		ELDO2		KNSO2	
Month	%	mm	%	mm	%	mm
October	-4.2	-.5	3.9	0.7	6.1	0.4
November	-37.3	-7.2	-38.5	-21.5	-5.0	-0.7
December	-49.6	-12.7	-20.9	-7.0	-50.4	-15.0
January	4.9	1.2	-16.1	-8.1	-34.4	6.8
February	-17.6	-2.2	7.9	1.6	-16.3	1.3
March	-16.3	-5.9	-32.6	-24.5	77.6	15.8
April	21.0	8.0	1.1	0.6	102.5	34.8
May	10.0	4.5	-21.7	-13.4	38.8	14.9
June	70.3	13.8	-43.7	-13.8	41.8	13.3
July	9.1	1.0	-44.7	-8.2	6/9	0.6
August	11.6	1.0	-65.2	-13.1	6.2	0.5
September	8.8	0.6	-36.5	-2.1	9.8	0.6
Total	0.5	1.8	-23.0	-108.8	0.7	73.1

Along with the MAPX/MAP ratio, Figure 3-5 presents the runoff bias for each month in the simulation period for WTTO2. The plots in this figure reveal that in general, the runoff volume bias corresponds to the MAPX/MAP ratio. It can be noticed, however, that the runoff bias lags the MAPX/MAP ratio for the first few months of the simulation period. For example, Figure 3-5 shows MAPX/MAP ratios less than 1.0 for October, November, and December of 1993, followed by two months in which the MAPX/MAP ratio is greater than 1.0. In April, 1994, the MAPX/MAP ratio climbs to 1.7. Examination of Figure 3-5 shows that while the MAPX/MAP ratio is greater than 1.0 for Jan and Feb, 1994, a corresponding positive bias in runoff volumes does not occur until April, 1994.

This delayed response of the runoff bias is logical considering the structure of the SAC-SMA. In those months in which MAPX values are less than MAP, larger soil moisture deficits are

created in the radar-forced model compared to the gage forced model. Even though in subsequent months the MAPX/MAP ratio is greater than 1.0, the larger deficits in the radar forced model require more precipitation to be satisfied before runoff can be produced.

Figure 3-5 shows that a large runoff volume bias was generated in June, 1995. Examination of the MAPX and MAP time series reveals that this bias is the result of a single precipitation event beginning on June 10. As shown in Figure 3-5, NEXRAD measured over 27 mm more precipitation than did the raingage network. Also, the most intense 6-hour period of rainfall in the MAPX time series occurred one time step earlier than the most intense period of gage-recorded rainfall.

The plot of the observed and simulated discharge hydrographs in Figure 3-8 reveals that the MAPX-forced simulation produced much more runoff than the MAP-forced simulation. While overpredicting the observed discharge, the MAPX-forced simulation is far better than the MAP-forced case. Examination of the radar rainfall patterns for this event reveal that some parts of the basin received little precipitation compared to others, implying that the gage network may have misrepresented the event in a similar fashion to the case discussed by Barge et al., (1979). Examination of the initial conditions in each simulation revealed no major differences, so that the simulated hydrographs in Figure 3-8 are the result of the differences in MAPX and MAP.

Results very similar to those in Figure 3-8 were also achieved for an event in January, 1995 in basin WTTO2. Initially, it was not clear whether the good fit produced using radar data was due to oversimulation of the precipitation due to bright band contamination, or whether the radar simply captured the precipitation better than the gage network. Subsequent analysis of the Stage III data by ABRFC personnel revealed that there was no bright band contamination for this event, indicating that the better simulation was the result of a better estimate of the precipitation
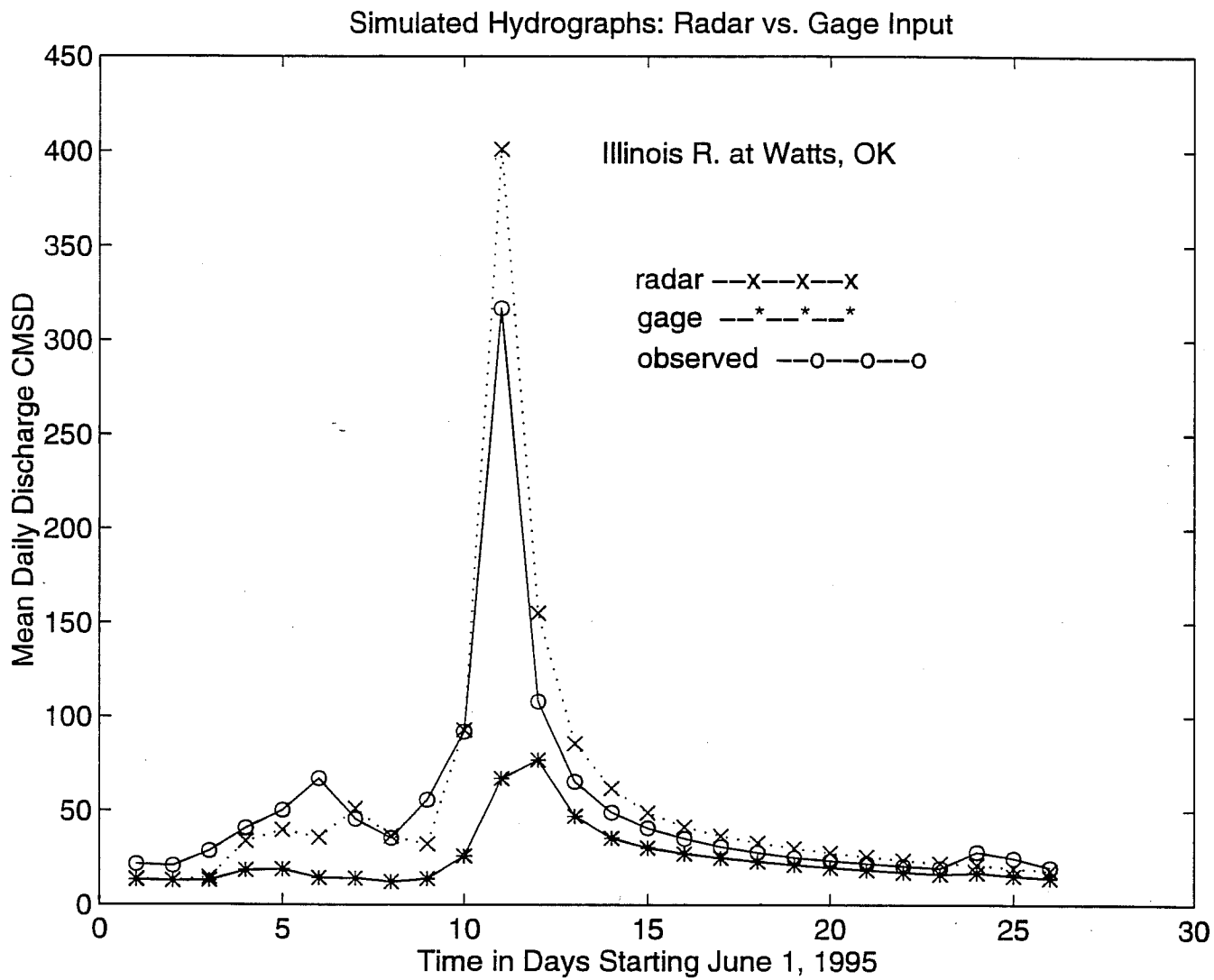
Figure 3-8 Simulated and Observed Hydrographe for Event of June, 1995.
Daily time step is used.

Table 3-6.   MAPX and MAP Values for June 10, 1995 Event in WTTO2

Date	Time	MAP Value mm	MAPX Value mm
June 8	24	8.00	8.61
June 9	6	3.12	1.60
June 9	12	2.62	8.71
June 9	18	0.0	0.03
June 9	24	8.26	5.38
June 10	6	0.02	0.0
June 10	12	0.10	7.26
June 10	18	6.78	33.88
June 10	24	21.18	14.12
June 11	6	0.0	0.0
June 11	12	1.65	0.15
June 11	18	3.33	2.79
total		55.13	82.53

Behavior similar to Figure 3-5 appears in Figure 3-6 for ELDO2. In general, the monthly runoff biases correspond in time to the MAPX/MAP ratio. In April, 1994 a large bias can be identified. In this case, the MAPX values for an event on April 5 are almost double the MAP values. As a result, the MAPX forced simulation exhibited a strong runoff response (not shown here), while the MAP-forced simulation showed almost hydrograph no rise at all. Observed streamflow records reveal no significant runoff response for this rainfall event, indicating that the radar greatly overpredicted the amount of precipitation for this event. From April, 1994 to the end of the simulation period, Figure 3-6 shows a quite strong negative bias in runoff volumes. This result is understandable in that the overall MAPX/MAP ratio of 0.88 indicates less rain detected by the radar.

Figure 3-7 shows the same erratic behavior of the runoff volume ratio for basin KNSO2 that was seen for basins ELDO2 and WTTO2. A large bias can be seen for the month of April, 1994, largely due to the event on April 9-11, in which the radar recorded 81.3 mm of rainfall and the gage network recorded 35.6 mm. Although not shown here, there is no observed discharge data for this event, so it is not possible to judge the simulations forced using the two data sources. After this event, Figure 3-7 shows a general positive runoff bias, which is reasonable considering that the average MAPX/MAP ratio is 1.15. The large bias in June of 1995 is due to a single event in which the radar greatly overestimated the precipitation compared to the gage network estimate.

While the purpose of the hydrologic modeling was to compare radar and gage network forced streamflow simulations with gage-calibrated model parameters, it was nonetheless interesting to also visually compare both simulations to observed streamflow records for storm events. In some cases, the MAPX-forced simulations performed better than the gage-forced simulations. However, in others, either the gage-forced simulations were better or the radar-forcing produced hydrograph responses that were not seen in the observed streamflow records. More comprehensive testing should address the issue of the accuracy of stream flow simulations generated by MAPX and MAP data.

3.2 Comparison of Mean Areal Precipitation Time Series Derived from Stage III vs. the Historical Calibration Rain Gage Network

3.2.1 Introduction

As in the previous section, the study area is nine basins in the region near the Oklahoma-Arkansas-Missouri state boundaries. This region was analyzed because of its dense gage network and the availability of archived Stage 3 radar products. MAP and MAPX time series were derived for the period from May 7, 1993 through December 31, 1993. This is the period in which the historical gage and discharge data overlap with archived radar products. The gage

MAPs were calculated using both the hourly and daily gage accumulations obtained from the National Climatic Data Center's 3200 precipitation data. Appendix A shows the gage network and station weights used by the calibration precipitation preprocessor software called MAP3 which was used to calculate the historical gage MAPs for the 9 basins in the study.

Summary statistics were generated for the 1- and 6-hour case, for all nine basins, and for the entire 7-month duration of the MAP and MAPX time series. Statistics include the mean, standard deviation, and coefficient of variation, all of which are conditioned upon the occurrence of precipitation. The conditional statistics provide information about the ability of radar and gage networks to detect precipitation, as well as their ability to estimate precipitation intensity. Cumulative sums for each basin and the percent bias of accumulations from radar vs. gage networks were also tabulated.

3.2.2 Results

Tables 3-7 and 3-8 show that for the 7-month period, the Stage III MAPX cumulative totals have a negative bias ranging from -10 to -25 percent as compared to gage MAPs. This long term under catch of the MAPXs exists for both the 1- and 6-hour cases. The fact that the 6-hour conditional mean of the MAPX is larger than MAP for some basins is attributed to the spatial and temporal averaging of point gage measurements to time increments and areas where it is not raining. This produces rain for time intervals where no rain was occurring, reduces the conditional mean, and hides the actual cumulative bias that exist at the 6-hour case. MAPX is approximately 25 percent greater at detecting the temporal variability in the time series than the gage MAPs, for the 1-hour case. However, the normalized mean (coefficient of variation) shows that the temporal variability of the MAPs and MAPXs is nearly equal at the 6-hour time step. This indicates that the radar's ability to capture the temporal variability in precipitation time series at a 1-hour time step is largely lost when averaging to a 6-hour time step.

Figure 3-9 illustrates how the cumulative sum of both the MAP and MAPX time series behave over the 7-month duration for the TIFM7 basin. Only this basin is shown because all nine basins exhibited similar behavior. The figure shows how the gages and radar have different estimates of the volume and timing of individual precipitation events. Figure 3-9 also shows a plot of the cumulative differences in the MAP and MAPX time series, which highlights the timing and volume biases of individual storm events for the two rainfall measurements. Both methods appear to be similar in their estimation of event timing, but a spike appears in the cumulative difference plot when their timing is off. MAPXs have a lower accumulation even in the summer, which may be due to averaging point gage measurements over areas where it is not raining. Or, the radar may simply be underestimating precipitation rates. Radar is generally better than gage networks at estimating precipitation during high intensity convective storms because of the radar's high resolution spatial coverage (Seo and Smith, 1996; Smith et al., 1996).
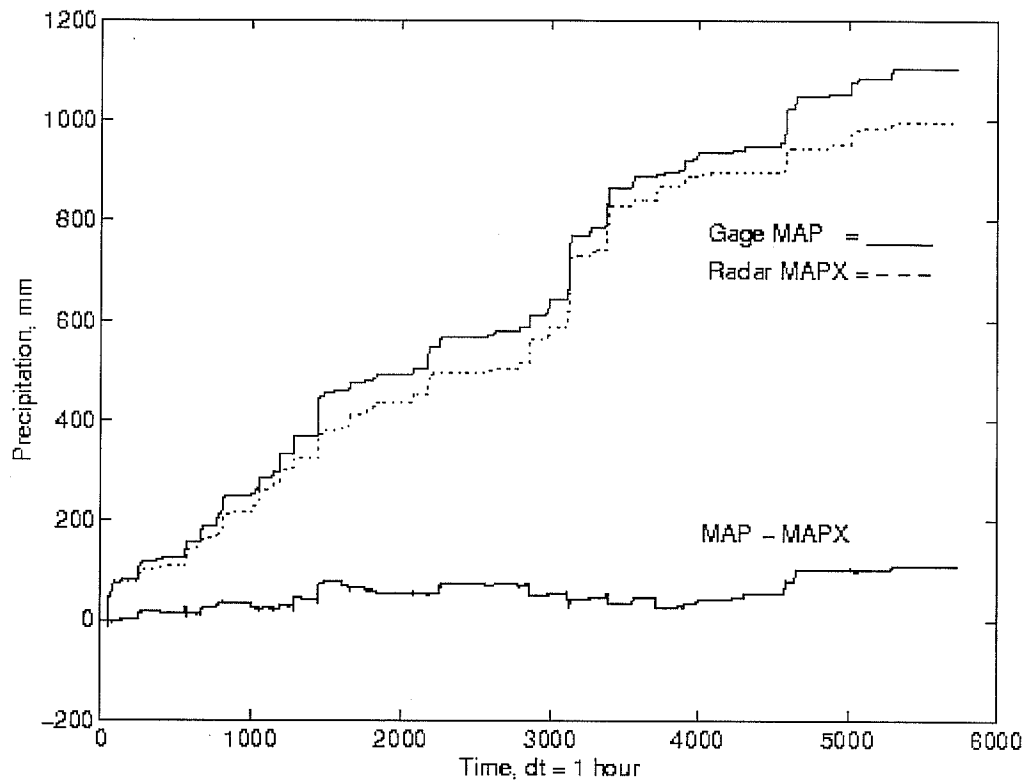
Figure 3-9 7-month cumulative sum of 1-hour MAP and MAPX time series for the TIFM7 basin. Time=0 is May 7, 1993 and time=5736 is December 31, 1993. The radar MAPX has a lower cumulative sum of precipitation for the period analyzed. The bottom of the figure shows a plot of the difference between gage and radar mean areal precipitation estimates (MAP - MAPX).

Table 3-7 - Conditional Summary Statistics for 9 Basins
Using 1-hour MAP and MAPX Time Series

Basin ID	SUM (mm)		HOURLY MEAN (mm)		HOURLY STD. DV. (mm)		COEF. of VARIATION		% BIAS of SUMS
	MAP3	MAPX	MAP3	MAPX	MAP3	MAPX	MAP3	MAPX	
JOPM7	1207	1040	2.07	1.51	3.26	3.26	1.575	2.160	-13.9
TIFM7	1104	996	1.48	1.32	2.69	2.66	1.820	2.020	-9.8
WTTO2	977	798	1.27	1.04	2.68	2.20	2.107	2.111	-18.3
KNSO2	948	837	1.50	1.41	2.67	2.83	1.782	2.000	-11.7
ELDO2	1056	930	1.51	1.34	2.55	2.90	1.680	2.176	-11.9
TALO2	933	839	1.47	1.33	2.77	3.28	1.880	2.460	-10.1
TENO2	979	784	1.62	1.18	2.85	2.90	1.755	2.460	-19.9
VBLA4	1055	798	1.73	1.07	2.99	2.29	1.730	2.128	-24.4
MLBA4	864	726	1.523	1.11	2.37	2.48	1.547	2.240	-15.9

$\%BIAS = [(MAPX - MAP)/MAP] \times 100$

Table 3-8 - Conditional Summary Statistics for 9 Basins
Using 6-hour MAP and MAPX Time Series

Basin ID	SUM (mm)		6-HOUR MEAN (mm)		6-HOUR STD. DV. (mm)		COEF. of VARIATION		% BIAS of SUMS
	MAP	MAPX	MAP	MAPX	MAP	MAPX	MAP	MAPX	
JOPM7	1207	1040	5.51	5.10	9.29	9.52	1.69	1.87	-13.9
TIFM7	1104	996	4.30	4.70	7.90	8.55	1.84	1.82	-9.8
WTTO2	977	798	3.60	3.82	6.94	6.89	1.93	1.80	-18.3
KNSO2	948	837	4.35	4.65	7.75	8.32	1.78	1.79	-11.7
ELDO2	1056	930	4.19	4.72	7.68	8.79	1.83	1.86	-11.9
TALO2	933	839	4.15	4.49	8.34	9.34	2.01	2.08	-10.1
TENO2	979	784	4.45	4.15	8.64	9.02	1.94	2.17	-19.9
VBLA4	1055	798	4.67	3.80	7.69	6.20	1.65	1.63	-24.4
MLBA4	864	726	4.23	3.65	6.58	6.77	1.56	1.85	-15.9

3.3 Consistency of Stage III MAPX Data

One of the issues for calibrating the Sacramento model is consistency of the precipitation forcing. Procedures within NWSRFS have been developed for analyzing the consistency of raingage precipitation information by creating double mass plots of the raingage data. Changes in the slope of a double mass plot may indicate a station move or other human influence that inappropriately affects the gage catch. In order for NEXRAD data to be useful for calibration, one of the criteria is that the data needs to be consistent. Changes in NEXRAD processing and increased skill on the part of the HAS forecaster may influence the 'catch' or consistency of these data.

Over 4 years of hourly MAPX data and 6-hourly MAP data for each of 9 sub basins was available for evaluation. This period of analysis spanned from June 1, 1993 through the end of July, 1997. The MAP3 calibration preprocessor was used to derive double mass plots using the following approach:

1. Each of the archived 6-hour MAP time series for the 9 basins was accumulated to create a 24-hour MAP time series. Thus, each MAP time series was used to represent a daily precipitation station.

2. Each of the archive hourly MAPX time series for the 9 basins was treated as an hourly station.

3. The 9 hourly and 9 daily time series were input to the MAP3 preprocessor as "station" data. The lat/lon coordinates of the approximate centroid of each basin were used as rain gage coordinates.

4. The 9 daily stations were flagged to constitute the group base for consistency plots. Since each of the MAP time series represents the Thiessen-weighted precipitation measurements of several point gages, the group base derived in this way represents a large, hopefully stable base.

5. No observation times were provided for the pseudo 24 hour stations.

6. The accumulation of each of the hourly MAPX time series was plotted against the accumulation of the group base. (Actually, the deviation of each station from the accumulation of the group base is plotted). The group base for the MAPX time series consists of the 9 MAP time series.

Figures 3-10 and 3-11 display the consistency plots of the MAPX data. While the plots were made using MATLAB, the format is identical to the consistency plots produced using MAP3. Positive and negative deviations from the accumulated group mean are plotted on the x axis, while the accumulation of the group mean is plotted vertically down.

These figures show quite a bit of wobble for each station. However, it must be remembered that less than 4 years of data are represented in each plot, and that the scale for such a short period
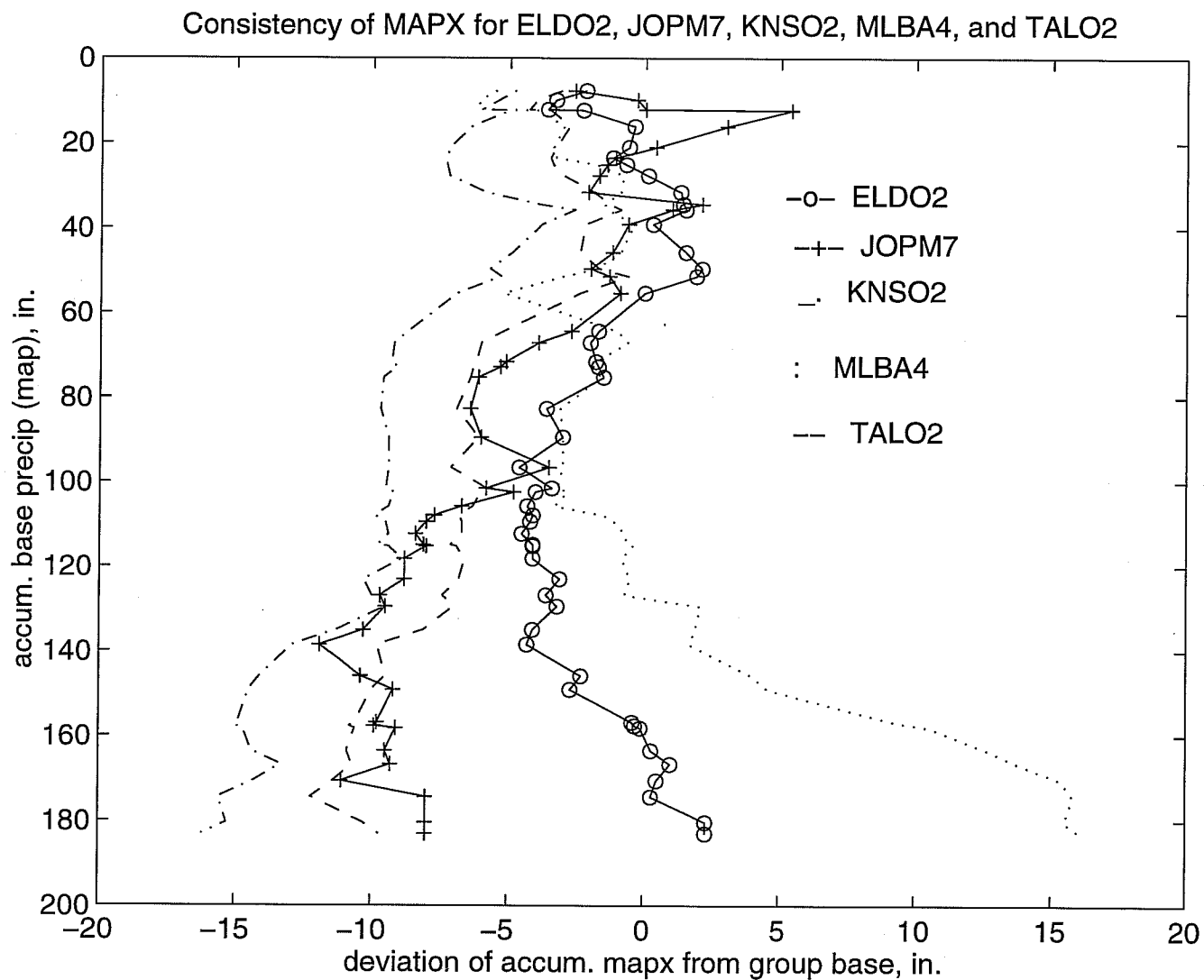
Figure   3-10   Double Mass Plots of MAPX Data for Selected Basins. Plots show deviation of station accumulation versus accumulation of the group base. Station accumulation here is accumulation of MAPX data. Group base here is comprised of the average accumulation of the MAP time series for all of the basins.
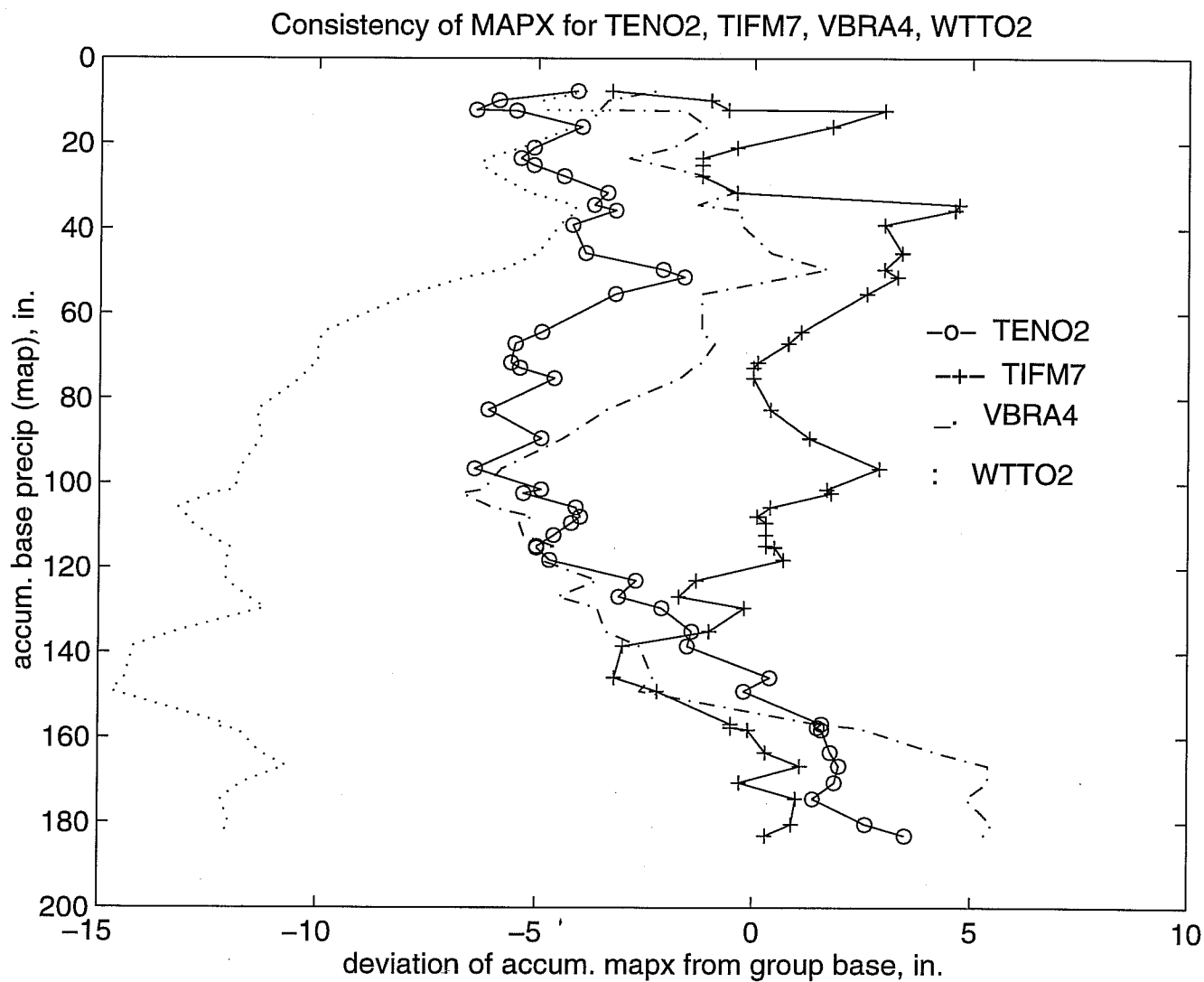
Consistency of MAPX for TENO2, TIFM7, VBRA4, WTTO2

Figure 3-11 Double Mass Plots of MAPX Data for Selected Basins. Plots
show deviation of station accumulation versus accumulation of the
group base. Station accumulation here is the accumulation of
MAPX data. Group base here is comprised of the average
accumulation of the MAP time series for all of the basins for
the corresponding time period.

may accentuate any deviations. It is not known whether these variations are significant and persistent. Usual double mass analysis involves 10 times the length of data represented here. In these two figures there is quite a bit of variation at the beginning of the plot. This may be due to the missing data in September, 1993 in which the data was lost due to a disk failure. The shortness of the analysis period makes any conclusions difficult to make. Personnel at ABRFC examined the consistency plots and could not reach definite conclusions. Figure 3.3-1 shows that basin MLBA4 displays an apparent increase in accumulation starting at a value of 100 inches. Review by Bill Lawrence in ABRFC and Eric Anderson indicated that this point might be a potential break point.

Further analysis led to the figures 3-12 through 3-20. In these figures, the deviation of the accumulated gage map from the group base is plotted with the deviation of the accumulated Stage III MAPX from the group base. For the gage map, the group base consists of the 9 MAP time series minus the gage MAP in question.

Once again, any conclusions regarding the consistency of Stage III derived MAPX time series are difficult to make. The gage MAPs for ELDO2 , WTTO2, and VBRA4 appear to be more of a straight line than the corresponding MAPX plot, indicating that the data is more consistent. For the remaining figures, it is difficult to state which data might be more consistent.
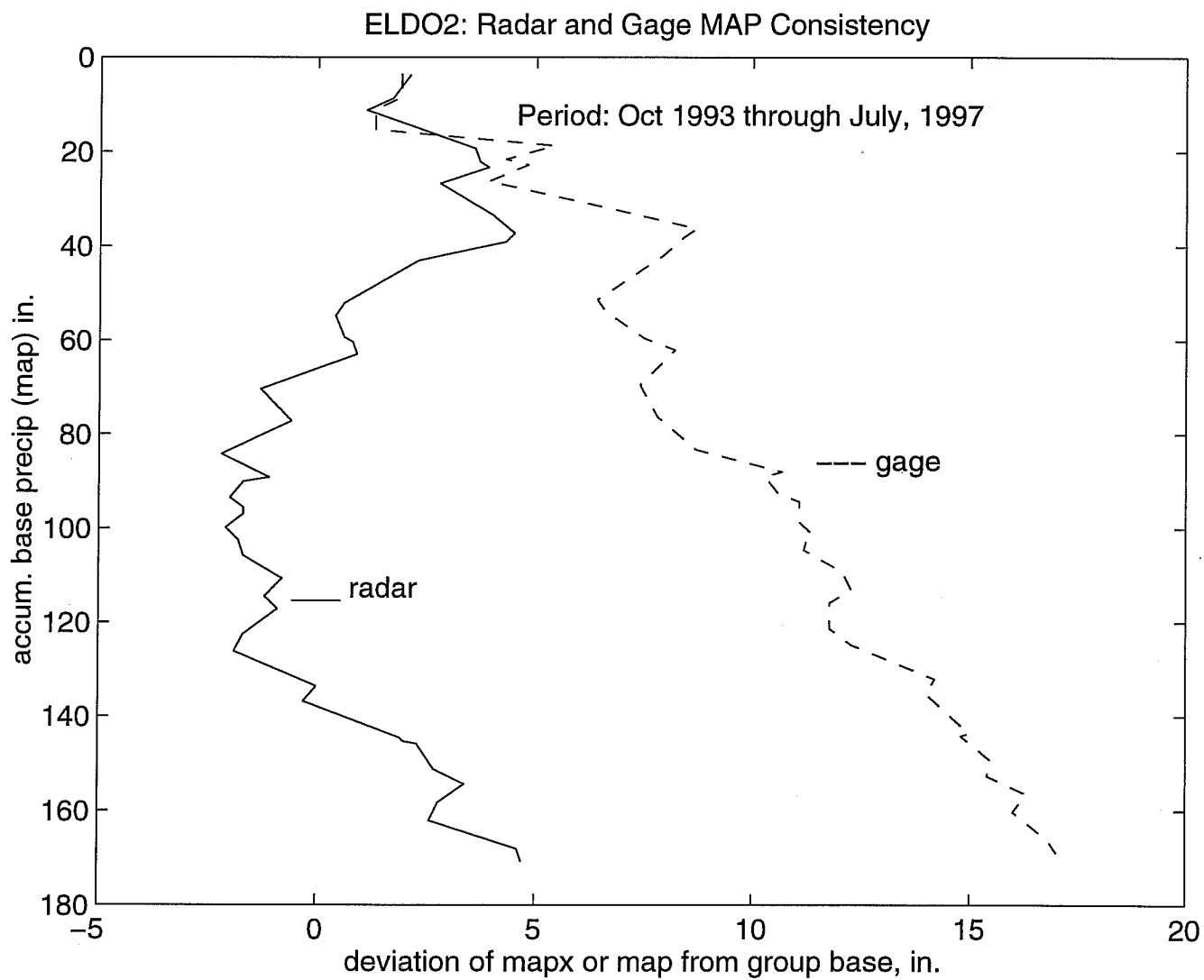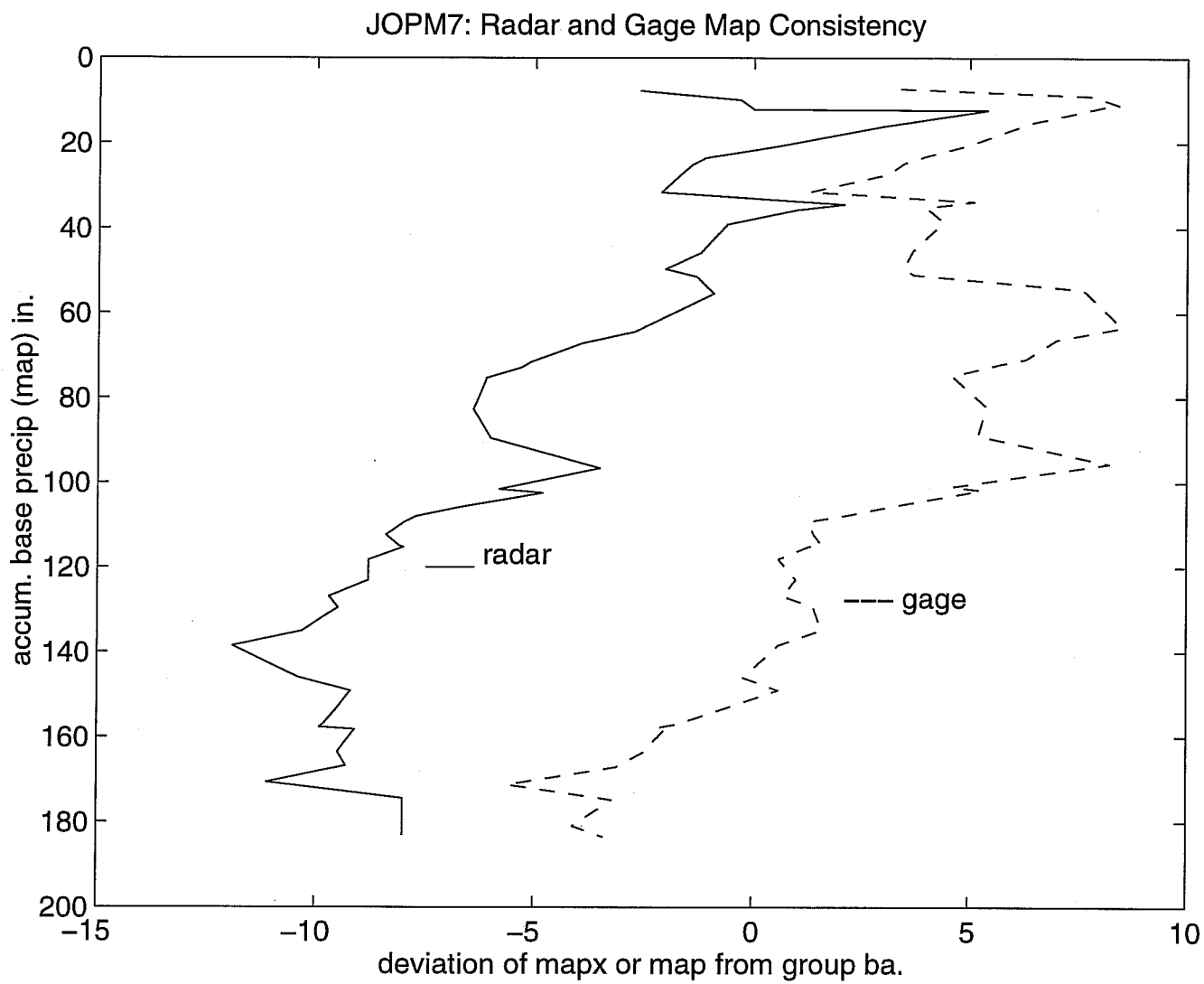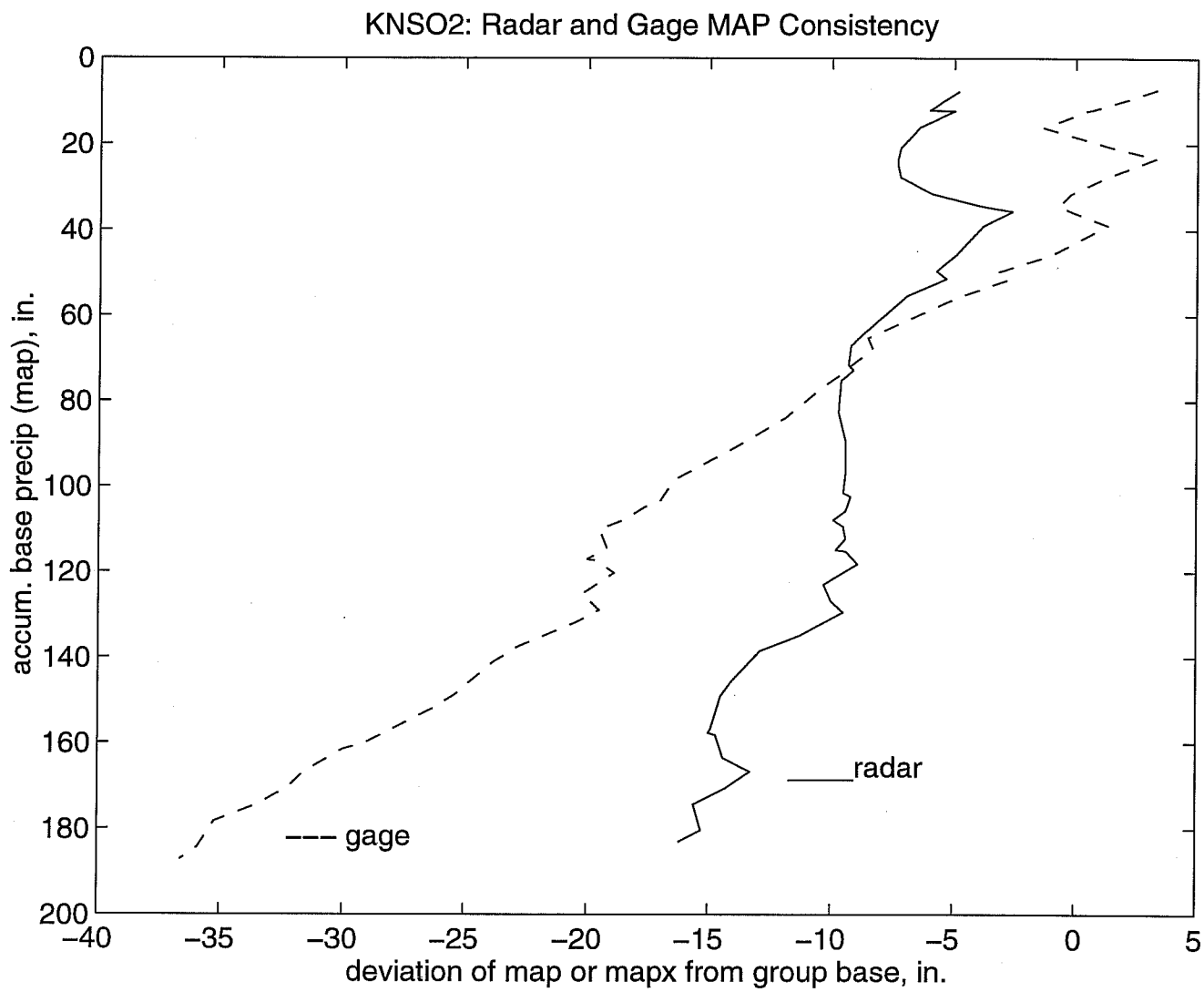
ELDO2: Radar and Gage MAP Consistency

Period: Oct 1993 through July, 1997

--- gage

radar

Figure 3-12

JOPM7: Radar and Gage Map Consistency

Figure 3-13

KNSO2: Radar and Gage MAP Consistency

accum. base precip (map), in.

deviation of map or mapx from group base, in.

— — gage

___radar

Figure 3-14

MLBA4: Radar and Gage MAP Consistency

Figure 3-15

3.33

TALO2: Radar and Gage MAP Consistency

Figure 3-16

TENO2: Radar and Gage MAP Consistency

Figure 3-17

TIFM7: Radar and Gage MAP Consistency

Period: October, 1993 through July, 1997

radar

--- gage

accum. base precip (map) in.

deviation of mapx or map from group base, in.
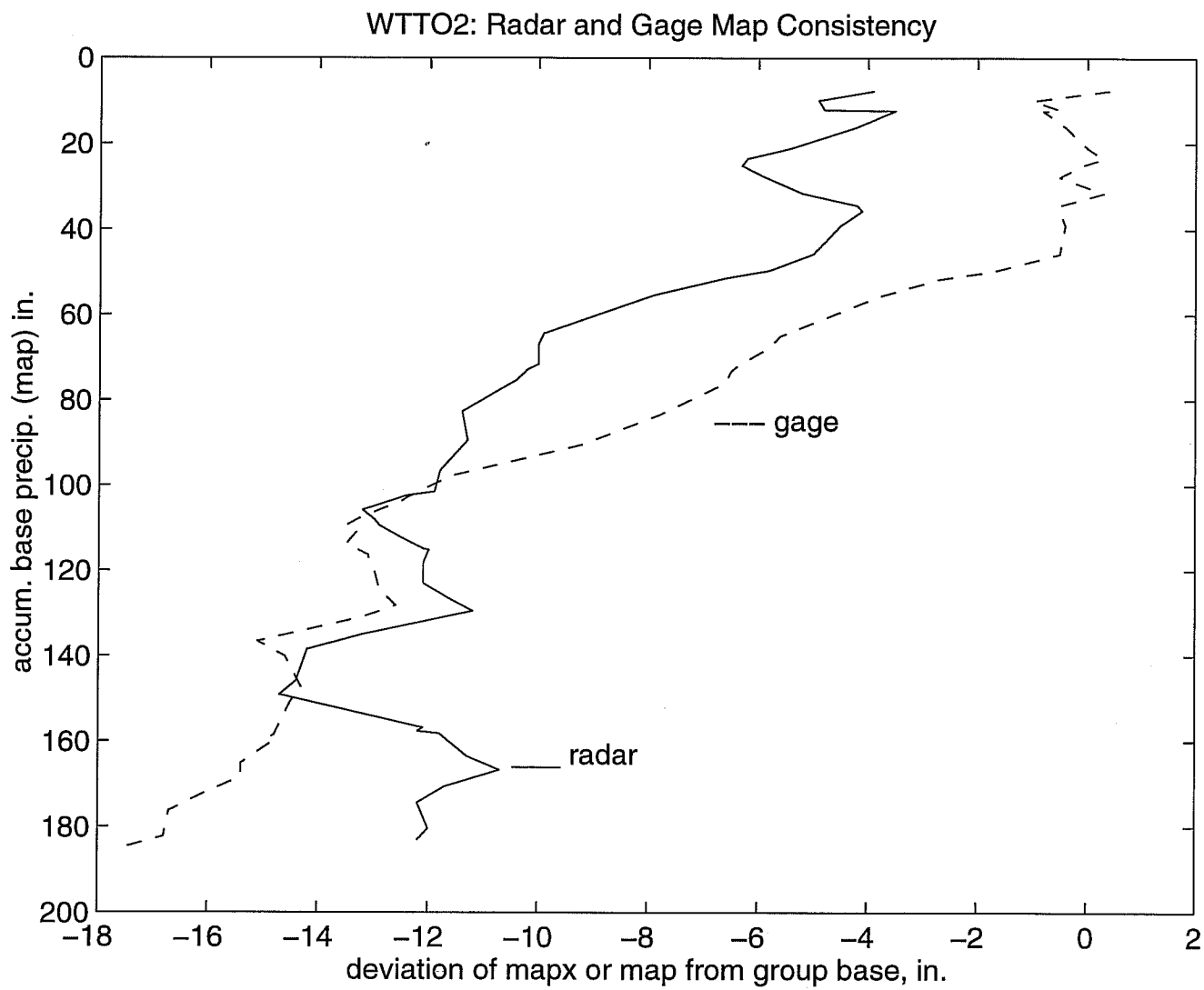
Figure 3-18
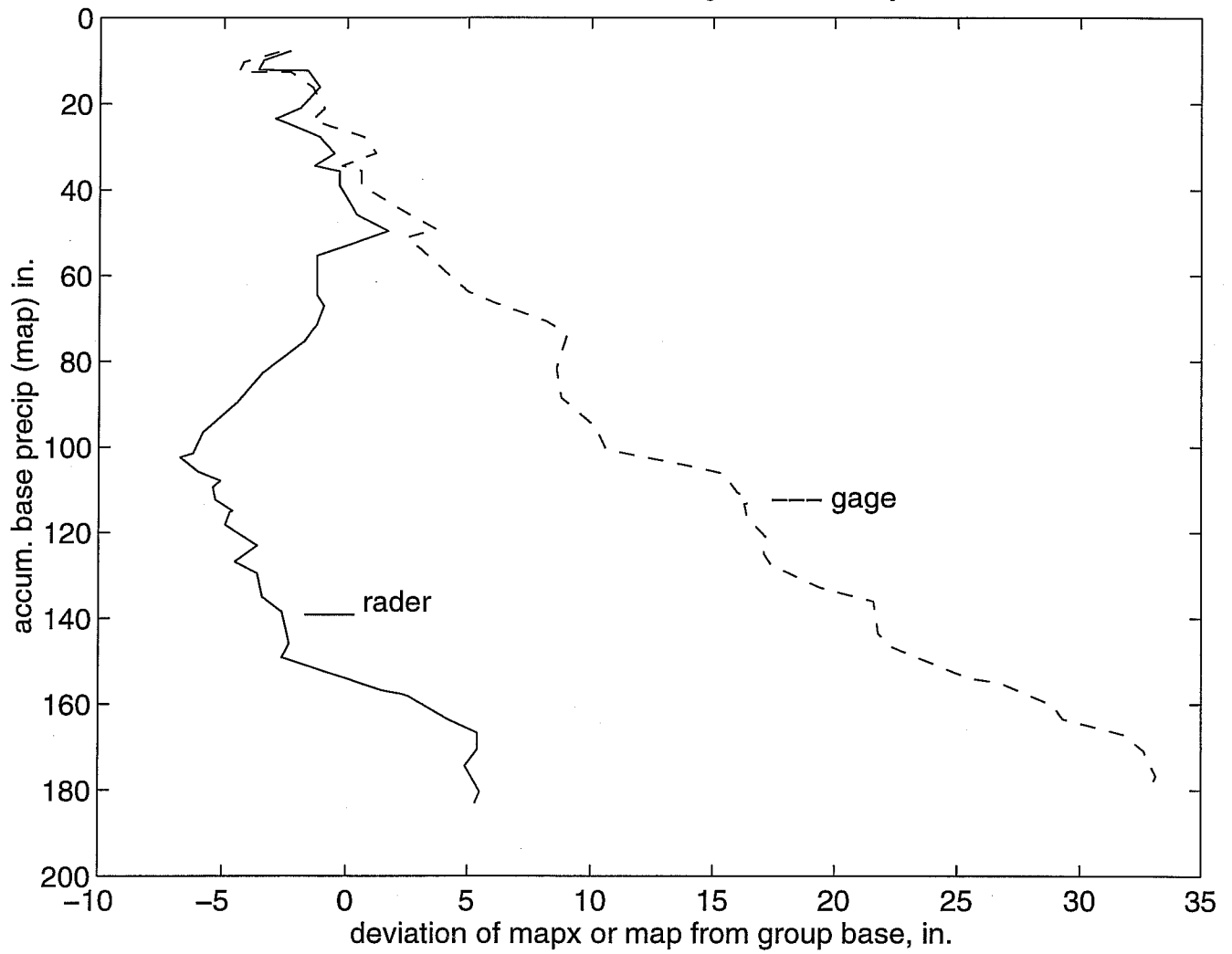
WTTO2: Radar and Gage Map Consistency

Figure 3-19

Figure 3-20

3.4 Conclusions

While much of comparison of MAPX and MAP values continues, some conclusions can be made at the present time. With regard to overall performance, the Next Generation Weather Radar system produces viable mean areal precipitation estimates. A problem of inconsistency is identified; however, the level to which these inconsistencies will affect hydrologic and climatologic models has yet to be determined.

Compared with gage only estimates of mean areal precipitation, the radar produces slightly lower values. This may effect climate and hydrologic models that rely on this data for calibration. We have shown that in the southern plains region, which has a relatively dense network of raingages and multiple overlapping radars, the radar estimates are approximately 5% to 10% lower than the gage estimates, after correction by NWS HAS forecasters. If historical gage networks are used to calibrate models, then use of the radar products may affect the model outcomes. The overall affect of this on NWS models is being investigated.

The bias appears to change throughout the year. Bright band reflectivity appears to be a contributing factor in apparently reducing the bias during certain periods of the year, thus caution should be applied when using data from months that may characterized by this climatological effect. Also, the bias appears to be decreasing (at least in Stage III products) as forecasters learn to better utilize and correct the radar. Again, it should be noted that Stage I precipitation products may also contain this bright band contamination and that Some Stage III products may have been corrected for this affect. Also, the removal of the bi-scan maximization may affect future winter results, producing some inconsistencies in the overall Stage III archives.

We have compared two operational products of the National Weather Service Tulsa River Forecast Center. Some of these products, particularly the NEXRAD precipitation products are available to the public. It is hoped that this work will provide some guidance for proper usage. Statistical differences in the MAPX and MAP time series resulted in significant impacts on streamflow simulations. Large biases can result in both runoff volumes and peak flows for certain events.

As one might expect, overall biases in runoff volumes correspond to biases in input forcing. For example, the long term MAPX/MAP ratio for basins WTTO2 and ELDO2 are 0.96 and 0.88 respectively, which lead to percent biases in the runoff volumes of 0.5 and -17.5. A percent runoff bias of 33.0 for basin KNSO2 resulted from the MAPX/MAP ratio of 1.04. Even larger monthly biases were seen in the simulations of the 3 basins. Inconsistent behavior was noted when storm events were examined. At times, the radar derived mean areal estimates of precipitation led to better streamflow simulations. At other times, the radar derived estimate led to simulated hydrograph responses that were not evident in the observed discharge records.

In comparison to MAP values derived from the historical network for model calibration, MAPX has a negative bias in the 7-month accumulations for all nine basins analyzed. The 1-hour MAPX detects more precipitation variability than the gage MAPs, but this effect was minimized when

averaging to a 6-hour time step. There are clear differences in each method's ability to estimate the timing and volume of individual events; however, no clear trend exists for all events. This suggests that hydrologic forecasting may benefit from having both measurement systems available to hydrologic forecasters, from which they can choose. Further analysis is required to evaluate what impact these differences between calibration MAPs and MAPX model inputs may have on operational hydrologic forecasting.

It is important the differences in long term means of the MAP and MAPX be resolved In the examples presented, the SAC-SMA was calibrated for 3 basins using multi-year MAP time series derived from an historical gage network. Use of these parameters may lead to sub-optimal simulations when forced with radar precipitation measurements or data from the operational gage network. It has long been assumed in the NWS that the MAP time series used for calibration are unbiased compared to MAP time series derived from the operational gage network as well as Stage III derive MAPX values. Further research should be performed to include a comparison of MAPs from the calibration network with the operational MAPX and MAP values. Additional hydrologic simulations should be performed after recalibration for use with one of the operational precipitation estimates.

Efforts are underway to enhance the bias correction algorithms in the processing of the NEXRAD data (Miller et al., 1998). Improvements to the mean field bias correction algorithm in Stage II allow for the inclusion of considerably more gage reports to be utilized in real time than the existing method by eliminating a gage-to-gage distance dependency requirement. In addition, a memory span parameter has been added to the mean field bias correction equation. A user specified value, this parameter allows the bias to consider a moving window of past gage-radar readings. (Breidenbach et al., 1998). When the memory span value is large, the bias approaches climatology. When the memory value is small, then the bias computation can respond quickly to the current sample bias.

A new procedure has been developed for the Stage II local bias adjustment as well. An optimal estimation procedure has replaced the original distance-weighted scheme for the adjustment of radar values near rain gage locations (Seo, 1997). Improvements have also been made in the estimation of rainfall values in areas covered by two or more radar umbrellas. Previously, the mean of all the estimates in the overlapping area was used. An option has been created in which the maximum rainfall value and not the mean can be used as the final value.

\

3.5 References

Barge, B.L., Humphries, R.G., Mah, S.J., and Kuhnke, W.K., 1979, 'Rainfall Measurements by Weather Radar: Applications to Hydrology', Water Resources Research, Vol. 15, No. 6, December, 1380-1386.

Battan, L.J., <u>Radar Observation of the Atmosphere</u>, University of Chicago Press, Chicago, Ill., 1973

Borga, M., Da Ros, D., Fattorelli, S., and Vizzaccaro, A., 1995, 'Influence of Various Weather Radar Correction Procedures on Mean Areal Rainfall Estimation and Rainfall-Runoff Simulation', Porceedings, 3rd International Symposium on Hydrological Applications of Weather Radar, August 20-23, Sao Paulo, Brazil, 146-157.

Breidenbach, J.P., Seo, D.J., and Fulton, R., 1998, 'Stage II and Stage III Post Processing of NEXRAD Precipitation Estimates in the Modernized Weather Service, 14th International conference on Interactive Information and Processing Systems for Meteorology, Oceanography, and Hydrology, 78th Annual Meeting of the American Meteorological Society, Phoenix, Arizona, Jan 11-16, 263-265.

Burnash, R.J.C., 1995, 'The NWS River Forecast system - Catchment Modeling", <u>Computer Models of Watershed Hydrology</u>, Chapter 10, Singh, V.P, editor, Water Resources Publications

Burnash, R.J.C., Ferral, R.L. and McGuire, R.A., 1973, A Generalized Streamflow Simulation System - Conceptual Modeling For Digital Computers', U.S. Department of Commerce, National Weather Service and State of California, Dept. Of Water Resources, March.

Collier, C.G., Harrold, T.W., and Nicholass, C.A., 1975, 'A Comparison of Areal Rainfall as Measured by a Raingauge-Calibrated Radar System and Raingauge Networks of Various Densities', Proceedings, 16th Radar Meteorology Conference, American Meteorological Society, 22-24 April, Houston, Texas, 467-472.

Finnerty, B.D, Smith, M.B., Koren, V., Seo, D.J., and Moglen, G., 1997, 'Space-Time Scale Sensitivity of the Sacramento Model to Radar-Gage Precipitation Inputs', Journal of Hydrology, in press.

Finnerty and Johnson, 1997, 'Comparison of National Weather Service Operational Mean Areal Precipitation Estimates Derived from NEXRAD Radar vs. Raingage Networks', to be presented at the International Association of Hydraulic Research (IAHR) XXVII Congress, San Francisco, Ca. August 10-15, 1997.3.41

Fulton, R.A., Briedenbach, J.P., Seo, D.J., Miller, D.A., and 0'Bannon, T., 1997, 'The WSR-88D Rainfall Algorithm', accepted for publication in Weather and Forecasting.

Goodhew, R., and Mylne, M, 1992, 'Measurement of Areal Rainfall by an Operational Radar at Medium Range', paper H2, Proceedings of 2nd International Symposium on Hydrological Applications of Weather Radar, University of Hannover, 7-10 September.

Holmes, M. 1995, 'Comparison of WSR-88D Precipitation Estimates with Gage Data for Phoenix, Arizona and Boise, Idaho', Western Region Technical Publication No. 95-30, National Weather Service Western Region Headquarters, Salt Lake City, Utah. (Also on www.wrh.noaa.gov)

Hopper, S.E., Illingworth, A.J., and Caylor, I.J., 'Bright-band errors in rainfall measurement: Identification and correction using linearly polarized radar returns', Hydrological Applications of Weather Radar, I.D. Cluckie, and C.G. Collier, editors, Ellis Horwood Series in Environmental Management, Science and Technology, 240-249, 1991.

Greene, D. R., and Hudlow, M.D., 1982, 'Hydrometeorological Grid Mapping Procedures,' AWRA International Symposium on Hydrometeorology, Denver, Colorado, June 13-17.

Klazura, G.E., and Imy, D.A., 1993, 'A description of the initial set of analysis products available from the NEXRAD WSR-88D System', Bulletin of the American Meteorological Society, 74, July

Kull, D.W, and Feldman, A.D., 1998, 'Evolution of Clark's Unit Graph Method to spatially Distributed Runoff', Journal of Hydrologic Engineering, Vol. 3, No. 1, January, 9-19.

Miller, D,. Seo, D.J., Breidenbach, J.P., and Fulton, R., 1998, '+
Evolution of the NEXRAD Precipitation Processing System (PPS) in the Open Systems ERA', 14th International conference on Interactive Information and Processing Systems for Meteorology, Oceanography, and Hydrology, 78th Annual Meeting of the American Meteorological Society, Phoenix, Arizona, Jan 11-16, 259-262

National Weather Service, 1993, 'OFS MAP Preprocessor Function', National Weather Service River Forecast System User's Manual, November.

Seo, D.J., 1997, 'Optimal Estimation of Rainfall Fields Using Radar Rainfall and Rain Gage Data', submitted to Journal of Hydrology.

Seo, D.J., Fulton, R., Breidenbach, J.P., Miller, D., and Friend, E., 1995, 'Final Report for October 1, 1993 to October 31, 1994', Interagency Memorandum of Understanding Among the NEXRAD Program, WSR-88D Operational Support Facility, and the National Weather Service Office of Hydrology, Hydrologic Research Lab.

Seo, D.J., and Johnson, E.R., 1995, 'The WSR-88D Precipitation Processing Subsystem- An Overview and a Performance Evaluation', Proceedings, 3rd International Symposium on Hydrological Applications of Weather Radar, August 20-23, Sao Paulo, Brazil, 222-231.

Seo, D.J., and Smith, J.A., 1996. Characterization of climatological variability of mean areal rainfall through fractional coverage. Water Resources Research, 33(7): 2087-2095.

Shedd, R.C., and Fulton, R.A., 1993, 'WSR-88D Precipitation Processing and its use in the National Weather Service Hydrologic Forecasting', Proceedings of ASCE Intl. Symposium on Engineering Hydrology, San Francisco, Ca. July 25-30.

Shedd, R.C., and Smith, J.A., 1991. Interactive precipitation processing for the modernized National Weather Service. Preprints, Seventh International Conference on Interactive Information and Processing Systems for Meteorology, Oceanography, and Hydrology, New Orleans, Louisiana, American Meteorological Society, pp. 320-323.

Smith, J.A., and Krajewski, W., 1994, 'Final Report - Estimation of Parameters for the NEXRAD Rainfall Algorithms', Submitted to NOAA National Weather Service, Office of Hydrology - Hydrologic Research Lab.

Smith, J.A., Baeck, M.L., and Steiner, M., 1997, 'Final Report: Hydrometeorological Assessments of the NEXRAD Rainfall Algorithms', submitted to NOAA, National Weather Service, Office of Hydrology, Hydrologic Research Laboratory, by the Dept. of Civil Engineering, Princeton University.

Smith, P.L., Cain, D.E., and Dennis, A.S., 1975, 'Derivation of an R-Z Relationship by Computer Optimization and its use in Measuring Daily Areal Rainfall', Proceedings, 16th Radar Meteorology Conference, American Meteorological Society, 22-24 April, Houston, Texas.

Smith, J.A., Seo, D.J., Baeck, M.L., and Hudlow, M., 1996, 'An intercomparison study of NEXRAD precipitation estimates', Water Resources Research, Vol. 32, No. 7, 2035-2045.

4. Numerical Experiments on the Sensitivity of Runoff to Level of Basin Disaggregation

4.1 Introduction

Sensitivity analyses using high resolution radar precipitation estimates in Chapter 2 pointed out that the Sacramento Soil Moisture Accounting Model (SAC-SMA) is sensitive to spatial scale. The fast runoff components, especially surface runoff, may be underestimated significantly if the model is calibrated at one scale and is applied to an other scale. Hillslope/Channel routing processes can also introduce discrepancies in an outlet hydrograph. To account for the spatial variability of rainfall and to reduce scale dependency, a semi-distributed approach is proposed here. However, a strategy of disaggregating a basin into an optimum number of sub-basins is not well defined.

Numerical experiments were conducted to get a quantitative estimate of simulated hydrograph sensitivity to sub-basin area. The SAC-SMA model was used to estimate the water balance components including total channel inflow. A linear distributed hillslope/channel routing reservoir type model (Koren and Barrett, 1994) was used to route total channel inflow through hillslope/channel reservoirs. It was assumed that the SAC-SMA and routing model parameters are uniformly distributed over the test area. The test area was located in the Red River basin over the Oklahoma-Arkansas border the eastern portion of the Tulsa RFC, Oklahoma. Input to the SAC-SMA model was gridded hourly precipitation estimated by NEXRAD with a resolution of approximately 4x4 km and monthly climatological potential evaporation averaged over the entire test area. The NEXRAD data set spans a 3 year period from May 7, 1993 through July 31, 1996. Nine headwater basins with areas from 329 km^2 to 4200 km^2 were selected for this study.

4.2. Disaggregation of Basins into Sub-basins

Software was developed to disaggregate a basin into a number of sub-basins based on the stream channel structure (cell-to-cell connectivity). The test area was gridded into rectilinear cells of approximately 4x4 km in size (HRAP projection), which match those of radar rainfall data. The connectivity of each grid cell was determined based on both digitized stream network and 30 arc second elevation data. As a result of this analysis, the connectivity file was created that consists of HRAP coordinates of each grid cell and a sequence number of the next connected grid cell.

Any basin defined in the connectivity file can be broken down into a number of sub-basins depending on a user-specified sub-basin threshold area. Sub-basin areas will vary around the desired area, and will depend on the stream channel topology.

4.3. Routing of Total Channel Inflow

Output from the SAC-SMA model, total channel inflow (TCI), was routed through the

connected grid cell network using a linear reservoir-type model. It is assumed that each grid cell consists of two reservoirs: a hillslope reservoir and a channel reservoir. The hillslope reservoir is the source of water for the 'main' grid channel reservoir. It is also assumed that all total channel inflow of a pixel reaches the 'main' channel reservoir of that pixel. The 'main' channel is the only source of water exchange between neighboring pixels. A linear reservoir routing model is used to route runoff within each cell to the stream (hillslope routing), and to move water from one grid cell to another (channel routing). Two parameters have to be defined to run the model: hillslope and channel reservoir lag times. In this study these parameters were estimated based on an existing unit hydrograph at the headwater basin outlet and the channel connectivity. The output of the routing can be a hydrograph at the outlet of any grid cell.

4.4. Numerical Experiment Description

Each headwater basin was disaggregated into a number of sub-basins for seven defined simulation scales based on threshold areas, as shown in Table 4-1.

Table 4-1. Sub-basin definition at different scales for the selected headwater basins in Tulsa RFC

Basin ID	Sub-basin threshold area, sq.km															
	60		100		150		250		350		500		800		Lumped	
	Mean area	No.	Mean area	No.	Mean area	No.	Mean area	No.	Mean area	No.	Mean area	No.	Mean area	No.	Mean area	No.
KNSO2	66	5	164	2											329	1
ELDO2	68	12	102	8	164	5	273	3	410	2					819	1
MLBA4	70	13	102	9	152	6	229	4	305	3	457	2			914	1
VBLA4	60	19	104	11	143	8	228	5	381	3	571	2			1142	1
JOPM7	66	18	99	12	148	8	296	4	394	3	592	2			1183	1
BMTA4	76	16	110	11	173	7	242	5	403	3	605	2			1210	1
WTTO2	73	22	107	15	161	10	268	6	403	4	537	3	805	2	1611	1
TIFM7	68	32	104	21	156	14	243	9	438	5	547	4	729	3	2188	1
TENO2			120	35			280	20	420	10					4200	1
Mean	68		112		158		257		394		552		817		1510	

Note: No. is a number of sub-basins in a headwater basin.

Two types of the numerical experiments were conducted at each simulation scale: 1) Rainfall averaging when the SAC-SMA input, rainfall, was averaged over each sub-basin, and 2) TCI averaging when the SAC-SMA output, total channel inflow (TCI), was averaged over each sub-basin.

Rainfall averaging was used in the combined study of water balance and routing process scale dependency. Simulations were performed for different sets of sub-basin definition, Table 4-1, from one lumped basin to 40-50 sub-basins with average area of 60 km². The SAC-SMA model was run for each sub-basin using rainfall averaged over that sub-basin. Output of the SAC-SMA model, total channel inflow (TCI), was disaggregated uniformly into NEXRAD grid resolution for input to the linear distributed routing scheme. The routing scheme was operated at the same scale, which was the radar pixel size, for all of the numerical experiments. Volumes of TCI from the SAC-SMA model can be different at each sub-basin scale depending on rainfall variability.

A second series of numerical experiments were conducted to estimate the routing contribution to scale dependency separately from runoff volume effects. To do this, the finest resolution SAC-SMA TCI output was averaged over different sets of sub-basin areas. Spatially averaged sub-basin TCI was then disaggregated uniformly into NEXRAD grid resolution for input to the linear distributed routing scheme. These experiments are referred to as "TCI Averaging" experiments. These experiments produce differences in the hydrograph shape at different sub-basin scales without changing the total runoff volume over the total headwater basin.

4.5. Results and Discussion

For each set of numerical experiments, simulated hydrographs from selected headwater basins, $X_{i,k}$, were compared to a reference hydrograph, $X_{i,fine}$, which was the hydrograph from the run at the finest grid resolution. Mean square differences, RMS, were calculated using Equation 4-1:

$$RMS_x = \sqrt{\frac{\sum_{i=1}^{N}(X_{i,k}-X_{i,fine})^2}{N}} \qquad (4-1)$$

where N is the number of data pairs, k is the scale identifier, and x is the type of statistic. RMS statistics were calculated using both hourly discharges and peak flow volumes. Peak flow volume was defined as a total runoff of hydrograph above 50% of the maximum discharge of a flood even as depicted in Figure 4-1 and in Equation 4-2:

$$V_k = \int_{t}^{t_2} \max[(Q_k(t) - \frac{Q_{ref,max}}{2}),0]\,dt \qquad (4-2)$$

4.3

where V_k is the volume in the reference hydrograph, Qref is the discharge of the reference hydrograph at time t, and $Q_{ref,max}$ is the maximum discharge of the reference hydrograph for the event.
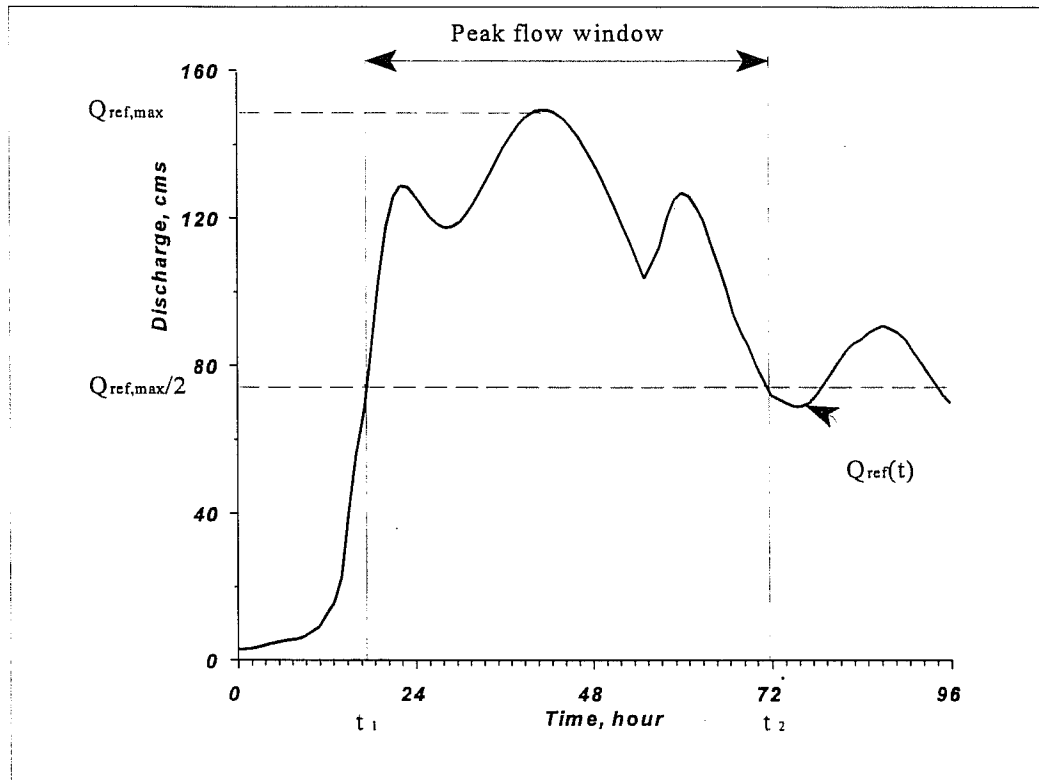

Figure 4-1 Schematic of the peak flow definition

4.5.1. Hourly discharge statistics.

Examination of the results revealed that mean square differences of hourly discharges usually increased with increasing size of sub-basin for the both Rainfall and TCI averaging experiments. Similarly, mean square differences of hourly discharges also increased with increasing size of a total headwater basin area when the basin was modeled as a lumped basin. However, differences in lumped model results for different total basin sizes can be larger than mean square differences depending on the sub-basin scale. Relative differences of a lumped run compared to the finest resolution run were in the range of 10-30% of the variability (i.e. STD) of hourly discharges.. The routing contribution (percent of *RMS* of TCI averaging experiments as compared to the *RMS* of Rainfall averaging experiments) we define as the Routing Ratio, and can be as much as 70% for the largest basin as seen in Figure 4-2. Although there is a tendency of increasing the routing contribution with increasing headwater basin area, there is no strong correlation. Other factors, such as the basin shape, channel network configuration or rainfall patterns, can contribute significantly to this dependency.
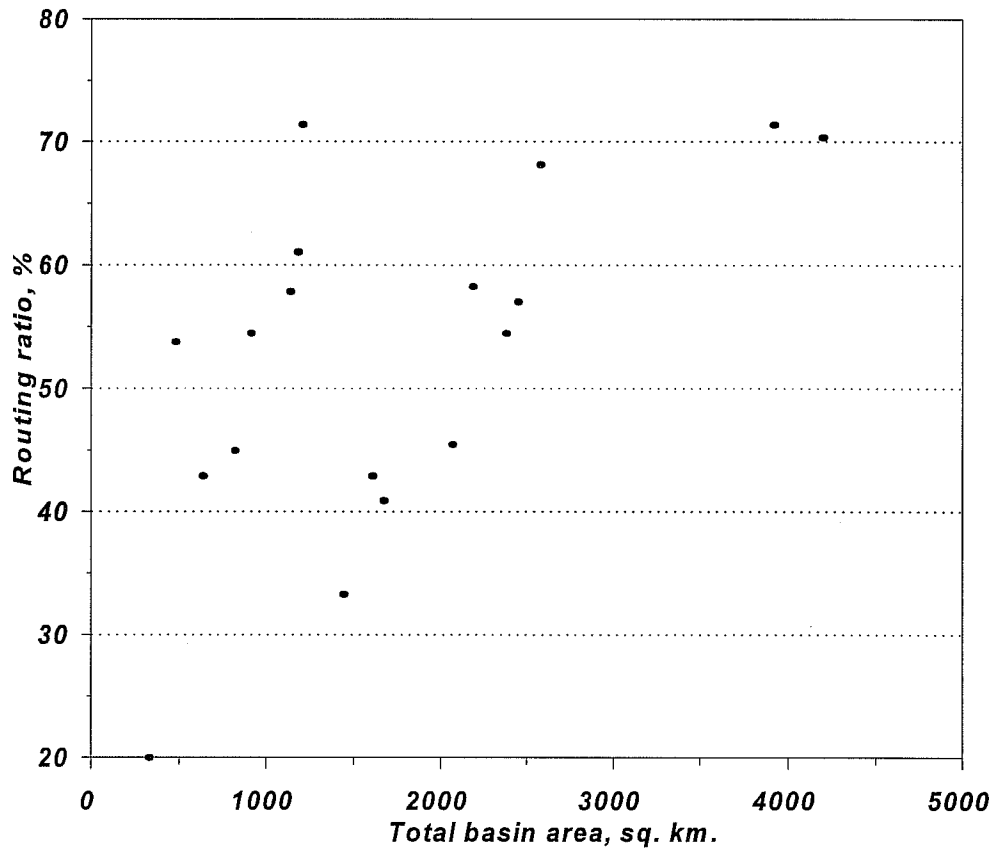
Figure 4-2. Routing contribution to the total mean square difference of hourly discharges for different basin areas, Tulsa RFC.

4.5.2. Peak flow statistics.

Examination of the results shows that the RMS statistic for peak flow volumes reflects a stronger water balance scale dependency. In addition to the mean square difference of the peak flow, *RMS*, a relative mean square difference, E_{STD}, was calculated as a ratio of the peak flow variance, *STD* of the reference hydrograph. The statistics were calculated for the Rainfall and TCI averaging

experiments. In both sets of numerical experiments, the Rainfall or TCI averaging lead to the reduction in peak flow.

The numerical experiment results indicate that it is important to consider two different aspects of scale when comparing hydrographs. These is the size of the sub-basins on one hand and the size of the total basin area on the other. The increase of the sub-basin size leads to the increase in relative peak flow differences compared to the finest resolution for both the Rainfall and TCI averaging cases. In contrast, the increase of the total headwater basin area leads to the decrease in relative peak flow differences, especially for the Rainfall averaging as seen in Figure 4-3. Although the TCI averaging is less sensitive to the total basin area, relative differences vary much from basin to basin, as seen in Figure 4-4.

It was possible to normalize peak volume differences to exclude the scale dependency on the total basin size. Mean square peak flow differences at each sub-basin scale k, RMS_k, were normalized by the peak flow difference at the total basin area (lumped basin), RMS_0, for each headwater basin

$$E_k = \frac{RMS_k}{RMS_0} \tag{4-3}$$

These values were plotted against a relative scale index calculated as the ratio of the total headwater basin area, A, to the sub-basin area, A_k. Figures 4-5 and 4-6 display these plots for the Rainfall and TCI averaging experiments. As expected, Rainfall averaging is more scale dependent. Fifty percent differences in the peak flow can be seen up to the scale index equals 10, i.e. a lumped basin was subdivided into 10 sub-basins. The same level of differences for the TCI averaging occurred only at scale index of 3-4. It is important that the relative mean square error does not vary much in a wide range of total basin areas (from 329 km^2 to 4200 km^2). A strong correlation exists between the normalized peak volume differences and the relative sub-basin scale, Figures 4-5 and 4-6. Equations 4-4 and 4-5 were derived for the Rainfall and TCI averaging, respectively

Rainfall averaging

$$E_k = \left(\frac{A}{A_k}\right)^{-0.38} \tag{4-4}$$

TCI averaging

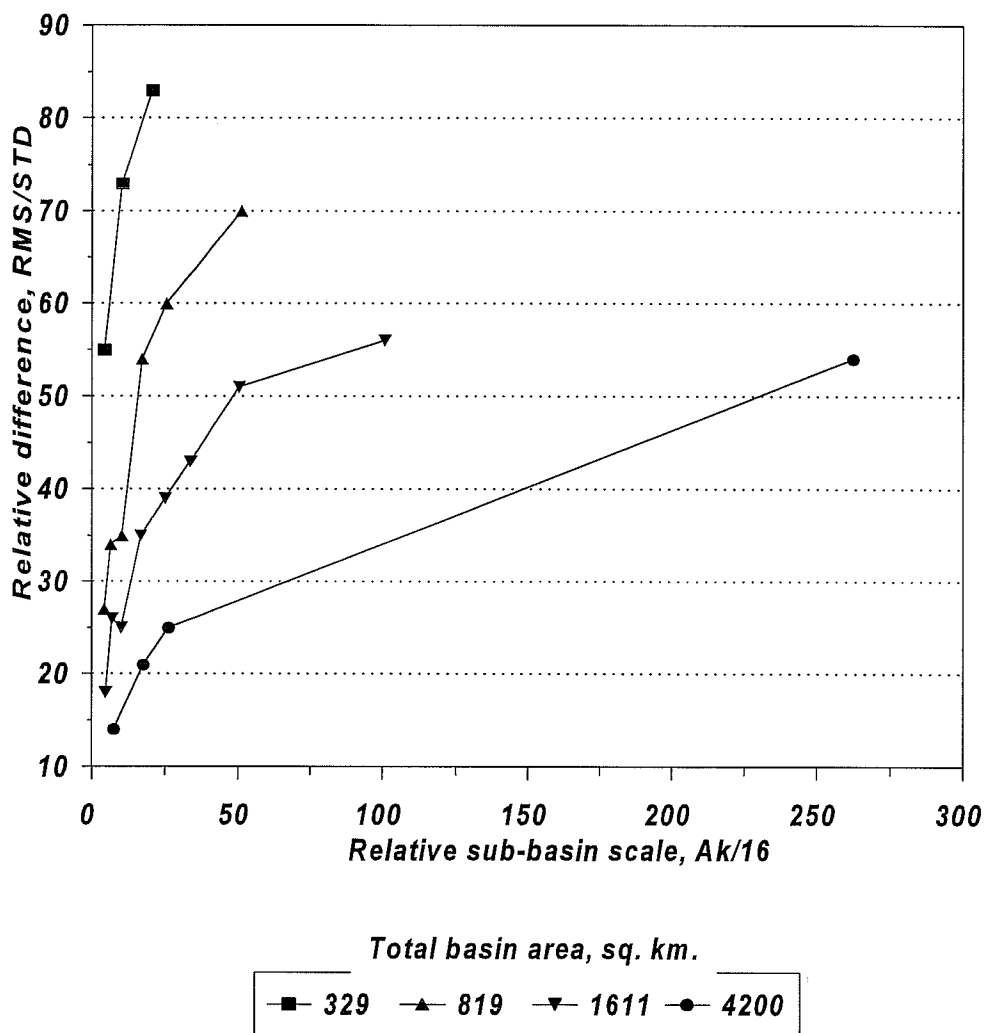$$E_k = \left(\frac{A}{A_k}\right)^{-0.965} \tag{4-5}$$

Figure 4-3. Peak flow differences compared to the finest scale at different sub-basin and total basin areas: Case of Rainfall averaging.
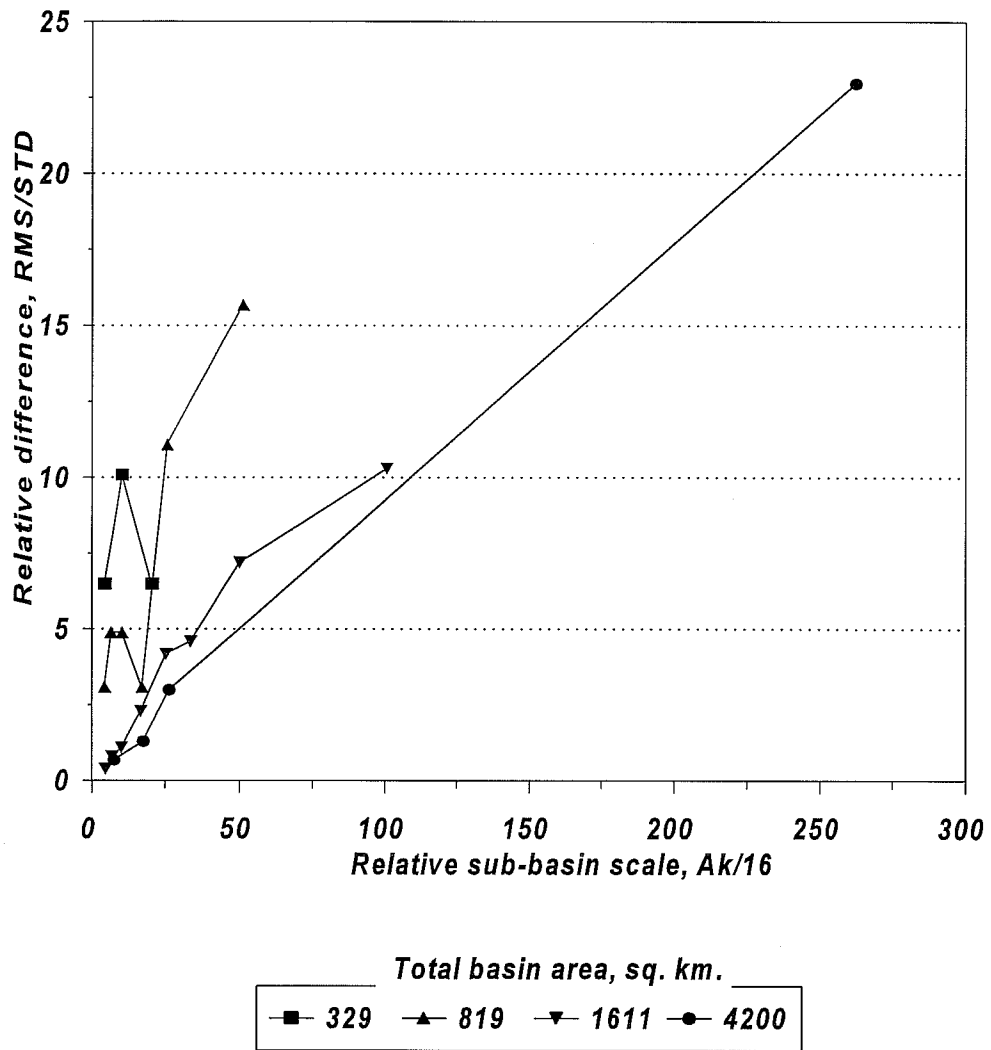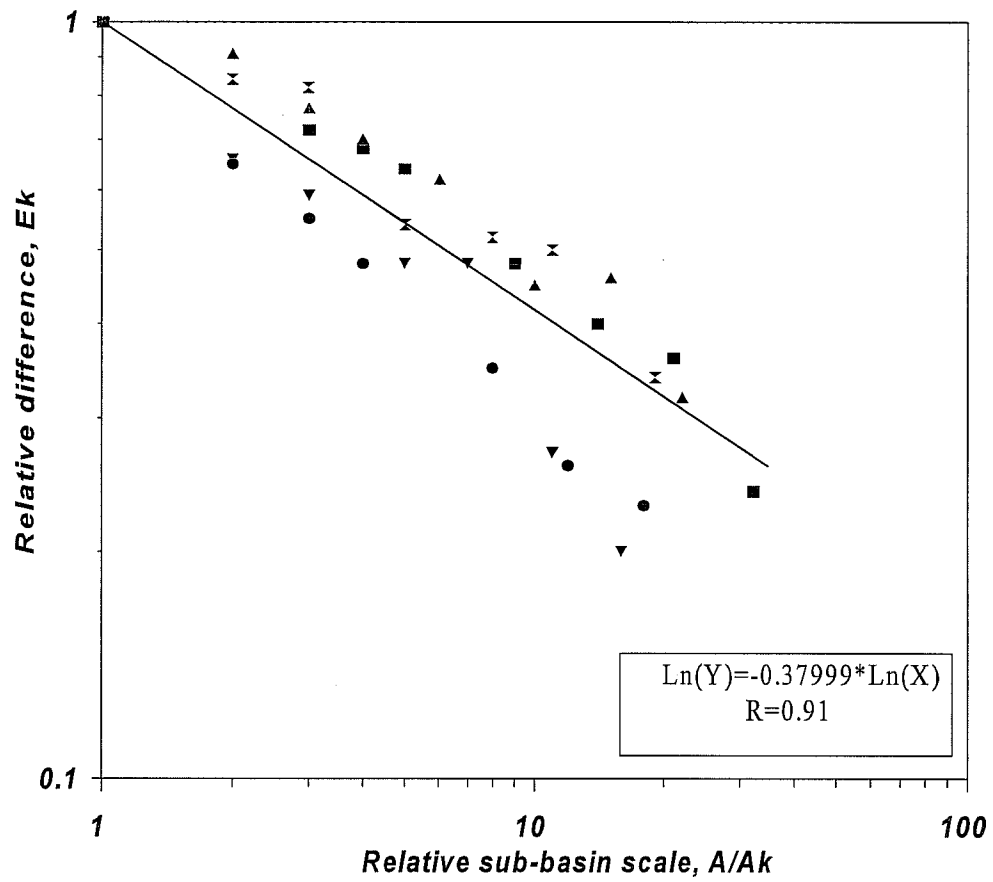
Figure 4-4. Peak flow differences compared to the finest scale at different sub-basin and total basin areas: Case of TCI averaging.

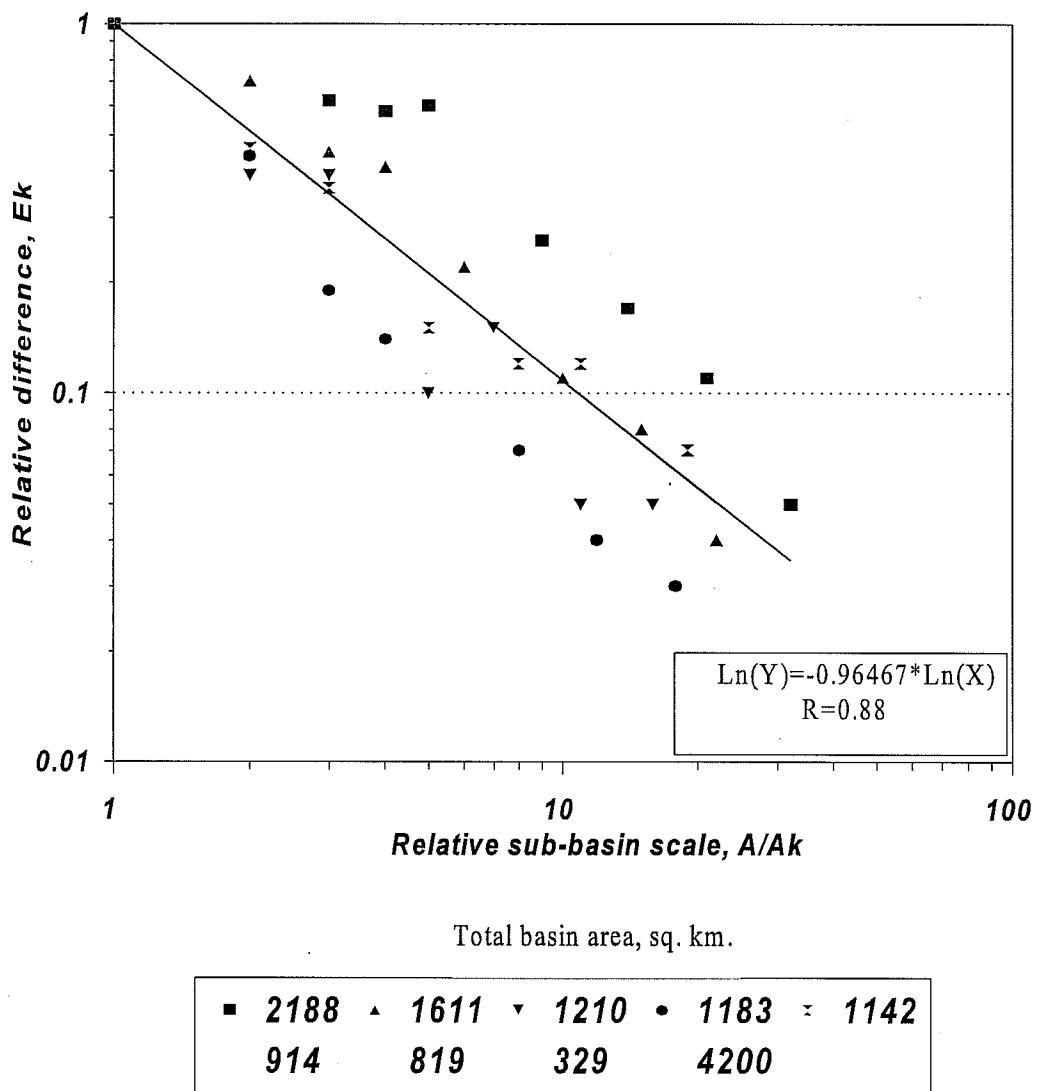Figure 4-5. Scale dependency of peak volumes for different headwater basins: Case of Rainfall averaging.

Figure 4-6. Scale dependency of peak volumes for different headwater basins: Case of Runoff averaging.

The theoretical basis of this type of scale dependency was presented by Gupta and Waymire (1990) to describe statistical properties of spatial rainfall and river flow distributions at different scales. Simple reformulation of the Equations 4-1 and 4-2 leads to the relationship between mean square differences of the peak flow at different scales:

$$RMS_{k+n} = RMS_k \left(\frac{A_k}{A_{k+n}}\right)^\alpha \qquad (4\text{-}6)$$

where it is assumed that sub-basin area decreases with increasing n. Equations (4-3) through (4-5) can be used to estimate relative differences of the peak flows simulated using different scales for the water balance and routing simulations. The numerical experiments present a potential advantage of basin subdivision. However, the real benefit can be smaller depending on the level of uncertainties in input/output data, the model structure, and the model parameter spatial variability.

The above numerical experiments did not account for noise in input data, specifically in rainfall information. Noisy input can eliminate any benefit realized by basin. The relative peak flow differences simulated using noisy rainfall are plotted versus the simulation scale in Figure 4-7 for one of the headwater basins. Unbiased noise from Gaussian distribution was applied to pixel rainfall values. Spatially non-correlated random noise of 25, 50 and 75 percent of a basin mean rainfall was generated in the analysis. Figure 4-7 indicates that the finest resolution run is very sensitive to the noise in rainfall. Differences in the peak flow at this scale using noisy data can be greater than differences at lower resolutions. When a high level noise was applied to each pixel, the finest resolution run gave bigger differences compared to the reference peak flow than a lumped run. However, small spatial averaging of noisy rainfall (e.g. four pixels) leads to very fast reduction in the effect of noise. As a result, all sub-basin scales bigger than one pixel size gave smaller differences in the peak flow than a lumped run.

4.6 Conclusions

Relative differences of hydrographs simulated by lumped and the finest resolution (16 sq. km.) were in the range of 10-30% on the basin areas from 400 sq. km. to 4200 sq. km. The routing contribution can be as much as 70% for the largest basin. Although there is a tendency of increasing the routing contribution with increasing headwater basin area, there is no strong correlation. Other factors, such as the basin shape, channel network configuration or rainfall patterns, can contribute significantly to this dependency.

Because of the big contribution of the routing, it is very important to account for the differences in routing from different areas of a basin. Using just a lumped unit hydrograph can eliminate benefit of the semi-distributed approach of the water balance calculations.

It is important to consider two different aspects of the scale when comparing hydrographs. These are the size of the sub-basins on one hand and the size of the total basin area on the other. The
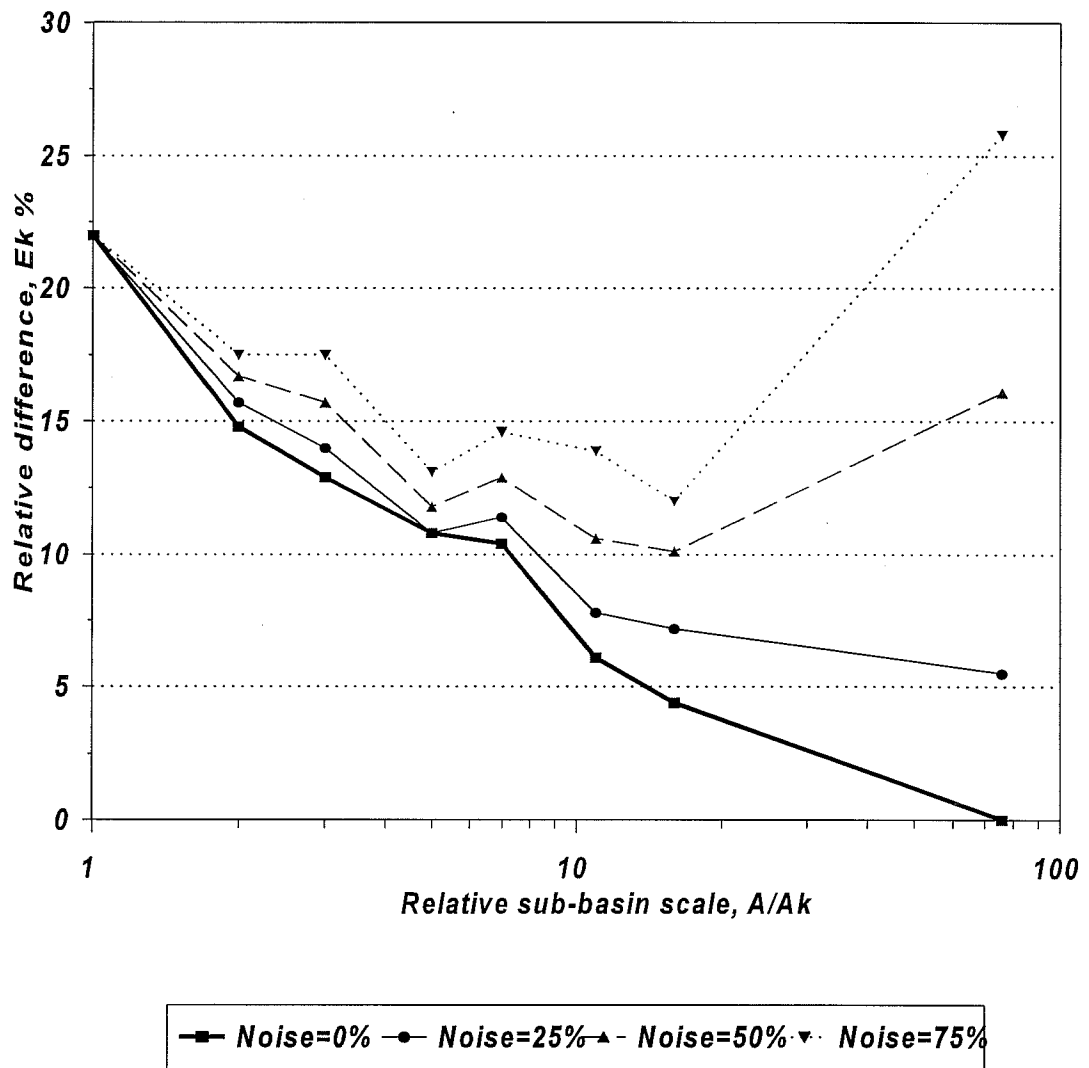
Figure 4-7. Effect of noisy rainfall on the peak volume at different sib-basin scales, BMTA4 basin, area 1210 sq. km.

increase of the sub-basin size leads to the increase in relative peak flow differences compared to the finest resolution for both the Rainfall and TCI averaging. In contrast, the increase of the total headwater basin area leads to the decrease in relative peak flow differences, especially for the Rainfall averaging.

The relationship between scale and peak flow volumes can be used for a rough estimate of the sub-basin size to account for the spatial variability of rainfall.

The numerical results indicate that some improvement in simulation capability can be realized by disaggregating basins. However, tests indicate that finer scale simulations are more sensitive to noise in the precipitation data. It agrees with results obtained by Kouwen and Garland (1989). Differences in the peak flow at the finest scale, 4x4 km, using noisy data can be greater than differences at coarser resolutions. However, small spatial averaging of noisy rainfall leads to fast reduction of the effect of noise.

4.7 References

Finnerty, B. D., M. B. Smith, D.-J. Seo, V. I. Koren, and G. Moglen, 1997. Sensitivity of the Sacramento Soil Moisture Accounting Model to Space-Time Scale Precipitation Inputs from NEXRAD. J. of Hydrol., 203(1-4): 21-38

Gupta, V. K., E. Waymire, 1990. Multiscaling properties of spatial rainfall and river flow distributions. J. of Geophysical Research, vol. 95, No. D3, 1999-2009

Koren, V., and C. B. Barrett, 1994. Satellite based distributed monitoring, forecasting, and simulation (MFS) system for the Nile River. Proceedings of the Second International Workshop on Application of remote sensing in hydrology. NHRI Symposium, No 14, October 1994, Saskaton: 187-200

Kouwen, N., and G. Garland, 1989. Resolution considerations in using radar data for flood forecasting. Canadian Journal of Civil Engineering, 16: 279-289.

5. Lumped and Semi-Distributed Modeling Tests

5.1 Calibration of Lumped Test Basins Using Historical Data

Calibration of the test basins was carried out in order to derive lumped, 6-hour simulations that would be used as a standard of comparison in subsequent tests using radar data in a lumped and semi-distributed mode. These standards represent the best simulations that can be attained using the current operational procedures. Lumped and semi-distributed simulations using radar data will be judged against these standard simulations as well as observed hydrographs.

Sacramento model parameters for the basins WTTO2, ELDO2, and KNSO2 were derived using standard procedures for time series development and manual calibration. Final parameters for these basins appear in Table 5.1-1. It can be seen that the parameters are quite similar. An graphical analysis of USGS mean daily flow records for each of these basins revealed that the basin response was quite similar, thereby supporting the final parameter sets. Figure 5-1 presents a semi-log plot of an event in June, 1985. Hydrographs for ELDO2, WTTO2, and KNSO2 are shown, and the similarities, especially in base flow, can be readily seen. ELDO2 shows a tendency to have more of a riparian vegetation effect, which is reflected in the higher RIVA value in Table 5.1-1.

Table 5.1-1   Final Sacramento Model Parameters from Manual Calibration

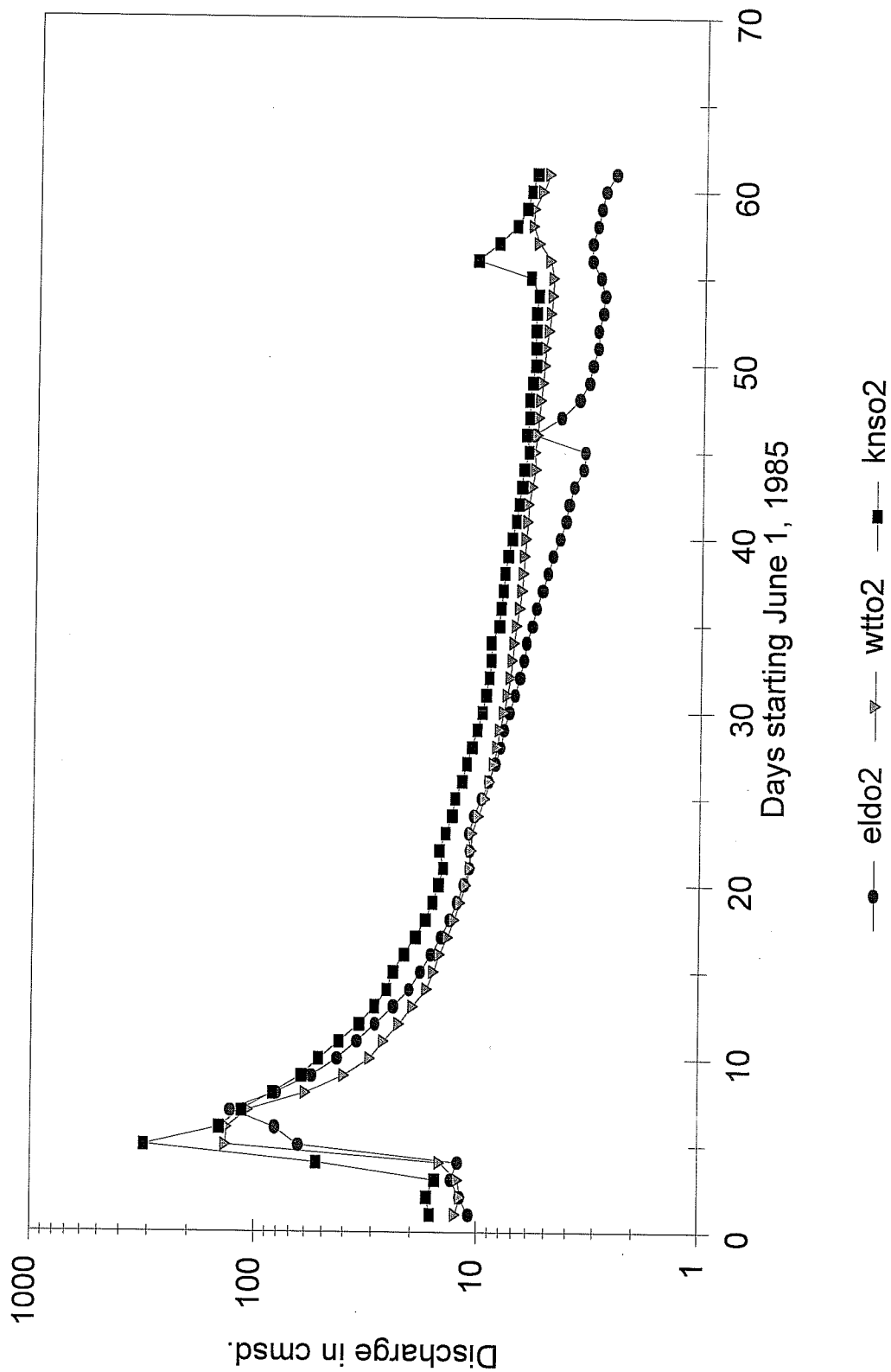| Parameter	KNSO2	ELDO2	WTTO2
uztwm	40	45	50
uzfw	25	30	25
uzk	0.3	0.3	0.3
pctim	0.002	0.00	0.005
adimp	0.0	0.01	0.0
riva	0.035	0.017	0.015
zperc	200	190	220
rexp	1.2	1.6	1.6
lztwm	200	175	265
lzfsm	25	25	24
lzfpm	72	40	79
lzsk	0.15	0.10	0.12
lzpk	0.006	0.008	0.009
pfree	0.15	0.10	0.15
side	0	0	0

Figure 5-1 Semi-log Plot of Observed
Flow - WTTO2, ELDO2, and KNSO2

5.1.1 Comments on Calibration with NEXRAD Data

In this section, a description of the process of manual calibration of the Sacramento model using MAPX will be discussed. One of the known concerns regarding the use of NEXRAD for calibration is the short period of record. University research (Univ. of Arizona, 1995) and the experience of many users have indicated that approximately 8-10 years of data are required to adequately determine the parameters of the Sacramento model. However, the longest record of NEXRAD data is approximately 4 years in duration, leaving open the question as to the suitability of the current NEXRAD archive for proper calibration. Nonetheless, experiments with lumped and semi-distributed basin formulations required that some level of calibration be attempted. The following are comments on efforts to manually calibrate basin WTTO2 at an hourly time step using NEXRAD data on a lumped scale.

As with calibration with rain gage precipitation products, one must be willing to investigate suspected errors in the precipitation forcing. For example, given the known problem with bright band contamination during winter months, it was not known whether the precipitation event on Jan, 5, 1995 was properly simulated. If the precipitation measurements were affected by bright band contamination and thus over estimated, then this event should be ignored during calibration. Adjustment of model parameters to simulate this event would likely result in parameters that would not be appropriate for other periods when good precipitation data was available. Discussions with ABRFC personnel revealed that for this event, there was no bright band contamination.

Tables 5.1.1-1 and 5.1.1-2 present a comparison of results achieved through manual calibration versus automatic calibration using MCP3 and the STAT-QME operation.. The automatic procedure attempted to minimize the RMS error statistic. From the monthly bias results in Table 5.1.1-1, it can be seen that except for the months of May and September, the manual method leads to results that are as good or better than the automated procedure when evaluated on a daily time step. The flow interval biases computed by the two methods are also quite similar, except that the biases for the highest two ranges switch.

What is different between the two calibration methods is the final value of the SAC-SMA model parameters . Table 5.1.1-3 presents the two sets of parameters. Several of the parameters are quite similar. For example, the sizes and release coefficients of the soil moisture zones are somewhat similar, with the exception of uztwm and lzfsm. However, striking differences exist between the parameters controlling the percolation demand curve. Manual calibration results in a percolation demand curve that is fairly linear (value of 1.2) between pbase and the value of 130 for zperc. In contrast, the automatic optimization resulted in rexp being 1.5 and zperc being only 40. Another great difference is the value of pfree: automatic calibration resulted in a much higher value than manual calibration. While it is known that it is difficult if not impossible to determine a "true" set of SAC-SMA parameters for a basin (Gupta, et al., 1998), manual calibration methods might not result in those derived by automatic calibration. While the optimized parameters are not outlandish, they are outside the range of parameters usually derived through manual calibration.

Table 5.1.1-1 Results from Manual and Automatic Calibration of WTTO2. Statistics computed by STAT-QME option using Mean Daily Flow.

Month	% Bias		Bias MM	
	Auto	Manual	Auto	Manual
October	-23.7	-23.9	-4.0	-4.0
November	-11.4	3.0	-6.7	1.8
December	-19.8	-6.4	-5.6	--1.8
January	-3.7	-2.5	-1.5	1.0
February	-19.7	-21.1	-3.5	-3.8
March	-12.9	-7.8	-5.5	-3.3
April	22.6	32.2	11.7	16.7
May	4.5	9.7	2.6	5.6
June	9.1	3.1	3.5	1.2
July	-6.9	-7.3	-1.1	-1.1
August	6.7	-4.1	0.6	-3.7
September	10.7	-14.1	-2.6	-3.5
total	-3.33	0.94	12.2	6.22

Table 5.1.1-2   Interval Bias from Manual and Automatic Calibration

	Flow Interval Bias	
Flow Range	Auto	Manual
0-.61	No cases	no cases
0.61-1.91	249	200
1.91-6.10	0.6	-1.4
6.10-19.05	-9.5	-9.0
19.05-60.96	-1.1	-3.1
60.96-190.51	4.2	22.1
above 190.51	-13.8	-3.18

Table 5.1.1-3 Hourly Parameters for WTTO2 Derived using Automated and Manual Calibration.

Parameter	Manual	Automatic
uztwm	40	93
uzfwm	35	28
uzk	.45	.66
pctim	.005	.005
adimp	.02	.015
riva	.015	0
zperc	130	40
rexp	1.2	1.51
lztwm	130	133
lzfsm	25	53
lzfpm	83	100
lzsk	0.13	0.12
lzpk	.006	.0097
pfree	.10	.412
side	0	0.

One of the difficulties with manual calibration and the current Interactive Calibration Program (ICP) is that X window versions of plotting function for hydrograph comparisons are limited to the WY-PLOT, which is limited to daily data. Statistical analyses are limited to the use of the STAT QME operation for mean daily flow. The use of daily data to calibrate hourly SAC-SMA parameters to hourly streamflow is at best difficult. For example, hourly plots of observed and simulated flows for a particular event may show a mult-peaked response, while in the WY-PLOT ICP display, only a single peak is visible due to the averaging from hourly to daily flow in the MEAN-Q operation.

If manual calibration is to be used in the future with finer scale data, then new ICP plot routines need to be developed. As of the date of this writing, an X windows version of the NWSRFS PLOT-TS operation is being developed and tested in HRL. This will add additional plotting capability to the Interactive Calibration Program. With this function, a user can plot simulated and observed hourly hydrographs with all of the panning and zoom capabilities present in the current WYPLOT routine of ICP.

5.2 Derivation of Synthetic Unit Hydrographs

Three methods of were used in Phase 1 to develop unit hydrographs for lumped and semi-distributed modeling tests. Each method is described below.

Method 1: S-Curve Transformation

The first method consists of the S-curve transformation, a method found in any text on hydrology. First, standard manual derivation methods were used to derive 6-hour unit graphs using historical 6-hour MAP data and USGS mean daily flow data. For some of the tests, these 6-hour unit graphs were converted to 1-hour unit graphs using the S curve technique.

Given the availability of a DEM and derived data sets, several synthetic methods were used to derive hourly unit graphs for lumped and sub-basins. These tests were conducted in order to investigate the importance of routing vs. runoff volume generation.

Method 2: Nash Cascade Approach

Another approach to the development of synthetic unit graphs is the Nash cascade of linear reservoirs. Nash's UHG is a two parameter gamma distribution

$$h(t) = \frac{1}{k\Gamma(n)} \left(\frac{t}{k}\right)^{n-1} e^{-\frac{t}{k}} \qquad (5.2\text{-}1)$$

where n is a shape parameter corresponding to the number of reservoirs in the cascade, k is a scale parameter representing storage, $\Gamma(n)$ is the Gamma function, and $h(t)$ are the ordinates of the unit hydrograph. Given appropriate precipitation and runoff data, the parameters n and k can be calibrated. Method 2 for derivation of unit hydrographs consisted of using 1 Nash cascade and calibrating the n and k parameters.

Method 3: Lumped Unit hydrographs Derived Using Spatial Data

In this section, unit hydrographs for lumped areas are derived by using spatially distributed data, either in the form of sub-basins information or Digital Elevation Model (DEM) data.

Method 3:1 Nash Method and Sub-basins

A somewhat non-traditional use of the Nash cascade was investigated for the Watts watershed in order to derive a lumped basin unit hydrograph. Given that the Watts basin was sub-divided into a collection of 8 sub-basins for semi distributed tests, the same configuration was used to derive a lumped unit graph. The following steps were followed in the unit graph derivation.

1. The SAC-SMA was run on a lumped basis using calibrated lumped parameters. A time series of total channel inflow (TCI) was generated.

2. An 8 sub-basin representation of Watts was derived, with the TCI time series applied to each of the sub-basins.

3. Assign a Nash cascade to each sub basin reflecting the movement of runoff (TCI) from each of the sub-basins to the main basin outlet. Rout the TCI from each sub-basin to the parent basin outlet. Simulated runoff at the main basin outlet is the sum of the routed runoff from each sub-basin.

4. Manually calibrate the k and n parameters in each sub-basin by comparing the simulated runoff to the observed runoff at the main basin outlet.

For the semi-distributed modeling studies, the individual unit hydrographs for each of the 8 sub-basins were used.

Method 3.2: Clark Time Area Approach.

The time-area approach is based on a drainage area distribution over a basin. Because the original version of this approach was based purely on translation, it usually overestimated the peak rate. To overcome this problem, Clark (Clark, 1943) suggested to route the time-area curve through a single element of linear storage (e.g., one Nash's reservoir). This has been a very widely used approach in watershed simulations. The calculations can be outlined in general as below:

    a) generate channel length distribution curve using DEM. Figure 5-2a presents the channel length distribution for the Illinois River at Watts, (WTTO2).

    b) derive the cumulative area vs distance curve, as shown in Figure 5-2b.

    b) estimate channel flow UHG ordinates $h_c(t)$ based on area-length curve

$$h_c(t) = \frac{A(L_t) - A(L_{t-1})}{dt} i$$

(5.2-2)

where i is the unit rainfall excess, dt is the time step of the UH, $A(L_t)$ is the total area below isochrone L_t (from area-length curve), the isochrone L_t can be estimated if the flow velocity, v_c, is available: $L_t = v_c\, t$.

c) estimate overland reservoir response using a single Nash Reservoir

$$h_h(t) = e^{-\frac{t-dt}{r_h}} - e^{-\frac{t}{r_h}} \qquad (5.2\text{-}3)$$

where r_h is a lag time of overland flow.

d) convolution of the channel UH and overland response

$$h(t) = \int_0^t h_c(g) h_h(t-g)\, dg \qquad (5.2\text{-}4)$$

The convolution integral in equation 5.2-4 results in the ordinates of the unit hydrograph h(t) according to the following example:

Time $t = 0$ $h(0) = 0$
Time $t = 1$ $h(1) = h_{c1} * h_{h1}$
Time $t = 2$ $h(2) = h_{c1} * h_{h2} + h_{c2} * h_{h1}$
Time $t = 3$ $h(3) = h_{c1} * h_{h3} + h_{c2} * h_{h2} + h_{c3} * h_{h1}$

There are two parameters that should be defined to generate the UH: overland flow lag time r_h, and average channel velocity v_c. The best approach is to estimate these parameters from rainfall-runoff time series.

The difference in time between rainfall excess and flood peak, t_p, can be used to estimate channel velocity:

$$v_c = \frac{L_{max}}{t_p} \qquad (5.2\text{-}5)$$

where L_{max} is the distance from outlet to the maximum of contributed basin area (from area-length curve). The overland flow lag time can be assumed to be equal to the difference in time between peak of flood and the center of mass of hydrograph.

If there is no observed data the parameters can be estimated from an empirical relationships.

Johnston (in Dooge, 1974) derived a relationship based on 19 catchments with areas between 25 and 1,624 sq. ml. in the Scotie and Sandusky basins. He proposed the relationship for the time of concentration (i.e., base of the time-area curve):

$$t_c = 5.0(\frac{L}{\sqrt{S}})^{0.5} \tag{5.2-6}$$

where t_c is the base time in hours, L is the length of the principal stream (from outlet to watershed limit) in miles, S is the average slope of the main stream in feet per mile. Similar relationships were obtained by Thomas (1974) for small Oklahoma watersheds (areas 5-20 sq. ml.)

$$t_c = 4.99(\frac{L}{\sqrt{S}})^{0.58} \tag{5.2-7}$$

and by Carter (in Thomas, 1974) for the Washington area:

$$t_c = 4.18(\frac{L}{\sqrt{S}})^{0.52} \tag{5.2-8}$$

The channel velocity can be estimated using these relationships. As an example, from Johnston's equation

$$v_c = \frac{L}{t_c} = 0.2(L\sqrt{S})^{0.5} \tag{5.2-9}$$

The overland flow lag time can be estimated from Eaton's equation (in Dooge, 1974)

$$r_h = 1.2(\frac{A}{L})^{2/3}(\frac{1}{R})^{1/3} \tag{5.2-10}$$

where R is the branching factor that varies from 1 to 2. A few case studies suggested that it is better to use a value of 2 for the branching factor. Equation 5.2-10 then becomes:

$$r_c = 0.95(\frac{A}{L})^{2/3} \tag{5.2-11}$$

Given the availability of precipitation and discharge data, t_p was derived for the WTTO2 basin, and a v_c was subsequently computed. Using v_c, Eq. 5.2-2 was solved go derive the channel

5.11

unit hydrograph for the WTTO2 basin. Eq. 5.2-11 was solved for r_c, and the overland response function for WTTO2 was derived. Convolution of Eq. 5.2-2 and 5.2-3 resulted in the optimal unit graph in Figure 5-3 and it can be seen how the optimal unit hydrograph resembles the stream length distribution.

For the WTTO2 basin, DEM-derived data sets such as flow connectivity were available. In addition, the USGS records specified an average channel slope. Using these data, Equation 5.2-6 was used to derive t_c, which was subsequently used to derive v_c. The resulting unit hydrograph is plotted in Figure 5-3 as the GIS_UH. The correspondence of the two derived unit graphs to each other and the stream length distribution can be seen in Figure 5-3.

Figure 5-4 presents two different unit hydrographs for Baron Fork at Eldon, OK. (ELDO2) The 6-hour unit hydrograph derived using manual calibration methods was translated to a 1-hour unit graph using a standard S-curve technique. A GIS-based unit graph was also derived. It is not clear why the jagged features in the GIS-based unit graph occur. It may be that the small size of the basin (308 sq. mi.) results in a small number of HRAP cells and thus an erratic stream length distribution plot. Nonetheless, it can be seen that the GIS based unit graph is an adequate representation of that derived from the calibrated 6-hour unit graph.

Figure 5-5 presents the relative contributions of the sub-basin unit graphs for the Watts lumped unit hydrograph basin. The ordinates for each sub-basin unit hydrograph can be derived from Figure 5-5 by subtracting the ordinates of the unit-graph plotted sequentially before it. The total unit hydrograph is represented by the outer shape of the double peaked hydrograph. The total unit hydrograph has a minor peak on the rising limb of approximately 14,000 cfs at about 8 hours. The major peak of the total unit graph is approximately 25,000 cfs at about 19 hours. It can be seen from the figure that the two-peaked shape resembles the stream length distribution and the unit graph derived using the Clark method.

Channel length distribution for the Watts outlet

(a)

Cumulative distance-area plot for the Watts outlet
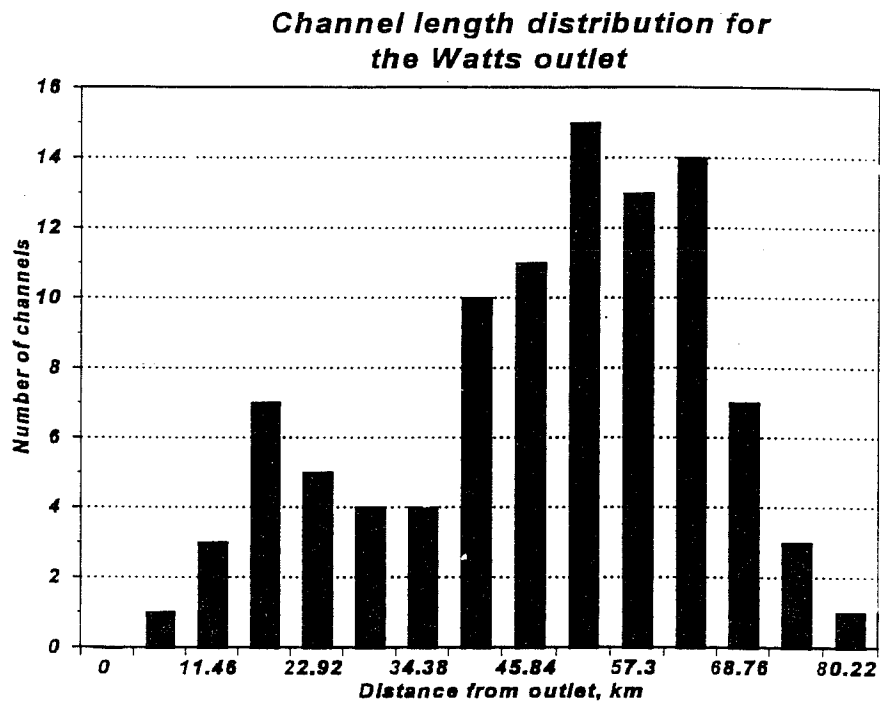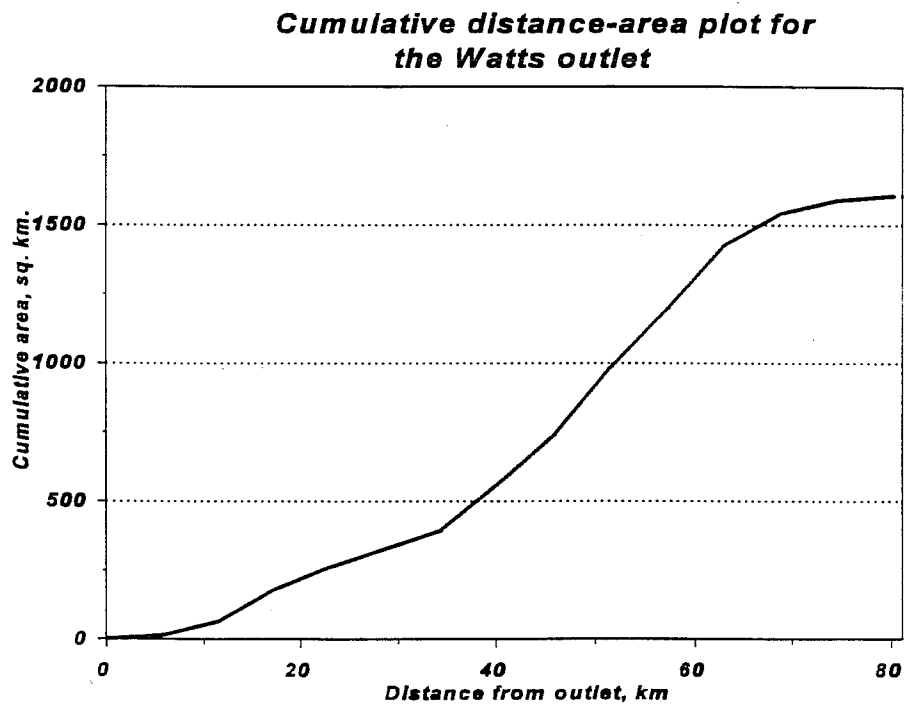
(b)

Figure 5-2   Channel Length Distribution (a) and
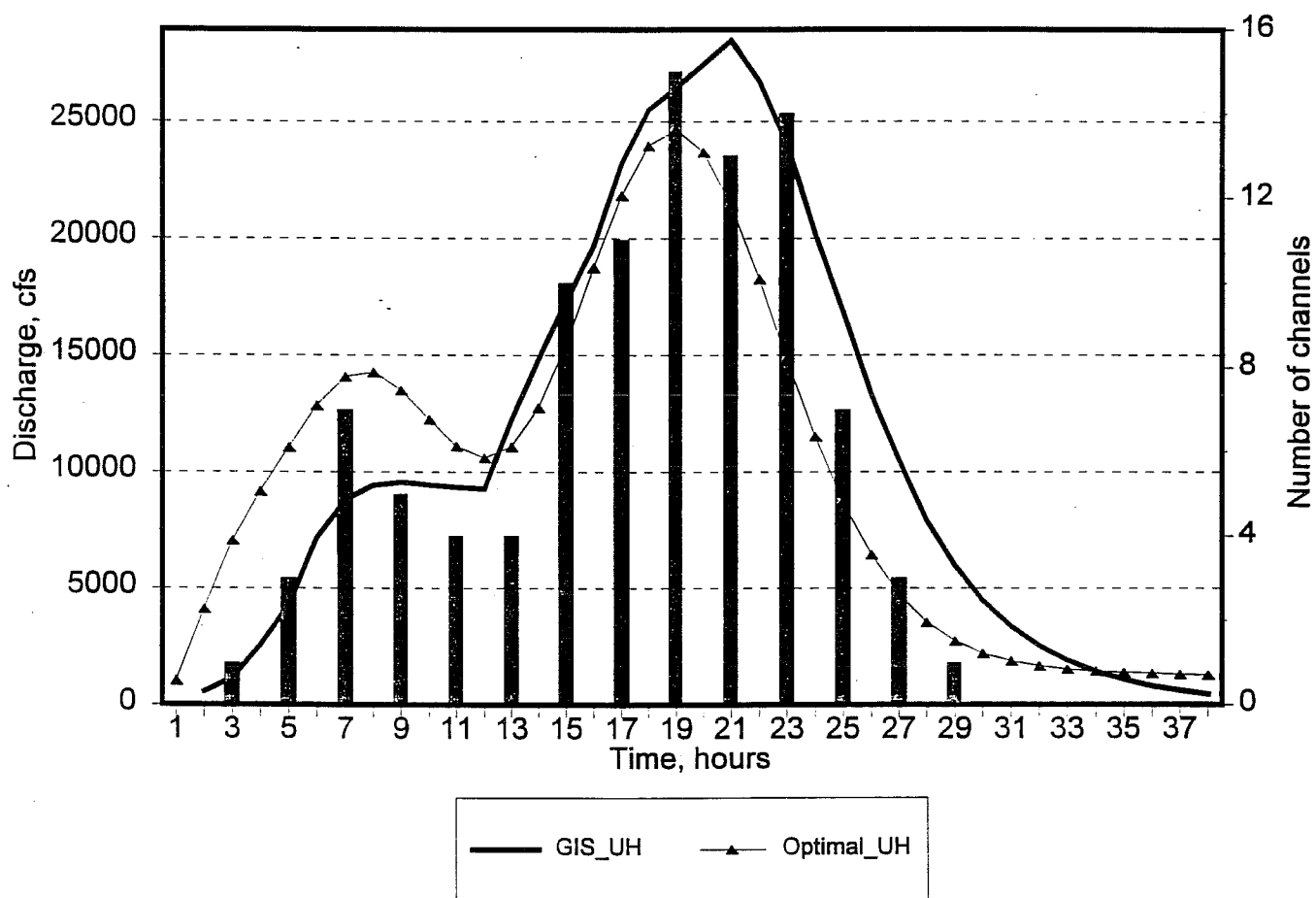Cumulative Distance-Area Plot (b) for
WTTO2.

Figure 5-3   Channel length distribution and synthetic unit hydrographs
derived using two methods.   The GIS_UH was derived using DEM data.   The
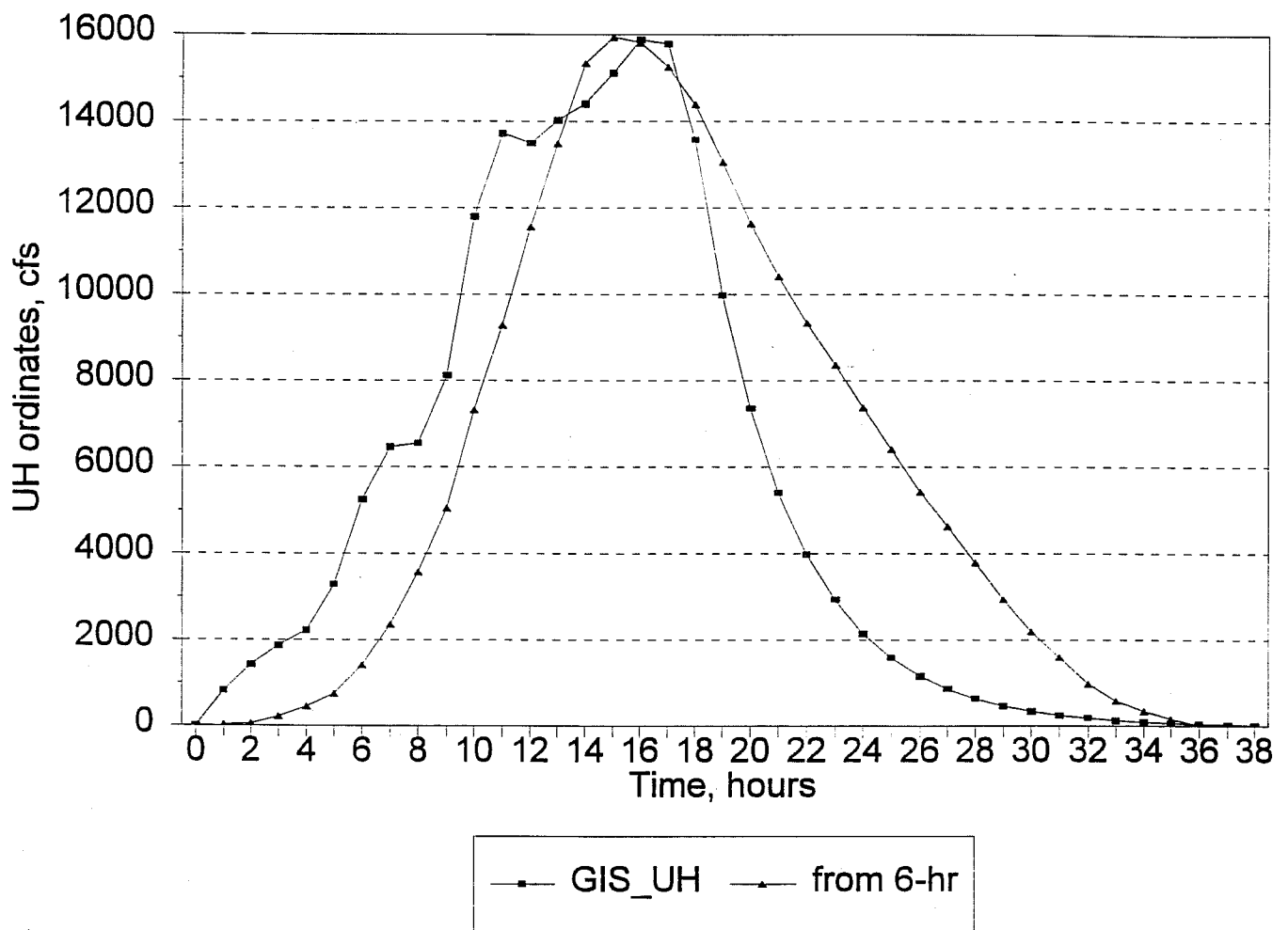Optimal_UH was derived using observed flow data to derive velocity and
timing parameters.

Figure 5-4 Unit hydrographs for ELDO2 derived using two different methods. The GIS_UH is derived from DEM data, while the other is derived from a calibrated 6-hour unit hydrograph. Both are 1-hour unit hydrographs.

5.15
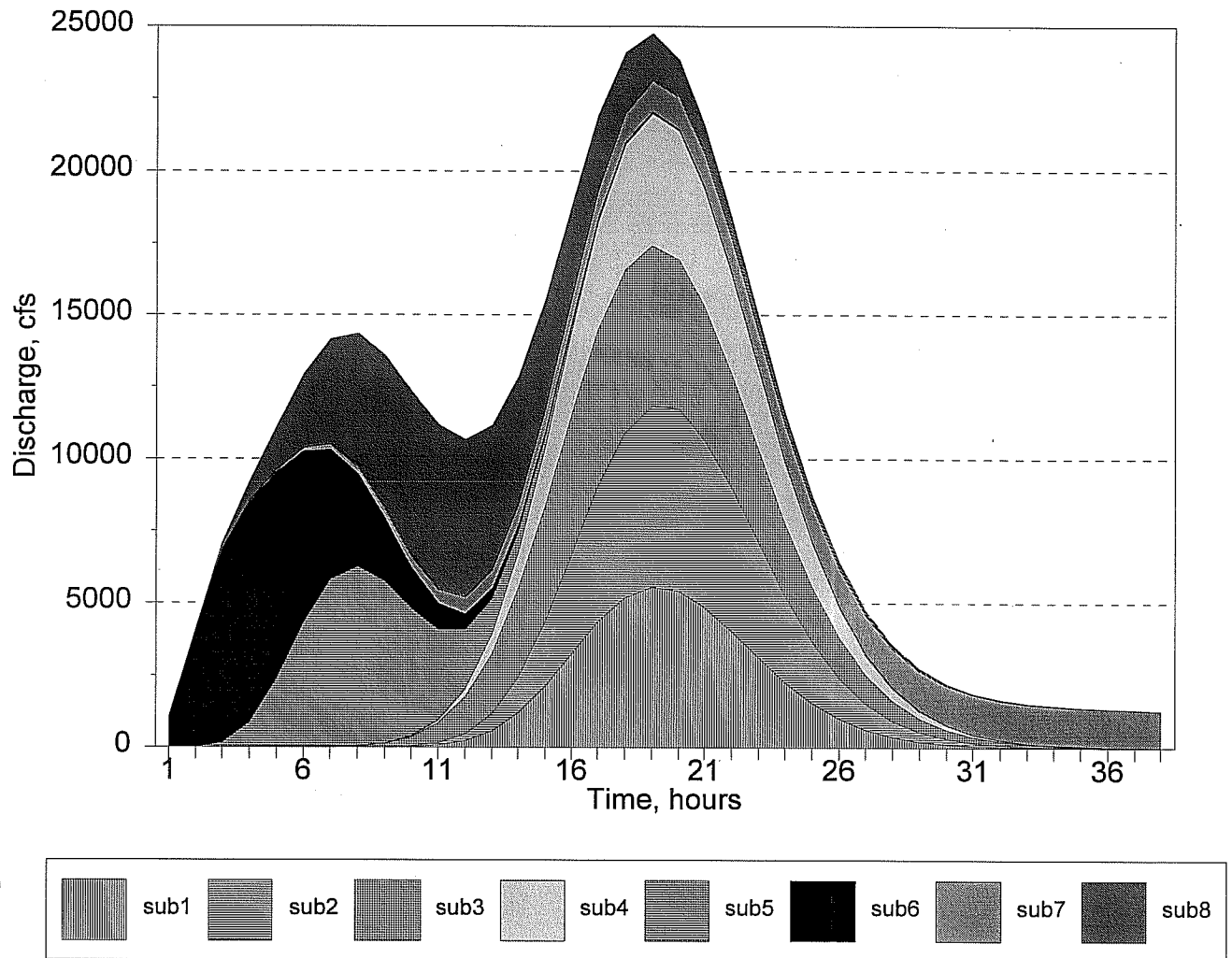
Figure 5-5 Relative Contribution of Sub-Basin Unit Hydrographs and
         Total Lumped Unit Hydrograph for WTTO2. The total lumped
         unit hydrograph is represented by the shape of the outer
         hydrograph. The shaded areas represent the relative,
         contribution of each sub-basin. The ordinates of each
         sub-basin unit graph can be derived by subtracting the
         ordinates of the unit graph plotted sequentially before it.

5.3 Lumped and Distributed Modeling Tests with Stage III and Basin WTTO2

5.3.1 Lumped Approach for WTTO2

A first series of hydrologic modeling tests was conducted on basin WTTO2 using a lumped approach. In these tests we hoped to determine the benefit of using Stage III data to define lumped MAPX input to the Sacramento model. Simulations were generated for the period October 1, 1993 to June 30, 1996 while statistics were generated for the period June 1, 1994 to June 30, 1996. In this way, any errors generated by initial conditions would not affect the statistics.

For the 1-hour lumped modeling tests, unit hydrographs were derived using the four methods described in part 5.2 discussed earlier:

1. 1-hour uhg derived using a standard S-curve technique applied to the calibrated 6-hour unit hydrograph: Method 1.

2. 1-hour unit graph derived using a single Nash cascade, with calibration of n and k parameters: Method 2.

3. 1 hour unit graph derived using spatial information:

   3.1 1-hour unit graph derived from the convolution of 8 Nash unit graphs (one for each of 8 sub-basins) Each sub-basin had a Nash unit hydrograph, reflecting the movement of water to the main basin outlet: Method 3.1
   3.2 1-hour unit graph defined using the Clark time area: Method 3.2

Even though there is some uncertainty regarding the consistency and length of period of Stage III data, an effort was made to recaibrate the SAC-SMA parameters for use with hourly MAPX data. Parameters for the SAC model were derived using automatic calibration techniques. Table 5.3-1 presents these parameters. Hourly stages were available from USGS gages and converted to discharge using the operational rating curve from the Tulsa River Forecast Center.

6-hour lumped simulations for WTTO2 were performed using archived operational MAPX and MAP time series discussed in Chapter 3. Recall that these time series are those which the ABRFC generated from using the operational MAP preprocessor and from StageIII data. These time series were subsequently used in their operational forecasting. The 1-hour MAPX time series were aggregated to form a 6-hour time series. In these simulations, SAC-SMA parameters were developed through standard manual calibration techniques using over 40 years of precipitation data. 6-hour simulations were also performed using parameters that were recalibrated for use with hourly Stage III data.

Table 5.3-1 Sacramento Model Parameters used in 1-Hour Simulations with WTTO2

parameter	value
uztwm	93
uzfw	28
uzk	0.66
pctim	.005
adimp	.015
riva	0
zperc	40
rexp	1.51
lztwm	133
lzfsm	53
lzfpm	100
lzsk	0.12
lzpk	.0097
pfree	.412
side	0

5.3.1.1 Results

Figures 5-6 through 5-8 display the results of these 1-hour lumped modeling tests in the WTTO2 basin using several unit graph derivation methods. Not shown in these figures are the simulations using the Clark time-area uhg, as they are very close to the simulations derived using method 3.1 (the Nash method). These figures show that the transformed 6-hour unit graph (Method 1 - S Curve) leads to damped responses in almost every case. For the April, 1996 case, the simulation derived using the transformed 6-hour uhg was not able to match the double peaked observed response. In all cases shown, the use of spatially distributed information, either in the form of channel length distribution in the case of the Clark uhg, or sub-basin responses in the case of the Nash method, leads to more accurate simulations of the observed hourly data.
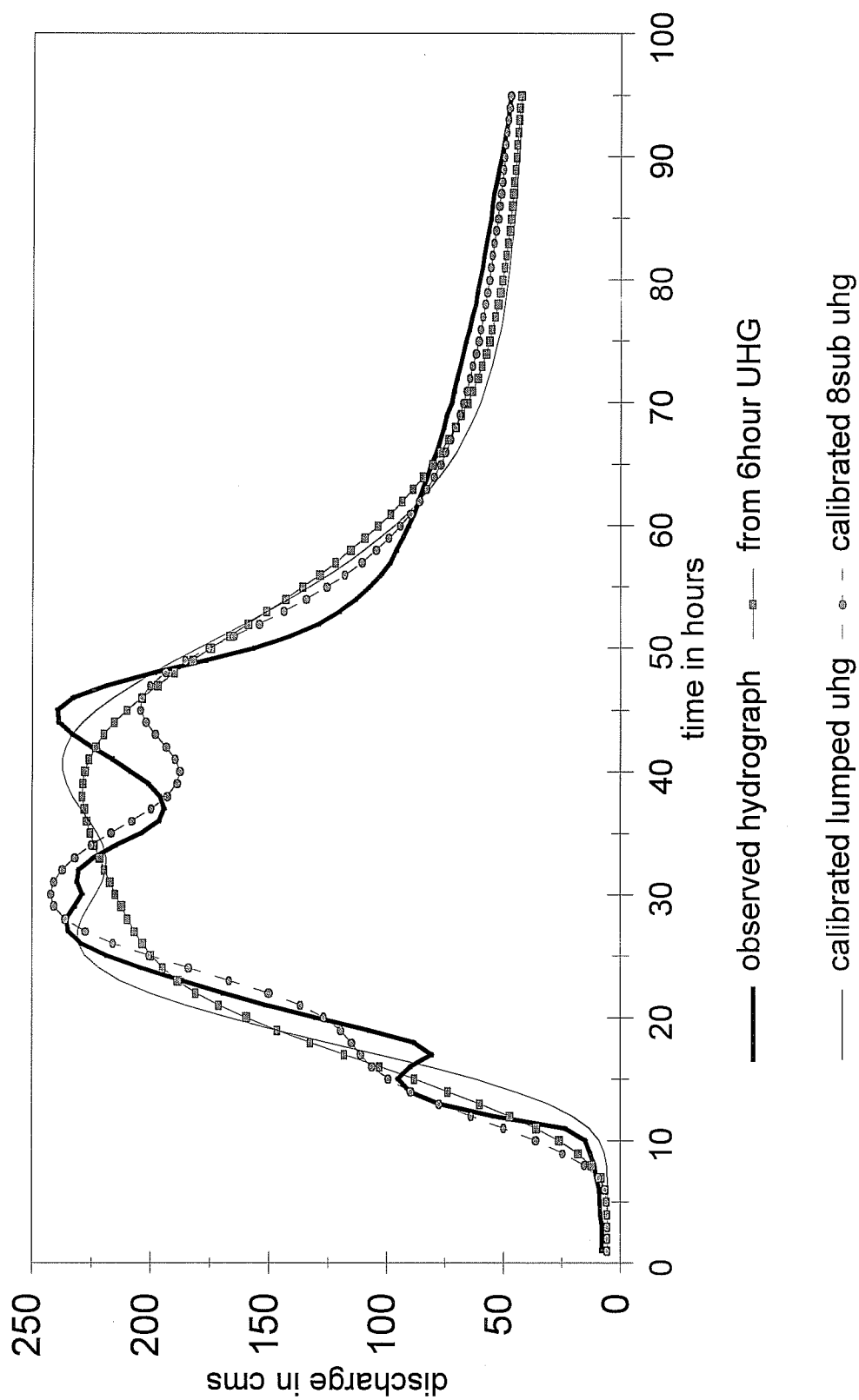
Figure 5-6 WTTO2 April 22, 1996
Sensitivity to UHG Derivation Method

legend: observed hydrograph — from 6hour UHG — calibrated lumped uhg — calibrated 8sub uhg
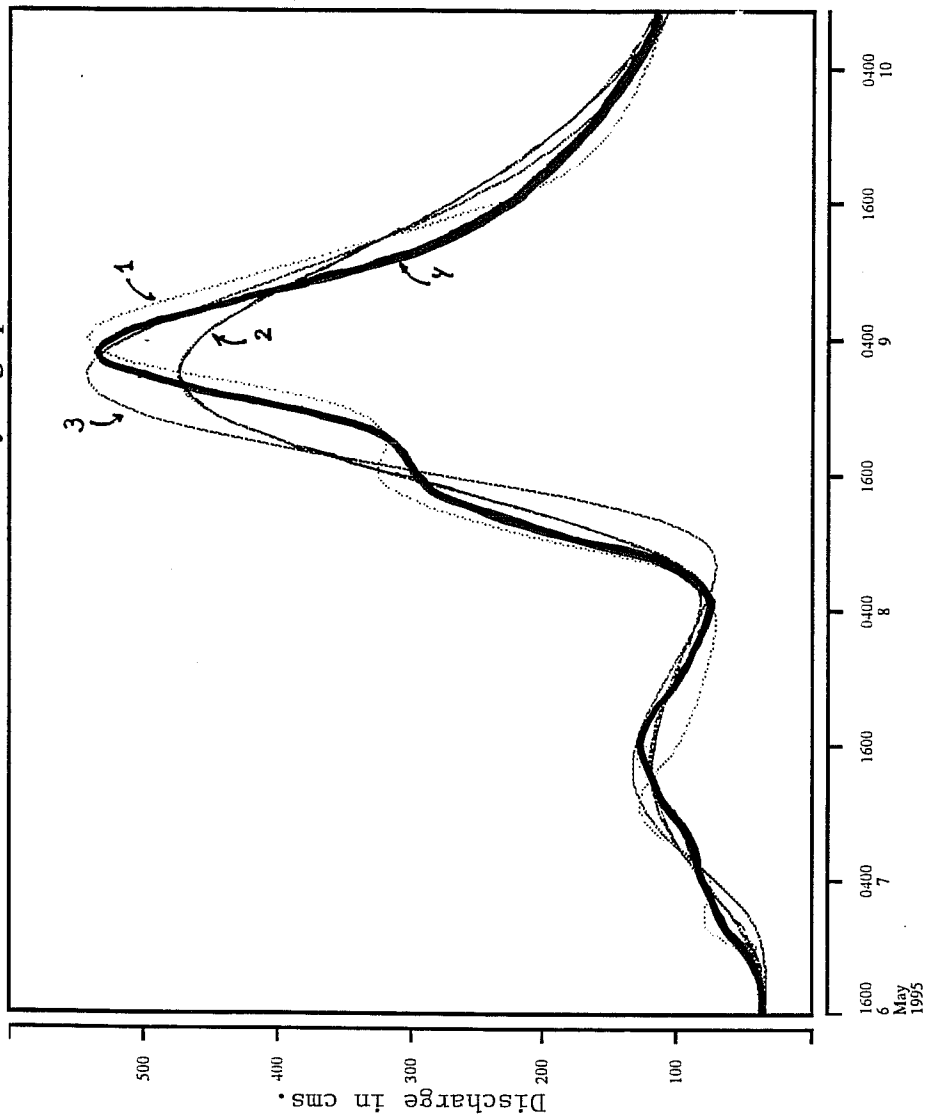
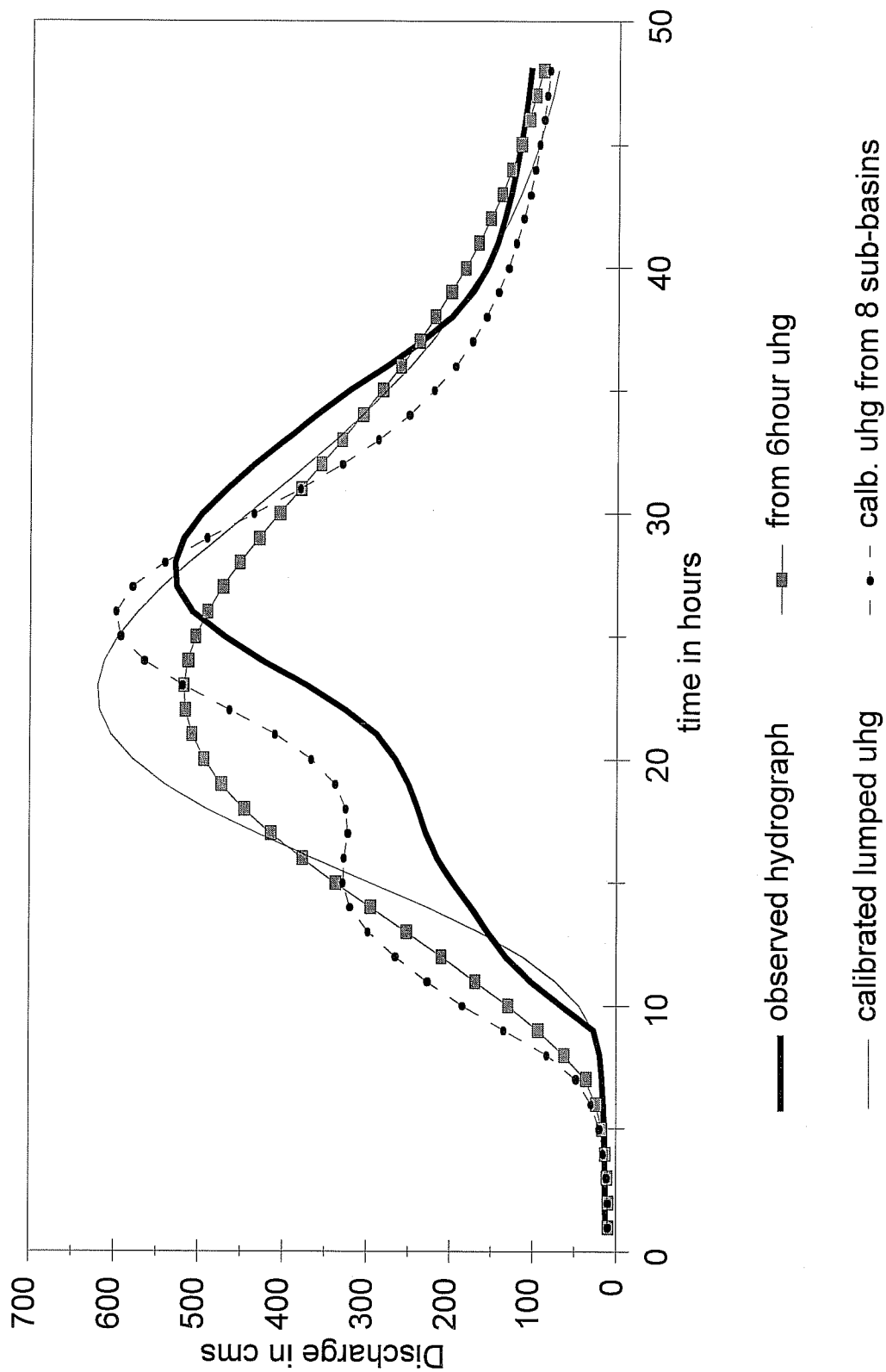Figure 5-7 WTTO2 May, 1995. Sensitivity to UHG Derivation Method

Figure 5-8 Wtto2 November 7, 1998
Sensitivity to UHG Derivation Method

Figures 5-9 and 5-10 show scatter plots of observed and simulated hydrograph peaks for two unit hydrograph methods. It can be seen in that the simulations from the 8 sub-basin Nash approach (and thus the Clark time-area method) produce the best agreement in peak flows.

Additional simulations were performed at a 6-hour time step, using the archived operational MAPX and MAP time series from ABRFC. Selected events from these simulations appear in Figures 5-11 and 5-12. From these figures it can be seen that the 6-hour MAPX simulation was consistently better than the 6-hour MAP simulation. For comparison, the 1-hour MAPX simulation using Method 3.1 for unit hydrograph generation is also plotted. It can be seen that the 1-hour MAPX leads to better simulations than either of the two 6-hour simulations. Hourly simulations using stage III more closely follow the multi-peaked observed streamflow.

5.3.2 Semi-distributed Modeling Tests

5.3.2.1 General Approach

For the semi-distributed modeling tests, the general emphasis was to test a very simple approach to capturing the spatial variability of precipitation. Recall that the goal of Phase 1 of the Distributed Modeling Project was to investigate the use of distributed precipitation information as a means of improving simulation capability. This would be accomplished through the use of sub-basins, each having its own lumped input. Subsequent to this effort would be investigations into the use of models with distributed hydrologic parameters. We have defined this effort to be Phase 2 of the Distributed Modeling Project

With this in view, WTTO2 was disaggregated into 8 sub-basins and for each a unit hydrograph was derived. These unit graphs modeled the movement of runoff volumes from each sub-basin to the main basin outlet. Unit hydrograph Method 3.1 was used for each sub-basin. Thus, in this modeling approach, there is no explicit channel routing. Future research may include the use of an explicit channel routing procedure such as Muskingum-Cunge to move water from sub-basin outlets to downstream computational points.

Gridded precipitation data is used to define MAP time series for each sub-basin. The same Sacramento model parameters were applied to each of 8 sub-basins and calibrated by uniformly adjusting the parameters up or down. Re-calibration of the 1-hour lumped parameters is necessary due to the change in spatial scale of the precipitation. Only the percolation parameters ZPERC and REXP were adjusted to recalibrate the model to semi-distributed input defined by the gridded radar values.
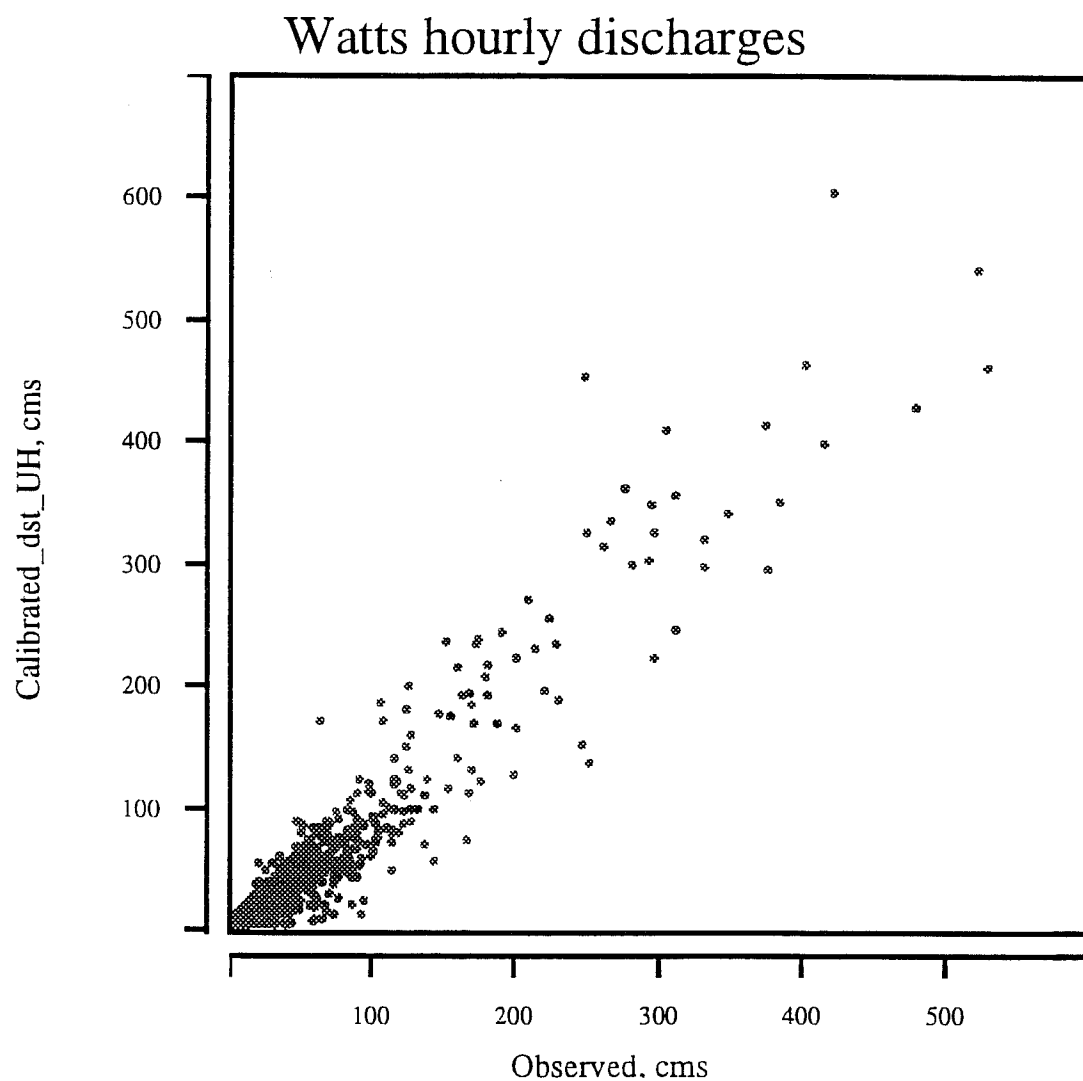
Figure 5-9   Scatter plot of observed discharges versus those
derived using a unit hydrograph derived using
Method 3.1

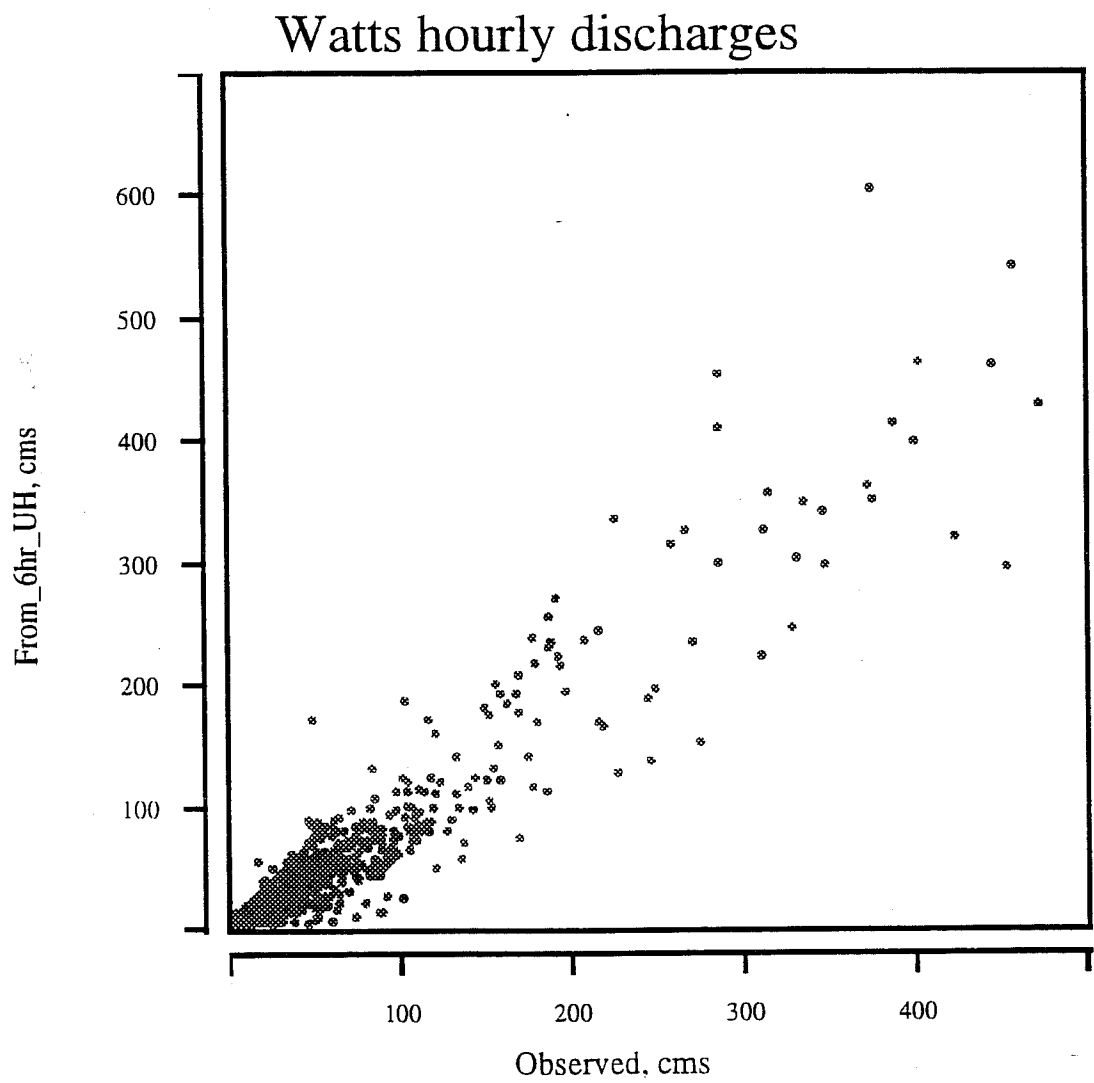Watts hourly discharges

Figure 5-10   Scatter plot of observed discharges versus those
              derived using an S-curve transformed 6-hour
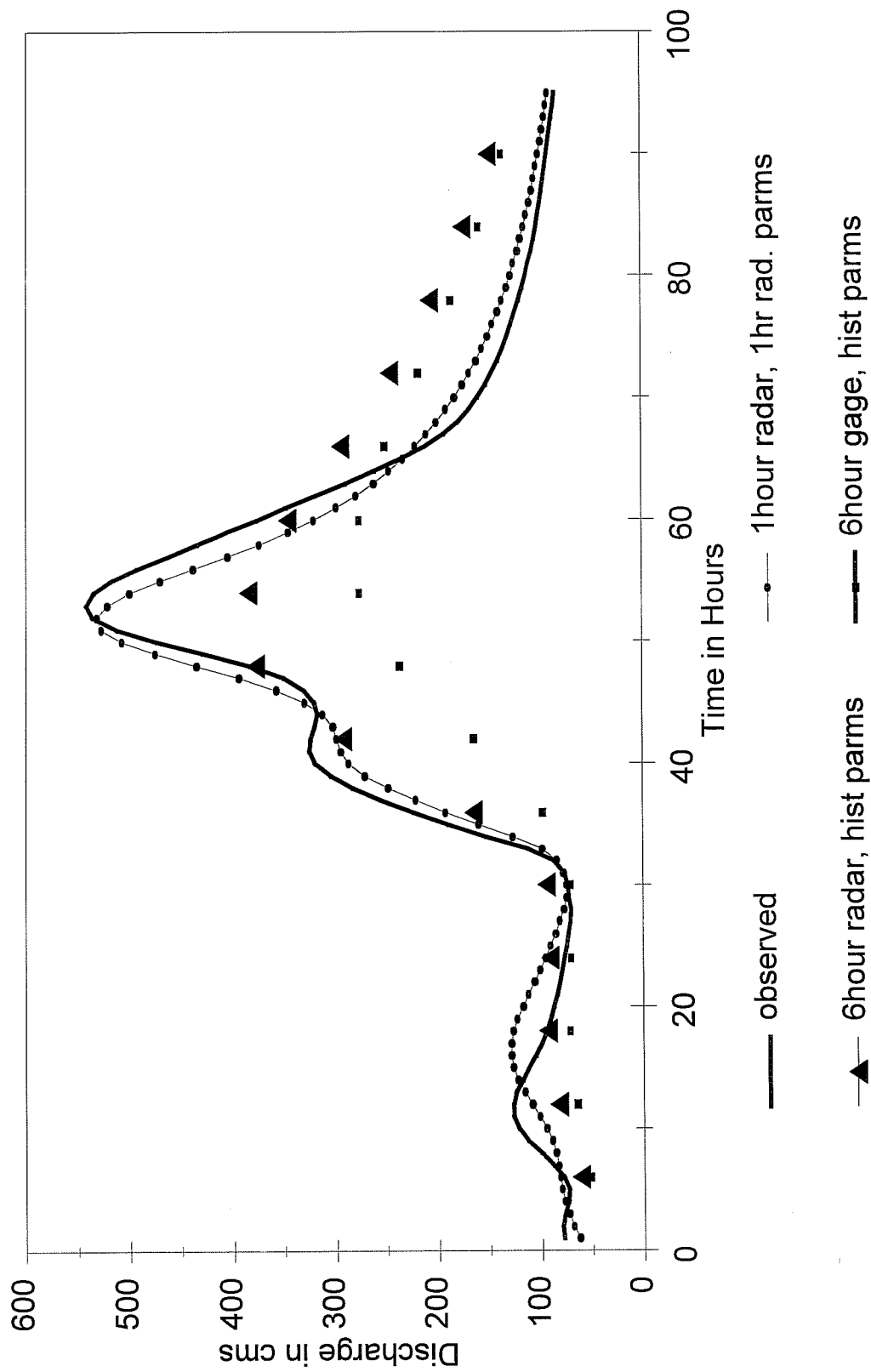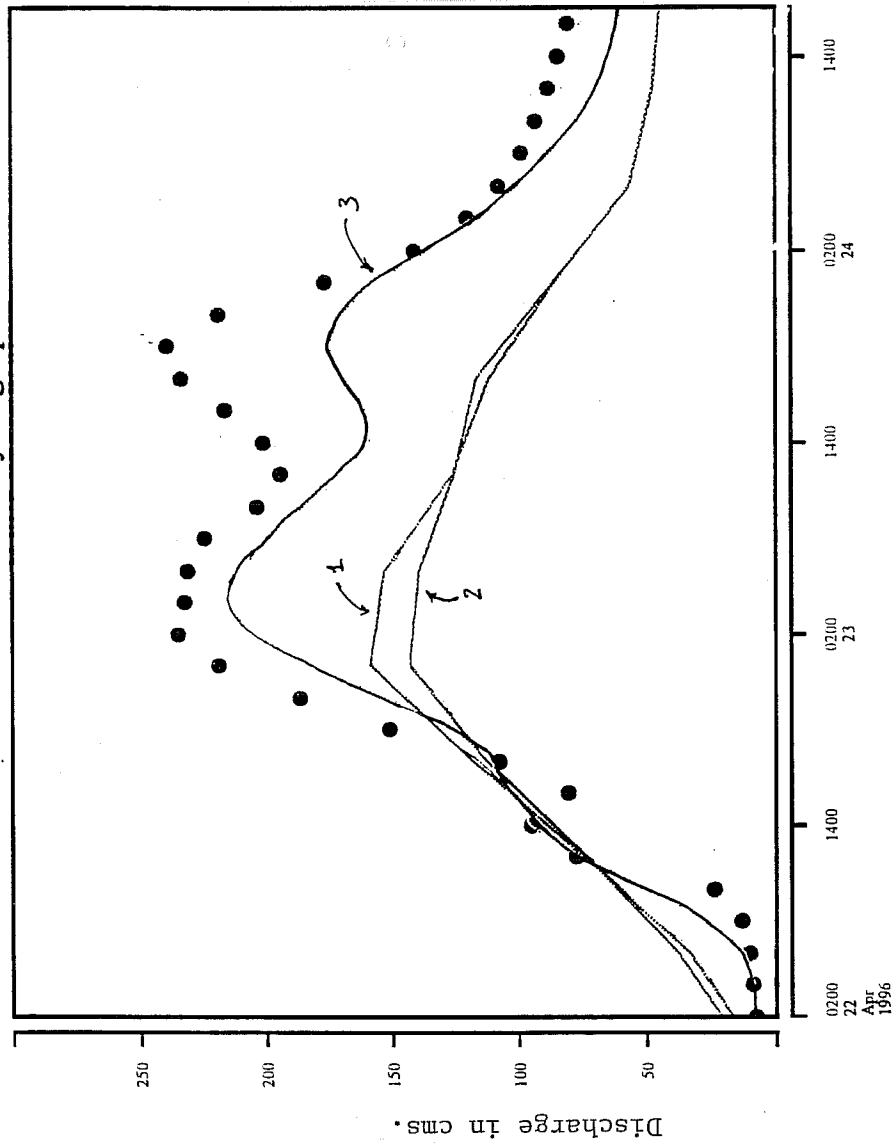   unit hydrograph.

Figure 5-11   WTTO2 May 7, 1995
6-Hour and 1-Hour Lumped Simulations

Watts hydrographs

observed
6-hour gage
6-hour radar
1-hour radar

1
2
3

Figure 5-12 WTTO2 April, 1996 6-Hour and 1-Hour Lumped Simulations

Continuous simulations were performed from October 30, 1993 to July 31, 1996. However, to minimize any biases arising out of inaccurate initial conditions, statistics were generated using only the period June 1, 1994 to June 30, 1996.

5.3.2.2 Results of Semi-Distributed Tests in WTTO2

Figures 5-13 through 5-15 present results from the semi-distributed tests for the Illinois River at Watts, Ok. In these tests, the unit hydrograph for the sub-basins was derived using Method 3.1 in which a Nash cascade was assigned to each of the 8 sub-basins. The Nash n and k parameters were calibrated so that the simulated discharge agreed with the observed discharge. The lumped simulations were derived using the unit graph from method 3.1. Surprisingly, the sub-basin approach does not dramatically improve simulation accuracy compared to the lumped simulations, which were already quite good. Figure 5-14 shows a case where the sub-basin approach led to better simulation of the rising limb of the hydrograph. Apparently, Stage III captures a good estimate of the areal mean precipitation, leading to a fairly good lumped simulation. In addition, examination of these rainfall events reveals that most of them were fairly uniform in a spatial sense, and thus adequately fulfill the assumptions of lumped hydrological modeling.

As mentioned earlier, the sub-basins were calibrated by uniformly adjusting up or down the SAC parameters in each basin. In this sense, we are modeling semi-distributed precipitation, not semi-distributed hydrologic parameters. One of the problems associated with a distributed or semi-distributed approach to modeling is the method of parameter estimation and calibration. Figure 5-15 illustrates a difficulty with assigning uniform parameters to each sub-basin. The sub-basin approach leads to a greatly overpredicted simulation. Examination of the individual MAPX times series for this event in Figure 5-16 revealed that the precipitation predominately occurred over one or two of the sub-basins, leading to the overpredicted streamflow response shown. From this, one might conclude that the parameters for this sub-basin should be different than those in the other sub-basins.

Table 5.3-2 presents the statistical results of the lumped and semi-distributed modeling tests with basin WTTO2. Versions 1,2, and 3 represent the results of lumped hourly simulations descriped in section 5.3.1. Versions 4 and 5 represent the semi distributed simulations. In version 4, the lumped hourly parameters were applied uniformly to each of the 9 sub-basins. Version 5 is the same as version 4 except that the SAC-SMA parameters have been recalibrated. 6-hour simulations are presented in versions 6 through 9. Version 9 represents the best results achievable using the standard lumped 6-hour rain gage based model of WTTO2 and historically calibrated SAC parameters. Version 8 is the same as version 9 except that the 6-hour MAPX data is used. Versions 6 and 7 are the same as versions 8, and 9 respectively except that the unit hydrographs are hourly and derived using method 3.1

By using a 6 hour MAPX data instead of rain gage data used in version 9, simulation bias can be improved as shown by the version 8 results. However there is a corresponding slight loss of
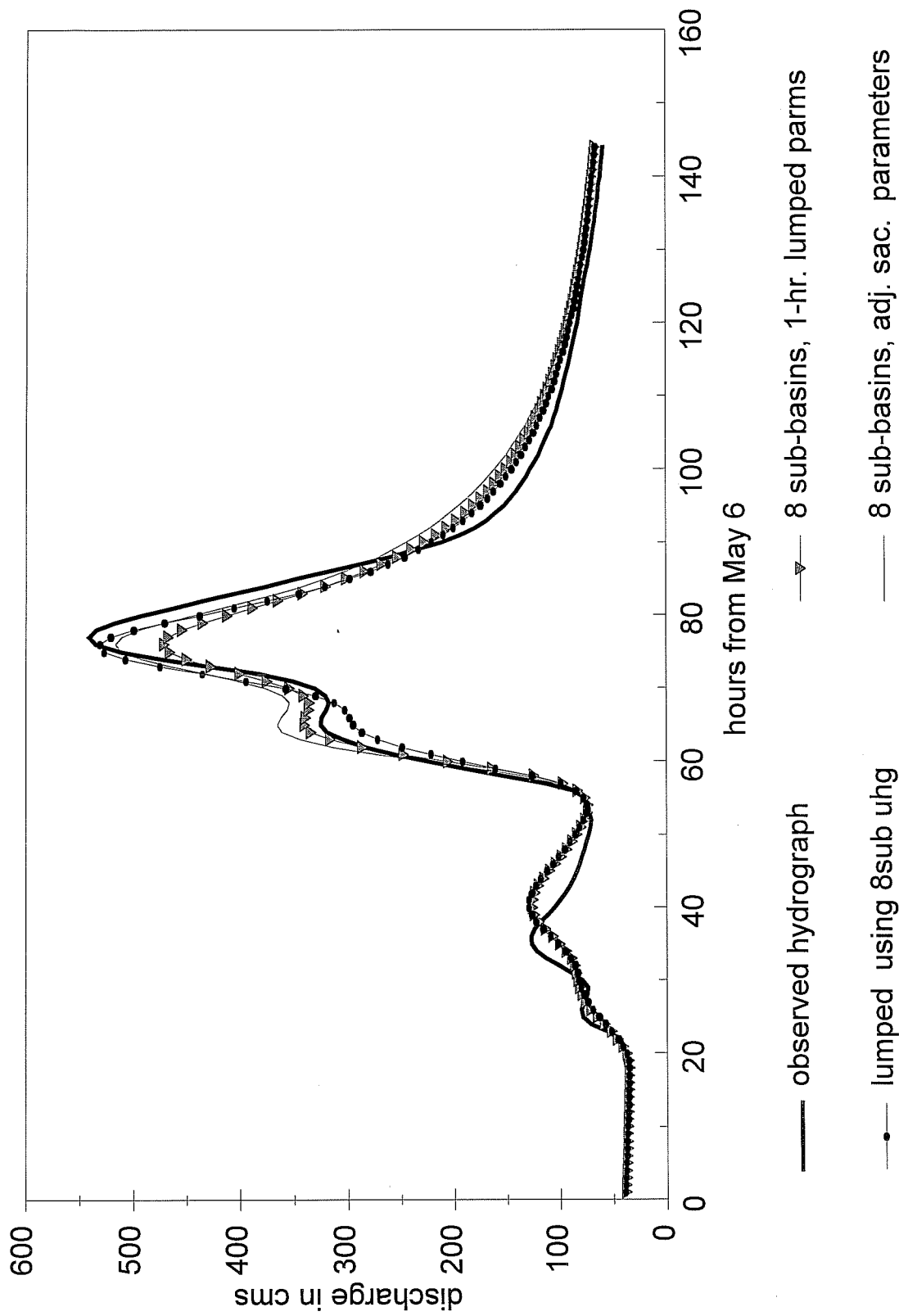
Figure 5-13   WTTO2 May 6, 1995
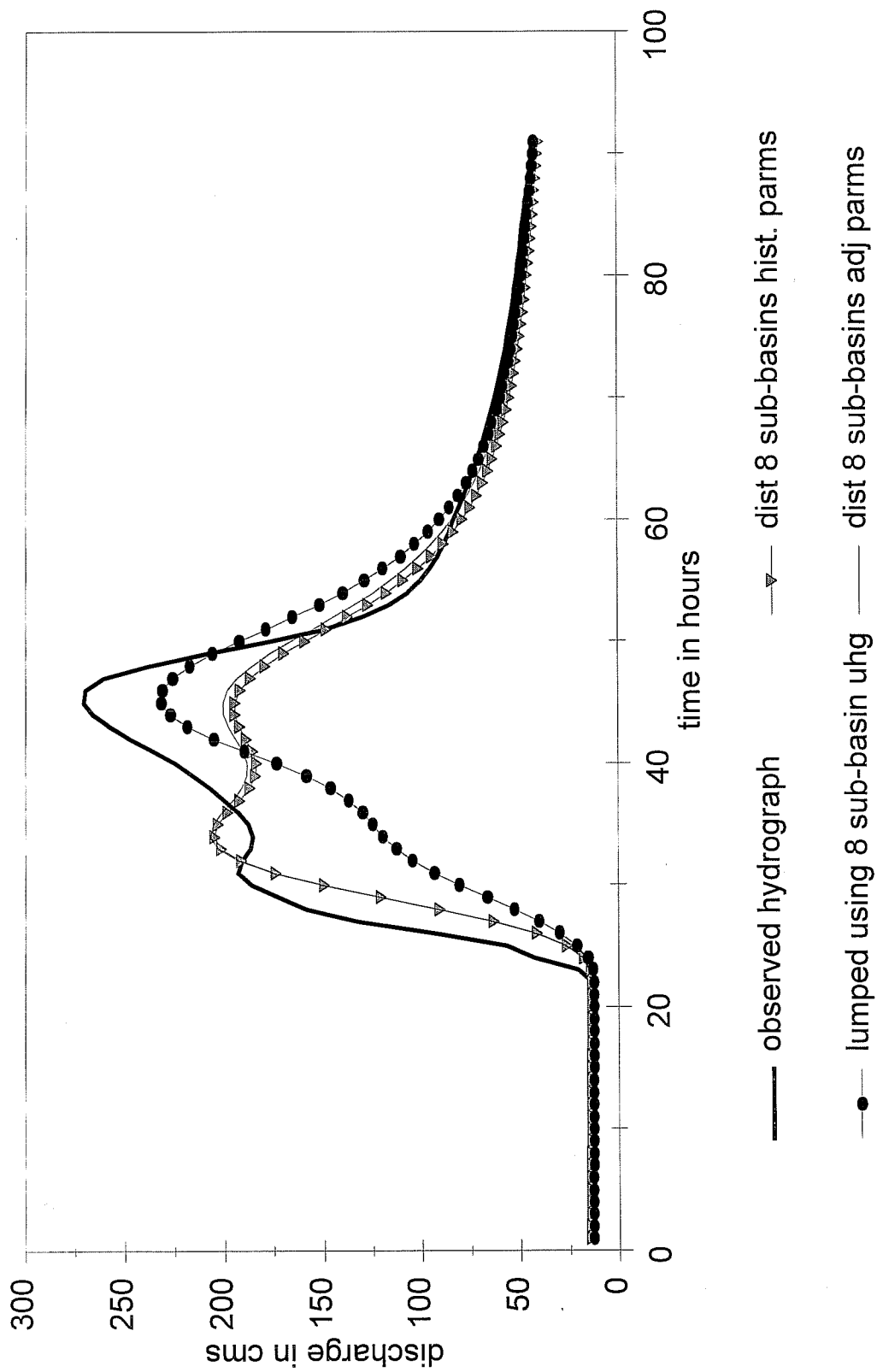Distributed and Lumped Simulations

Legend:
— observed hydrograph
— lumped using 8sub uhg
— 8 sub-basins, 1-hr. lumped parms
— 8 sub-basins, adj. sac. parameters

Figure 5-14   WTTO2 May 10, 1996
Distributed and Lumped Simulations

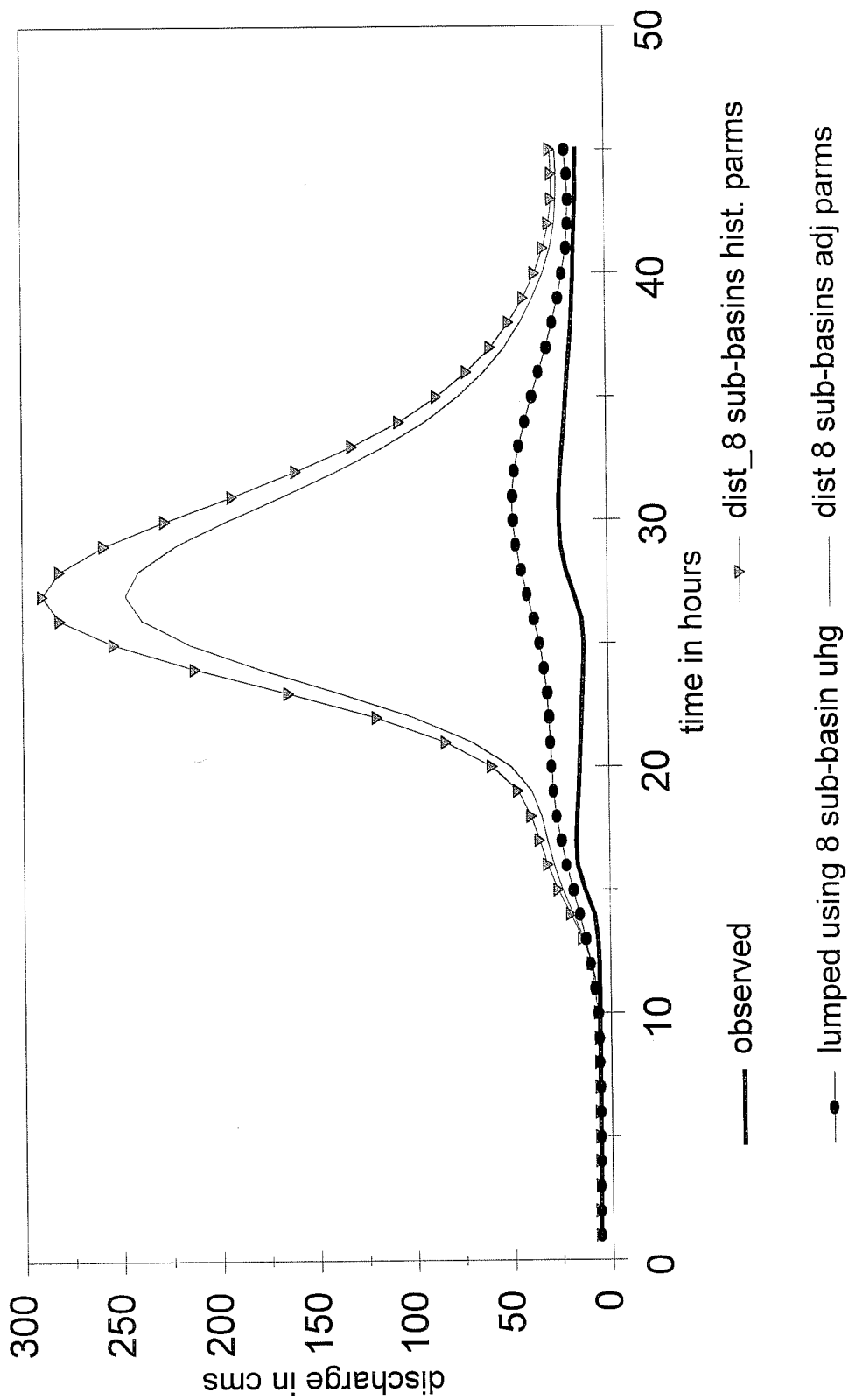Figure 5-15   WTTO2 July 15, 1994
Distributed and Lumped Simulations

Legend:
— observed
—▽— dist_8 sub-basins hist. parms
—●— lumped using 8 sub-basin uhg
— dist 8 sub-basins adj parms

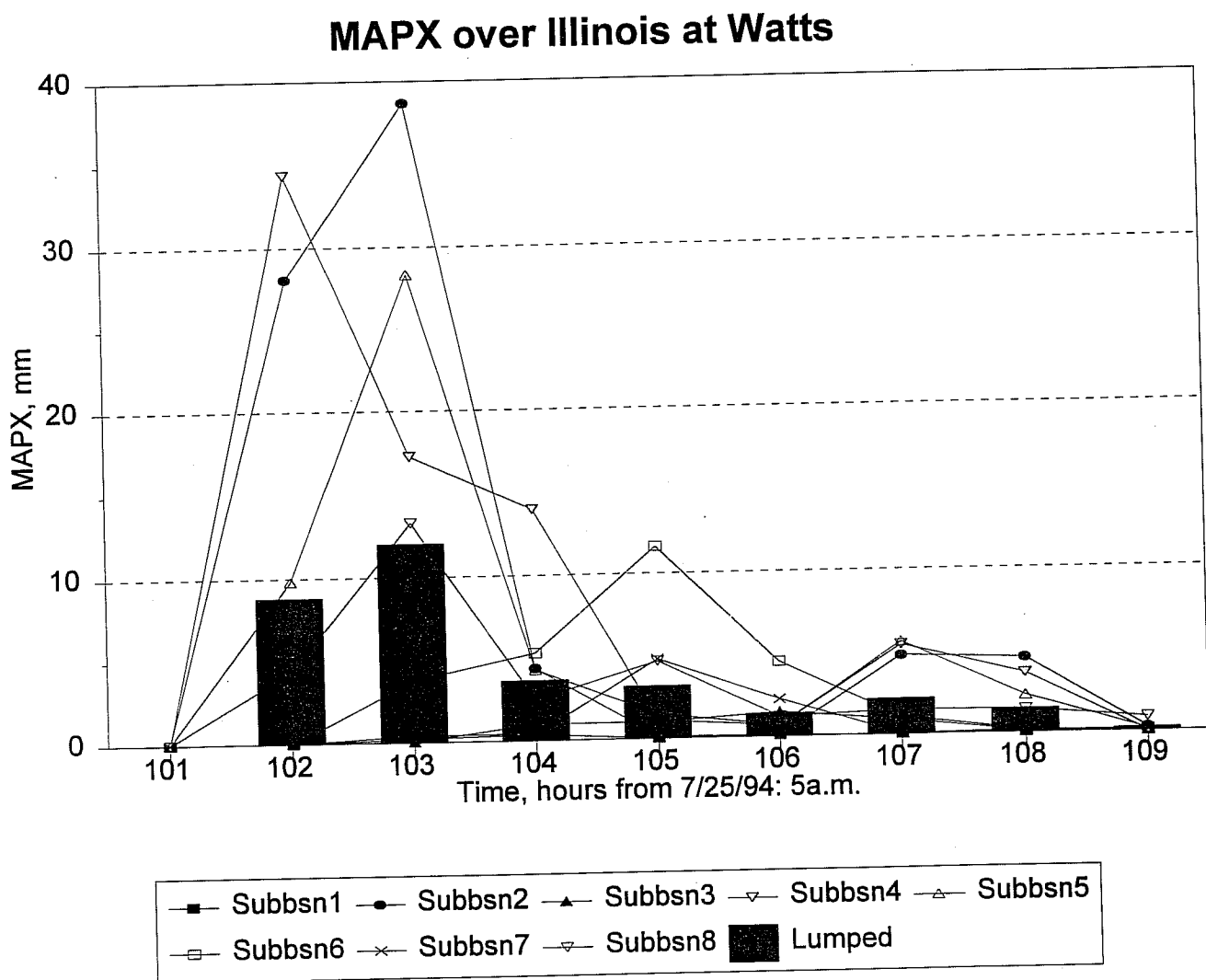(Graph: discharge in cms vs time in hours)

Figure 5-16   Distribution of Sub-basin MAPX Values for Event
of July 25, 1994.

accuracy as noted in the RMS value. The standard deviation of the discharges increases from 23.76 to 34.44, indicating more variability in the hydrographs. It can be seen that the simulations using the operational 6-hour MAPX and 6-hour MAP time series produce significant bias. It is interesting to note that the %bias improves in version 8 compared to version 9. This is a surprising result in that the long term MAPX/MAP ratio for WTTO2 is 0.96 as reported in Table 3.1.2, indicating that the MAPX values are biased low compared to the MAP values. Apparently, the lower bias of -19.87 is dominated by the event of June, 1995, in which the MAPX values were much greater than the MAP values.

For this reason, these 6-hour simulations were repeated with a set of Sacramento model parameters that were used with the 1-hour NEXRAD tests. These tests are versions 6 and 7. Here it can be seen that an improvement in the RMS error from 14.7 to 11.74 was achieved, as was a reduction in the bias from -13.2 to -8.52. A slight increase in the variability was noticed as seen in the STD increasing from 28.44 to 29.42.

In general, 1-hour lumped simulations using Stage III derived MAPX information led to an increase in simulation accuracy, as seen in the results for versions 1,2 and 3. Statistically, the best results in this group were achieved by using a 1 hour unit hydrograph derived from the summation of 9 sub-basin unit graphs (method 3.1). Apparently, deriving a unit hydrograph using spatially varied information is better than unit hydrographs based solely on lumped information. The S-curve unit hydrograph and the lumped Nash unit hydrographs (methods 1 and 2) did not represent the definition of the hourly observed hydrographs.

Two sets of semi-distributed simulations were run with MAPX data from Stage III. In version 4, the Sacramento Model parameters from the lumped simulations were applied to each sub-basin.. Version 5 is the same as version 4, except that some Sacramento model parameter recalibration to the semi-distributed Stage III forcing was attempted. While visual inspection of the hydrographs in Figures 5-13 through 5-15 reveals a fairly good fit, the statistical results for this version show a slight degradation compared to any of the 1-hour lumped cases (version 2, 3, and 4) Apparently, the RMS statistic, which tends to emphasize peak flow differences, is worsened by cases such as those in Figure 5-15. In essence, while a 1-hour semi-distributed representation WTTO2 shows a slight general improvement in visual agreement between simulated and observed hydrographs, any statistical improvement is masked by the peak flow errors in a few events.

In general, plots of the simulated and observed hydrographs and statistical results indicate that the greatest improvement over the current 6-hour rain-gage based strategy is to use a lumped model forced by NEXRAD-derived mean areal precipitation estimates in conjunction with a redefined and calibrated 1 hour unit hydrograph. Further increases in simulation accuracy can be achieved by using a semi-distributed approach. However, such increases are slight and must be weighed against the difficulty in parameterizing and calibrating a semi-distributed model.

Table 5.3.1-2. Statistical results from Lumped and Semi-distributed tests of WTTO2. Simulation Period is June 1, 1994 through June 30, 1996

Version	Hourly			6-Hourly			Daily		
	STD	RMS	%BIAS	STD	RMS	%BIAS	STD	RMS	%BIAS
Observed Streamflow	33.98			33.68					
Hourly Simulations				Hourly Simulations Averaged to 6-hour time step					
1 Lumped MAPX, Method 1 uhg	35.10	10.87	2.12	34.97	10.22	2.09		7.70	2.07
2 Lumped MAPX, Method 2 uhg	36.73	11.97	1.71	36.51	11.17	1.68		8.12	1.66
3 Lumped MAPX, Method 3.1 uhg	34.40	10.07	1.71	34.24	9.50	1.68		7.47	1.67
4 Distributed Parms (lumped 1-hour) MAPX	38.52	13.24	4.25	38.01	12.47	4.22		8.64	4.22
5 Distributed Parms (recalibrated 1-hour) MAPX	36.87	12.55	3.18	36.59	11.58	3.16		8.39	4.80
6-hourly Simulations									
6 Lumped, Method 3.1 uhg, 6-hr, MAPX				29.42	11.74	-8.52		8.91	-8.50
7 Lumped, Method 3.1 uhg, 6-hr gage MAP				28.44	14.70	-13.2		11.77	-13.2
8 Lumped, calb. uhg, 6-hr MAPX, parameters from historical calibration				34.44	18.95	-19.87			
9 Lumped, calb. uhg, 6-hour MAP parameters from historical calibration				23.76	17.84	-25.52			

5.4 Lumped and Semi-distributed tests with Basin ELDO2

5.4.1 Approach for ELDO2

Unit hydrographs for the basin ELDO2 were derived using the methods in section 5.2. For the semi-distributed modeling tests, ELDO2 was disaggregated into 5 sub-basins along natural topographic ridgelines. A unit hydrograph for each sub-basin was derived using method 3.1.

A 1- hour unit graph was derived by summing the sub-basin unit hydrographs. For 6 hour lumped simulations, the manually calibrated 6-hour unit hydrograph was used. Manual calibration of SAC model parameters was performed using standard trial and error approach using MAP time series derived from NCDC data.

For tests with the NEXRAD data, recalibration of the SAC parameters was performed using automated optimization techniques. The same parameters were used for the semi-distributed and distributed representations and are listed in Table 5.4.1-1

Lumped 6-hour simulations were performed using MAPX and MAP time series from the archives of operational data. These simulations used SAC parameters calibrated using standard manual methods and NCDC cooperative observer data.

5.4.2 Results

As with the tests with basin WTTO2, simulations were run from October, 1993 to July, 1996. However, statistics were generated only for the period of June 1, 1994 through June 30, 1996. In this way, any biases caused by improper initial conditions in October, 1993 would be minimized by allowing the model to cycle through almost a complete year.

Figures 5-17 through 5-20 show typical events from the 6-hour time step simulations using the archived operational MAPX and MAP time series and manually calibrated parameters using historical raingage data. It can be seen in all these figures that the simulations with both radar and gage data are predominately poor, with the rain-gage simulations showing a slightly better agreement. The November 5, 1994 event was best simulated using the 6-hour rain gage data. In this case, the radar based storm total precipitation over a 3 day period is 4.968 inches, while the rain gage network mean areal values totaled just slightly more, 5.117 inches. However, examination of the MAPX and MAP time series reveals that the rain gage network recorded a 6 hour period with over two inches of rain, while the radar recorded only a bit over 1 inch for the same period. This is puzzling, in light of Figure 3-3, which showed that the radar precipitation estimates are usually more intense. For this event, the Sacramento model generated fast responding surface runoff for this period using the more intense MAP data, leading to the peaked hydrograph response. Using the less intense MAPX data, the Sacramento model simulated this event as slower responding interflow. The intensity was not extreme enough to fill the upper zone tension water reservoir so as to generate fast responding surface runoff.
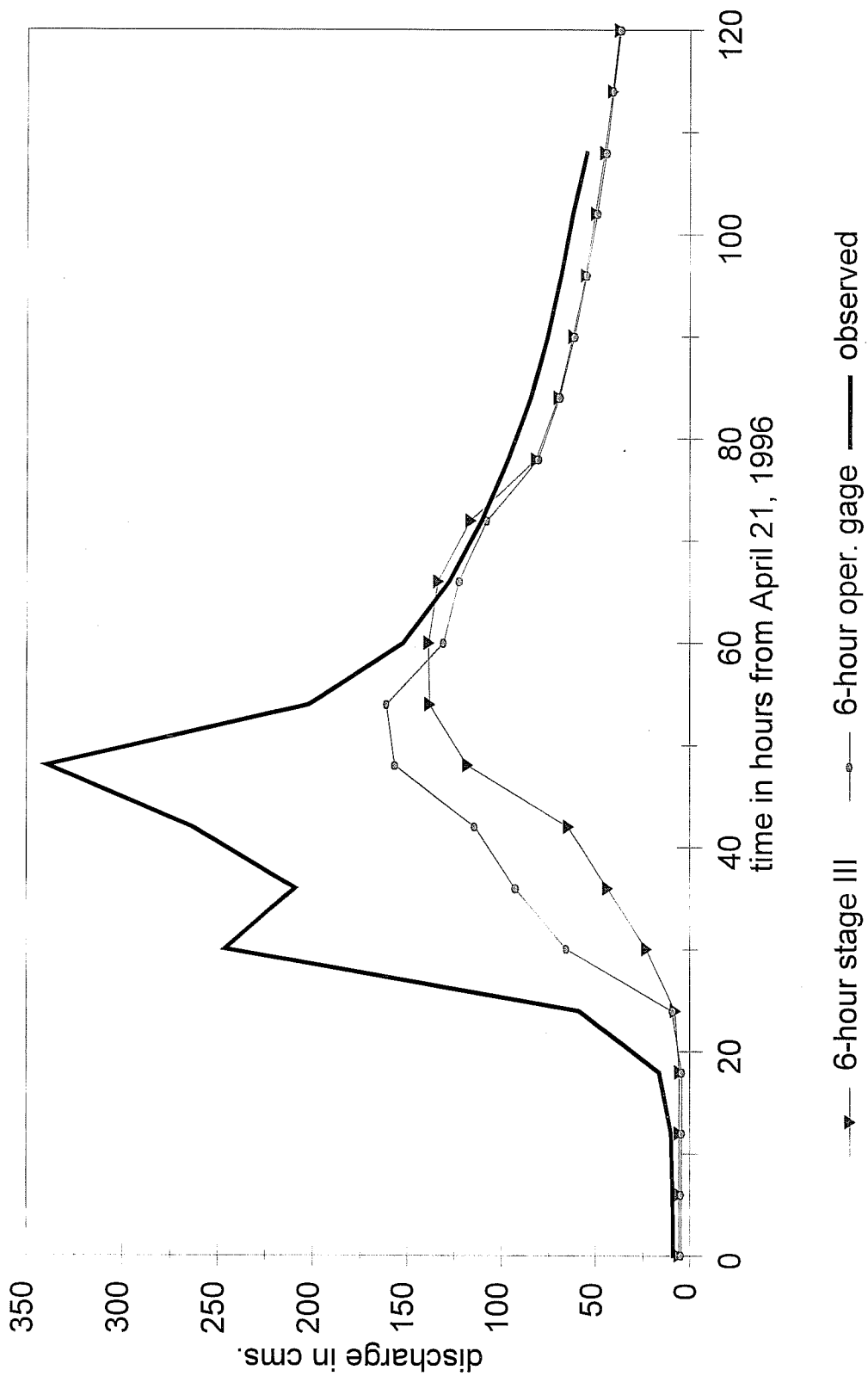
Figure 5-17 ELDO2 April, 1996
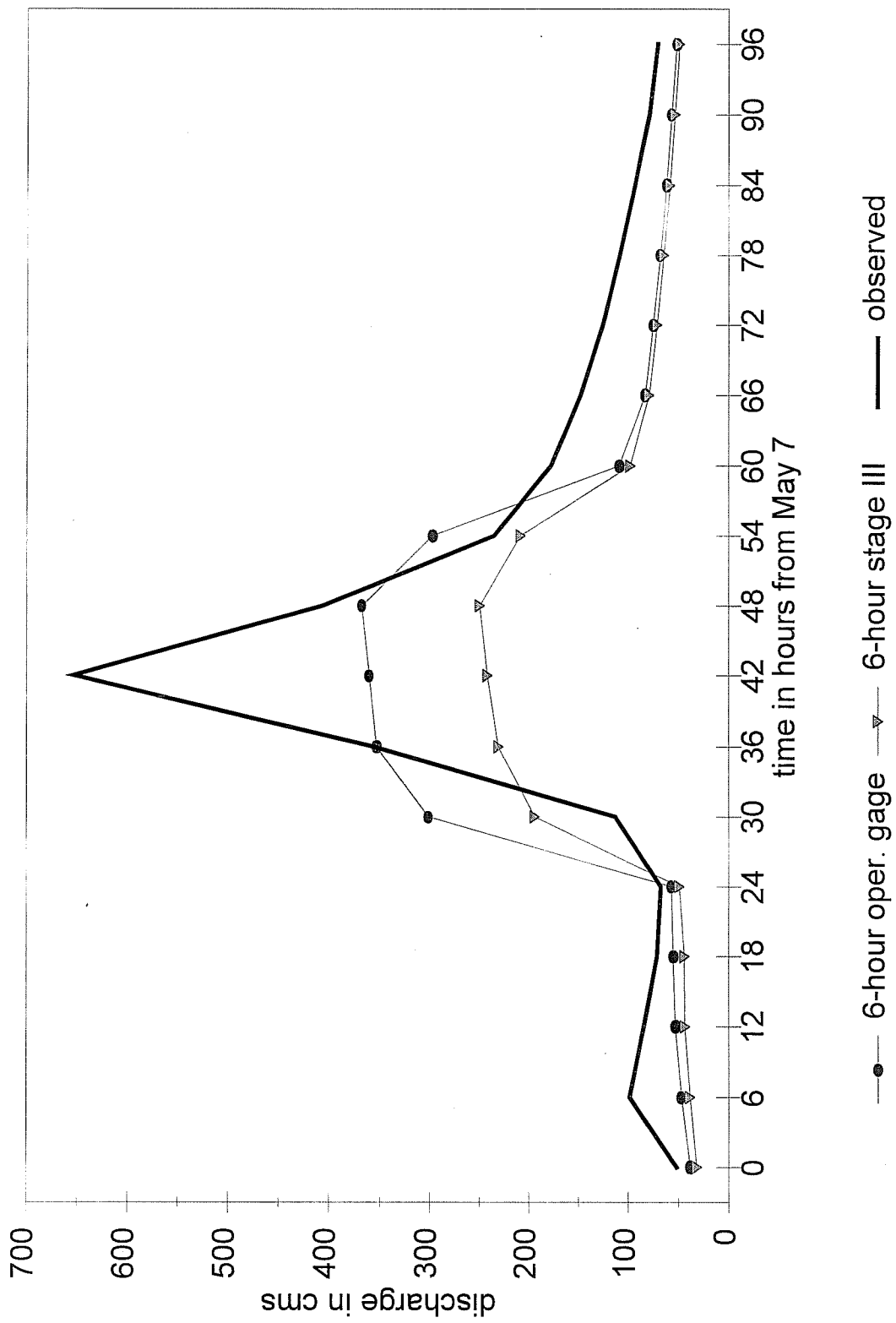Lumped 6-hour Radar and Op. Gage Tests

Legend: 6-hour stage III   6-hour oper. gage   observed

Y-axis: discharge in cms.

X-axis: time in hours from April 21, 1996

Figure 5-18 ELDO2 May 7, 1995
Lumped 6-hour Radar & Op. Gage Tests

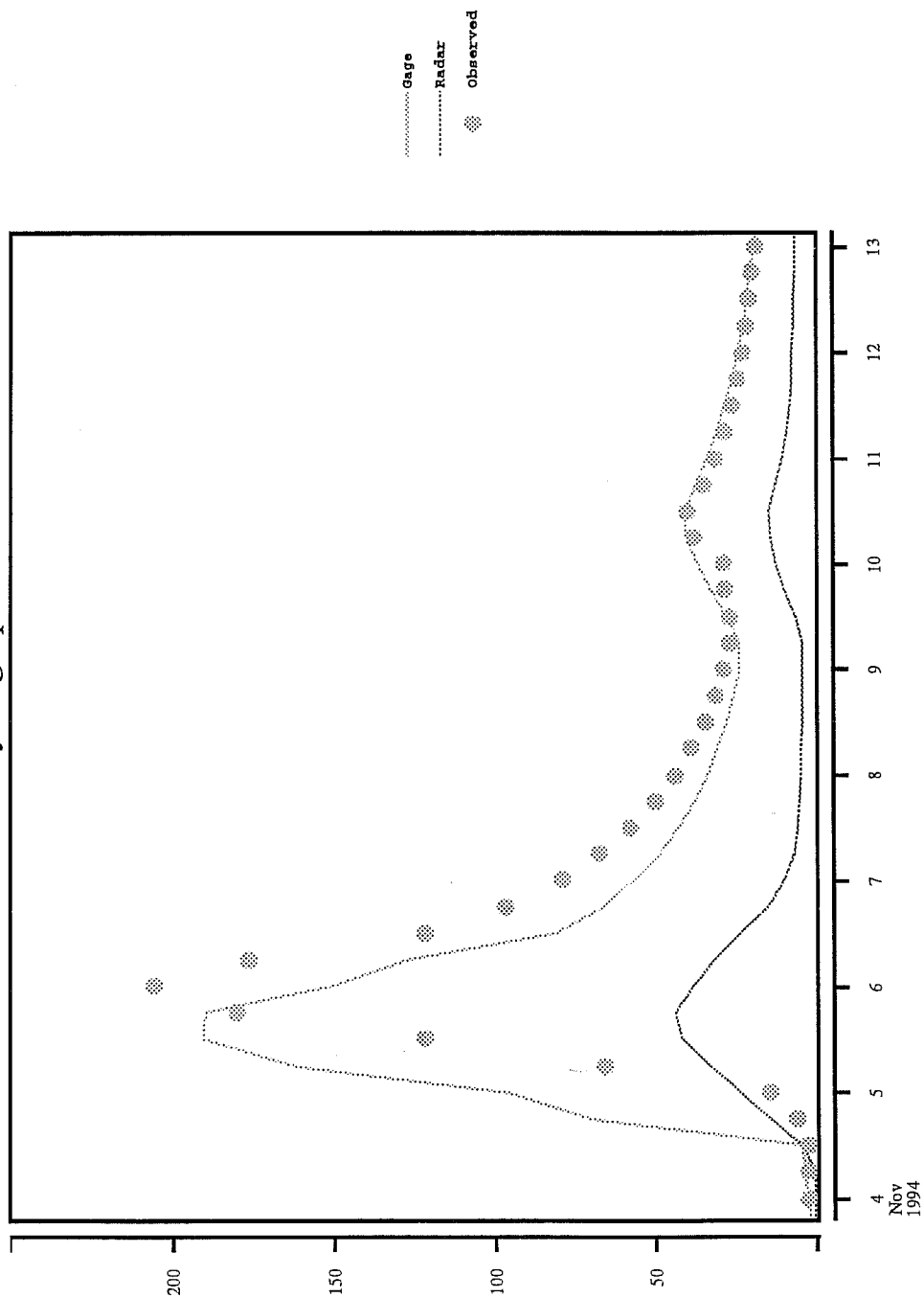—●— 6-hour oper. gage   —▽— 6-hour stage III   —— observed

6-hour hydrographs at Eldon

Figure 5-19   Lumped 6-hour Radar and Operational Gage Simulations for
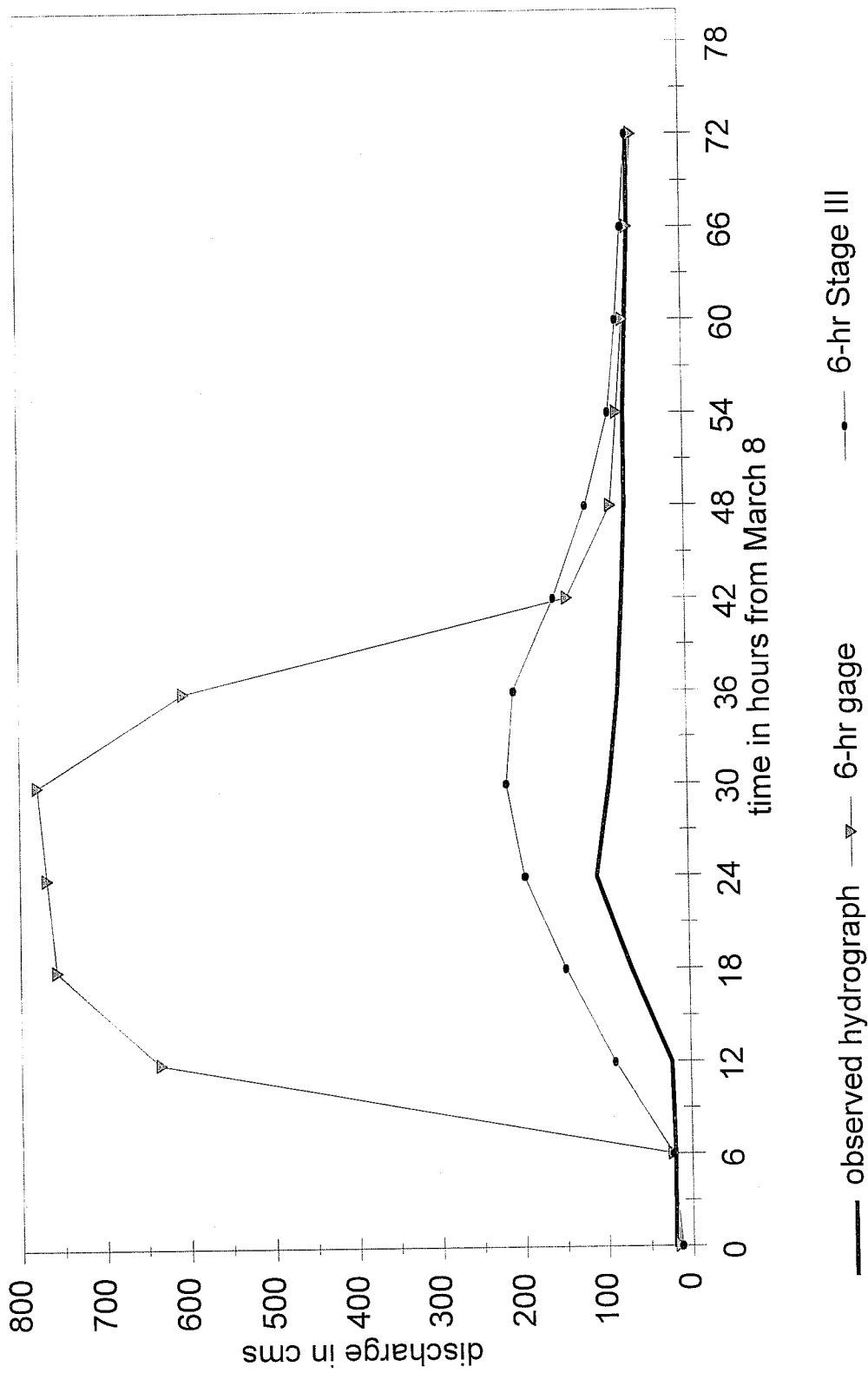Event in November, 1994.

Figure 5-20 ELDO2 March 8, 1994
Lumped 6-hour Radar and Op. Gage Tests

Table 5.4.1-1 Sacramento Model Parameters for 1 Hour Lumped and Semi-Distributed Simulations.

parameter	value
uztwm	45.0
uzfw	30.0
uzk	0.3
pctim	0.0
adimp	0.01
riva	0.017
zperc	190.0
rexp	1.5
lztwm	175
lzfsm	25
lzfpm	40
lzsk	0.10
lzpk	0.008
pfree	0.1
side	0.0

Figure 5-20 presents an event in which the precipitation as measured by the operational raingage network led to an extreme overprediction, while the MAPX based simulation was more reasonable. Examination of the MAP time series indicated that on March 8, 4.33 inches of precipitation fell over the entire ELDO2 basin as a 6 hour areal mean. However, a closer look at the NCDC climatological data for this month revealed that none of the point precipitation stations recorded more than 2.6 inches for any day. Clearly this MAP value of 4.33 inches is an error. In addition, from an examination of NCDC snowfall data and temperature data for March 7-9, 1994,

it is evident that this event was a snowfall event. So, in addition to the errors in the 6-hour MAP, the event was also mistyped as a rainfall event when it was most likely a snowfall event. Recall that the SNOW-17 model is not used on the simulations in this report. While snow does occur in the area, it is not a dominant part of the hydrological cycle. Discussions with personnel at the Tulsa River Forecast Center reveal that while snow may occasionally occur, it quickly melts.

Figures 5-21, 5-22, and 5-23 present typical results from the lumped and semi-distributed results of basin ELDO2 using radar data. Recall that in these simulations, some recalibration of the historical parameters to the radar data was performed. As with WTTO2, semi-distributed modeling scenarios did not greatly improve hydrograph simulation beyond the lumped approach. Lumped results based on hourly NEXRAD were quite good for the single peaked events in Figures 5.4-5 and 5.4-7, and the semi-distributed approach was not able to achieve much better accuracy. Neither the lumped nor semi-distributed approaches were able to adequately reproduce the second peak in Figure 5.4-6

Table 5.4-1 presents the statistical results for the simulations for basin ELDO2. Version 4 represents the operational rain gage data with SAC-SMA model parameters calibrated using historical.. This simulation should represent the best possible using the current lumped, 6-hour gage-based modeling strategy. It is important to note that the use of the operational MAP time series with historically calibrated parameters led to a -23% bias. Use of MAPX data (1 hour data accumulated to a 6 hour time step) with the historically calibrated SAC-SMA parameters (Version 3) led to a further decrease in simulation accuracy, with a two fold increase in bias to -49.71. It is unclear why the bias using operational 6-hour gage data would be greater than that computed using the historical 6-hour gage data. Comparison of versions 3 and 4 indicates that SAC-SMA parameters should not be the same for rain gage and Stage III forcing.

As with the tests with basin WTTO2, there is a great increase in accuracy over the lumped 6-hour tests by using 1-hour lumped MAPX based simulations. Comparison of the results for version 4 and Version 1 show that the RMS error statistic is halved by using MAPX and a re-defined unit hydrograph. Disaggregation of the ELDO2 basin into 5 sub-basin, each with its own unit hydrograph, only slightly improves the RMS and %BIAS statistics. As for WTTO2, it appears that the greatest gain in simulation accuracy compared to current modeling methods is to use hourly MAPX values with a re-calibrated SAC model and re-defined hourly unit graph. One must question whether the slight gain in simulation accuracy justifies the effort involved with the disaggregation of ELDO2 into 5 sub-basins.
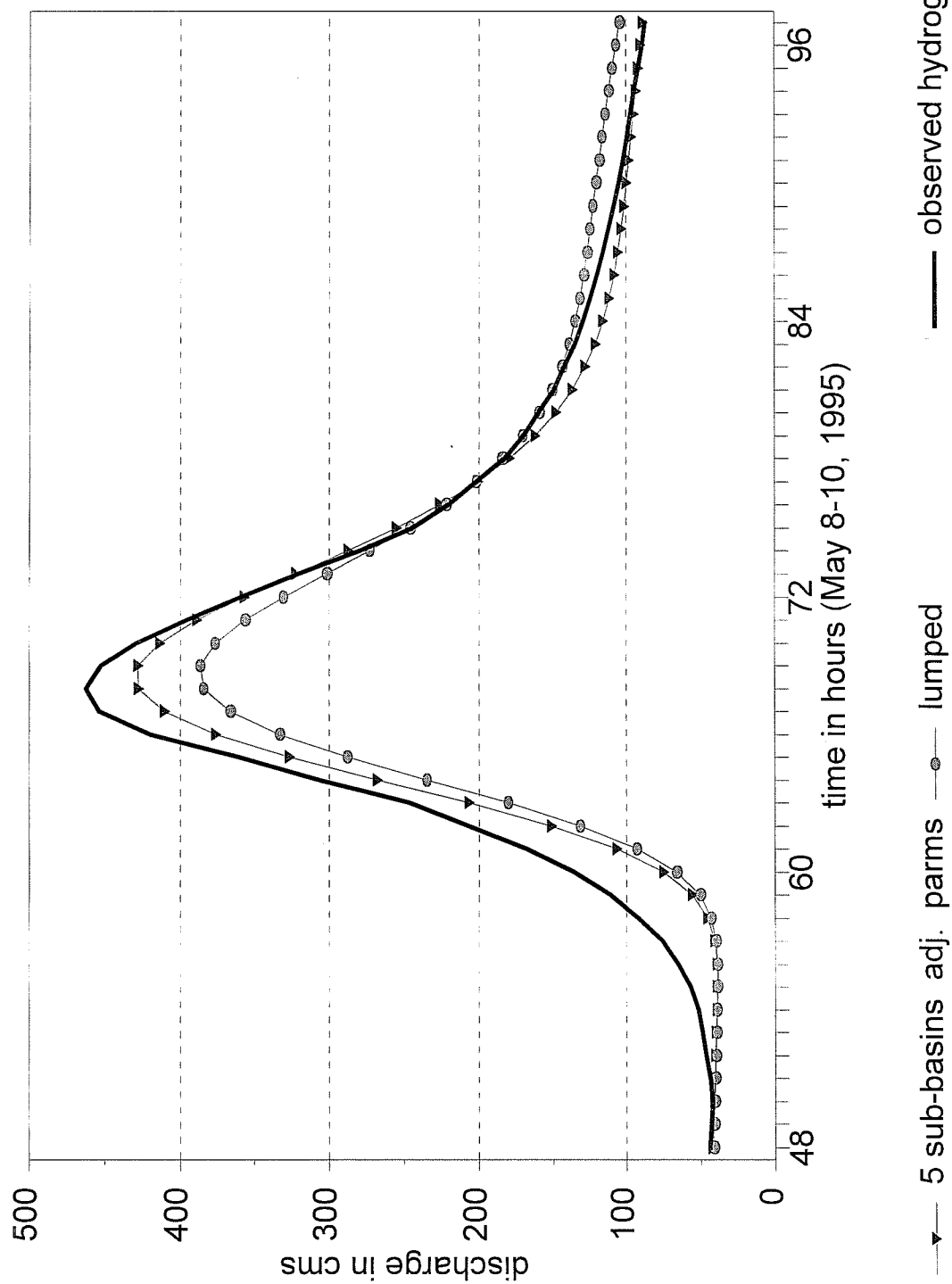
5.40

Figure 5-21 ELDO2 May 8-10, 1995
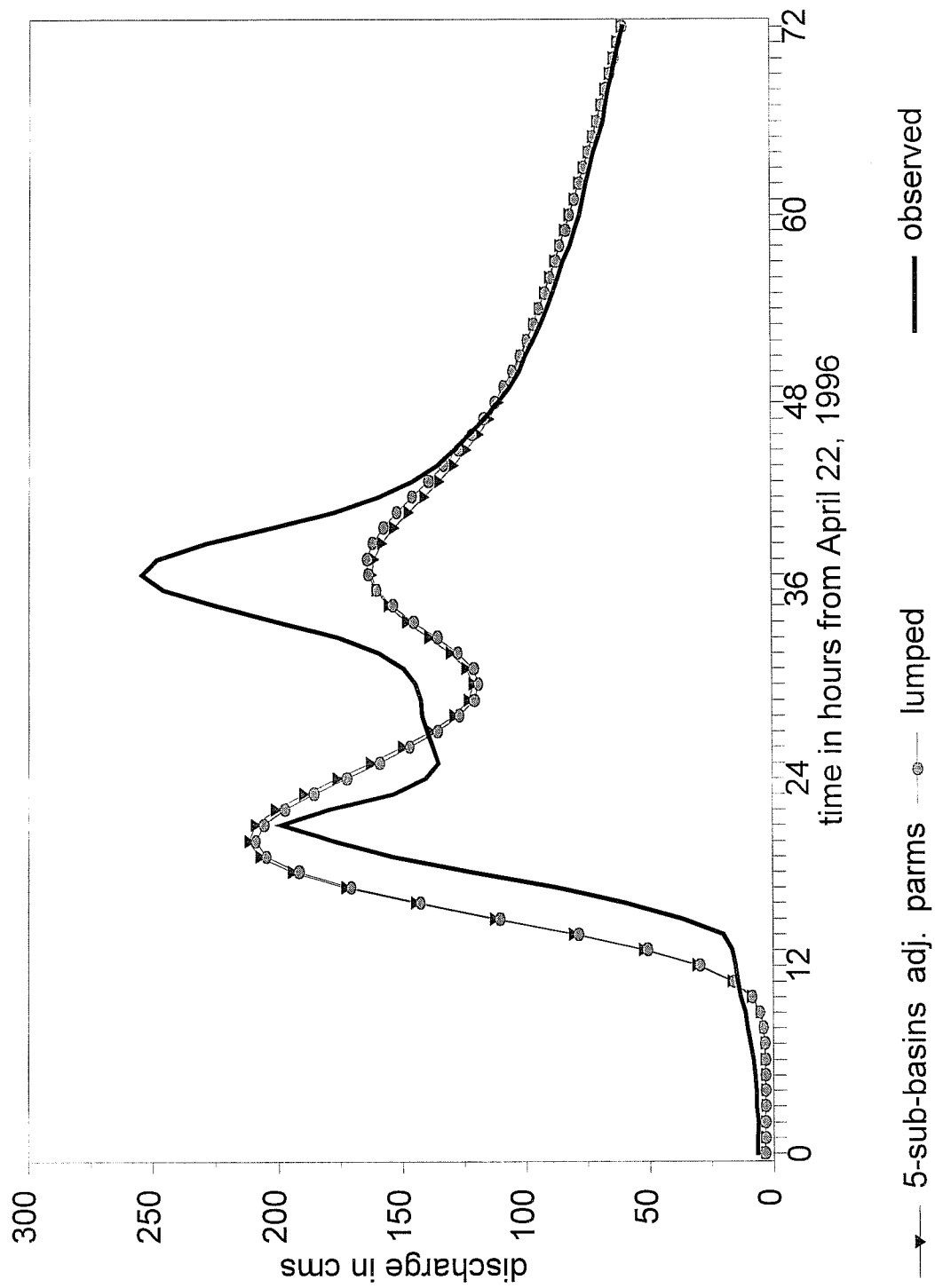Semi-Distributed & Lumped Simulations

Figure 5-22 ELDO2 April 22-25, 1996
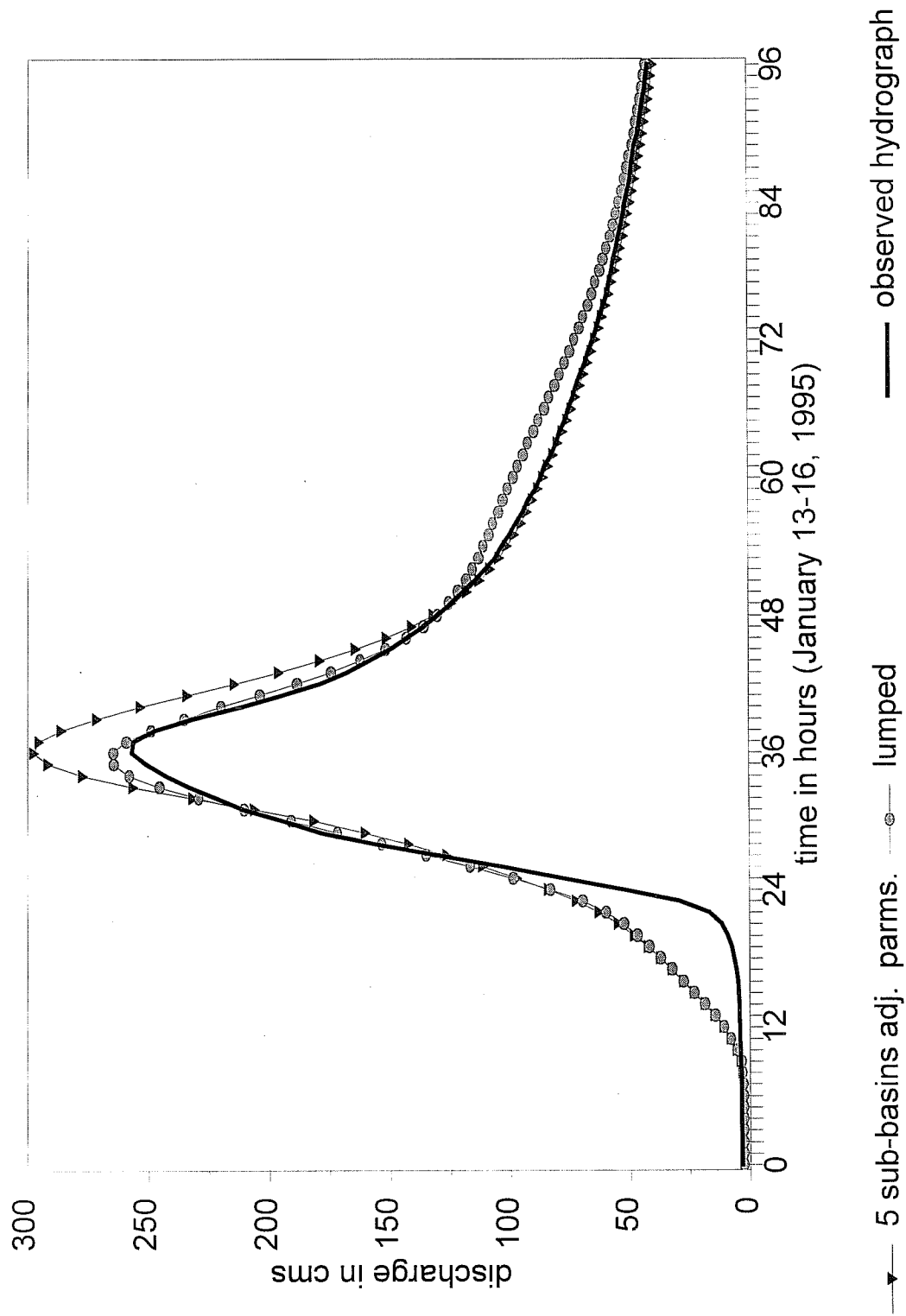Semi-distributed & Lumped Simulations

Figure 5-23   ELDO2   Jan. 13, 1995
Semi-distributed & Lumped Simulations

Table 5.4-1 Results for Lumped and Semi-distributed Modeling Tests for Basin ELDO2. Period is June 1, 1994 through June 30, 1996

Version	Hourly			6-hourly			Daily		
	STD	RMS	%Bias	STD	RMS	%Bias	STD	RMS	%Bias
Observed streamflow	19.36	-	-	19.12	-	-	-	-	-
Hourly Simulations				Hourly averaged to 6-Hourly					
1 Lumped, MAPX, Method 3.1 uhg,	17.36	7.38		17.20	7.10		6.1	-15.5	
2 Distributed, lumped parms, Method 3.1 ugh	17.98	7.22		17.79	6.91		5.7	-13.7	
6-Hourly Simulations									
3 Lumped, Operational 6-hour MAPX, parameters from historical calibration	-	-	-	16.10	16.24	-49.71			
4 Lumped, Operational 6-hour MAP, parameters from historical calibration.	-	-	-	21.70	14.37	-23.42			

5.44

5.5 Lumped and Semi-Distributed Simulations at Talequah.

5.5.1 Approach

Lumped and semi-distributed simulations for the basin defined by the gage on the Illinois River at Talequah, OK (TALO2) followed the same methodology used with basins ELDO2 and WTTO2. The total area of basin TALO2 (959 sq. mi or 2484 sq. km) contains the headwater basins WTTO2 and KNSO2. TALO2 is treated as a local area in the operational model used by the Tulsa River Forecast Center, with basins KNSO2 and WTTO2 flowing into it. In lumped modeling tests described herein, TALO2 was treated as a single headwater basin in order to perform tests on a basin larger than WTTO2, KNSO2, and ELDO2. In semi-distributed modeling tests, TALO2 was disaggregated into 9 sub-basins.

As the basin above the gage is not modeled operationally as a lumped area, no operational rain gage derived MAP time series is available for the entire area. Thus, all simulations for basin TALO2 were performed at a 1-hour time step using the Stage III product to define precipitation input for lumped and semi-distributed simulations. Parameters for the Sacramento model were derived through automatic calibration against observed hourly streamflow values and are presented in Table 5.5-1

Table 5.5-1 Hourly SAC-SMA Parameters used for Lumped Simulations in Basin TALO2

parameter	value	parameter	value
uztwm	123.0	lzfsm	95.9
uzfw	49.4	lzfpm	289.0
uzk	.749	lzpk	0.0097
pctim	.005	lzsk	0.122
adimp	0.0	pfree	0.693
riva	0.015	side	0.0
zperc	30.5		
rexp	1.3		
lztwm	249.0		
lzfsm	95.9		
lzfpm	289.0		

5.5.2 Results

Figures 5-24 through 5-26 present typical results from hourly lumped and semi-distributed simulations of basin TALO2. Once again it was surprising to see the close agreement between the lumped and semi-distributed simulations. Moreover, both simulations appear to be reasonably accurate compared to the observed hourly streamflow hydrographs.

Figure 5-27 presents hourly simulations for the event in July, 1994. This is the same event presented for WTTO2 in Figure 5-15. These results indicate that the semi-distributed formulation performed worse than a lumped representation. This is most likely due to the problems of Sacramento model parameterization in sub-basins which were discussed in Section 5.3.1

Table 5.5-2 presents the statistical results of lumped and semi-distributed tests for TALO2 from June 1, 1994 to June 30, 1996. These statistics verify that there is very little simulation improvement gained by using a semi-distributed formulation versus a lumped model. While figures 5-24 through 5-26 indicate quite close agreement between lumped and semi-distributed formulations, Table 5.5-2 shows that the hourly statistics actually slightly worsen when using a 9 sub-basin formulation. As with the statistical results for basin WTTO2, this is most likely due to events such as that is Figure 5-27, which would tend to emphasize the RMS error statistic.
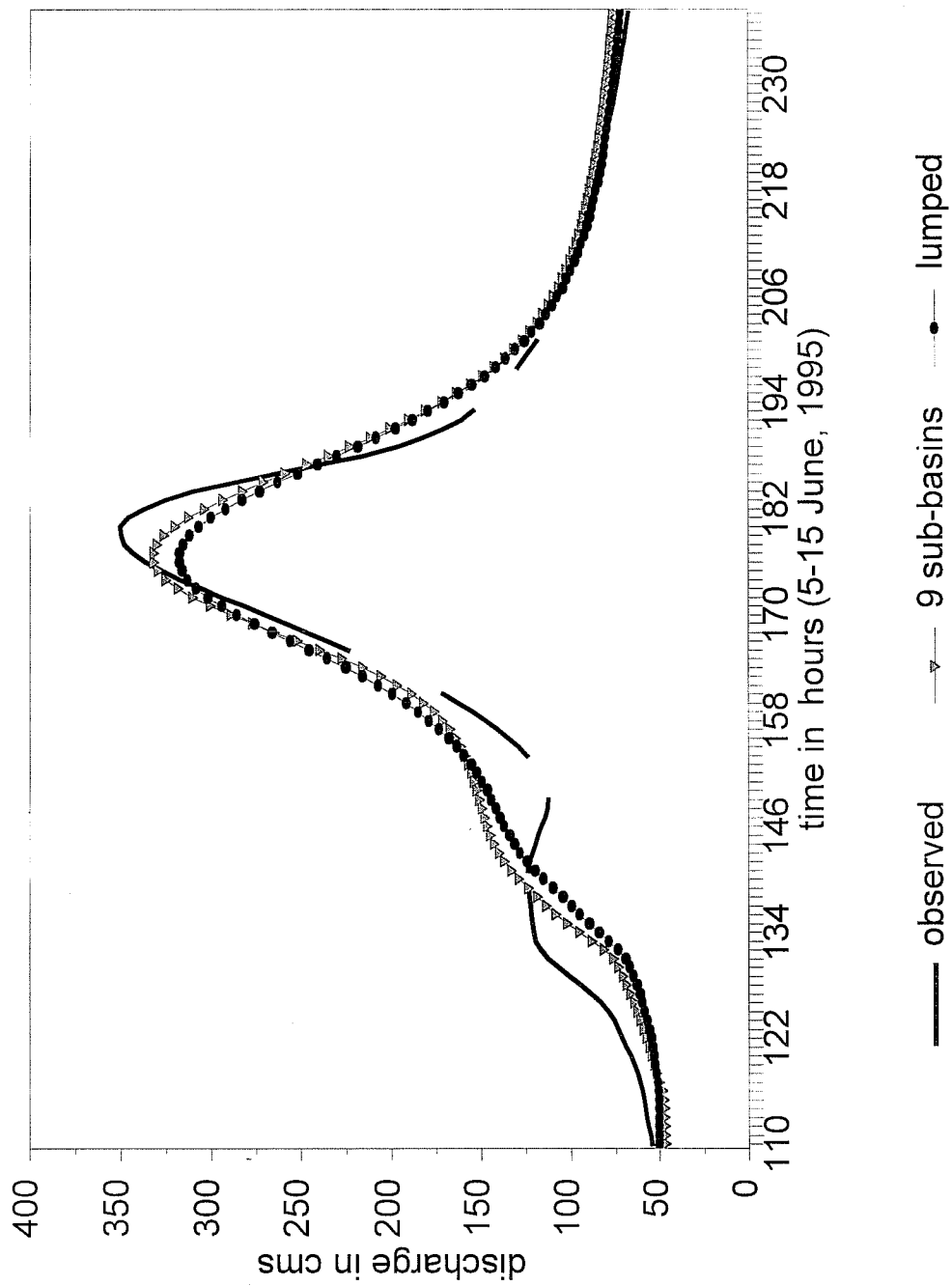
Figure 5-24 TALO2 June, 1995
Semi-distributed & Lumped Simulations

legend: observed — 9 sub-basins — lumped

time in hours (5-15 June, 1995)
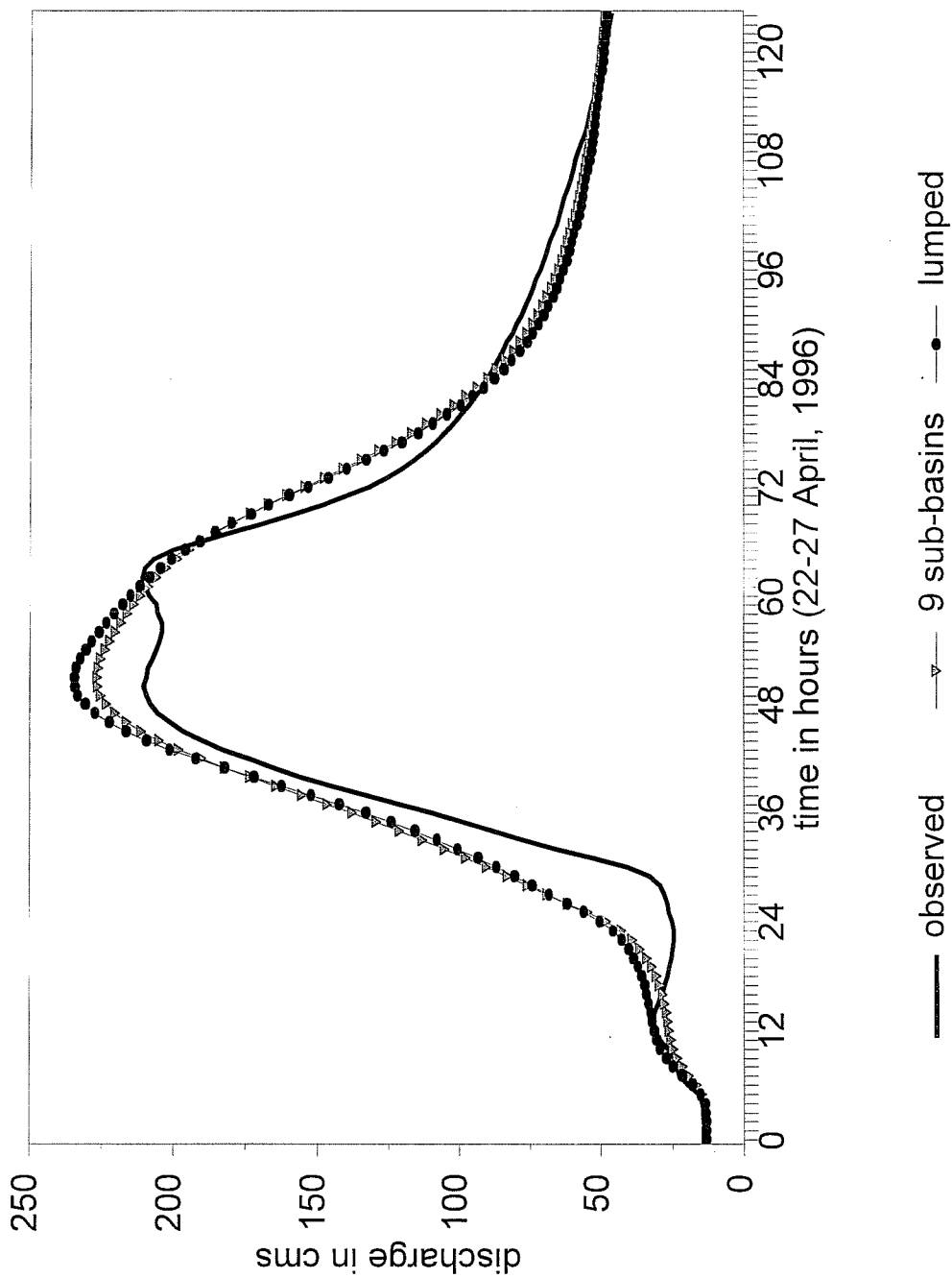
discharge in cms
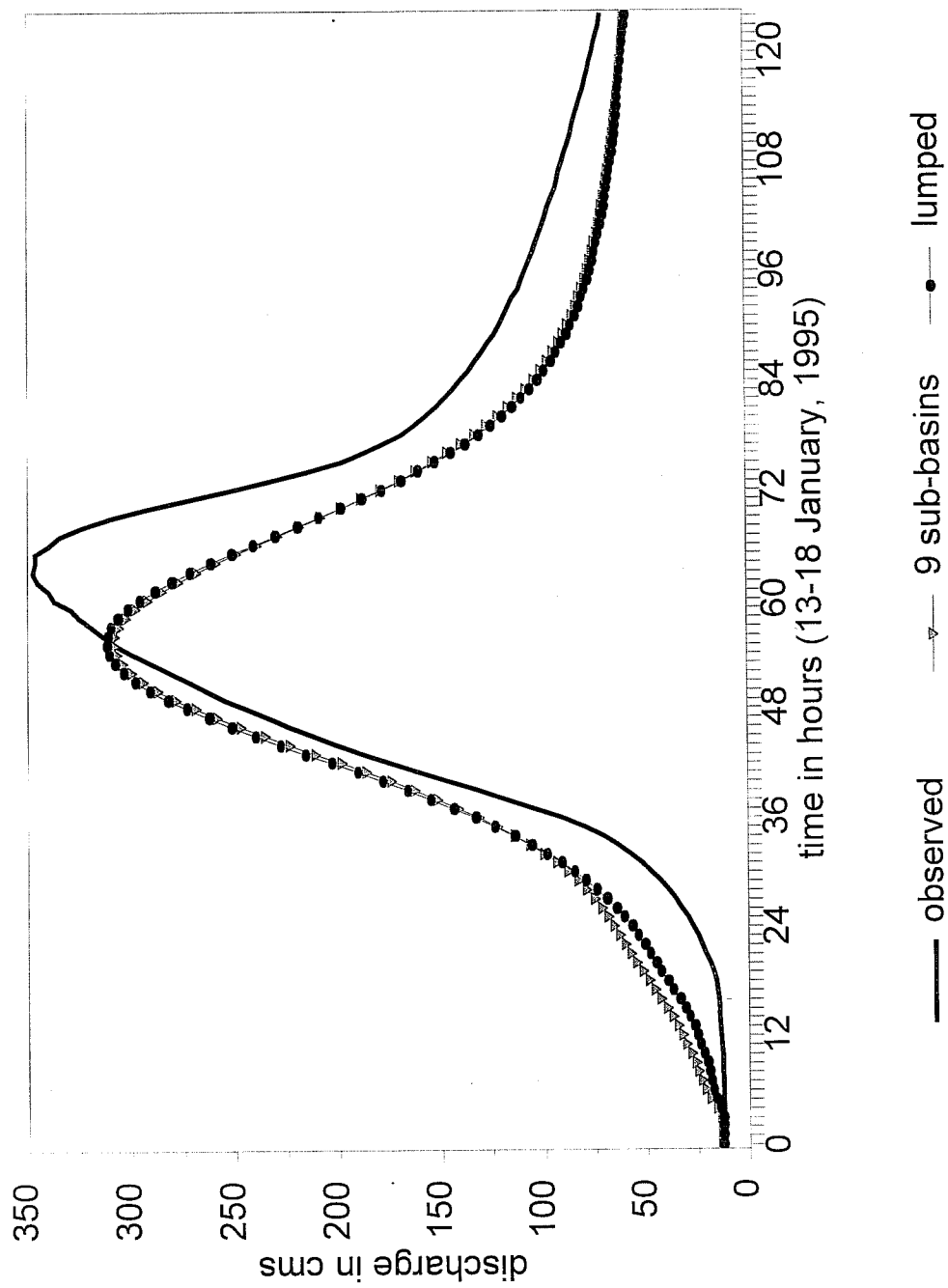
Figure 5-25 TALO2 April 22, 1996
Semi-distributed & Lumped Simulations

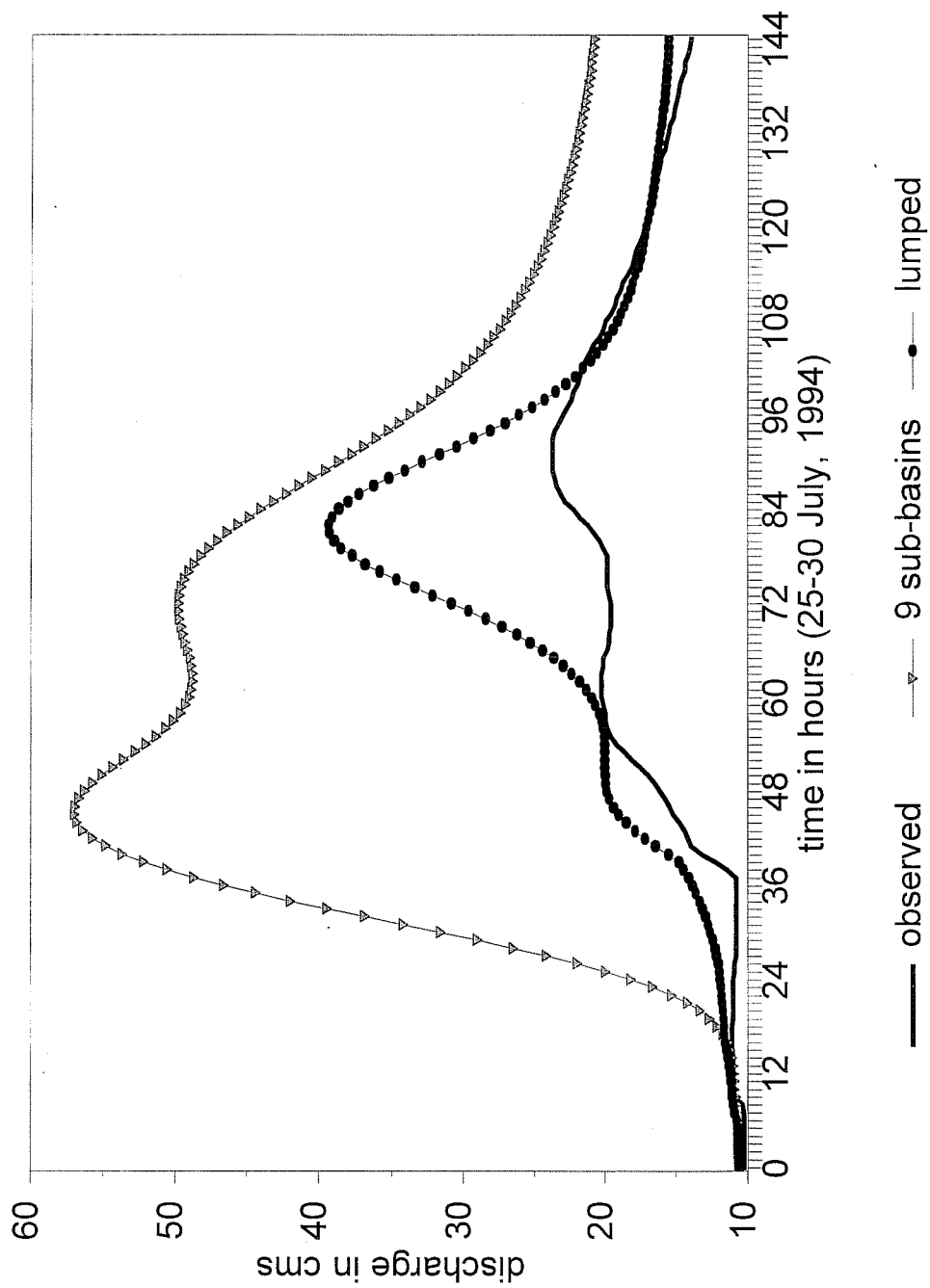Figure 5-26 TALO2 Jan., 1995
Lumped & Semi-distributed Tests

Figure 5-27 TALO2 July, 1994
Lumped & Semi-distributed Tests

Table 5.5-2   Lumped and Semi-distributed results for TALO2 for Period June 1, 1994 to June 30, 1996

Version	STD	RMS	%BIAS	STD	RMS	%BIAS	STD	RMS	%BIAS
observed hourly streamflow	28.9			28.9					
1	Lumped, hourly MAPX	28.8	9.22		28.9	9.07		8.0	8.6
2	Semi-distributed, 9 sub-basins, hourly MAPX	28.5	9.55		28.5	9.40		8.6	12.1

5.51

5.6 Discussion of Results from Lumped and Semi-Distributed Tests with NEXRAD.

It is important to present the results of the preceeding section in light of past research on the effect of precipitation variability on basin outflows. Numerous studies have been conducted in the past two decades that point to the sensitivity of runoff hydrographs to spatial and temporal variations in precipitation. Many of these studies examined the effects of raingage sampling errors on the outflow hydrograph. In an early and oft-quoted work, Wilson et al., [1979] showed that the spatial distribution of rainfall had a marked influence on the runoff hydrograph from a small catchment. On the other hand, Beven and Hornberger [1982] stated that rainfall patterns have only a secondary effect on runoff hydrographs, while a correct assessment of the global volume of rainfall input in a variable pattern is more important in simulating streamflow hydrographs. On a small watershed, Krajweski et al., [1991] found a higher sensitivity to the temporal resolution of precipitation than to the spatial resolution. Ogden and Julien [1994] performed tests that identified when spatial and temporal variability of precipitation was dominant. Troutman, [1983], Ogden and Julien [1994], and Shah et al.,[1996a,b] also investigated the effects of precipitation variability on hydrologic simulations.

It is interesting to note that the majority of these and other studies were based on synthetically generated precipitation and streamflow records. Usually, comparisons were made against a 'reference' or 'truth' hydrograph generated by running the hydrologic model at the finest data resolution. Synthetically generated data were often used due to the lack of appropriately long periods of observed data. Moreover, it can be seen from the research listed in Table 5.6-1 that the majority of studies emphasizing the importance of the spatial variability of precipitation used models containing the Hortonian runoff generatiion mechanism. It is now recognized that runoff results from a complex variety of mechanisms and that in some basins, a significant portion of runoff hydrographs is derived from slower responding subsurface runoff [Wood et al., 1990].

Obled et al., [1994] commented that the numerical experiments in the literature were based on the use of models which may be only 'a crude representation of reality'. Furthermore, they argued that the actual processes at work in a basin may not be those predicted by the model. Thus, the research in the literature may have shown the sensitivity of a particular *model* to the spatial variatiability of precipitation, not the sensitivity of the actual *basin*. The work of Obled et al. is significant in that they were perhaps the first to examine the effects of the spatial variation of rainfall using observed precipitation and streamflow data. In addition, the model used in their studies focused on saturation excess runoff as the main runoff generation mechanism. In simulations against observed data, they were unable to prove the value of distributed inputs. A semi-distributed representation of the basin did not lead to improved simulations compared to a lumped basin modeling scenario. In some cases, their model responded to a rainfall event which the basin either ignored or dampened. In a reformulation of their earlier model, Lindstrom et al, (1997) were able to improve their semi-distributed model

performance, but concluded that they could not expect further breakthroughs as long as standard input data is used and models are judged only by analysis of river runoff.

It is surprising to note that in all three watersheds in the tests herein, disaggregation of the parent basin into sub-basins did not greatly improve simulation accuracy beyond that achieved by the 1-hour lumped Stage III-based simulations. In some cases, the semi-distributed approach led to a slight improvement in timing. Yet, it was surprising to find that little improvement was gained even though strong rainfall gradients existed across the parent basin. In fact, the statistics show that for WTTO2, the RMS error actually increases a small amount when a semi-distributed formulation was used. In support of the findings of Pessoa, et al.[1993] and Obled et al. [1994], a sub-basin approach to capture the critical spatial variability of precipitation did not produce the expected improvements in streamflow simulation. It appears that consideration of the spatial variability of the rainfall was important only insofar as it facilitated a more accurate measure of the basin average volume. Any information contained in the spatial pattern of precipitation did not lead to improvements in simulation.

These findings are counter-intuitive in that one would think that higher resolution information would lead to better results. Obled et al. [1994] investigated similar surprising results and postulated that they may be due to the type of runoff generating mechanism. In basins marked by Hortonian i.e, infiltration excess, type of runoff generation, variability of both precipitation and soil characteristics is important and is reflected in the basin outlet hydrograph. In areas where saturated areas dominate the runoff generation process, most of the rainfall infiltrates and spatial variations in the intensity of precipitation are dampened by the storage and delays in the soil layers. They argued that while the spatial variability of precipitation is important, it is not 'sufficiently organized in time and space to overcome the effects of smoothing and dampening' when routed through a watershed

Finding similar results, Pessoa et al. [1993] noted that appropriately spatially averaged precipitation seemed sufficient for the 840 sq. km. basin in their study. In their investigation, a distributed model containing both Hortonian and saturation-excess mechanisms in each computational grid element was used. In their synthetic analyses, all simulations were begun when the basin was in a 'wet' state, and when the dominant runoff generating mechanism (measured by the number of pixels predicting each type of runoff) was rapidly changing from Hortonian to saturation-excess.

Although counter intuitive, the results presented herein do not seem surprising when viewed in light of the discussion presented in Obled et al. [1994]. In that work, the authors challenged the generally accepted idea that the spatial and temporal variation of rainfall has a strong effect on the outlflow hydrographs from natural catchments, arguing that this concept has been taken for granted and has been based on numerical experiments and not simulations against observed data. Numerical studies with synthetic data were performed in part due to the lack of a sufficiently long record (Krajewski et al., [1991], Beven and Hornberger, [1982]).

In discussing their semi-distributed results,   Obled et al. [1994] also noted that:

' *the results do no degrade with distributed information, but just remain at the same already high level.* '

However, it was noticed in several cases in our results where the semi-distributed approach actually produced worse results than the hourly lumped simulations. Investigation into one such event in the WTTO2 basin (not shown) revealed that the precipitation occurred predominately over a few of the sub-basins. In this case either the Stage III estimate of precipitation is drastically wrong or the parameters in the sub-basins need to be quite different, indicating the method of calibrating a semi-distributed model outlined above needs to be refined. Apparently, assigning the same SAC-SMA parameters to each sub-basin is not a valid approach, even if calibrated to observed basin outlet hydrographs.   Assuming that the Stage III gridded precipitation estimates are valid, then it is clear from such examples that hydrologic model parameters may need to vary across sub-basins rather than be uniform.

Table 5.6-1   Survey of Research on the Importance of the Spatial and Temporal Variability of Precipitation

Author	Model Type, Runoff Mechanism	Analysis Type	Data	Basin Size, type	Conclusions
Dawdy and Bergman, 1969	Infiltration excess	Parameter optimization using 9 events		25 sq. km ; high moisture retention and absorption	Parameters from caibration are different for different patterns of rainfall.
Wilson et al, 1979	SCS (Hortonian?)	Numerical, point sampling, 1 vs 20 gages; 15 events	Synthetic Rainfall and Streamflow	26.5 sq. mi.	Rain volume from 1 gage same as vol from 20 gages Spatial distribution of rain and accuracy of the precipitation input have a marked influence on outflow hydrograph from a small catchment.
Shanholtz, et al., 1981,	Holtan I/E Finite Element model	Numerical, Thiessen weighting	1. hypo-thetical 2. actual	n/a ?	1. Large errors result when ignore spatial variability of precipitation 2. Rainfall dist. significantly affects peak, vol.
Beven and Hornberger 1982	Semi-distributed., bucket model	Numerical	Synthetic	287 sq. km homogenous	**Rainfall pattern per se has only 2nd order effect on hydrograph. Correct vol. of input in a highly variable pattern far more important than pattern itself.** Peak timing most sensitive to pattern.
Hamlin, 1982	HYSIM	Point sampling of synthetic rainfall	Synthetic rainfall, 'true' response		Sampling errors have a large effect on outflow hydrographs. Rainfall variation is imp. for small basins; for large catchments, general averaging balances out variations in catchment processes and rainfall.
Troutman, 1983	Green-Ampt Infil.-Hortonian (I/E)	Numerical	Synthetic		
Milly and Eagleson 1988	Hortonian (I/E) Saturation Excess (S/E)	Numerical	Synthetic	n/a	**Where I/E flow is significant, rain/runoff process is extremely sensitive to storm scale.** Fixed volume of rain produces more runoff when concentrated over smaller area. **When this is significant, must account for pattern *and* vol.**

Reference	Model	Method	Data	Area	Findings
Wyss, Williams, and Bras, 1990	Subsurface flow, all infiltrates, dist. routing, 2 velocities		Observed radar, Souhegan Squannacook	440 sq. km, 160 sq. km	**Large rainfall gradients appear to have only limited effect on response of basins.** Application to a basin dominated by Hortonian flow would justify use of gridded kinematic streamflow model
Chandrasekar, et al, 1990	DPM., SCS infil.,	Point sampling of radar	synthetic radar and 'true' streamflow	7.5 sq. km. Reynolds Ck.	Detailed radar data gave best sim.lumped radar input to dist.model like Pessoa gave less bias. Response times on small basins important. For large basins, aggregation of input data not as important. Performance may actually improve due to input-error averaging. MAP and lumped model gave worst results
Krajewski et al, 1991	SCS (Hortonian?) DPM and lumped	Point sampling of Monte Carlo rainfall fields	synthetic	7.5 sq. km Reynolds Ck.	Higher sensitivity to temporal than spatial variation.. 1, 5, 87 gages gave same results for small basins.
Naden, 1992.	Unit hydrograph, hillslope and channel routing	Semi -distributed	observed rain gage data	7,000 sq. km.	**Hillslope response is dominant; as a result a semi-distributed model is not a significant improvement over lumped.**
Pessoa, Bras, and Williams, 1993	**Hortonian & Dunn, DPM**	numerical, point sampling of radar, DPM with observed, averaged.	real radar for convective events, parial coverage	840 sq. km	**Distributed inputs to DPM same as lumped inputs to DPM** Use of isolated rain gages leads to large errors, agreed with Wilson, 1979.
Duncan, et al, 1993	Holtan infil excess, gridded DMP Not calibrated	10 sampling densities of radar data, then thiessen weights 256 trials each	real radar, synthetic flow	4800 sq. km	Shape of hydrographs from the 10 sampling densities is very sensitive to spatial variability of the rainfall.
Ogden and Julien, 1993	No infiltration, ie all runoff, DPM	numerical, monte carlo	synthetic	31.64 sq. km 121 sq. km.	Results only applicable to low permeability soils or high rain rates. Found conditins where spatial variability is dominant: $T_R < T_E$
Obled, Wendling, Beven, 1994	TOP-model Saturation Excess	point sampling of gages semi-dist & lumped;	**real raingage and flow data**	71 sq. km	Dense network gives better results. **Spatial variability of rainfall must be taken into account to get better total volume, not pattern. Semi-distributed modeling didn't help over lumped. Consider natural dampening in basin. Model produces hydrograph features not seen in observed data**

Ogden & Julien, **1994**	CASC-2D, Green-Apt Infil.	Synthetic; with and w/o infiltration	synthetic	32 sq. km 121 sq. km both Hortonian	'Storm smearing', 'watershed smearing' parameters computed for infiltration, no infiltration cases.
Shah et al, **1996**	SHE	point sampling of rainfall	synthetic	10.55 sq. km	Errors increased (compared to ref. hydrograph) when variability of rainfall field is increased.
Winchell, **1997, 1988**	Modified TOP-Model: Hortonian I/E and Saturation Excess	NEXRAD	synthetic 'true' streamflow	102 sq. km	I/E very sensitive to spatial, temporal precip variability **S/E not sensitive**

Notes

1. S/E: Saturation Excess runoff
2. I/E: Infiltration Excess runoff
3. DPM Distributed Parameter Model

5.7 References

Beven, K.J., and G.M. Hornberger, Assessing the effect of spatial pattern of precipitation in modeling stream flow hydrographs, *Water Resources Bulletin*, 823-829, 1982.

Bradley, A.A., Use of Weather Radar with Lumped Parameter Hydrologic Models', paper presented at the 13th Conference on Hydrology, 70th Annual Meeting of the American Meteorological Society, Long Beach, California, February 2-7,1997, J87-J88.

Bradley, A.A., and A. Kruger, 'Recalibration of Hydrologic Models for Use with WSR-88D Precipitation Events', Preprints, 78th Annual American Meteorological Society Meeting, Special Symposium on Hydrology, Phoenix, Arizona, 1998, 302-305.

Burnash, R.J.C., 1995, The NWS River Forecast System - Catchment Modeling, in *Computer Models of Watershed Hydrology*, Chapter 10 , Singh, V.P., Editor, Water Resources Publications.

Burnash, R.J.C., R.L. Ferral, and R.A. McGuire, 1973, A Generalized Streamflow Simulation System - Conceptual Modeling For Digital Computers, *REP* U.S. Department of Commerce, National Weather Service and State of California, Department of Water Resources, March.

Chandrasekar, V. W.F. Krajewski, and V. Lakshmi, A monte-carlo study of radar-ranfall sampling for hydrological applications, paper presented at the Eighth Conference on Hydrometeorology, Kananaskis Par, Alta., Canada, October 22-26, 1990.

Clark, C.O., Storage and the unit hydrograph, *Transactions of the Americal Society of Civil Engineers, 110*, 1419-1446, 1945

Dawdy, D.R., and J.M. Bergmann, Effect of rainfall variability on streamflow simulation, *Water Resources Research, Vol 5(5), 958-966*, 1969.

Duncan, M.R., B. Austin, F. Fabry, and G.L. Austin, The effect of gauge sampling density on the accuracy of streamflow prediction for rural catchments, *Journal of Hydrology 142, 445-476, 1993*.

Duan, Q. V.K. Gupta, and S. Soorochian, A shuffled complex evolution approach for effective and efficient global minimization, *Journal of Optimization Theory and Its applications, Vol. 61(3)*, 1993.

Finnerty, B.D. and D. Johnson,, Comparison of mean areal precipitation estimates derived from NEXRAD radar vs. rain gage networks, paper presented at the 27th congress of the Int'l Assoc for Hydraulic Research   - Managing Water: Coping with Scarcity and Abundance, Proceedings of Theme A., Water for a Changing Global Community, Water Resources Engineering

Division/ASCE, San Francisco, Ca., August 10-15, 1997, Ca. 601-606.

Finnerty, B.D., M.B. Smith, D.J. Seo, V. Koren, and G.E., Mogen, , Space-time scale sensitivity of the Sacramento model to radar gage precipitation inputs, *Journal of Hydrology*, 203, 21-38, 1997.

Gupta, V. K., and E. Waymire, Multi scaling properties of spatial rainfall and river flow distributions. *Journal. of Geophysical Research, Vol. 95, No. D3*, 1999-2009, 1990.

Hamlin, M.J., The significance of rainfall in the study of hydrological processes at basin scale, *Journal of Hydrology, 65, 73-94,* 1983.

Hudlow, M.D., Technological developments in real-time operational hydrologic forecasting in the United States, Journal of Hydrology, 102, 69-92, 1988.

Jones, A.T., B.E. Vieux, and M.D. Eilts, Aspects of Calibrating a Distributed Rainfall-Runoff Model Using WSR-88D Rainfall Estimates in the Illinois Basin, Preprints, 78th Annual American Meteorological Society Meeting, Special Symposium on Hydrology, 11-16, January, Phoenix, Arizona, 294-297, 1998.

Kenner, S.J., S. Brich., Y. Yang., M.R. Hjelmfelt, and R.A. Pielke, Atmospheric and surface hydrologic simulation of an extreme event, Preprint Volume of the Second Internaitonal Scientific conference on the Global Energy and Water Cycle, 17-21 June, Washington, D.C., 1996,17-18

Kite, G.W., and N. Kouwen, Watershed Modeling using Land Classifications, *Water Resources Research, 28(12)* 3193-3200, 1992.

Koren, V., and C. B. Barrett, Satellite based distributed monitoring, forecasting, and simulation (MFS) system for the Nile River, paper presented at the Proceedings of the Second International Workshop on Application of remote sensing in hydrology. NHRI Symposium, No 14, October 1994, Saskatoon, 1994, 187-200

Koren, V.I., B.D. Finnerty, J.C. Schaake, M.B. Smith, D.J. Seo, and Q.Y. Duan, Scale dependencies of hydrologic models to spatial variability of precipitation, accepted for publication in the *Journal of Hydrology*, 1998.

Kouwen, N., and G. Garland, Resolution considerations in using radar rainfall data for flood forecasting, *Canadian Journal of Civil Engineering*, 16, 279-289, 1989

Krajewski, W.F., V. Lakshmi, K.P. Georgakakos, and S. C. Jain, A monte -carlo study of

rainfall sampling effect on a distributed catchment model, *Water Resources Research*, Vol. 27, No. 1, 119-128, 1991.

Kull, D.W. and A. D. Feldman, Evolution of Clark's Unit Graph Method to Spatially Distributed Runoff , *Journal of Hydrologic Engineering*, January,9-19 1998.

Larsen, J.E., M. Sivapalan,., N.A., Coles, and P.E. Linnet, Similarity analysis of runoff generation processes in real-world catchments', *Water Resources Research, 30(6)*, 1641-1652, 1994.

Lindstrom, dG., B. Johansson, M. Persson. M. Gardelin, and S. Bergstrom, Development and test of the distributed HBV-96 hydrologic model, Journal of Hydrology, Vol. 201, 272-288, 1977.

Michaud, J. and S. Sorroshian, Comparison of simple versus complex distributed runoff models on a midsized semiarid watershed, *Water Resources Research, Vol. 30, No. 3*, March, 593-605, 1994.

Milly, P.C.D., and P.S. Eagleson, Effect of storm scale on surface runoff volume, *Water Resources Research, Vol 24(4) 620-624, 1988.*

Naden, P.S., 1992, Spatial Variability in flood estimation for large catchments: the exploitation of channel network structure, Hydrological Sciences Journal, 37(1), 53-71.

Nash, J.E., The form of the instantaneous unit hydrograph, IAHS, 45(3-4),14-121, 1957.

Obled, C.H., Wendling, J., and Beven, K., The sensitivity of hydrological models to spatial rainfall patterns: an evaluation using observed data, *Journal of Hydrology, 159*,305-333, 1994.

Ogden, F.L., and P.Y. Julien, Runoff sensitivity to temporal and spatial rainfall variability at runoff plane and small basin scales, *Water Resources Research, Vol. 29, No. 8*, 2589-2597, 1993

Ogden, F.L, and P.Y. Julien, Runoff model sensitivity to radar rainfall resolution, *Journal of Hydrology, 158, 1-18,* 1994.

Pessoa, M.L., R.L, Bras,. and E.R. Williams, Use of weather radar for flood forecasting in the sieve river basin: a sensitivity analysis, *Journal of Applied Meteorology, 32 (3)*, 462-475, 1993.

Refsgaard, J.C., Parameterisation, calibration, and validation of distributed hydrological models, *Journal of Hydrology, (198)*, 69-97, 1997.

Schaake, J.C., Importance of the HRAP grid for operational Hydrology, paper presented at the U.S./Peoples Republic of China Flood Forecasting Symposium, Portland, OR. NOAA/NWS,1989, pp 331-355.

Shah, S.M.S., P.E. O'Connell, and J.R.M Hosking, Modelling the effects of spatial variability in rainfall on catchment response. 1. Formulation and calibration of a stochastic rainfall field model, *Journal Hydrology, 175,* 66-88, 1996a.

Shah, S.M.S., P.E. O'Connell,, and J.R.M. Hosking,, Modelling the effects of spatial variability in rainfall on catchment response. 2. Experiments with distributed and lumped models, *Journal of Hydrology, 175,* 89-111, 1996b.

Shanholtz, V.O., B.B. Ross, and J.C. Carr, Effect of Spatial Variability on the Simulation of Overland and Channel Flow, *Transactions of the American Society of Agricultural Engineers, Vol 24(1), 124-138,* 1981.

Smith, MB, V. Koren, D. Johnson, B.D. Finnerty, and D.J. Seo, Distributed Modeling: Phase 1 Results, Rep., 210 pp., National Weather Service Hydrologic Research Lab, 1998

Troutman, B.M., Runoff Prediction Errors and Bias in Parameter Estimation induced by Spatial Variability of Precipitation, *Water Resources Research, Vol 19. No. 3,* 791-810, 1983.

University of Arizona, 1995. Progress Report. 1995-1996 Cooperative Agreement NA37who385 by the Department of Hydrology and Water Resources, The University of Arizona, to the Hydrologic Research Laboratory of the U.S. National Weather Service, June, 1995.

Wilson, C.B., J.B. Valdes, and I. Rodriquez-Iturbe, On the Influence of the spatial distribution of rainfall on storm runoff, *Water Resources Research, Vol 15(2), 321-328, 1979.*

Winchell, M., H.V. Gupta, and S. Sorooshian, Effects of radar-estimated precipitation uncertainty on different runoff generation mechanisms, *Rep. HWR No. 97-080, 285 pp.,* Department of Hydrology and Water Resources, University of Arizona, 1997.

Winchell, M., H.V. Gupta, and S. Sorooshian, On the simulation of infiltration and saturation excess runoff using radar based rainfall estimates: Effects of algorithm uncertainty and pixel aggregation, Water Resources Research, Vol 34, (10), 2655-2670, 1998

Wood, E.F., M. Sivapalan, and K. Beven, Similarity and scale in catchment storm response, *Review of Geophysics, 28(1),* 1-18, 1990.

Wyss, J., E.R. Williams, and R.L. Bras, Hydrologic modeling of New England river basins using radar rainfall data, *Journal of Geophysical Research, Vol. 95(D3), 2143-2152, 1990.*

6. Case study in Upscaling and Downscaling of SAC-SMA Parameters

6.1 Introduction

As described earlier, an initial approach to capturing spatial variability in precipitation is the semi-distributed model where a lumped basin is disaggregated spatially into a group of smaller constituent sub-basins and the lumped parameters are uniformly distributed to all sub-basins. The semi-distributed formulation may then be recalibrated by adjusting all sub-basin parameters simultaneously and uniformly to improve the simulations. This semi-distributed approach is a simple rainfall averaging technique that neglects the variability in model parameters across the sub-basins and does not explicitly address scale dependencies in runoff models. Some attempt at accounting for scale is done when recalibrating the semi-distributed formulation to the basin outlet hydrograph. The evaluation of the semi-distributed approach is performed by comparing continuous 1 hour simulations of observed hydrographs from lumped and semi-distributed applications of the Sacramento model.

In this section, the process of downscaling of model parameters refers to the assignment of lumped parameters to constituent sub-basins. The validity of downscaling lumped parameters to sub-basins is tested by calibrating an interior sub-basin and comparing simulations from the interior sub-basin using its parameters vs. the parent basin parameters. This test helps to evaluate the validity of applying parameters from a lumped basin to constituent sub-basins. This is a critical test of the assumption that lumped model parameters are appropriate and representative of the parameters required for the simulation of interior sub-basins.

The concept of upscaling of sub-basin parameters to the semi-distributed formulation is tested by comparing simulations of the semi-distributed model run with the lumped parameters vs. the sub-basin parameters. In addition, these nested sub-basin verification tests highlight the errors and problems associated with regionalizing head water basin parameters by applying them to neighboring head water and local basins of differing spatial scales. Regionalizing runoff parameters is a very common practice in modeling when data or time for calibration is limited.

This section presents the results of a nested sub-basin calibration and simulations. The results are relevant to understanding how the parameters from a lumped basin apply, if at all, to an interior sub-basin, and how small scale parameters apply to larger basins. Although the sub-basin is nested inside the lumped basin, the results are relevant to cases where the sub-basin is outside the lumped basin, as in the case of applying headwater basin parameters to local basins and adjacent basins of varying sizes.

The experiments described above were performed on the Watts basin (1645 km²) discussed in earlier sections. An 8 sub-basin formulation was used for the semi-distributed model. Three years of 1 hour, 4x4 km Stage III radar-gage NEXRAD precipitation data were used to simulate and calibrate the Sacramento model at Watts. The interior headwater sub-basin

of Savoy (433 km²) was calibrated using an MAPX time series derived from 14 months of Stage III precipitation data. USGS provisional 1 hour discharge data was used for the observed hydrographs. Savoy is represented by 2 of the 8 sub-basins in the semi-distributed formulation.

6.2 Down Scaling from Lumped Parent Basin to Sub-Basins

In testing the validity of down-scaling model parameters, three sets of SAC-SMA parameters are analyzed: 1) the lumped parameters from the 6 hour historically calibrated Watts basin, 2) manually adjusted and optimized parameters using the 1 hour radar and discharge data and 8 sub-basin formulation of Watts, and 3) a manually calibrated lumped parameter set from Savoy using 1 hour radar and discharge data. All cases used a time-area unit hydrograph for Savoy. The 12 ET-demand curve values were the same for all simulations. Table 6.2-1 shows a list of the three parameter sets used in the study.

Simulation experiments on the interior sub-basin of Savoy illustrated that the parameters from the larger lumped basin of Watts were somewhat useful for Savoy, but resulted in clear systematic errors. The long term continuous simulation at Savoy using the Watts 6-hour historically calibrated parameters did not produce the flashy peak runoff observed in the headwater basin and also simulate too much base flow as shown in Figure 6-1. The figure shows an example of the outcome of historically calibrating a basin, and then uniformly distributing those parameters to smaller sub-basins. The results in Figure 6-1 are expected after analyzing Figure 6-2, which shows the scale dependent runoff characteristics exhibited in hydrographs from the three nested basins of Talequah (2482 km2, TALO2), Watts (1645 km2, WTTO2) and Savoy (433 km2). The observed hourly discharge shown in Figure 6-2 have been normalized by the drainage area of Watts to highlight the systematic differences in runoff volume and hydrograph shapes for the various scales of the basins analyzed. The basins received approximately the same input depth of rainfall as estimated by radar, yet much more runoff is generated from Savoy than Watts. The hydrograph is attenuated as it moves down the drainage network, and it is assumed that there are greater losses from the larger basins which reduces the overall runoff volume in the water balance. Smaller scale headwater basins generate more runoff per unit area which is potentially attributed to fewer losses associated with less groundwater storage and shallower soils. Steeper headwater slopes generally produce faster response runoff that may not have time to become held in tension soil storage or river bank storage where it will later be lost to atmospheric evaporative demands.

The Watts 6-hour parameters were recalibrated to reduce baseflow and generate more rapid response surface runoff seen at the Savoy gage. Table 6.2-1 shows how the parameters were calibrated to the observed Savoy hourly discharge hydrographs. Although the 6 hour historical gage network parameters in Table 6.2-1 are not identical to the parameter set used in Section 5.1 of this report, these parameters are an alternate parameter set and experiments with either parameter set

Table 6.2-1: Sacramento Model Parameter Sets used in Upscaling and Downscaling Tests

parameter	Watts Historical, gage, 6 hour	Watts 8 sub-basin, radar, 1 hour	Savoy, radar, 1 hour
uztwm	40	93.1	60
uzfwm	25	28.4	20
uzk	0.25	0.694	0.3
pctim	0.005	0.005	0.001
adimp	0	0	0.01
riva	0.015	0.015	0.02
zperc	120	40.1	200
rexp	2.0	1.4	1.8
lztwm	160	133	100
lzfsm	40	50.3	20
lzfpm	100	100	25
lzsk	0.014	0.119	0.2
lzpk	0.009	0.0097	0.009
pfree	0.15	0.612	0.3
side	0	0	0
Upper Storage	65	121.5	80
Lower Storage	300	283	145
Total Storage	365	404	225

Savoy Simulations with Parameters from Savoy and Watts

Discharge, cms

Time, hours (April-July, 1996)

observed — — savoy — · — watts

Figure 6-1

6.4
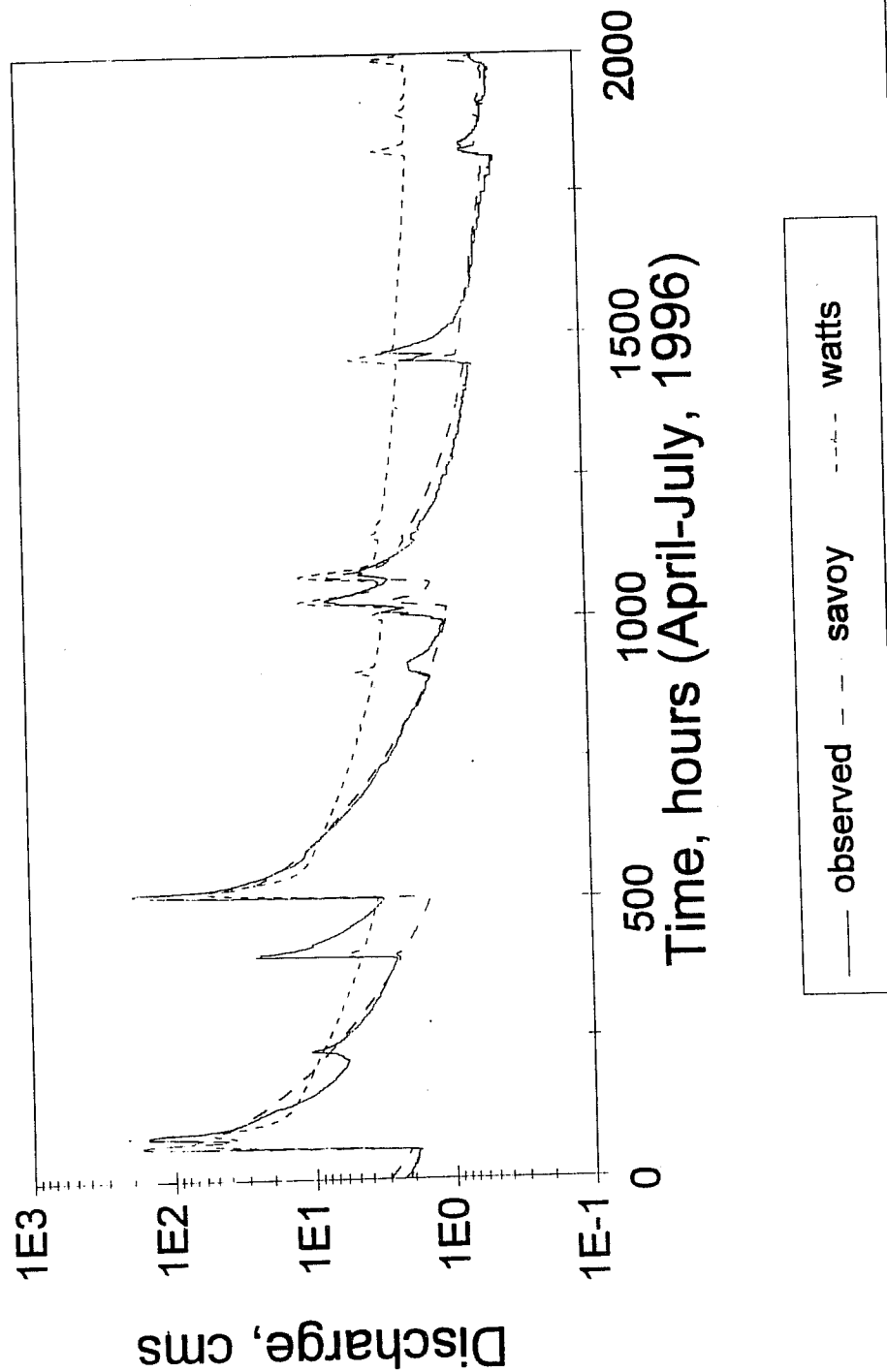
Runoff per unit area for nested basins
April 10th – May 20th, 1996

Discharge, cms
Time, hours

taloz (2482 km) —— watts (1645 km) ----- savoy (433 km)
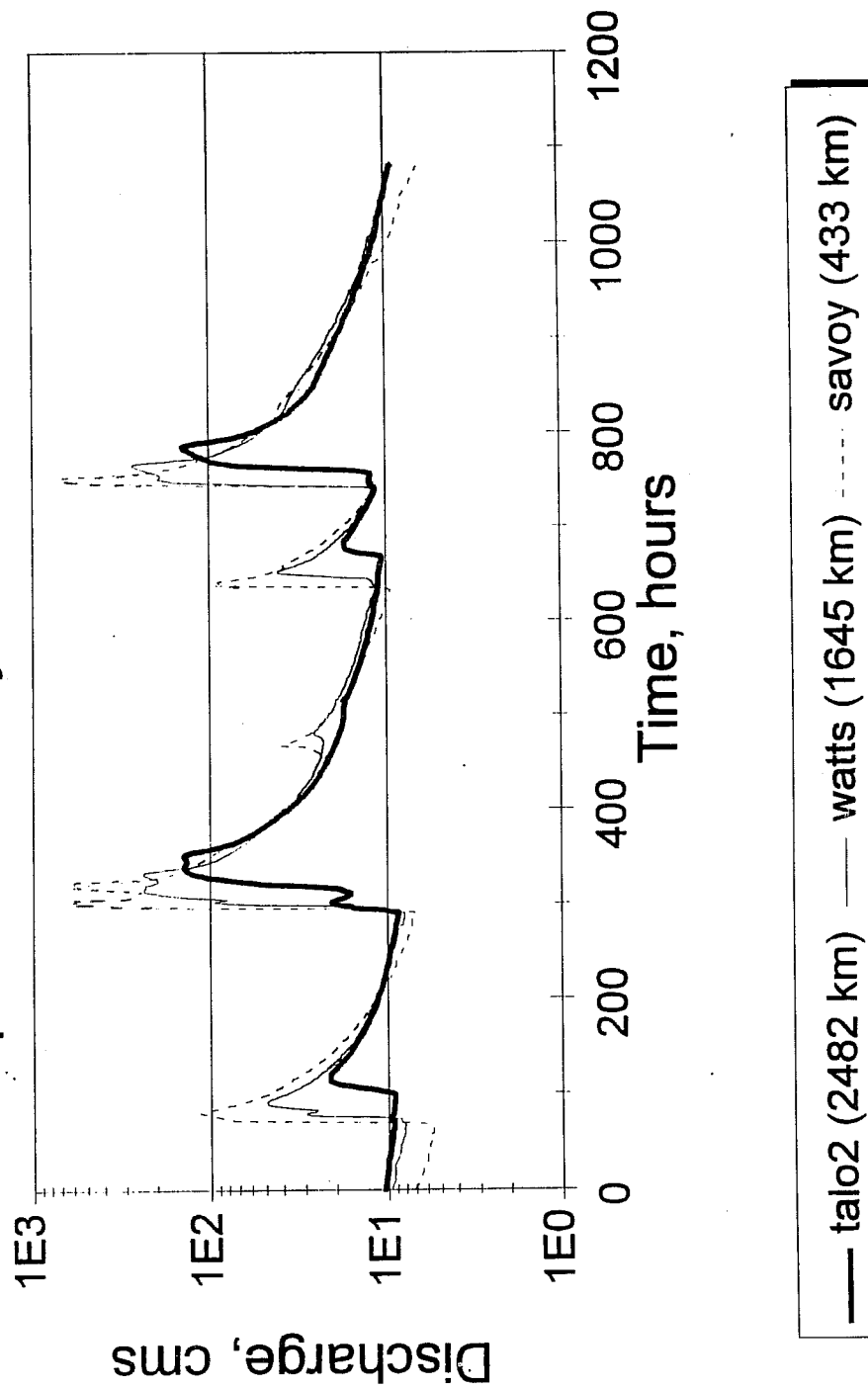
Figure 6-2

support the same conclusions. Notice that the storage of Savoy was greatly reduced from the storage at Watts. The unit hydrograph was also recalibrated with a sharper rising limb and a smaller tail to reduce slow response runoff (see Figure 6.2-15 in the following section on unit hydrographs). Down scaling of lumped parameters did not directly represent the local heterogeneities in the Savoy sub-basin, or the general hydrologic response of a smaller headwater basin.

Figure 6-3 presents simulated and observed hydrographs for an event on April 22, 1996 at the Savoy gage. This event exhibited very fast response times and steep rising and falling limbs. This complex event was best simulated with the calibrated Savoy parameters. Both of the Watts parameter cases produced a dampened response that greatly underestimated the peak volume and magnitude. The Watts 8 sub-basin parameters performed slightly better than the historically calibrated 6-hour lumped Watts parameters.

Figure 6-4 shows a moderate single peaked flood event a few weeks later on May 10, 1996. All cases underestimated the observed peak at Savoy. However, the Savoy parameters performed very well in the timing of the peak while underestimating the magnitude. The Watts parameters responded slowly in both the time to peak and peak discharge, as compared to the observed and Savoy simulations. The significant underestimation of all parameter sets may be related to errors in initial conditions or radar underestimation.

Figure 6-5 shows a large flood event at Savoy on September 26, 1996, which unfortunately is missing observed data. Interestingly, the case serves to illustrate that varying results are generated as a function of discharge magnitude. Here, the Savoy and Watts lumped parameters produced very similar results in the timing, magnitude and shape of the hydrograph, with the lumped being slightly greater. This is a reversal in simulation results that we observed in Figures 6-2 and 6-3 where Savoy parameters produce almost twice as much runoff as the Watts parameters for the moderate sized events. The Watts 8 sub-basin parameters produced the least amount of runoff, which is not consistent with the results shown in Figures 6-2 and 6-3. These results may be a function of the storage or percolation rates of the 3 parameter sets analyzed. Initial soil moisture states are also different for the 3 parameter sets, and therefore create differences in the hydrographs.

Figure 6-6 shows another moderate sized event that occurred at Savoy on November 6, 1996. This event shows the similar trends from Figures 6.2-2 and 6.2-3 where the Savoy parameters produce twice as much runoff as the Watts parameters. However, in this event, all parameter sets produce nearly the same time to peak. It is difficult to evaluate which parameter set best represents the observed data because the observed hydrograph looks as if it has data errors because of the flat peak shape. It should be noted that the 1 hour observed discharge data obtained for these tests is considered provisional by the U.S.G.S..
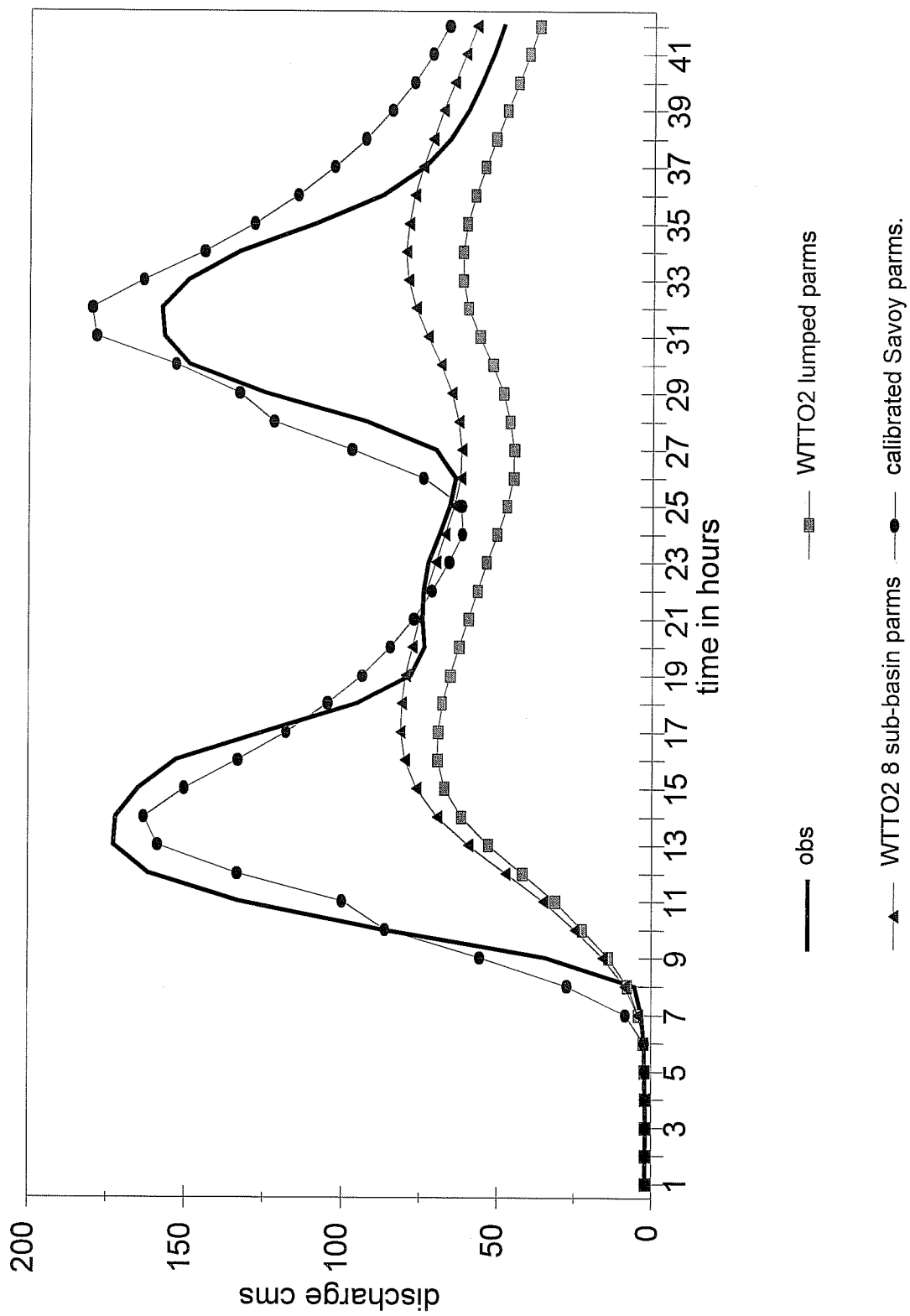
Figure 6-3 Savoy April 22, 1996
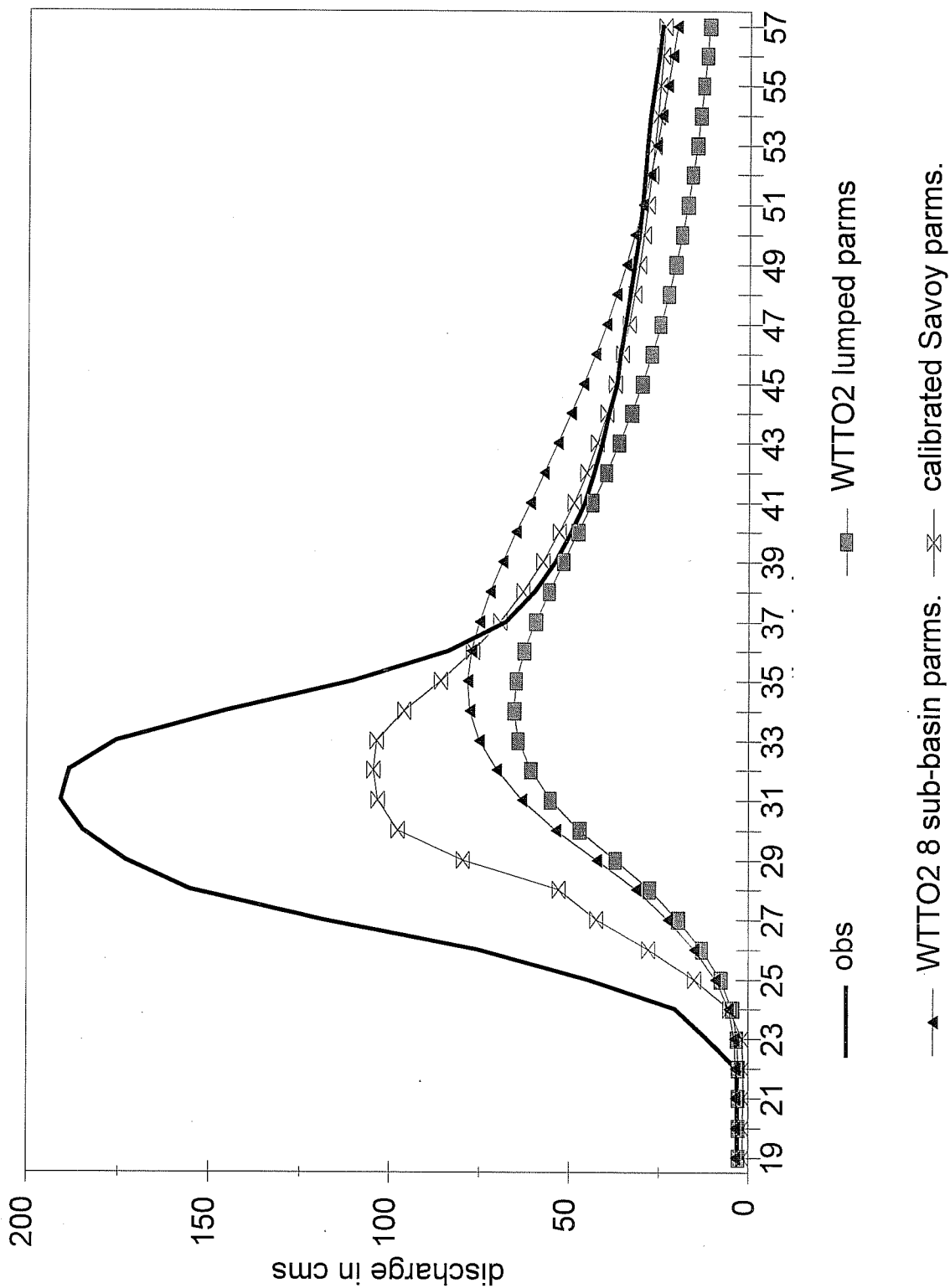Lumped Simulations - Various Parms

obs ——— WTTO2 lumped parms

WTTO2 8 sub-basin parms ——▲— calibrated Savoy parms.

Figure 6-4   Savoy, May 10, 1996
Lumped Simulations - Various Parms.

obs ——   WTTO2 lumped parms
WTTO2 8 sub-basin parms.   calibrated Savoy parms.
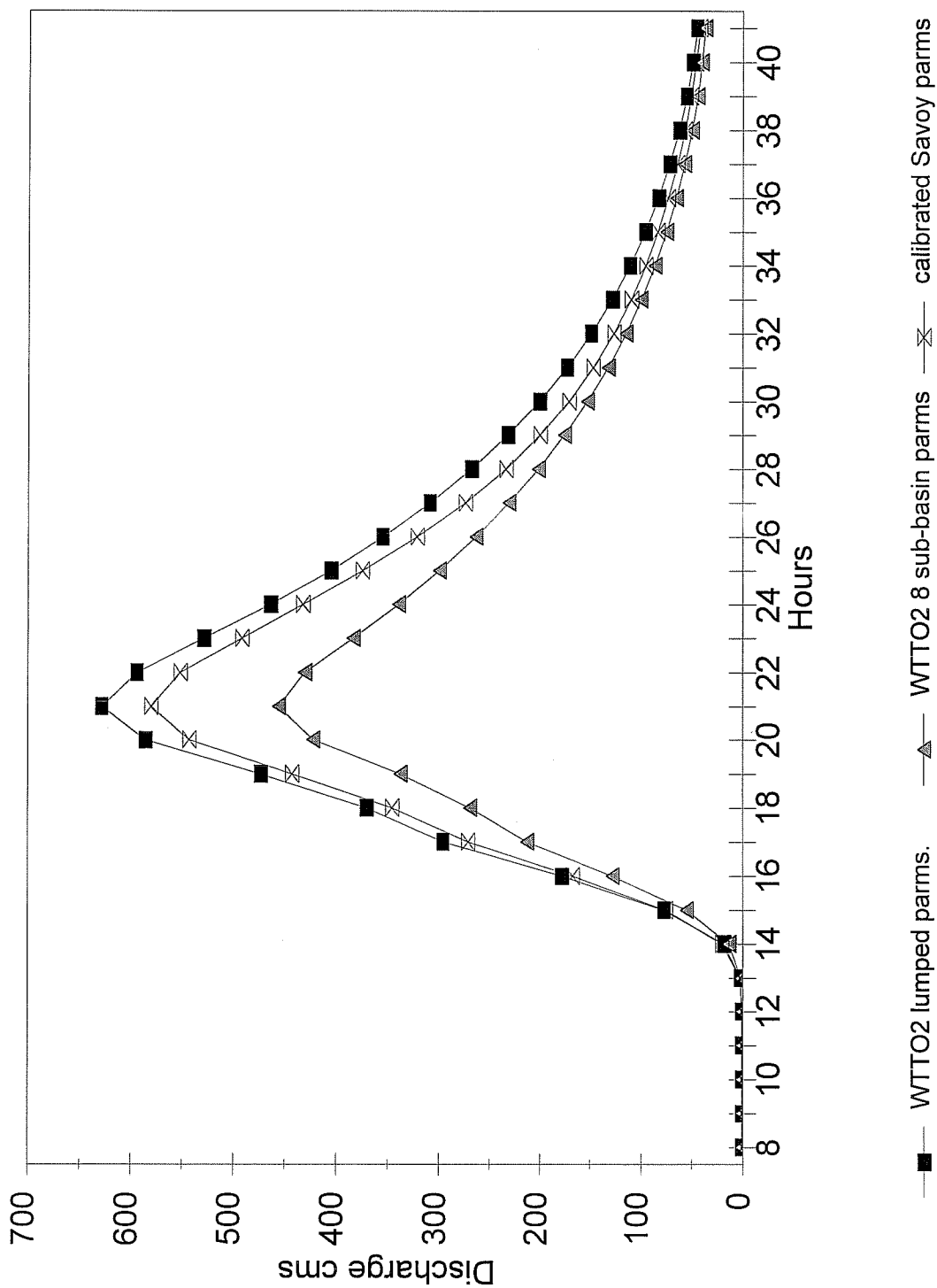
Figure 6-5 Savoy   Sept. 26, 1996
Lumped Simulations with Various Parms

— WTTO2 lumped parms.   —▲— WTTO2 8 sub-basin parms   —✕— calibrated Savoy parms
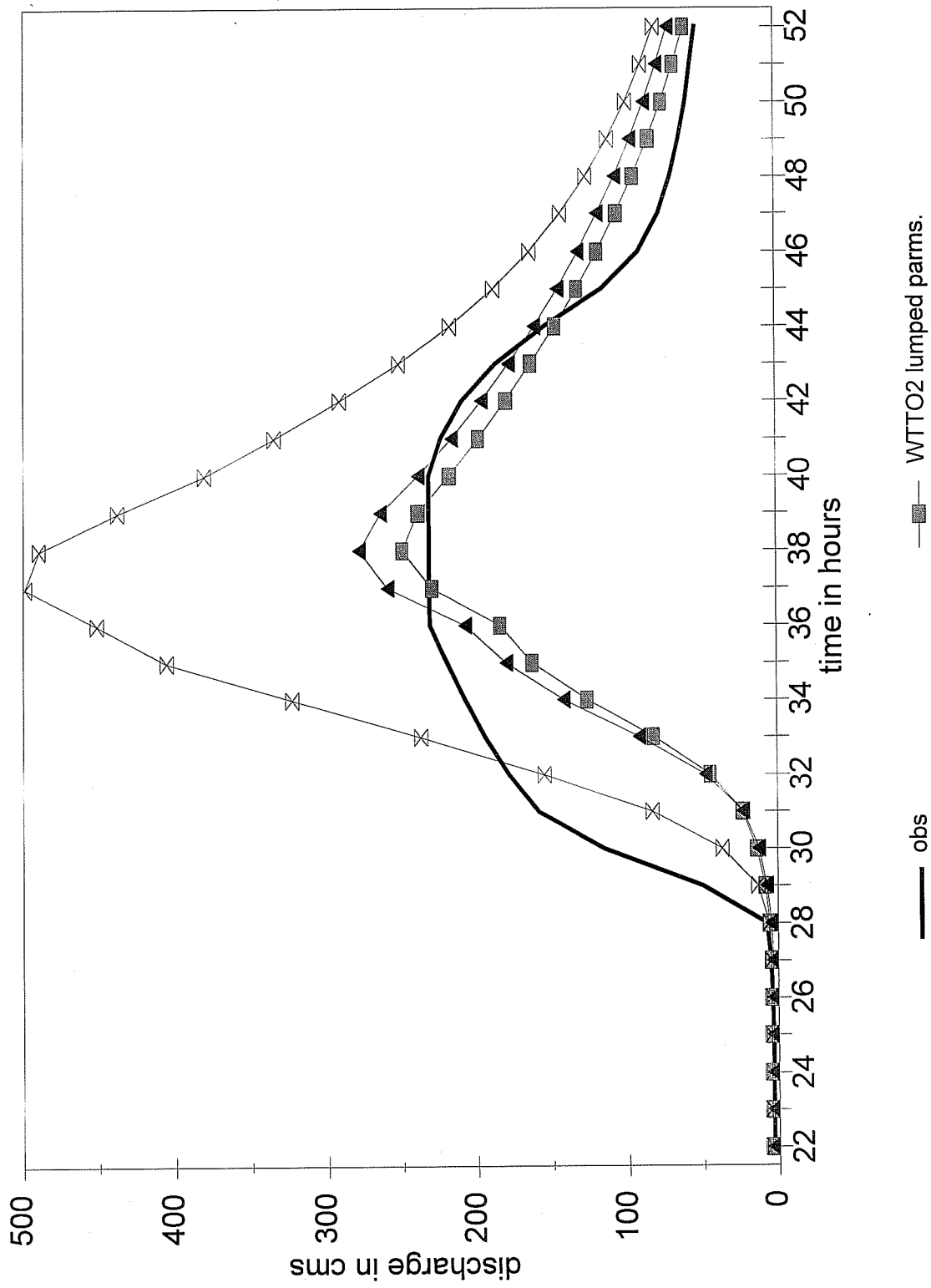
Figure 6-6 Savoy Nov. 6, 1996
Lumped Simulations with Various Parms.

Figure 6-7 is a good example of data problems that occurred on November 23, 1996. The first peak shows that all parameter sets underestimated the moderately sized event, probably due to an underestimation of the rainfall volume by the radar. Again, the Savoy parameters almost reproduce the peak magnitude and the timing was slightly delayed. The Watts lumped parameters generated a dampened response. All three parameter sets led to simulated secondary peaks, while the observed discharge hydrograph is continuously receding. This is a common calibration problem where there are errors in the discharge data or the radar products, and these errors can significantly bias calibration statistics to the point that they are misleading or not useful. There is reason to believe that this event was a wintery mix which the radar is not designed to observe.

6.3 Upscaling from the Savoy Sub-basin to the Watts Parent Basin

In this series of tests, the 8 sub-basin formulation of WTTO2 is used with two different paramterizations: 1) the 1-hour calibrated Savoy parameters applied to each of the e sub-basins, and 2) the 1-hour semi-distributed parameters derived through the calibration of the 8 sub-basin formulation of WTTO2 described in section 5.3.2. Recall that the 1-hour Savoy parameters were developed through calibration at the interior stream gage at Savoy, while the second set of parameters was calibrated to the observed discharge at the outlet of the parent WTTO2 basin.

Figure 6-8 shows a four month simulation of the 8 sub-basin formulation at Watts using the 1 hour calibrated 8 sub-basin Watts parameters and the Savoy calibrated parameters. The figure shows that uniform application of the Savoy parameters to all of the 8 Watts sub-basins resulted in too much runoff being simulated in the long term, and particularly in medium sized events. This result is expected after analyzing the natural scale dependent hydrograph characteristics shown in Figure 6-2. However, large isolated flood events existed where the Savoy parameters simulated less runoff than the Watts parameters in the semi-distributed formulation. The results in Figure 6-8 illustrate that the parameters from a single sub-basin may not be representative of the other sub-basins, and do not necessarily result in an improved simulation for the larger basin.

The degraded simulation performance at Watts with Savoy parameters may be attributed to increased sensitivity of the sub-basin runoff to increased precipitation spatial variability. Direct mapping of high intensity precipitation on sub-basins causes the semi-distributed model to become more sensitive to parameter variability and Stage III precipitation errors across the basin. Unit hydrograph estimation for the sub-basins and the scale dependent behavior of the Sacramento model may have been contributing factors. Runoff simulations may also have been affected by non-uniform initial soil moisture conditions in the semi-distributed case because moisture states are a function of the recent space-time distribution of rainfall across the basin. Lateral subsurface transfer between sub-basins was neglected.
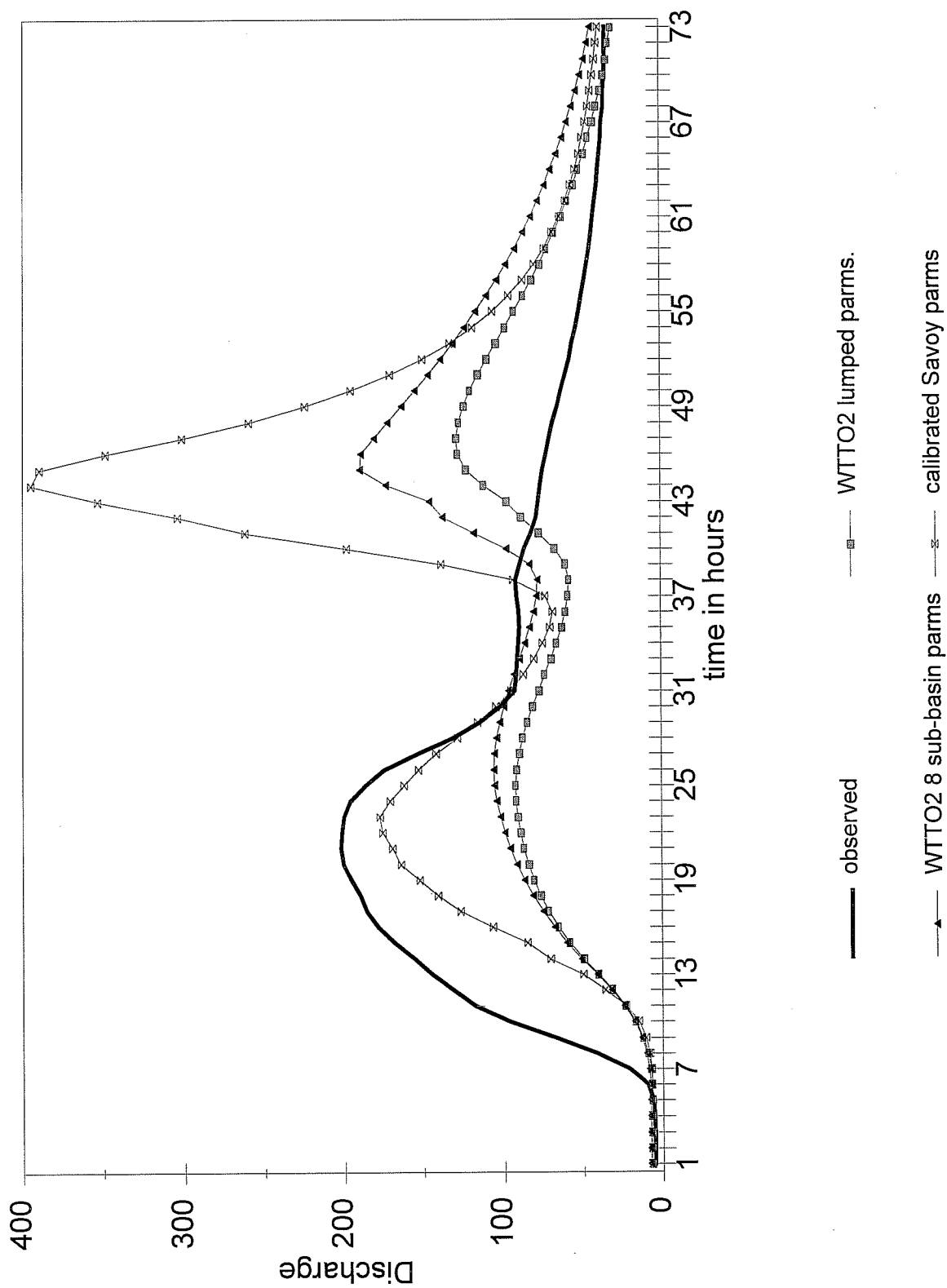
Figure 6-7 Savoy Nov. 23, 1996
Lumped Simulations with Various Parms.

— observed ——— WTTO2 lumped parms.

——— WTTO2 8 sub-basin parms ——— calibrated Savoy parms

Watts 8 Subbasin Case, May-July, 96
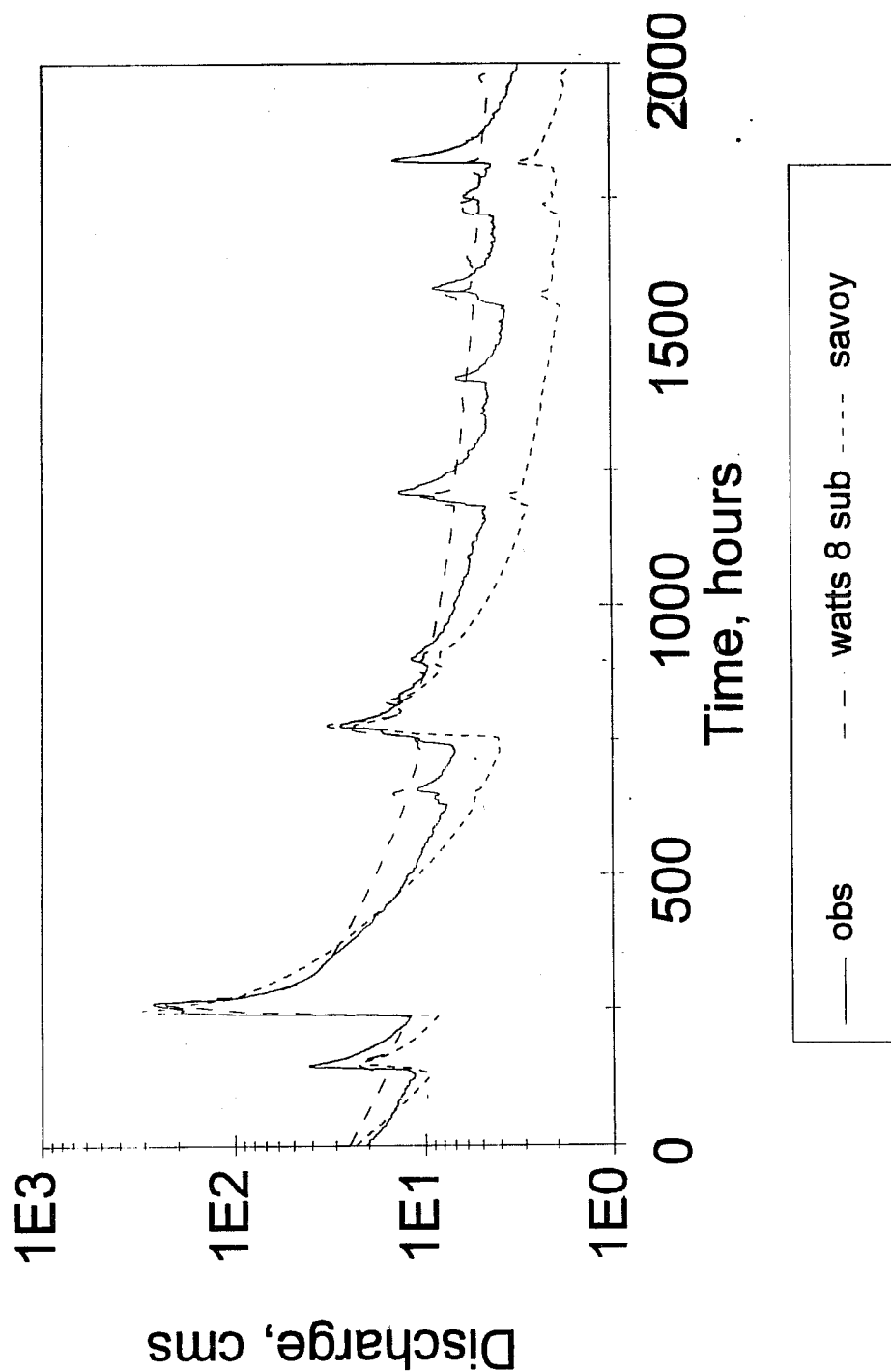Parameters from Watts and Savoy

Figure 6-8

Figures 6-9 through 6-13   present simulated hydrographs derived using the two parameterizations for the 8 sub-basins. In general, the use of the Savoy parameters in each of the 8 sub-basins for the parent WTTO2 basin leads to marked over simulation of the observed streamflow response. While the Savoy parameters are sufficient for the Savoy sub-basin, their uniform application to all of the 8 constituent sub-basins in WTTO2 is not appropriate.

6.4 Summary and Conclusions

Down scaling of parameters from the larger Watts basin to the nested headwater sub-basin of Savoy caused systematic simulation biases in the long term simulation and conflicting results on individual storm events. These results indicate that the parameters of a lumped basin are not representative of its constituent sub-basins. The lumped parameters generally produce too much baseflow for an upland headwater sub-basin, and not enough of flashy, fast response runoff. Up scaling of sub-basin parameters to the larger parent basin resulted in over simulating volume and acceleration of the timing and steepness of the rising limb of the hydrograph. This indicates that smaller basins may have different hydrologic processes than larger basins, even when one is a subset of the other. These results agree with the general physics of small basins which have less groundwater flow and more surface runoff than larger basins. That is why baseflow is over estimated when down scaling and under estimated when upscaling. The small basins generate more fast response surface flow and therefore more sensitive to rainfall rates, which leads to over estimating when upscaling.

The sub-basin formulation of the Sacramento is an attempt to capture the spatial variability of precipitation. However, uniform application of the lumped model parameters to all the sub-basins ignores the scaling effects of rainfall forcing on model runoff generation and the local heterogeneities that exist within a basin. Natural soil moisture distributions generally follow the rainfall distribution immediately after the storm. Over the inter storm period soil moisture drains into the low lands. If the sub-basin are smaller than the natural hydrologic boundaries, then the subsurface transfer of water will not be modeled and soil moisture states may not be physically realistic. This causes differences in the temporal evolution of soil moisture states for the various model formulations, even when using the same parameters, which can result in runoff hydrograph differences. Differences in soil moisture states are obviously greater for the cases where different model parameters were used.

Numerical scale runoff simulation experiments performed with the Sacramento model in Chapter 2 of this report showed that parameters applied at finer scales produced more surface runoff and less baseflow. These results were attributed to the increase in storm intensity at fine rainfall averaging scales which increased the rainfall excess. However, rainfall averaging clearly does not fully account for the spatial scale dependency of runoff that is observed in the nested basins studied. This analysis of observed and simulated hydrographs from real nested basins indicates that parameter adjustments are required when modeling at different space-time scales
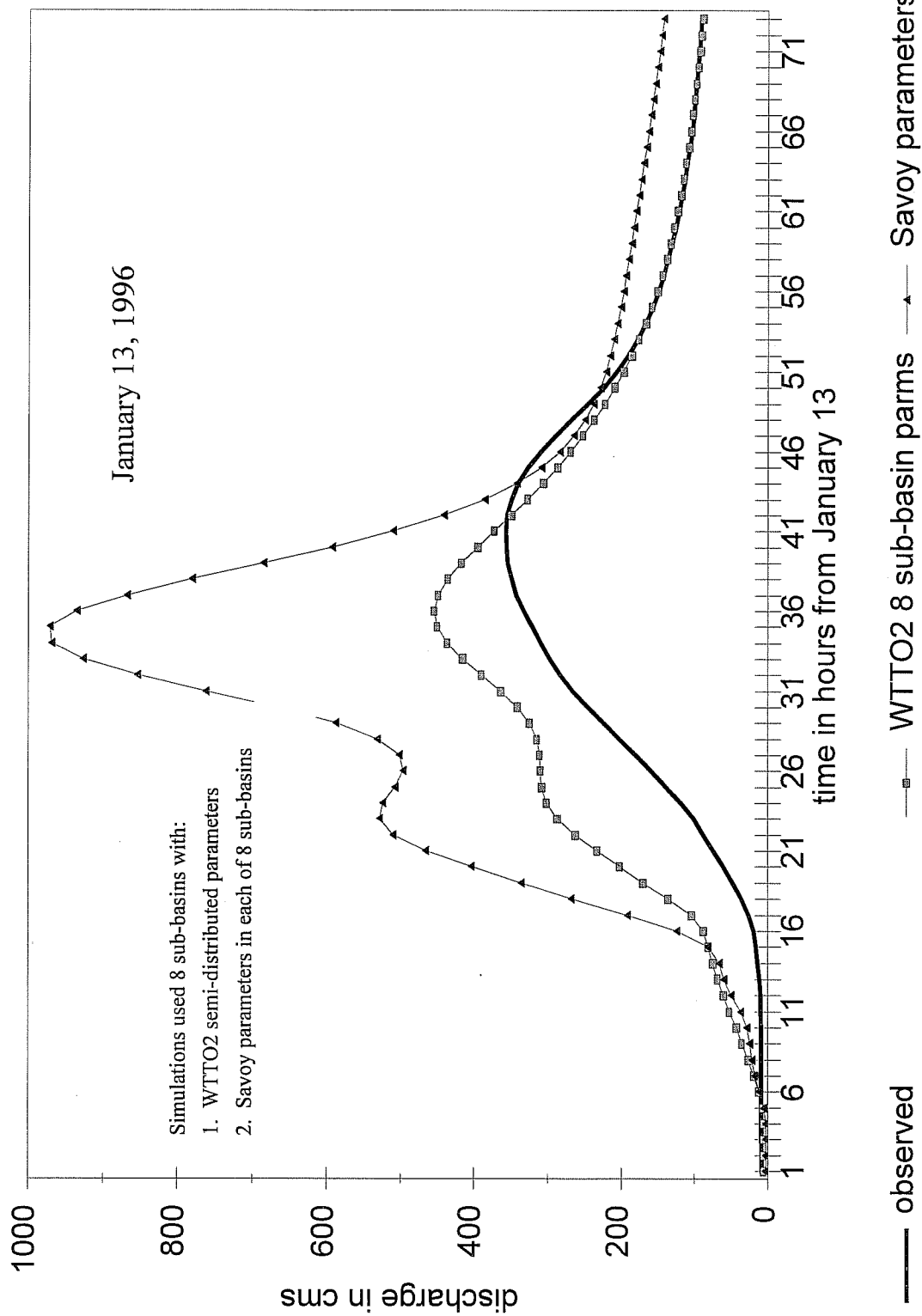
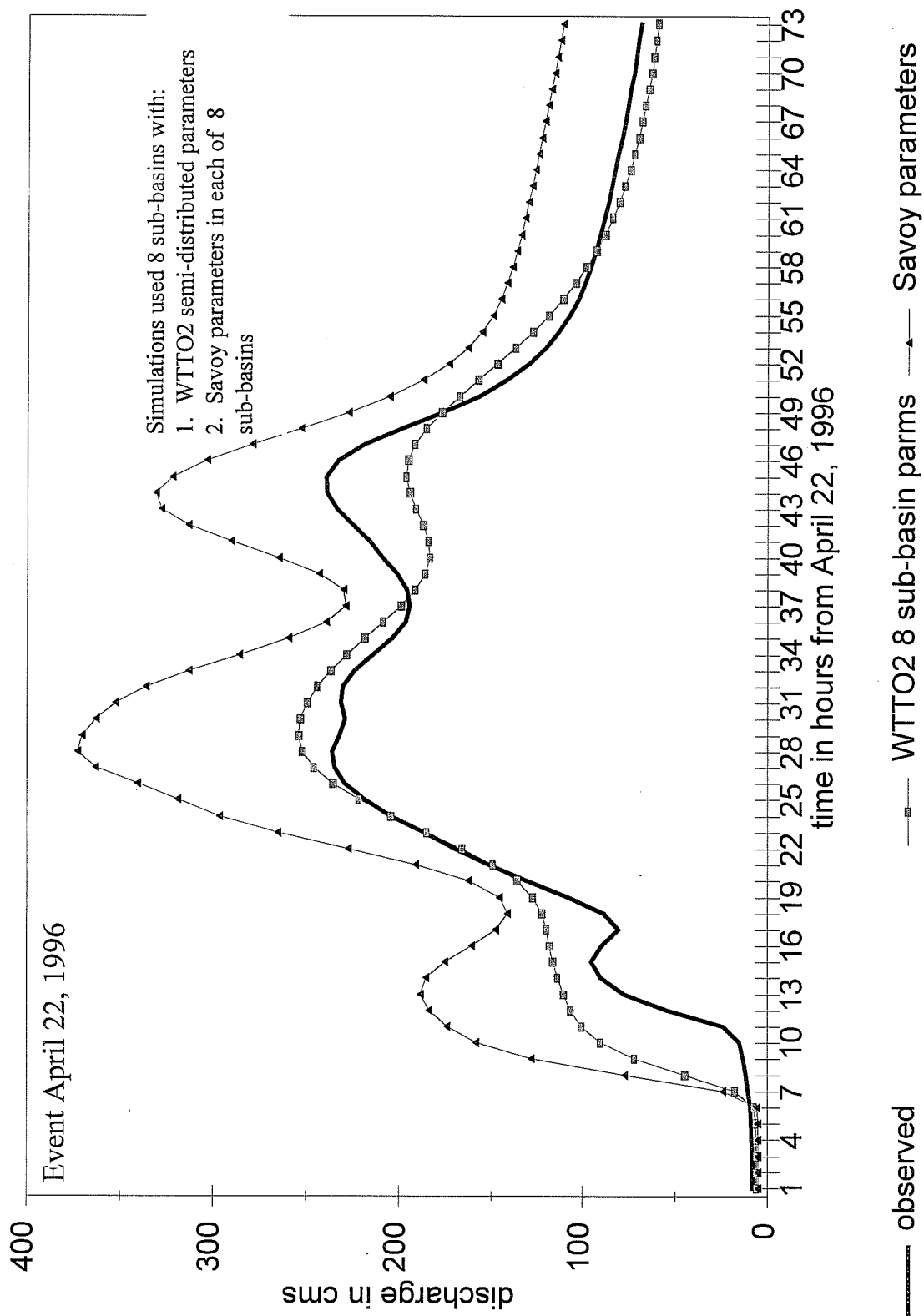Figure 6-9 Semi-Distributed Tests
with two parameter sets

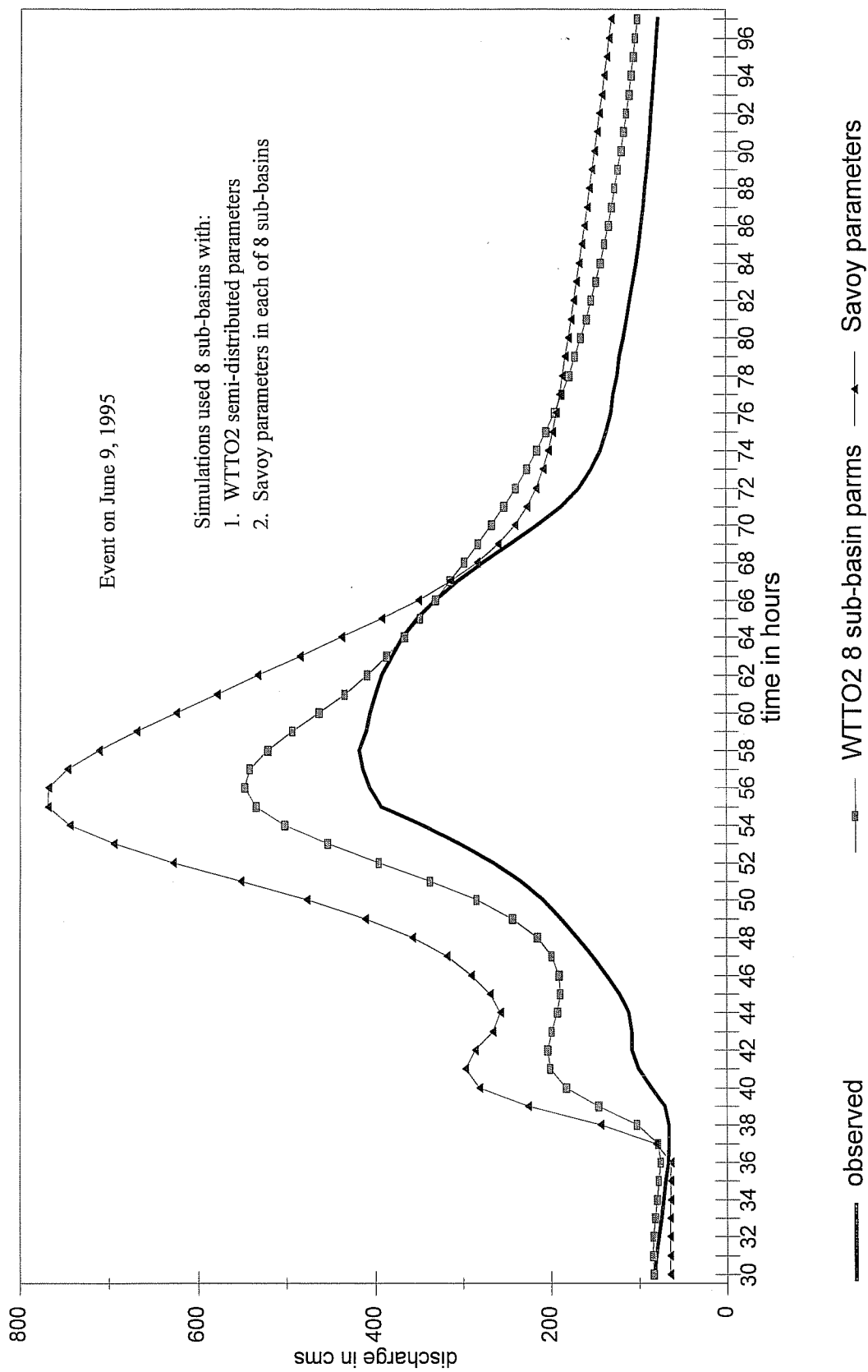Figure 6-10 Semi-Distributed Tests
with Two Parameter Sets

Event on June 9, 1995
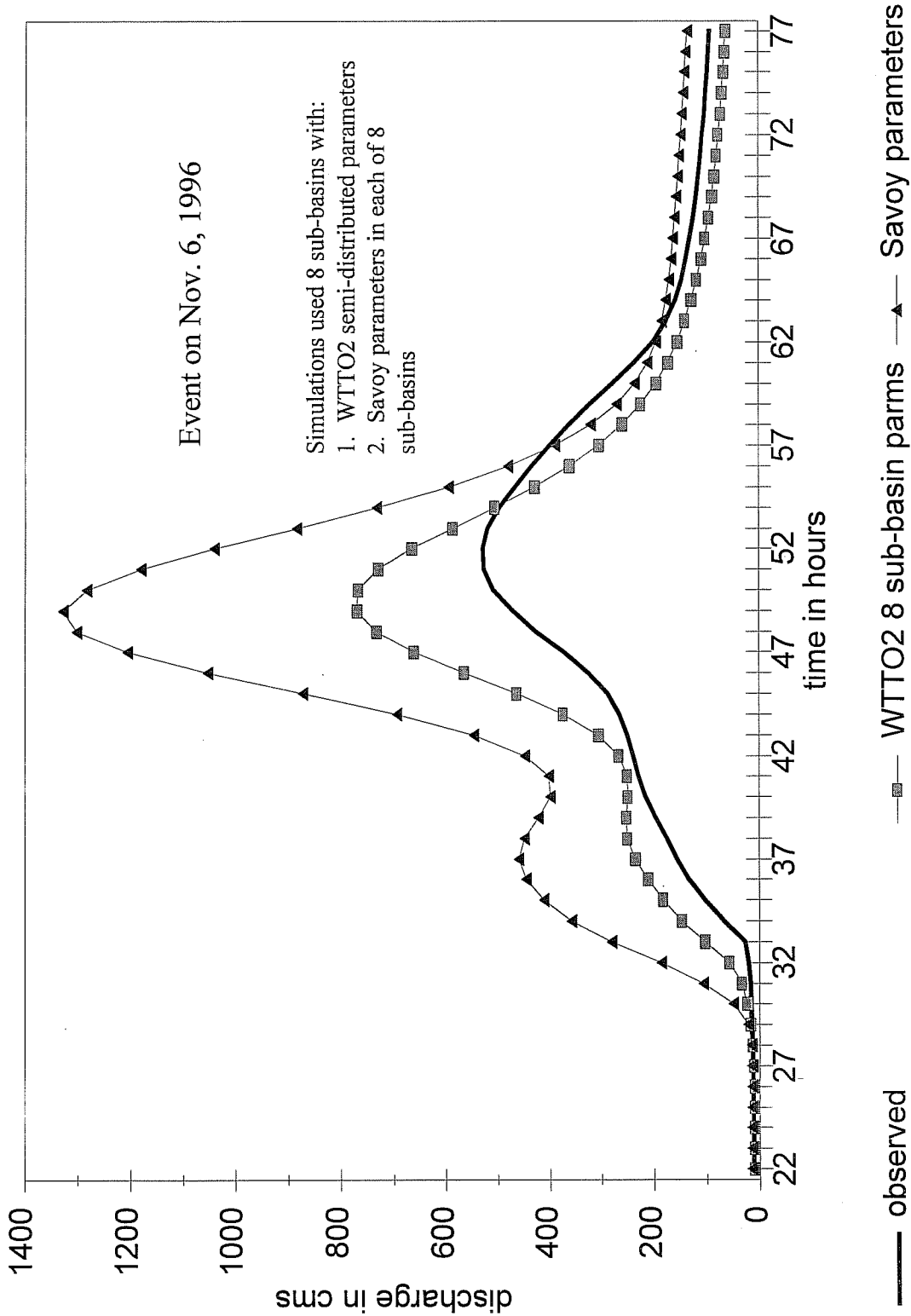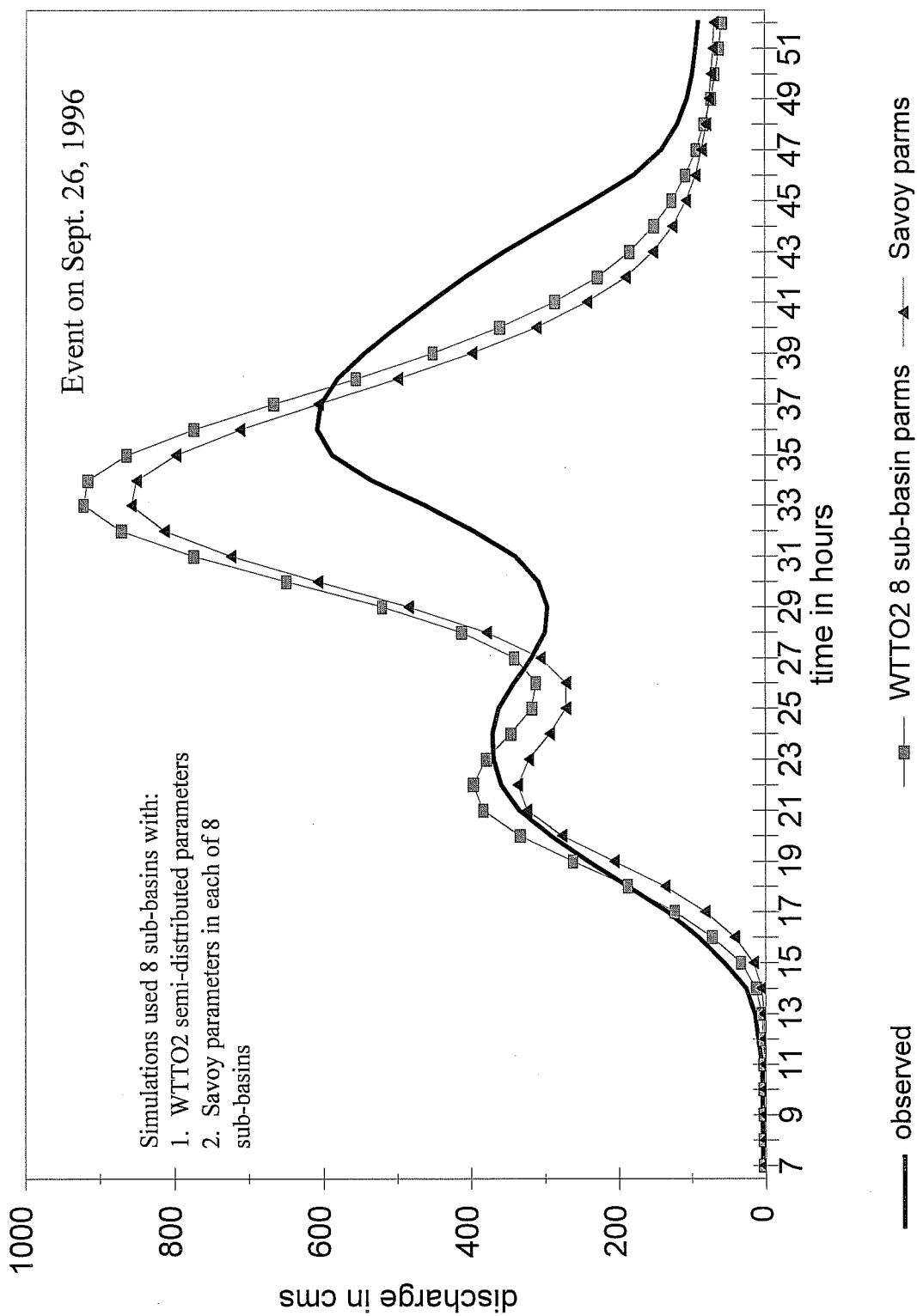
Simulations used 8 sub-basins with:
1. WTTO2 semi-distributed parameters
2. Savoy parameters in each of 8 sub-basins

time in hours

discharge in cms

—— observed   —■— WTTO2 8 sub-basin parms   —▲— Savoy parameters

Figure 6-11 Semi-Distributed Tests
with Two Paramter Sets

Figure 6-12 Semi-Distributed Tests
with Two Parameter Sets

Figure 6-13 Semi-Distributed Tests
with Two Parameter Sets

with the Sacramento model. Furthermore, calibrated parameters of a given basin are probably not fully representative of the heterogeneities that exist in near by basins of similar or differing scales, as shown in the up scaling regionalization experiments. Therefore, the spatially variability of hydrologic model parameters should be accounted for when applying distributed type models, and accounting for the spatial variability of rainfall may not be sufficient enough to improve results attained from lumped modeling approaches.

6.5 Unit Hydrograph Analysis

The Savoy 1-hour calibration required a different unit hydrograph than the 6-hour Watts parent basin unit hydrograph. A number of automatic and manual calibration methods were tested to derive one. This experiment illustrates the importance of the unit hydrograph in the semi-distributed modeling approach.

The S-curve method may be used to derive a 1 hour uhg from the 6 hour uhg at Watts. Assuming that the sub-basin has the same hydrograph shape as the parent basin, scale the volume of the Savoy unit graph according to a ratio of the area of Savoy and Watts to a power (0.65 in the Savoy case). This power is a largely unknown and is generally calibrated or estimated using judgement or trial and error. It is recommended that this method be used only if there is no other information about the basin.

Terrain data may be used to derive unit hydrographs as a function of the time-area curve for the basin, provided there is DEM (digital elevation model) data available. The DEM of the basin is used to determine the distance of every pixel to the basin outlet, and the basin area that drains through each pixel. This method is described be in section 5.2 of this report.

Routing of a unit depth of runoff from each pixel may also be used to evaluate the unit hydrograph. The routing unit hydrograph may assume constant travel time in the hill slope and the channel, or it may use a travel time that is a function of pixel slope, or any other information available about slope, channel roughness, land use, vegetation, etc. This method was used assuming constant travel velocities for the entire Savoy basin for the hill slope and for the channel. This method may be used effectively with a reasonable assumption about travel time constants, and may be calibrated if other information is available. A minimum of 10 pixels is recommended. This method may also be effective at deriving unit hydrographs when the basin experiences only partial coverage from precipitation and only a fraction of the basin is contributing runoff.

Since 14 months of hourly discharge data were available at Savoy, a manually calibrated unit hydrograph was also derived for use in the Savoy experiments. The results of the four methods of unit hydrograph derivation are shown in Figure 6-14. The figure shows that all methods produce similar and reasonable unit hydrographs with respect to timing and volume, but with some noticeable differences in shape. Both of the terrain-based methods, time-area and routing, result in more volume in the tail of the unit graph than the other methods. This may be attributed to the routing coefficients or the geomorphology of Savoy. The routing method has a less peaked round top that may be attributed to the assumption of constant travel times in all the hill slopes and channels, regardless of the true pixel slope, or roughness. The S-curve method had the most irregular shape due to interpolation between 6 and 1 hour ordinates, but it has a very reasonable shape given that it was derived from Watts the parent basin. The manually calibrated unit graph has the steepest rising limb and highest peak. This is due to the

preservation of volume when it was estimated to remove the estimated interflow contribution to the unit hydrograph. Due to the timing parameters in the Sacramento model runoff components from interflow and the subsurface, the unit graph is not supposed to incorporate the timing coefficients.

Figure 6-15 shows the effects of the various unit hydrograph methods on simulated discharge from the Savoy event on April 22, 1996. Since this is a surface runoff type event as simulated by the Sacramento model, the shape, timing, and peak of the simulated discharge hydrographs look very similar to the shapes plotted in Figure 6-14.
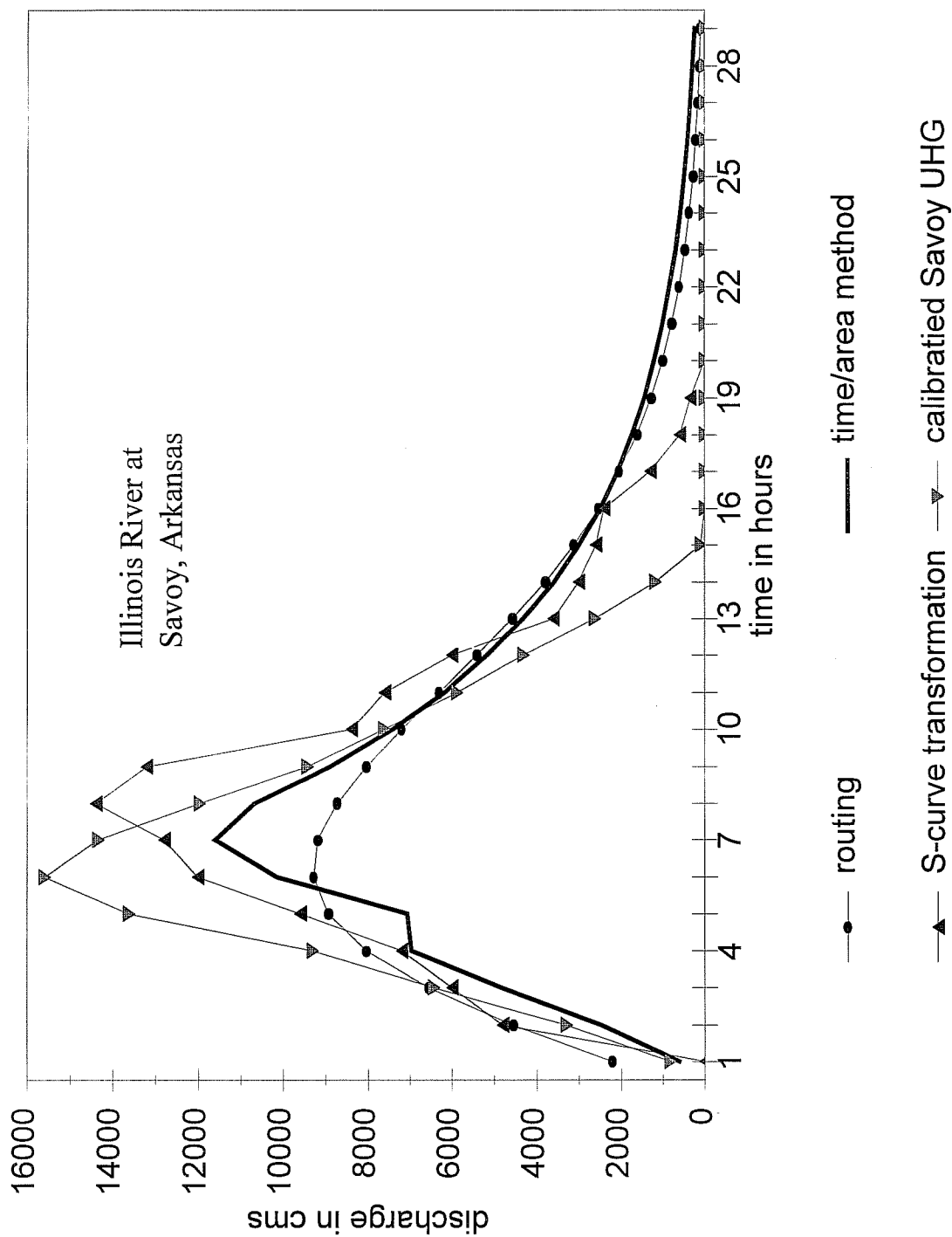
Figure 6-14 Unit Hydrographs Derived
Using 4 Different UHG Methods
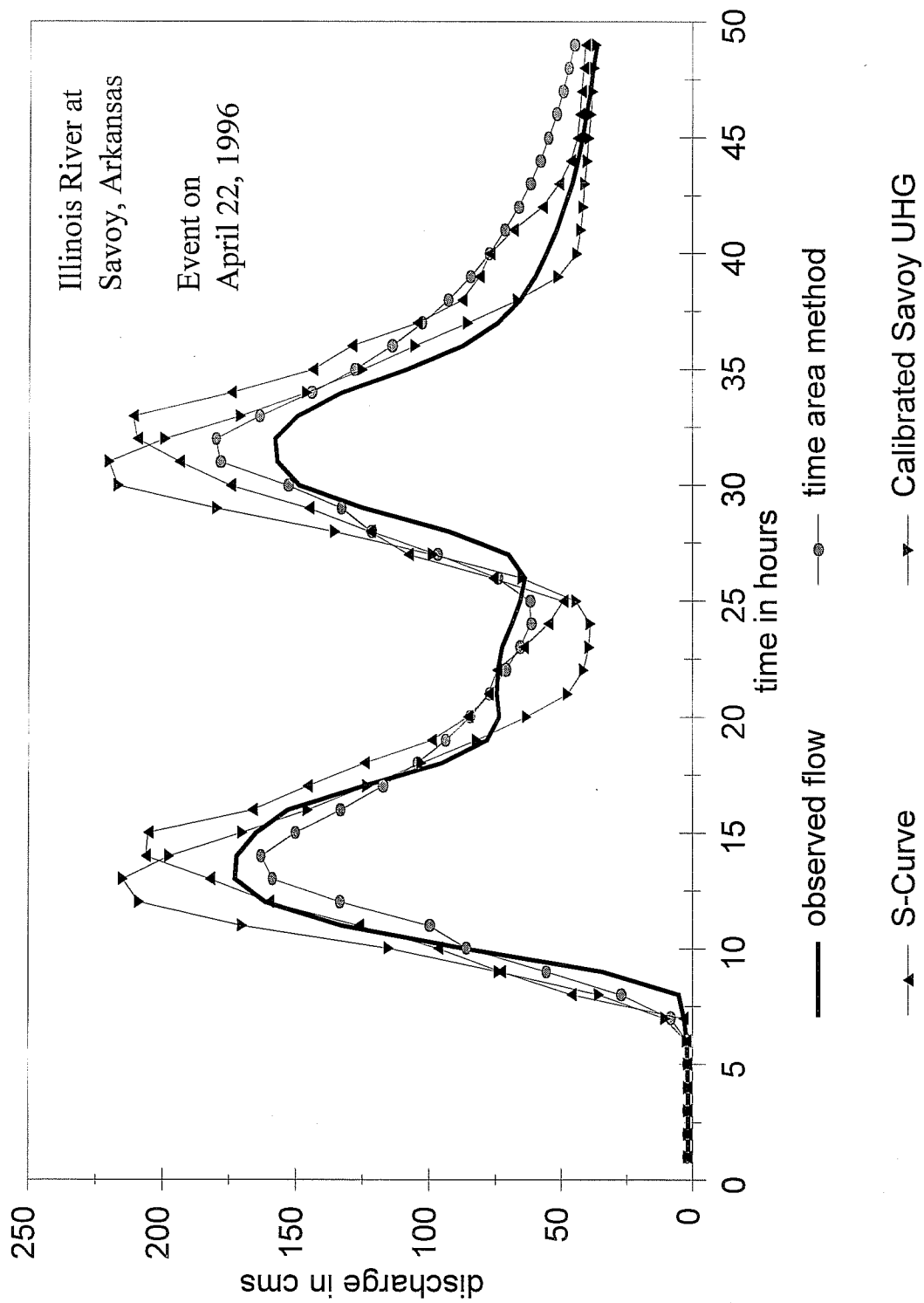
Figure 6-15 Flow Simulations using Three Unit Hydrographs

7. Major Conclusions

While each of the preceding chapters contained specific conclusions, a review of the major conclusions will be presented here in order to tie together the entire effort.

In general, the use of Stage III precipitation estimates provides clear benefits over the use of rain gage data for hydrologic modeling in the three basins studied. The most dramatic improvement over the current RFC lumped 6-hour rain-gage based modeling approach was realized by using the following:

   a. Lumped approach
   b. 1 hour time step
   c. Precipitation input defined by MAPX derived from Stage III
   d. Unit hydrograph initially defined by incorporating spatial data, ie. a time area approach
      or a Nash unit hydrograph.

These results support the findings of Pessoa et al., (1993) and Obled (1994). In WTTO2, 6 hour time step simulations with MAPX also showed improvement over the 6 hour rain gage based simulations.

Surprisingly, disaggregation of the WTTO2, ELDO2, and TALO2 basins did not provide a significant improvement in simulation accuracy beyond the approach outlined above. Although the results presented in Chapter 4 indicated that simulated hydrographs were sensitive to the level of headwater basin disaggregation, we could not utilize this effect when tests observed data was used. Our results also contrast some other research which has highlighted the influence of the spatial variability of precipitation on outflow hydrographs. However, like the analyses in Chapter 4, the majority of these past studies based their conclusions on the use of synthetically generated streamflow. While hydrograph shape and timing of the rising limb appeared to be slightly improved in some of our cases, the statistics showed a slight decrease in accuracy compared to the lumped simulations. This is most likely due to the RMS error statistic being dominated by several badly simulated events.

While the semi-distributed approach did provide limited improvement, several results indicated a weakness in the approach for parameterization and calibration of the sub-basin SAC-SMA parameters. Since the SAC-SMA parameters cannot be easily derived from physical watershed data, the same parameters were assigned to each sub-basin. Correspondingly, with discharge data only at the outlet of the basins, a strategy of uniformly adjusting model parameters in all sub-basins was adopted for calibration with the Stage III data. However, several events indicated that some sub-basins could have been parameterized differently. This was seen in the over-prediction of some events in which the precipitation was concentrated on a few sub-basins. Yet, due to the short 4 year period of data, too few spatially variable precipitation events were available for explicit sub-basin calibration.

It is uncertain whether the Stage III archive and operational MAPX data are of sufficient quality for Sacramento model calibration. Double mass plots of 8 MAPX time series were only

available for approximately 4 years, which is one tenth of the period for which consistency plots are currently derived using NCDC data. Guidelines for consistency corrections suggest that a correction be computed for prolonged changes in slope that last several years or more. Subjectively, the MAPX double mass plots appeared to have less wobble or variation than the operational MAP time series for the same period. However, due to the short period, it is difficult to ascertain whether prolonged slope breaks are present. In addition, the detected differences between the long term means from the MAP and MAPX time series need to be resolved before proper implementation of calibration results in the operational system can be achieved. It is uncertain whether changes in the NEXRAD computational algorithms can be seen in the double mass plots. Another factor adding to the uncertainty regarding the quality of the xmrg files is that the P1 processing system has been in use at ABRFC in addition to Stage III, which may introduce biases in the detected rainfall.

Based on 7 months of data, the runoff components of the Sacramento model were found to be dependent on the scale of precipitation forcing. Surface runoff, generated when the upper zone tension and free water storages are filled, is the most sensitive component of total runoff. Slower responding base flow components proved to be the least sensitive to changes in the spatial scale of precipitation forcing. A reformulated version of the SAC-SMA was found to be less dependent on scale than the current version of the model.

An effort was made in Chapter 2 to derive guidelines for a priori SAC-SMA parameter adjustment so that a basin could be calibrated using conventional techniques and then the parameters would be adjusted for use with Stage III data. It was hoped that these guidelines would enable the user to adjust lumped 6-hour SAC-SMA parameters for use with different spatial and temporal scales. In essence, it was hoped that the user could recalibrate the parameters in the absence of a sufficient period of Stage III data. These tests were performed with a single data source, the Stage III xmrg files for ABRFC. One of the underlying assumptions of these tests was that the Stage III data and archived operational MAP products would lead to the same long term mean in areas where there is little spatial variability in the long term catch of gages. Comparison of archived MAP and MAPX data (Chapter 3) revealed that the MAPX have a long term tendency to be biased low compared to the operational gage derived MAP data. Preliminary comparisons of 7 months of archived MAPX data and calibration MAP data for basins in ABRFC revealed a similar tendency. Thus, one of the underlying assumptions of the parameter adjustment guidelines is invalidated, and the issue of a priori parameter adjustments to account for changes in spatial and temporal scale becomes more cloudy.

An analysis of over 3 years of archived MAPX and Map data found that the two precipitation products have different statistical properties. First, long term means for the two can be up to 10% different. This has implications for calibration and operational forecasting. Also, Stage III derived MAPX values were found to represent precipitation events a occurring in fewer time intervals than the gage derived MAP data. This could be the result of several factors. First, there are fundamental differences in the computational algorithms. The operational MAP preprocessor generates a 24 hour MAP value and then distributes it over four 6-hour time intervals. The MAPX preprocessor generates hourly mean values. Also, the MAP preprocessor uses hourly, 3-hourly, 6-hourly, and daily rain gage reports, while the MAPX preprocessor predominately uses hourly rain gages that report at the top of the hour.

Simulations with archived operational MAP time series and historically calibrated model

parameters indicated that larger biases were generated compared to the bias derived in calibration This result indicates that the calibration MAP and operational MAP time series might be statistically different. A direct, long term comparison cannot be made yet due to the limited overlap of the time series. At the time of this writing, NCDC data is only available at HRL through the end of September, 1993, while the archived operational MAP data begins in May of 1993.

Synthetic methods can be used to derive initial unit hydrographs for simulation. Most extensively used in hydrologic simulations was the Nash method. The Clark time area method was also used to generate unit hydrographs for comparison to the Nash unit hydrograph for one basin. However, some calibration of the unit hydrographs was performed.

References

Obled, C.H,. Wendling, J., Beven, K., 1994, 'The Sensitivity of Hydrological Models to Spatial Rainfall Patterns: An Evaluation Using Observed Data', Journal of Hydrology, 158, 1-18.

Pessoa, M.I., Bras, R.L., Williams, E.R., 1993, 'User of Weather Radar for Flood Forecasting in the Sieve River Basin: A sensitivity Analysis', Journal of Applied Meteorology, 32 (30, 462-475

8. Recommendations

Based on the work conducted so far, several recommendations can be made for further research topics. In addition, several practical software development efforts have already begun.

Strategies need to be developed for parameterizing and calibrating the SAC-SMA when used in a sub-basin mode. This is part of the general problem of calibrating a semi-distributed conceptual model when observed streamflow data is only available at the parent basin outlet. Modeling results showed that calibrating a semi-distributed model by uniformly adjusting parameters in all sub-basins can lead to poor simulations in certain instances. Perhaps precipitation events occurring over individual sub-basins could be isolated and used to adjust hydrologic model parameters. The problem remains in that SAC-SMA parameters are not readily derived from physiographic data. Other continuous models that might be more easily parameterized should be identified for testing.

Efforts are underway in HRL to import spatial data sets such as soils information into ARC/Info and ARC-VIEW in order to assess parameter variability. Initially, these data will be used to visually examine inter-basin and intra-basin variability of physical watershed data. As a start, such information could be used to guide sub-basin delineation and justify the use of different SAC-SMA parameters in different basins.

At the time of this writing, several ongoing research efforts may provide direction for future NWS hydrological model usage. MIT has recently been awarded a 3 year research grant from another agency to perform extensive comparative tests of their physically based distributed parameter model against the SAC-SMA. Their model uses a gridded approach for each computational element and is able to compute saturation excess and infiltration excess types of runoff. Planned cooperation with HRL includes the provision of data sets and modeling results for one of the basins studied in this report as well as 5 or 6 from other parts of the United States. The University of Arizona is conducting research to address the problem of calibrating a semi-distributed conceptual model. The Hydrologic Engineering Center of the U.S. Army Corps of Engineers has plans to modify their event-based MODClarke model to perform continuous simulations.

Given the usefulness of Stage III data for hourly lumped hydrologic simulation, enhancements are underway in the Interactive Calibration Program to enable users to display hourly simulation results for manual calibration of model parameters. Currently, the only display option is associated with the WY-PLOT operation, which is limited to the display of mean daily flow. As outlined in section 5.1.1, calibration of an hourly model by examining mean daily flow values cannot be effectively performed. To alleviate this problem, design requirements have been detailed for a new display function based on the PLOT-TS operation, and at the time of this writing, a beta version of this plotting function is being tested in HRL. With this capability, a user will be able to plot data at variety of time steps and will be able to construct his own displays. As with the ICP WY-PLOT display, the user will be able to scroll through the entire run period as well as change plotting scales. The plotting routine will be developed in such a way that it will be easily converted to a stand alone version for the eventual inclusion into an off-line research modeling system.

The semi-distributed modeling results presented herein used MAPX time series computed using in-house developed software. For future research, a beta version of a calibration MAPX preprocessor has been developed and has been tested in HRL. In addition, a beta version is being tested as an off-line preprocessor at OHRFC and SERFC. It is planned that this software could eventually be delivered to the field to be used to develop MAPX time series for hydrologic model calibration in the same way that MAP3 is used. As input, it uses Stage III xmrg files and produces hourly or six hourly MAPX time series in OH DATACARD format. It requires a basin boundary defined by lat/lon pairs. Testing with 9 basins defined using IHABBS basin delineation software generated MXCO HRAP line segments that are identical to those in ABRFC files. In addition, MAPX values derived that were identical to archived ABRFC MAPX time series. This software uses the sfbdrv.f subroutine that is used in the DEFINE BASIN command of NWSRFS. In this way, any further research will use the same algorithms that are used operationally in the field. More importantly, use of this tool by RFCs would ensure that the same precipitation processing algorithms are used in calibration as in operational forecasting with Stage III data. Recall that the algorithms in the Calibration MAP3 program are different than those used to compute MAP values in OFS.

Procedures need to be developed for the generation of synthetic unit hydrographs. As seen in Chapter 5, hourly lumped unit hydrographs developed from synthetic methods performed better than those generated by using an S-curve technique with the 6-hour unit graphs. For the Nash and Clark methods of unit hydrograph derivation outlined in Chapter 5, HRAP (4km.) connectivity was used. At the time of this writing, the IHABBS software developed by NOHRSC is being modified to include both the Soil Conservation Service (Now the National Resource Conservation Service-NRCS) and Clark methods of generating unit hydrographs. This effort was begun for the purpose of generating unit hydrographs for the Site Specific model. IHABBS is based on 500m. resolution data. Once completed, this capability needs to be further tested for developing initial hourly unit graphs that can be used with the SAC-SMA.

Continued work needs to be directed at both manual and automatic calibration using NEXRAD. For the majority of the lumped and semi-distributed tests, automatic calibration was used to derive SAC-SMA parameters due the short period of data. Manual calibration efforts should be continued in order to gain insight as to how the SAC model behaves with input of greater intensity.

A comparison of the calibration MAP time series and the operational MAP time series for the 8 test basins in ABRFC needs to be performed. This can be done once the latest NCDC precipitation data is mounted. The calibration time series need to be extended beyond the current ending point of September, 1993 so as to overlap as much as possible the operational MAPX time series that start in May, 1993. Efforts are underway to make available the hourly and daily NCDC precipitation data so that a calibration MAP time series can be derived up to 1998. At the time of this writing, analyses are being conducted using the operational MAPX and MAP time series from ABRFC from 1993 to 1998, thus extending the analyses presented in Chapter 3. The Calibration MAP time series will be included this analyses as soon as the hourly precipitation data is put on the HRL system.

In addition, comparison of operational MAP and MAPX data should continue so as to monitor the change in bias due to the implementation of improved Stage II and Stage III

processing procedures. Given longer time series of these two types, more significant conclusions can be made regarding the suitability of the Stage III data for calibration.

The Muskingum-Cunge channel routing procedure needs to be completed. Parameters for this method could be developed from physiographic data. The reformulated SAC-SMA model should be tested further with observed stream gage data. In order for this model to ever be used in OFS, modifications to the operational MAPX preprocessor need to be made so that the coefficient of variation and percent of rain covered area are computed hourly and passed to the reformulated SAC-SMA.

The scaling studies in Chapter 2 were limited to the 7 month period of archived xmrg data at the time. Given the existence of a longer period of Stage III data, the scaling studies should be extended in order to validate the results presented.

Tests are already underway to extend the semi-distributed analyses of Chapter 5 to the basin TIFM7, which is the largest of the 9 test basins. A historical calibration has been performed, and attempts are now being made to re-calibrate the SAC-SMA parameters for use with MAPX in a lumped approach. Semi-distributed tests will soon follow. With continued testing of a semi-distributed approach, we hope to evaluate the sensitivity of observed and computed outflow hydrographs to the spatial variability of precipitation.

Appendix A

Scatter Plots of MAP Values vs MAPX Values for 9 Basins in ABRFC

Period of Analysis: June 1993 to November, 1996

Gage vs Radar Mean Areal Precipitation: ELDO2

Figure A-1

Gage vs Radar Mean Areal Precipitation: JOPM7

Figure A-2

Gage vs Radar Mean Areal Precipitation: KNSO2

Figure A-3
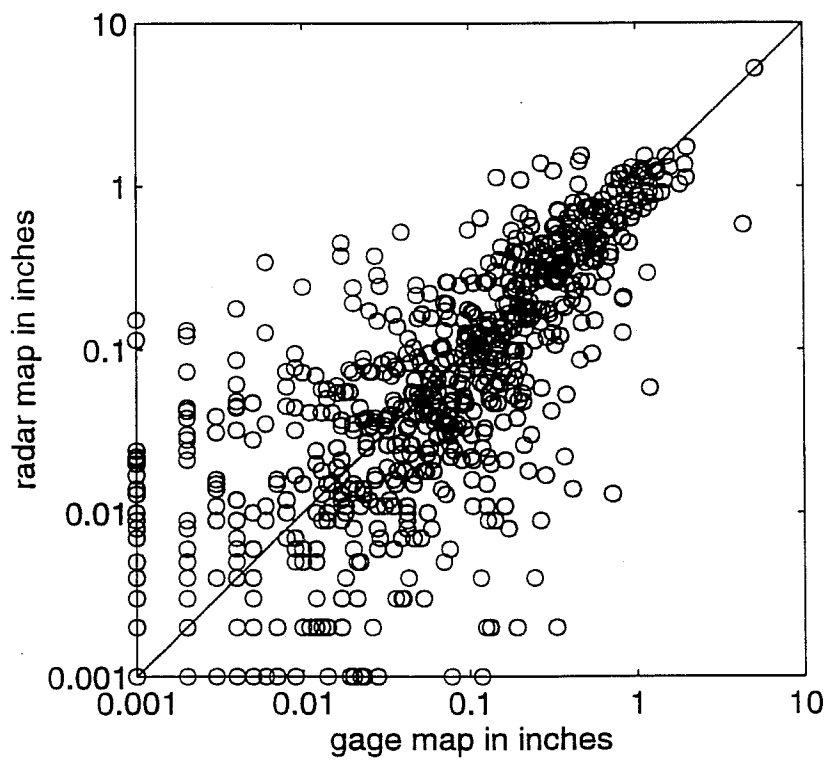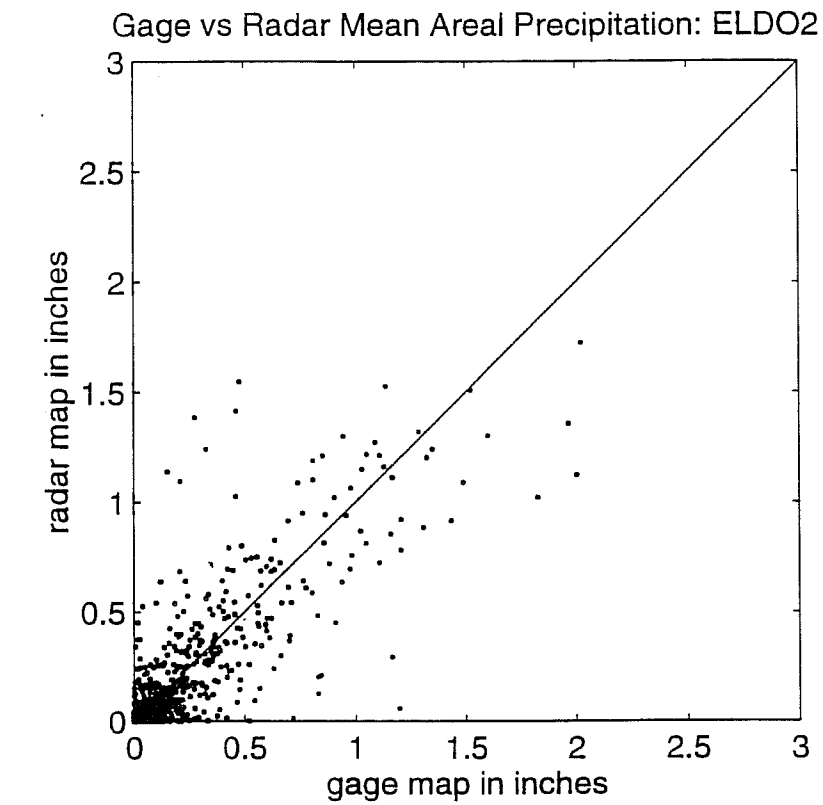
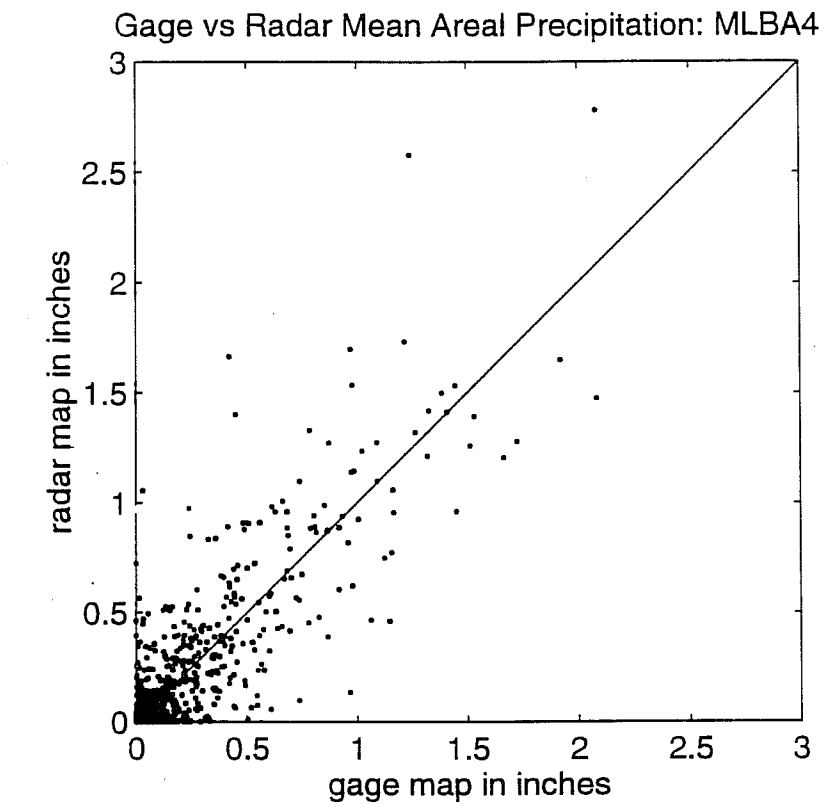Gage vs Radar Mean Areal Precipitation: MLBA4
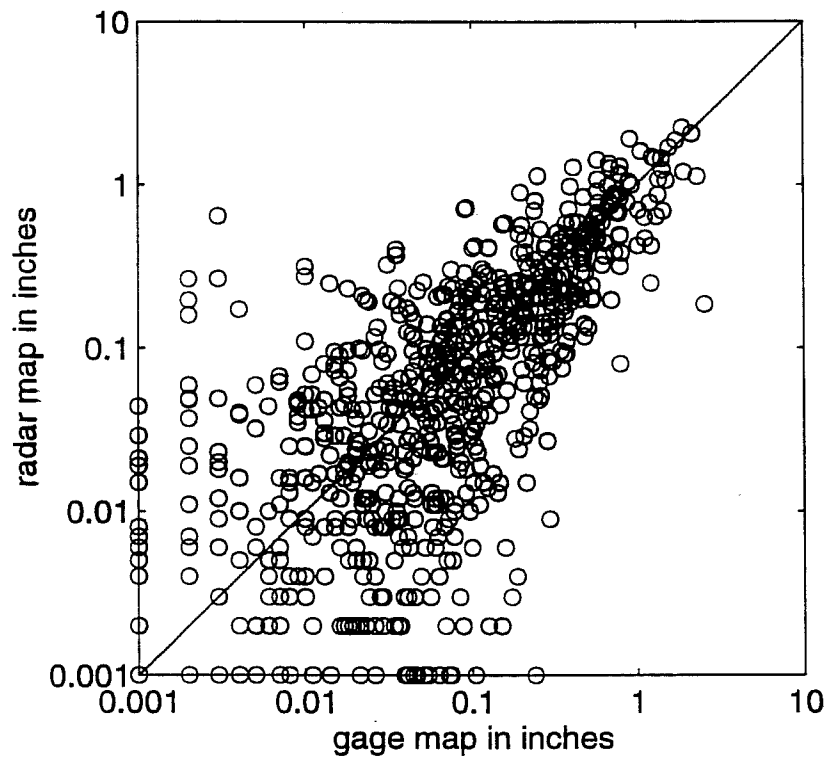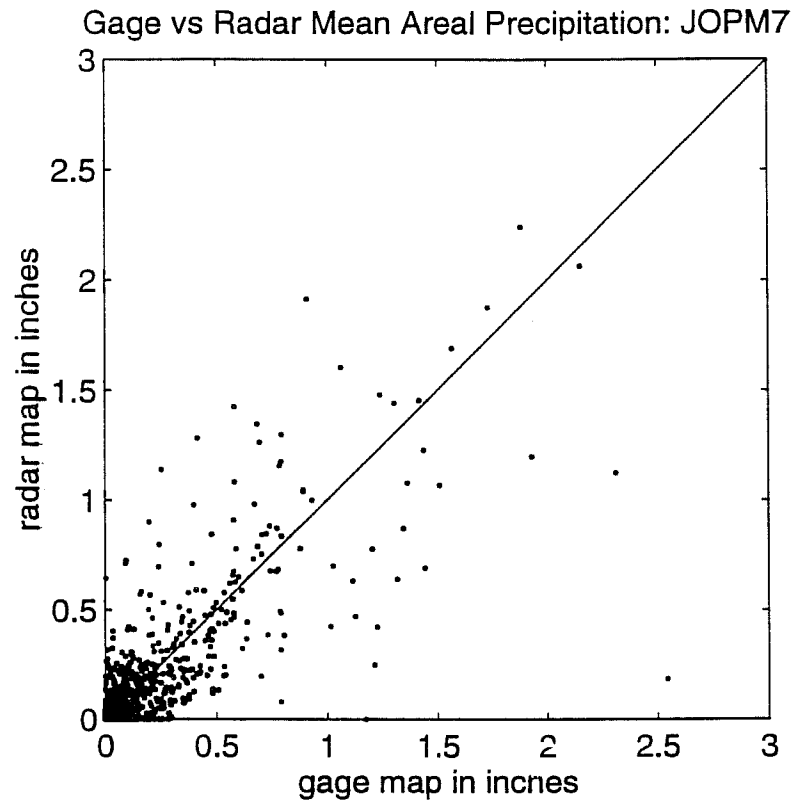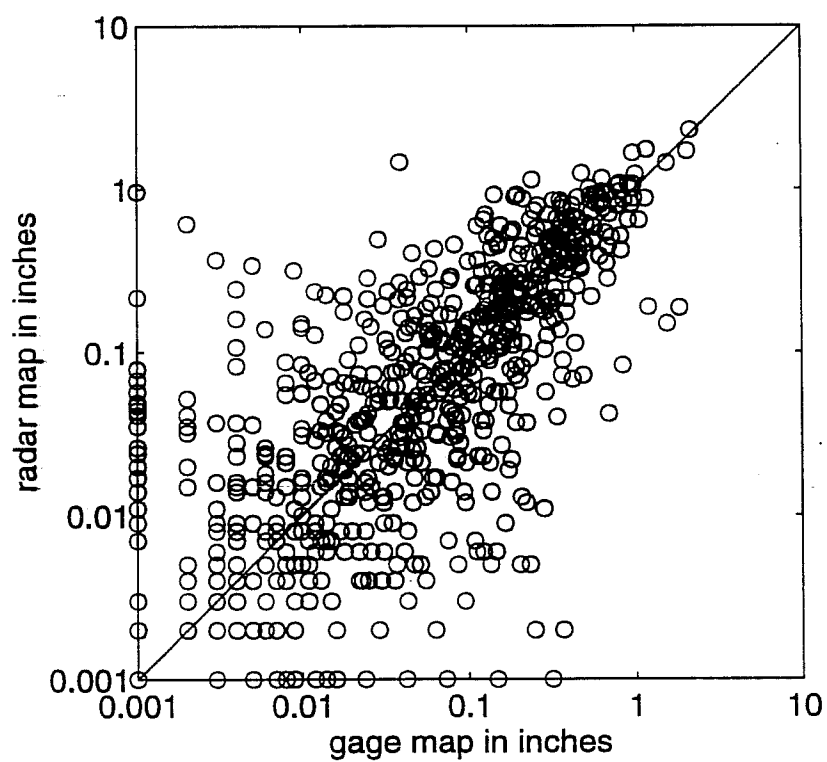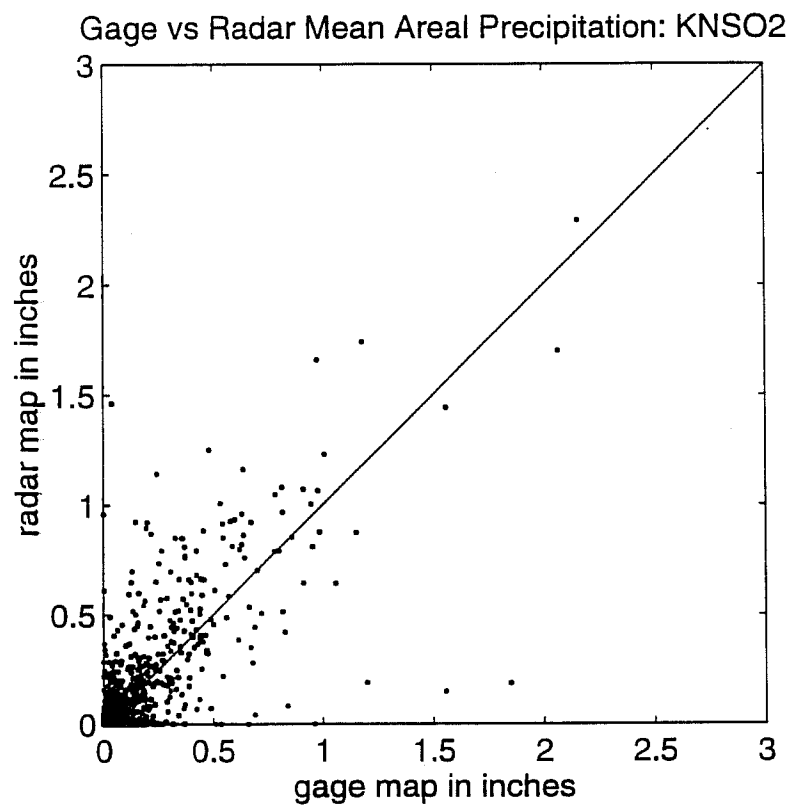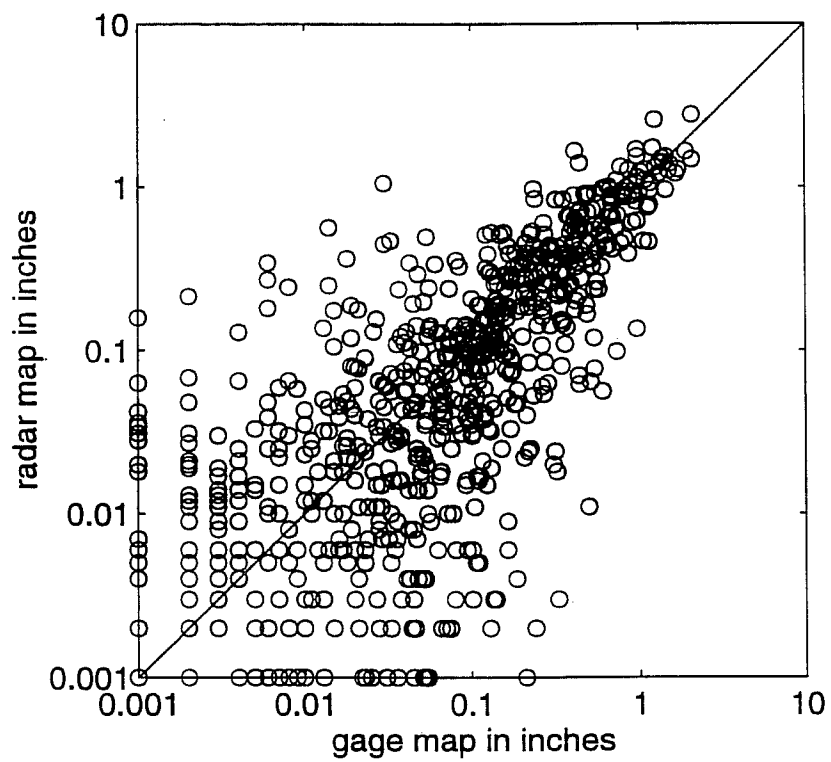
Figure A-4
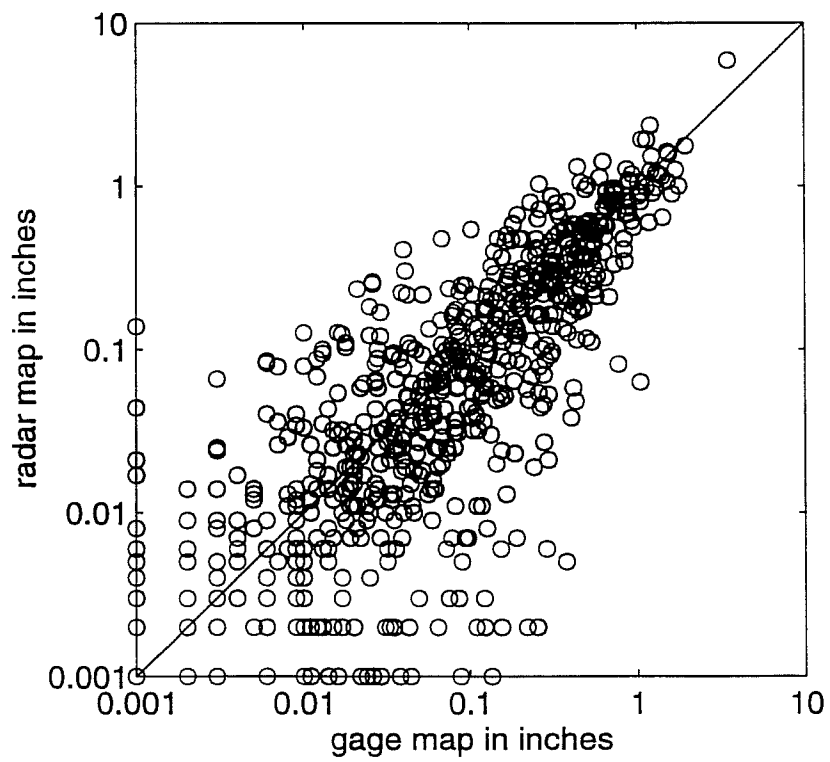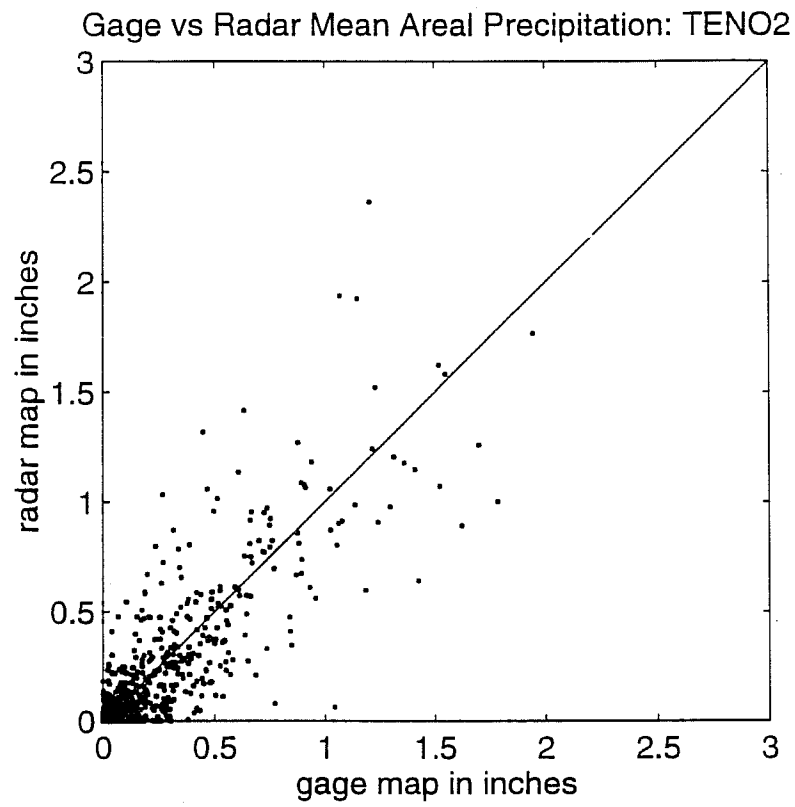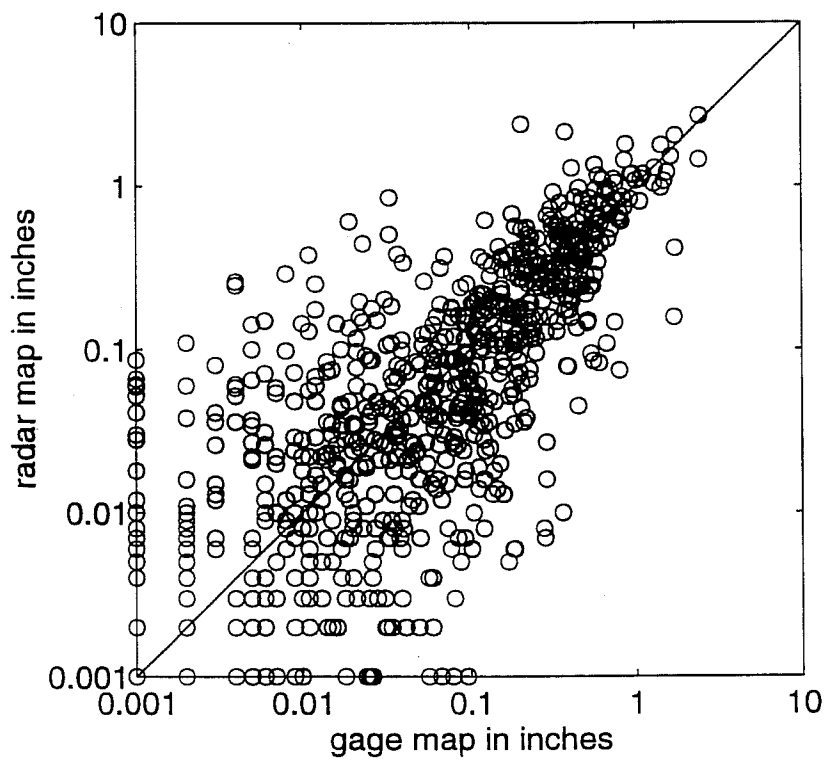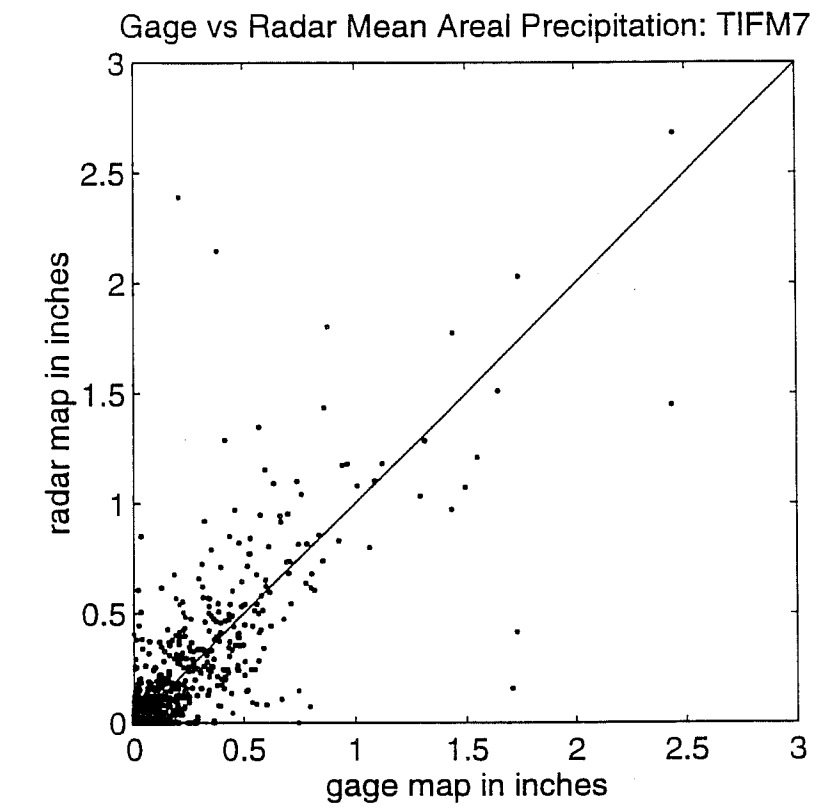
Gage vs Radar Mean Areal Precipitation: TALO2

Figure A-5

Gage vs Radar Mean Areal Precipitation: TENO2

Figure A-6

Gage vs Radar Mean Areal Precipitation: TIFM7

Figure A-7

A.8
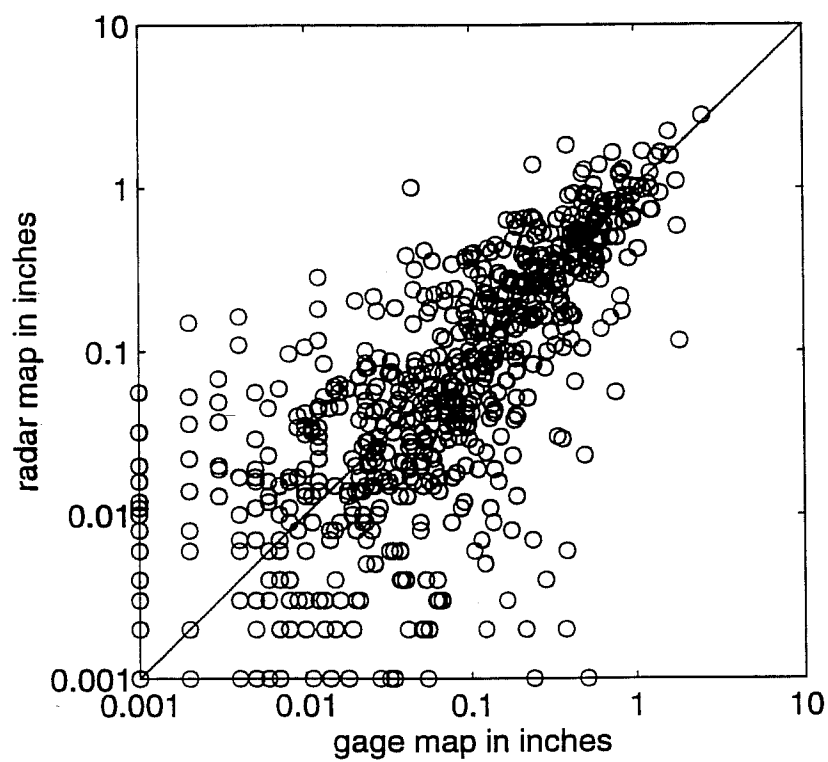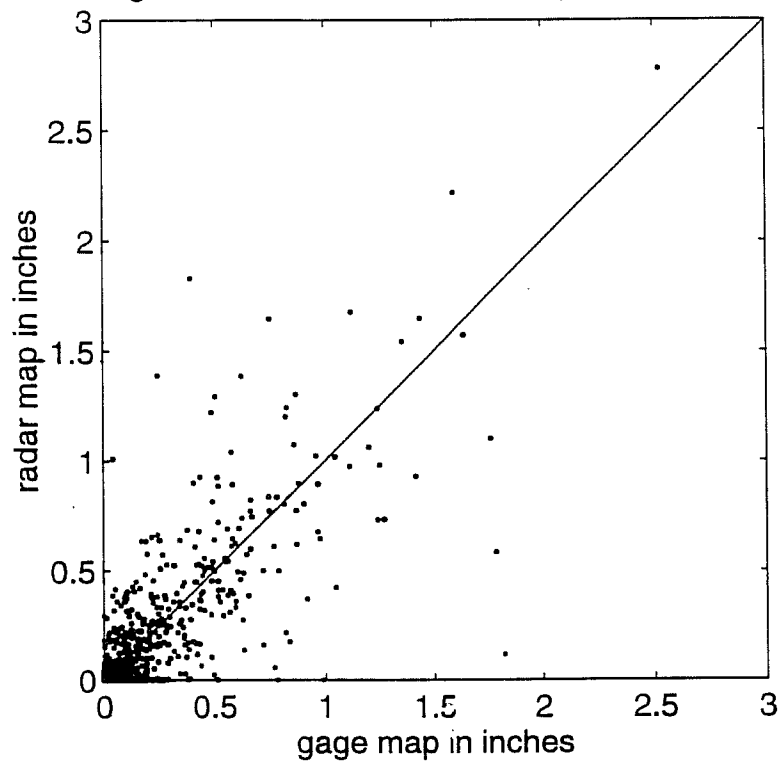
Gage vs Radar Mean Areal Precipitation: VBRA4
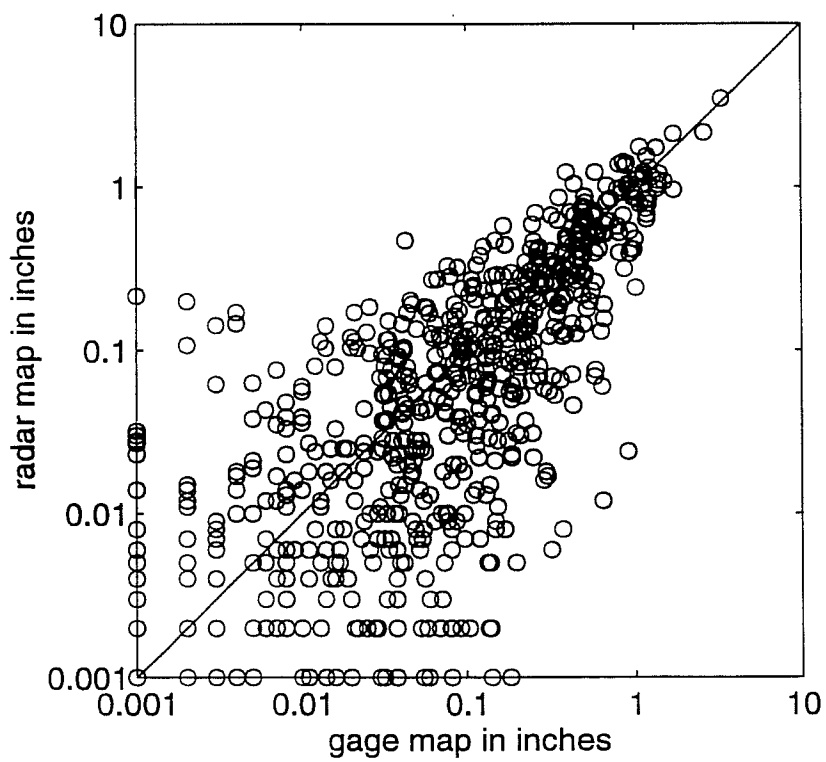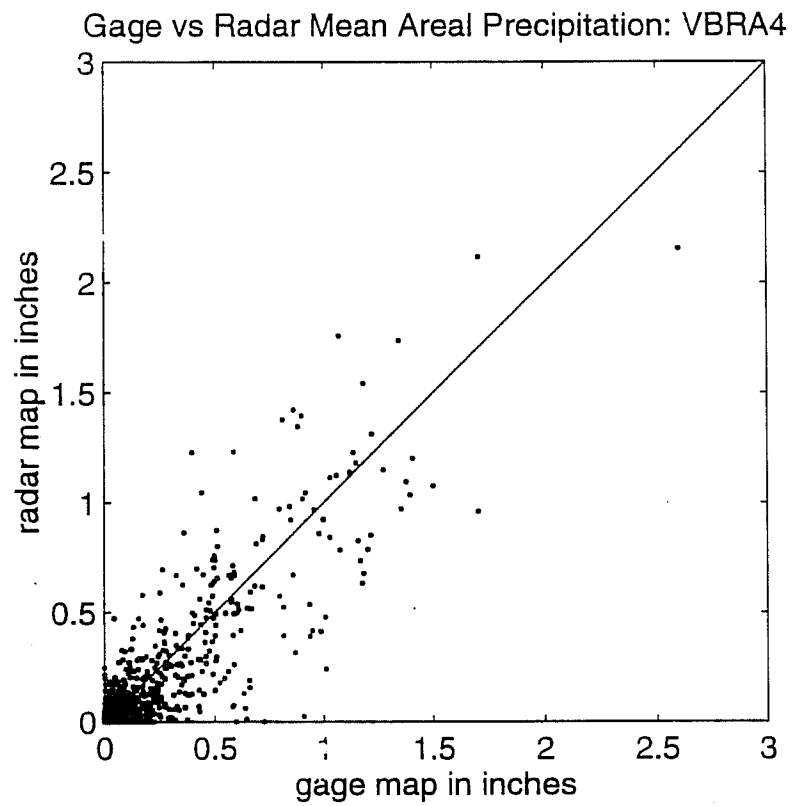
Figure A-8

Gage vs Radar Mean Areal Precipitation: WTTO2
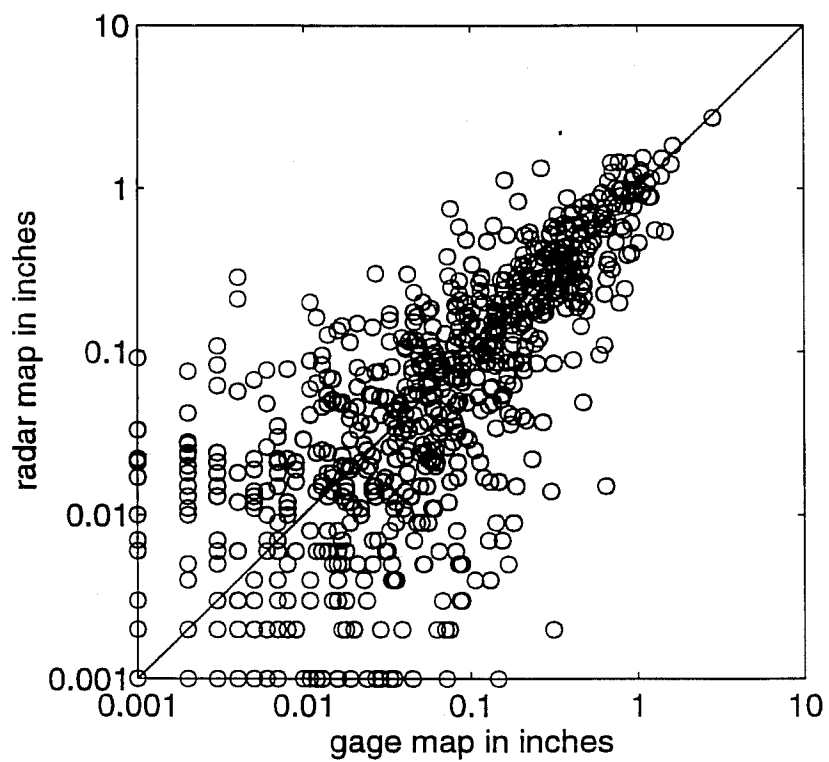
Figure A-9

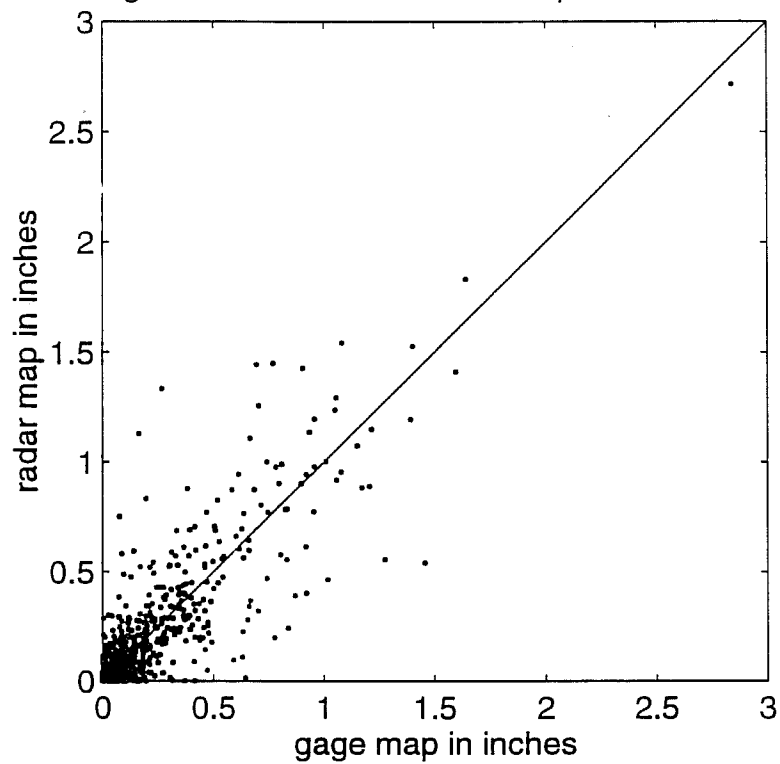# Appendix B

Monthly Ratio of MAPX to MAP for 8 Basins in ABRFC
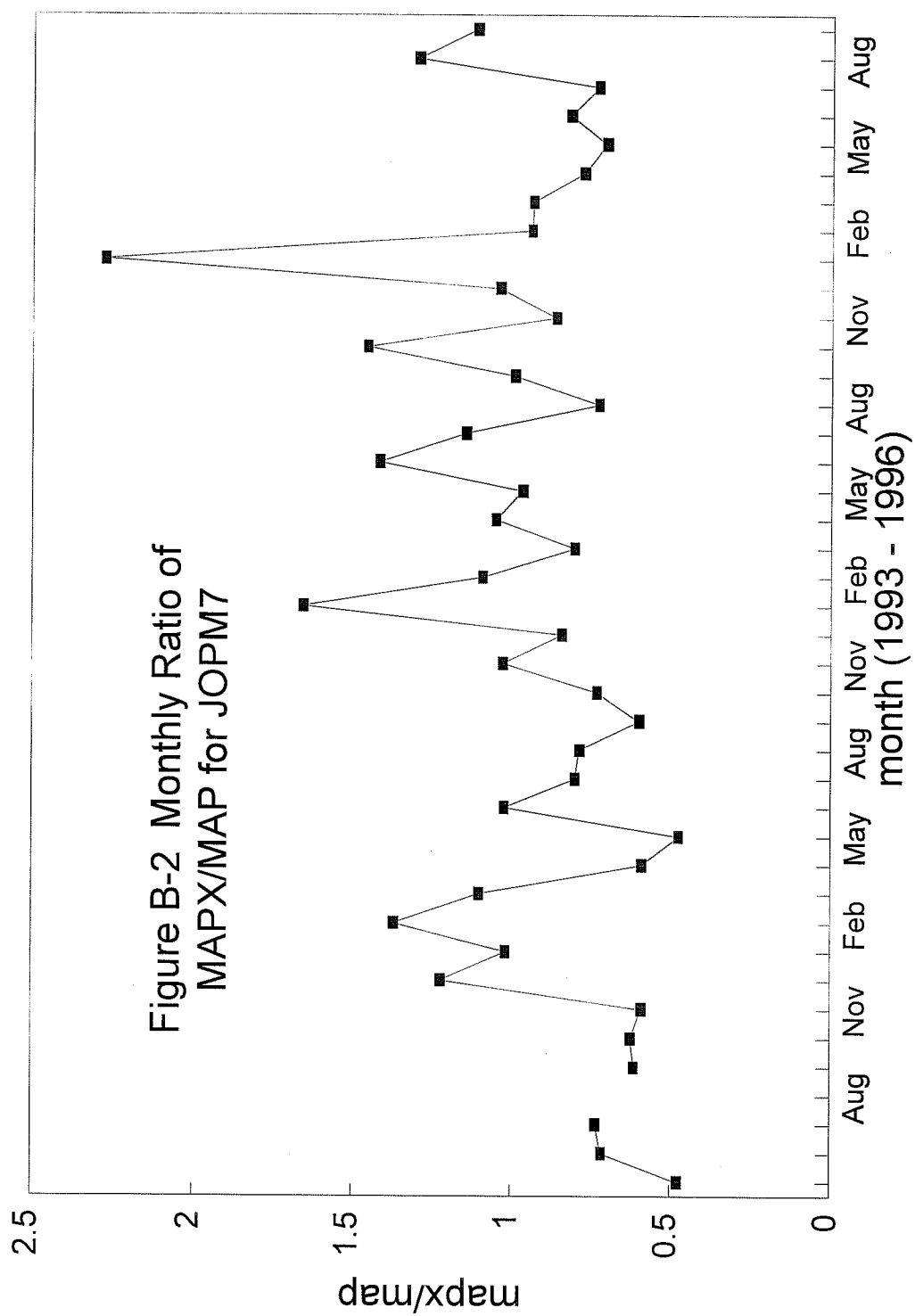
Period: May 1993 to September 1996

Figure B-1   Monthly Ratio of
MAPX/MAP Ratio and for ELDO2

Figure B-2 Monthly Ratio of MAPX/MAP for JOPM7

Figure B-3 Monthly Ratio of
MAPX/MAP for KNSO2

Figure B-4 Monthly Ratio of
MAPX/MAP for MLBA4

Figure B-5 Monthly Ratio of MAPX/ MAP for TALO2

Figure B-6 Monthly Ratio of MAPX/MAP for TENO2

Figure B-7 Monthly Ratio of
MAPX/ MAP for TIFM7

Figure B-8 Monthly Ratio of MAPX/MAP for WTTO2